HEAT AND MOISTURE TRANSFER IN BUILDING

W040

CIB Proceedings

ISBN 90-6363-017-4

Publication 245

HEAT AND MOISTURE TRANSFER IN BUILDING

CIB Proceedings **Publication 245**

A collection of 31 Refereed Papers prepared in conjunction with the meeting of CIB Working Commission W040 - Heat and Moisture Transfer in Building which was held at the Faculty of Civil Engineering, Czech Technical University in Prague, Czech Republic from 30th August to 2nd September 1999

EDITORS

PROFESSOR INGEMAR SAMUELSON

Coordinator W040

SP Swedish National Testing and Research Institute

Building Physics Department

AND

PROFESSOR ROBERT CZERNY

Department of Structural Mechanics

Faculty of Civil Engineering

Czech Technical University

ASSOCIATE EDITOR

CHRISTOPHER POLLINGTON

Deputy Secretary General CIB

ISBN 90-6363-017-4

February 2000

CONTENTS

WHOLE BUILDING HYGROTHERMAL PERFORMANCE

A. Karagiozis, M. Salonvaara

WHOLE BUILDING HYGROTHERMAL PERFORMANCE

Achilles Karagiozis[1] and Mikael Salonvaara[2]

[1]Oak Ridge National Laboratory,
1 Bethel Valley Rd, Oak Ridge,
TN, 37831-6070, US
Karagiozisan@ornl.gov

[2]VTT Building Technology
P.O. Box 1804, FIN-2044 VTT
Finland,
Mikael.Salonvaara@vtt.fi

ABSTRACT

Many recent, moisture-originated failures in low-rise residential and high-rise residential/commercial buildings have put a significant pressure to change construction codes in North America and Europe. However, solutions to moisture induced problems may be difficult when several interacting mechanisms of moisture transport are present. Recently, a new approach to building envelope durability assessment has been introduced in North America. The approach employs moisture engineering, which requires system information about the wall systems as constructed or with aging characteristics coupled with advanced modeling to predict the long-term performances of building envelope systems. This permits the comparison and ranking of individual building envelope systems with respect to total hygrothermal performance. While critical information can be obtained by investigating the one to one relationships of a building envelope to interior and exterior environments, the total behavior of the actual whole building is not accounted for. This paper goes one step further, by incorporating the individual hygrothermal performances of all walls, roof, floor and mechanical systems. The direct and indirect coupling of the building envelope and indoor environment with HVAC system are included in the analysis. The full house hygrothermal performance of an aerated concrete wall system and a wood frame wall system are examined for a mild climate. The hour by hour drying potential of each system was then numerically analyzed using real weather conditions of Knoxville TN. The results clearly demonstrate the drying potential for the wall system in that climate. Furthermore, the selected exterior thermal insulation strategies and interior vapor control strategies in this study clearly show the critical behavior of the full house with respect to drying initial construction moisture. The results show the importance of the total hygrothermal behavior of the whole house to the coupling between the various envelope parts, interior and exterior environments and HVAC system. From these results moisture control strategies are identified for the whole house hygrothermal performance.

KEYWORDS: Moisture Control, Hygrothermal Modeling, Integrated Building Analysis

INTRODUCTION

Moisture transport through a building envelope influences not only the durability, indoor air quality, health and safety of the inhabitants, but also the energy efficiency of the envelope system. The influences of moisture transport are experienced differently in lightweight (hygroscopic) or heavy weight (moisture massive) building envelope systems. Recently several catastrophic large scale moisture related failures have appeared in wall systems that were not designed properly with moisture control principles. Current stucco clad

wall systems in Vancouver Canada belong to this class of building systems that are prone to moisture damage. Moisture induced damage of more than 1 billion dollars annually in premature failures have been documented (Buske, 1999). Similarly, improperly designed exterior insulated finish systems, EIFS, have caused major moisture related damages in Wilmington NC (Nisson, 1995). In almost all cases of moisture related damage, the building envelopes were not designed to handle the moisture loads that were present due to the imposing environment. In both locations, Vancouver BC and Wilmington NC, the need for proper moisture control analysis of building system is clearly demonstrated. However, solutions to moisture induced problems may be difficult to achieve when several interacting mechanisms of moisture transport are present.

Recently, a new approach to building envelope durability assessment has been introduced, and is becoming an acceptable norm in North America. The approach employs experimental and advanced modeling analysis to predict the long-term performances of building envelope systems to various levels of interior and exterior environmental loading. This permits the comparison and ranking of wall systems with respect to an overall hygrothermal performance. Elaborate experiments are conducted to measure the various hygrothermal properties such as sorption and suction isotherms, vapor permeabilities, liquid diffusivities, and drainage which are then complimented with full scale laboratory building envelope testing to determine system and sub-system performances. Modeling is then initiated to predict the hygrothermal performances of the individual building envelope part. This approach has been termed as Moisture Engineering (Trechsel 1998, Karagiozis, 1997b).

Further advances in the area of moisture engineering are currently been achieved by taking a broader wholistic approach to moisture design (Salonvaara, 1999) (Karagiozis and Salonvaara, 1999). In most applications, building envelope designers and researchers attempt to quantify the hygrothermal performance of an individual building envelope, for example a wall, roof or basement by uncoupling the system not only to the interior environment but the interactions of the other envelope components to both the exterior and interior environments. Understanding the hygrothermal performance of the one to one interaction of a small part (section of a wall system perhaps to the exterior environment) of a building is termed today as state-of-the-art analysis. The stand-alone analysis of specific envelope parts is important in understanding the influences of various controlling elements (vapor retarder, air barriers, building papers) in terms of their effect on the hygrothermal performance of the envelope, but provide limited performance information on the overall heat and mass transfer of a building. This limitation becomes more and more serious in retrofitting applications and when highly insulated structures are employed.

An novel iterative open loop approach of complete hygrothermal analysis of a building is demonstrated which requires the direct coupling of all building envelope systems with the interior environment and mechanical systems (HVAC) and the exterior environmental loads.

In this paper, the authors present a new model and approach to wholistic moisture engineering analysis. This paper demonstrates an application of wholistic moisture engineering modeling to quantify the drying performance of a composite polystyrene bead concrete block building and a light weight wood frame EIFS building. All building elements, such as the walls, roofs are included in the analysis. The source of water considered is due to the initial construction moisture in the composite polystyrene bead concrete block, or the exterior sheathing oriented strand board. The study will attempt to shed some light in some (not all) of the issues present in the integrated moisture performance of a complete building.

OBJECTIVES OF PRESENT STUDY

The present work is concerned with the hygrothermal performance (drying potential) of two building systems, one with a composite concrete polystyrene bead block home, and the other with a conventional exterior insulated finish system (EIFS). Both of these buildings were subjected to two selected vapor diffusion control strategies. The objective of the work was to determine the long-term hygrothermal performance of the buildings to various vapor control and thermal insulation strategies while subjecting the exterior boundary to real weather data. A wholistic approach is employed by using moisture engineering principles that integrate intensive numerical analysis and accurately defined material property measurements. All wall and roof envelope components were employed in the analysis. The weather data used in this study analysis are representative of a mild-climate found in the east-southern portion of United States (TN).

VAPOR CONTROL THEORY

Moisture entry into the wall structure can be caused mainly by five processes: initial construction moisture, vapor diffusion, liquid diffusion, water leakage and moist air leaking inward or outward (being more important for cold climates) through the building envelope. Moisture transport by diffusion occurs under the influence of a vapor pressure or moisture content (capillary suction pressure) gradient acting across the wall structure. Additional factors of significant importance are the overall integrity of the building material (i.e. cracks and openings), the interface contact and surface moisture resistances, but have not been included in this analysis. To control moisture flow into the wall structure, vapor barriers have been devised. The application, location and selection of the vapor retarders is strongly dependent on wall design (whether or not special buffer zones have been provided) and on climatic conditions. However, only a limited number of studies exist that have integrated both the vapor and liquid transport performance of building systems including the effects of wind-driven rain see [Salonvaara and Karagiozis, 1998].

MATERIAL-PROPERTY DETERMINATION

Hygrothermal material properties for composite concrete was measured at VTT (Salonvaara, 1999) and the interior and exterior stucco were extracted from a paper presented by one of the authors [Karagiozis, 1997a].

DESCRIPTION OF THE MODEL

A new model, developed by the authors [1999] provided a structured framework allowing the integration of the individual heat, air and moisture performances of various oriented walls systems and roof assemblies, by lumping the building dependent geometries to the interior and exterior environment as well as the mechanical equipment of the building.

PROBLEM DESCRIPTION

The hygrothermal performance (drying potential) of composite concrete block wall home, and an EIFS building wall was analyzed with two different interior vapor control strategies. The composite concrete polystyrene bead wall system was composed 12 mm of conventional stucco, 50 mm of expanded polystyrene, 198.4 mm (200 kg/m^3) of composite

polystyrene bead concrete, 6 mm of interior stucco and interior vapor paint coats. The lightweight wall was composed of a 5 mm acrylic exterior stucco, 50 mm EPS, 12 mm OSB, 89 mm glass fiber insulation, building paper and 12.5 mm gypsum board.

The house was rectangular in cross section (15 x 20 m) and the roof was inclined at 20 degrees. Windows and doors occupied the approximately 20 % of the exterior building surface, and were represented with U-value thermal performances of 2.0 W/m^2K. The roof consisted of 300 mm mineral wool insulation with polyethylene vapor/air retarder and gypsum board on the interior side.

The inside surface of the gypsum plaster was coated with either a vapor open paint (permeance approximately 200 ng/m^2sPa or 4 perms). Variations of these walls consisted of the case with a vapor impermeable (57 ng/m^2sPa or 1 perms) paint coat.

The composite concrete was initially assumed at 22 % moisture content, and the oriented strand board was at 30 % moisture content. This represents wet initial moisture conditions in both wall systems. All other layers in the wall system were assumed to be in equilibrium at 80 % relative humidity.

Wind driven rain water was included in the analysis, the exterior surfaces were exposed to the amount of rain that typically hits a vertical wall. This amount depends on the intensity of precipitation, wind speed and wind direction as well as the location on the wall surface [Karagiozis and Hadjisophocleous, 1995].

The wall was exposed to outside air temperature, relative humidity, wind speed and orientation and rain precipitation that varied hourly according to the weather data from the selected location (Knoxville). The simulations were carried out for a three year exposure starting on the 1st of August. The solar radiation and long wave radiation from the outer surfaces of the wall were included in the analysis. In this study, no air infiltrating or exfiltrating was considered; therefore the primary mode of water transmission is due to diffusion processes, both vapor and liquid transport. For the simulations of the wall and roof assemblies the LATENITE 3.0 VTT [Salonvaara, 1999] version was employed for all simulations.

BOUNDARY CONDITIONS

Internal conditions were analytically resolved by the transport of moisture and heat through the wall systems and the mechanical heating and air conditioning controls. The interior inhabitants were also modeled as heat and moisture sources and sinks, by allowing daily variations of thermal and moisture production and dissipation. A typical 24 hour schedule is depicted in Figure 1 for a 2 adult and 2 children household [Salonvaara, 1998a]. The interior space was dehumidified, and 0.3 air change per hour was assumed for air quality purposes. The US National Climatic Weather Center [1995] data for Knoxville during the years 1961-1963 were used in the simulations. The 1961 yearly average temperature and vapor pressure in Knoxville is 14.8 °C, and 1296 Pa, respectively.

The heat and mass transfer coefficients for external and internal surfaces were variable depending on the temperature, the wind speed and orientation (only the for the exterior surfaces). The heat and mass transfer coefficients for the exterior were assigned values that varied from hour to hour depending on the exterior weather conditions.

SIMULATION RESULTS

Figure 2 shows spatial relative humidity distributions through the cross section of the composite concrete wall (a) and light weight wall (b) system during week 120 from the start

of the simulations. Results for the two interior vapor control strategies are displayed, one that employed a vapor open paint coating and the other with a vapor impermeable coating. In all wall orientations, when the impermeable vapor control strategy was employed, the walls displayed slower drying potential for the weather location of Knoxville. Differences of up to 60 % in relative humidity in walls are present between the cases with and without vapor permeable paint coatings, displaying the critical importance of the choice of interior vapor control. Results also show that limited drying occurs within the wall even after 120 weeks for the case that employed the impermeable interior vapor coating.

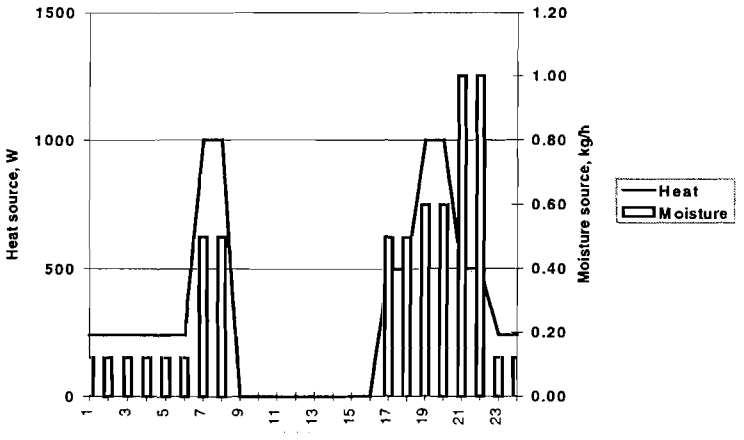

Figure 1. Heat and moisture sources in the building at various times of day. Daily heat and moisture sources total 7.9 kWh and 6.1 kg.

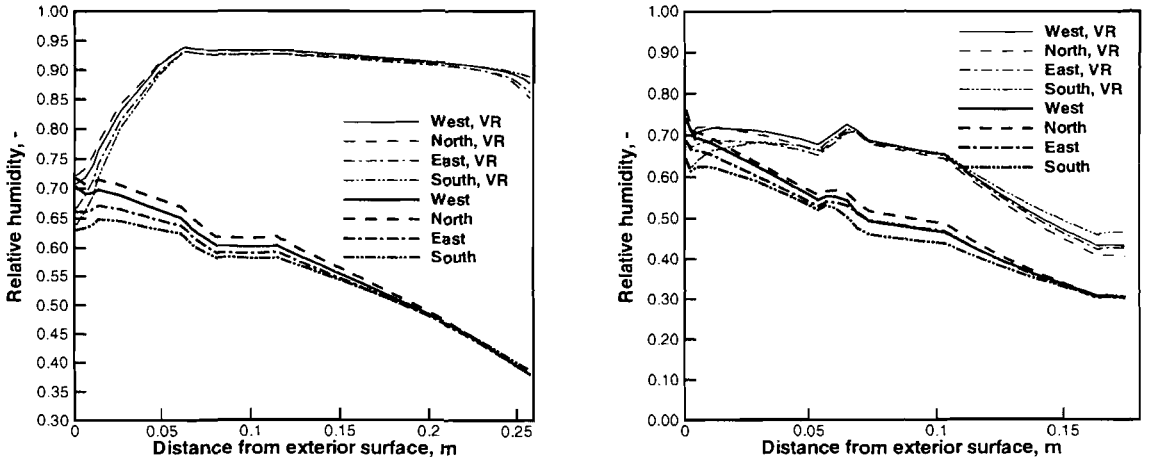

(a) (b)

Figure 2. Relative humidity distributions in walls after 120 weeks from the start of the simulations. (a) Concrete wall, (b) light weight wall.

An analysis of the weather data for a 30 year period (1961-1990) shows that a mild climatic region is present in Knoxville TN with only very short cold periods during winters and hot and quite humid summers. The 30 year mean temperature is 14.45 C and the mean relative humidity is 71.53 %, which represent conditions that may be classified as mild for possible moisture damage.

In Figure 3a, the mold index as formulated by Viitanen, is displayed for the exterior side of the oriented strand board, as a function of time in days. Figure 3b shows the relative humidity as a function of time. The results show that the initially wet conditions cause risk of mold on the OSB surface, as mold growth index of 4 represent the case of mold growth with the probability of 10 % of the OSB surface covered with mold. However, in the no-retarder case the mold growth index rapidly drops to very safe levels, showing that this particular light weight wall without a 6-mil polyethylene vapor retarder has rapid drying performance and the long run performance of the wall is satisfactory in term of durability exposure to mold. Vapor retarder on the inside slows drying and high relative humidities exist for an extended period and extremely high risk for mold growth (calculations show 50% of the surface covered by mold) as well as for rotting is present in the vapor retarder case for the light weight wall (Figure 3).

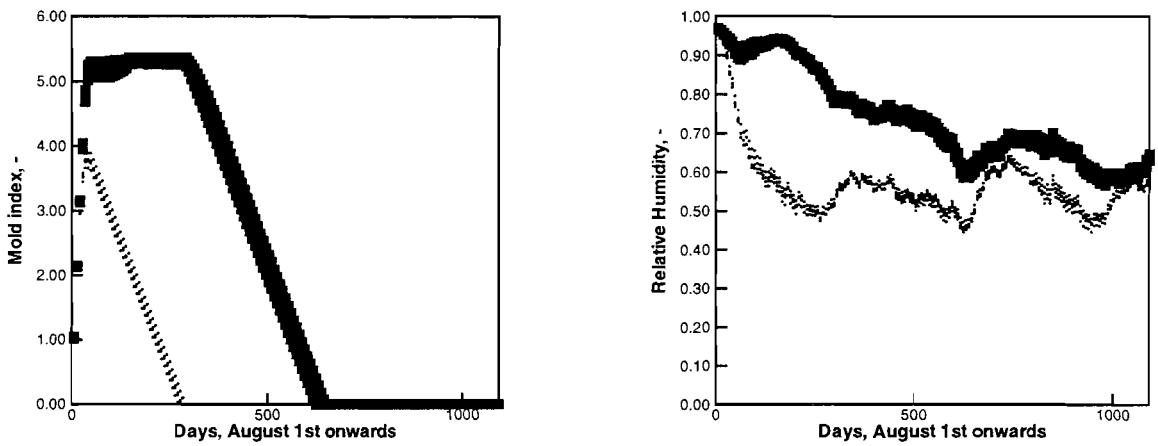

(a) (b)

Figure 3. (a) Mold Growth Index for EIFS wall (OSB). Larger symbols for the case with vapor retarder. (b) Relative humidity for the same wall and location.

Figure 4 shows the effective (whole house) U-value for the four wall and roof systems (averaged for all orientations). The results are plotted out on a monthly basis, and display all seasonal effects. High initial effective U-values are displayed for the No VR case, and

this is attributed solely to the faster drying out that occurs when the resistance for drying is

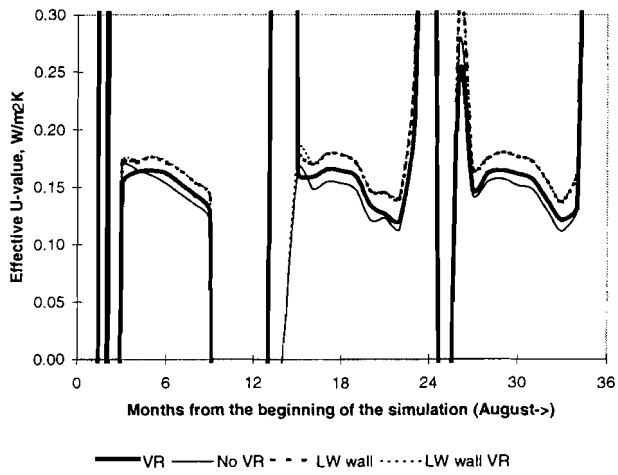

Figure 4. 'Whole house average' U-value for envelope systems (walls and roofs).

less. The building was equipped with a heating and cooling system that turned on heating if the temperature fell below 20°C and cooling if the temperature rose above 22°C.

Evaporation of initial moisture from the walls (no vapor retarder cases) resulted in increased indoor air relative humidity in comparison to buildings with vapor retarder. The maximum increase in the relative humidity was approximately 7%. Example of time-wise behavior of indoor air temperature and relative humidity is given in Figure 5.

Buildings with vapor retarder needed on average -2.8% less dehumidification during the first three years, but the three years separately gave -8.2%, +1.9%, +2.3%, first, second and third year, respectively, i.e. VR case needs 8.2% less dehumidification during the first year, but slightly more in the following years to come, because of no dampening effect of hygroscopic walls interacting with the indoor air.

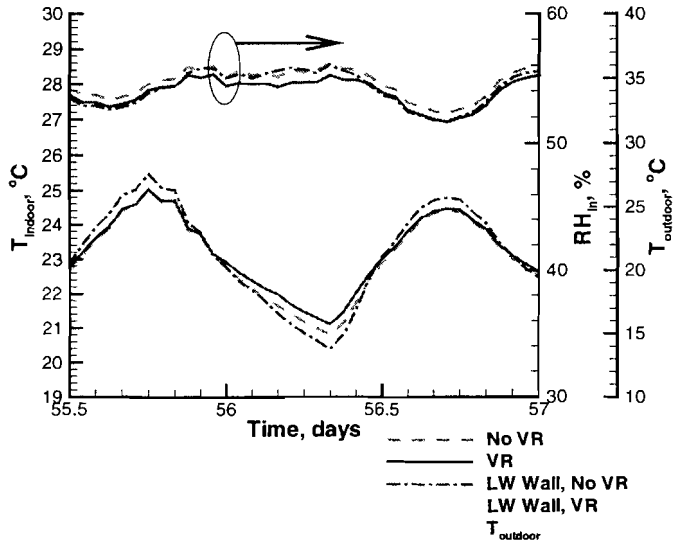

Figure 5. Indoor air temperature and relative humidity as a function of time for different wall systems.

The same comparison for the sum of heating and cooling during the three years is: +1.6%, +2.2%, +2.2% for heating and +5.4%, -1.4%, -1.1% for cooling (the energy of the concrete building with vapor retarder minus the energy for the concrete building without vapor retarder) first, second and third year, respectively. The heat loss through the walls and roofs are higher for the building with vapor retarder than without one: +0.7%, +5.6%, +4.6%, first, second and third year, respectively. This is simply due to higher thermal conductivity of polystyrene concrete in the case with vapor retarder (high moisture contents). The light weight wall building consumes 3% more heating energy and 7% more cooling energy than the concrete wall building per each year. The first year is slightly but not significantly different than the following years after the initial drying. The effective 'whole house' U-value of the light weight wall building is approximately 7% higher than that of the concrete building with vapor retarder and 15% higher than that of the concrete building without vapor retarder (dryer walls).

Figure 6 shows the dehumidification of indoor air, as a function of time in months (starting August 1). Results are shown for all four wall systems. With the exception of the initial effects of drying, the differences diminish.

CONCLUSIONS

Vapor diffusion control and insulation strategies have a significant effect on the hygrothermal performance (drying potential) of composite concrete polystyrene bead walls and light weight wood frame walls (EIFS) in a cold climate. This study, which included the effects of vapor and liquid transport found that the use of a tight interior vapor control may not be beneficial to drying the initial construction moisture in cold climates. The results showed rapid drying for the no-retarder case as the drying potential for climatic conditions of Knoxville are very favorable.

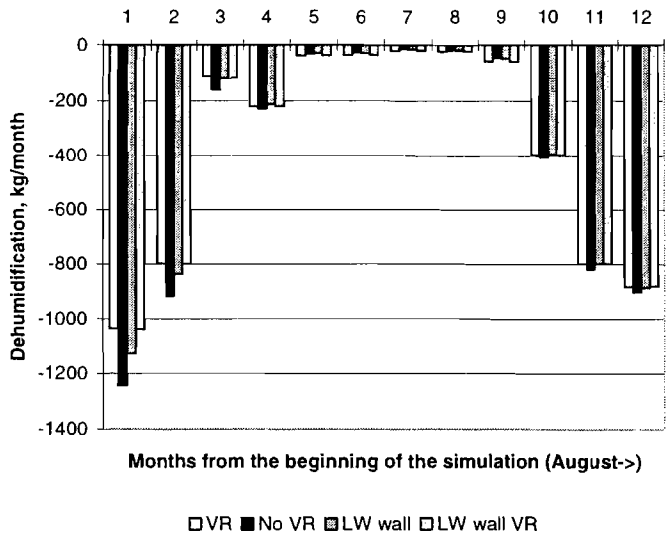

Figure 6. Building dehumidification as a function of wall system (first 12 months).

The proper combination of interior and exterior vapor control and insulation control must be employed, as demonstrated in this study. If buildings are equipped with an air conditioning equipment, moisture transport from the interior can be regulated. Additional research is needed to determine the critical range of interior climatic conditions that owners of the building must adhere to. Buildings must be designed to accommodate some form of synchronized moisture control that utilizes drying towards the interior as well as the exterior. Aerated concrete walls that incorporate such features can be developed with substantially higher moisture load tolerances for any climatic region, without necessarily requiring special special cavities or other expensive changes in design.

The results provided in this paper are only applicable to the specific materials, wall specifications and weather conditions employed. Further work is needed to characterize the effects of defects in the exterior surface or possible moisture infiltration or exfiltration from the interior or exterior environments.

ACKNOWLEDGEMENTS

The authors of this study would like to thank ORNL for the development of a moisture engineering research project, to address integrated construction technologies, in particular to Andre Desjarlais the Program Manager.

REFERENCES

ASTM Standard Designation C 755 - 73. 1976. Standard Recommended Practice for Selection of Vapor Barriers for Thermal Insulations, 1976 Annual Book of ASTM Standards, pp. 527-543.

Burch, D.M. and Thomas, W.C. 1991. An Analysis of Moisture Accumulation in a Wood Frame Wall Subject to Winter Climate, National Institute of Standards and Technology Report NISTIR 4674.

Buske, P., 1999. Levelton Engineering Limited, Personal communication.

Kunzel, H.M. 1996. Humidity controlled vapor retarders reduce risk of moisture damage, Proceedings of the 4th Symposium, Building Physics in the Nordic Countries, Espoo, Finland, Sept. 9-10, pp.447-454.

Karagiozis, A. and Hadjisophocleous G. 1995. Wind-Driven Rain on High-Rise Buildings, Thermal Performance of Exterior Envelopes of Buildings VI, Clearwater Beach, Florida, 4-8.

Karagiozis, A., Salonvaara, M. and Kumaran, K. 1994. "LATENITE Hygrothermal Material Property Database, IEA Annex 24 Report T1-CA-94/04, Trondheim, Norway

Karagiozis A., 1997a. Porous Media Transport in Building Systems, *CFD Society of Canada*, Victoria, May 25-27, 7-21 to 7-25

Karagiozis A., 1997b. Moisture Engineering, Proceedings of the Seventh Conference on Building Science and Technology, Durability of Buildings-Design, Maintenance, Codes and Practices, Mar. 20, Toronto.

Nission, E. 1995. Energy Design Update.

Salonvaara M. and Karagiozis A. 1994. Moisture Transport in Building Envelopes using an approximate Factorization Solution Method, CFD Society of Canada, Toronto, June 1-3.

National Climatic Data Center, 1999, CD data for US locations.

Salonvaara M. 1998a. Ph.D. Candidate

Salonvaara M. and Karagiozis A., 1998. "EIFS Hygrothermal Performance due to Initial Construction Moisture as a function of Air Leakage, Interior Cavity Insulation and Climate

Conditions", Thermal Performance of Exterior Envelopes of Buildings VII, Clearwater Beach, Florida.

APPLYING RISK ANALYSIS TO ROOF CONSTRUCTIONS: TWO EXAMPLES FROM PRACTICE

H. Hens, A. Janssens

Applying Risk Analysis to Roof Constructions: Two Examples from Practice

H. Hens[1], **A. Janssens**[2]
[1,2] Laboratory of Building Physics, Department of Civil Engineering, KU-Leuven, Celestijnenlaan, 131, B-3001, Leuven, Belgium

Abstract
The last two decades, building codes changed from prescriptive to performance based. Identical performance requirements, however, may generate solutions with differ substantially in buildability. To detect problems of poor buildability, risk analysis is of great help, risk being defined as the probability of occurrence of a defect multiplied with the size of the malfunctions it generates. The paper first describes risk analysis in more detail. Then the methodology is applied on two roofs, one above a swimming pool and one above a school building. Albeit a vapor retarder was included, reflecting the intention to achieve good moisture design, both roofs demonstrated a deficient condensation behavior. Main reason for that was poor buildability of the vapor retarder, resulting in air leakage and condensation. Thanks to a risk analysis, a case-specific upgrade could be proposed.

Key words: risk analysis, roofs, metallic construction, vapor and air flow retarder

1 Introduction
The performance approach reflects a key interest within building engineering, performances being defined as all properties and qualities of a construction, (1) which can be expressed in an exact way, (2) are predictable at the design stage and (3) controllable during and after construction (see e.g. [1]). Many countries adopted a performance based legislation in energy efficiency. Some rewrote their building code on the basis of performances. However, albeit both performance requirements and prediction help in generating correct decisions at the design stage, they do not guarantee a problem-free construction. Identical requirements may generate solutions which differ in buildability. To detect problems with that, risk analysis may be of great help

2 Risk analysis
In the context of building assessment we define risk as the probability (p) of occurrence of a defect multiplied with the size of the malfunction it causes (See e.g.[2])

$$\text{Risk} = p.\text{Size} \tag{1}$$

A risk is quoted as acceptable when the probability of occurrence of a defect is high but the malfunction it causes small or vice versa. Risk analysis includes two stages. (1) risk identification and (2) risk assessment. In the first stage all defects are identified. In stage two three questions ask for an answer: (1) what is the probability of occurrence of each

defect; (2) what is the magnitude of the malfunctions it causes; (3) is the risk acceptable? If the answer on question (3) is negative, safer solutions should be proposed on the basis of one or more of the following strategies: (in decreasing order of effectiveness) inherent, engineered or procedural. The inherent strategy uses redundancy and diversity to increase reliability. As a typical example of redundancy in roof construction figures the combination of a vapor permeable exterior finish with a vapor retarding interior lining.

3 Malfunctions of a roof construction

We consider as main malfunctions: (1) collapse, (2) rain leakage, (3) dripping moisture by interstitial condensation, (4) fungal defacement, (5) shortened service life, (6) higher energy expenses. Albeit exceptional, collapse represents the worst malfunction. Its size is very high. Rain leakage on the contrary is perceived as a nasty but less devastating consequence. It anyhow reminds the tenants that the roof does not behave properly. Dripping moisture by interstitial condensation gives more distress. Rain is understandable for the tenant, interstitial condensation not. Moisture coming from nowhere dripping down! The same holds for fungal defacement. A shorter service life is perceived as a malfunction only in extreme cases. The time window of the tenants in fact is narrow in comparison with even a shorter service life. Deficient thermal performance finally does not feel risky. Energy is too cheap for that, while nobody knows the reference, i.e. the energy consumption in case thermal malfunctioning was not a point. Table 1 gives the distress scores for the six modes of malfunctioning considered. Normally the score should range from 0 to 1, 1 for a problem distressing everybody, 0 when nobody takes it seriously. We nonetheless multiplied the score with a seriousness factor. Costs generated by the malfunction is one of the elements which help in defining that factor. Collapse got a seriousness factor 10, all other malfunctions 1.

Table 1 Classification of the problems in order of (guessed) distress magnitude

Order	Problem	Importance	Score
1.	Collapse	Highest	10.00
2.	Dripping moisture by interstitial condensation	Very high	1.00
3.	Fungal defacement	Very high	1.00
4.	Rain leakage	High	0.95
5.	Shorter service life	Low	0.10
6.	Higher energy expenses	Extremely low	0 to 0.01

4 Defects responsible for interstitial condensation and dripping

We restrict the discussion to interstitial condensation and dripping moisture. Design flaws and workmanship imperfections which could generate that malfunction are listed in table 2. Where in the past D1 was a common flaw, today D3 and W1 are the problem. To our experience, a vapor retarder is even prescribed in cases where it is not needed. However, neither time is spend in evaluating buildability nor does the contractor care

for leaks. At least nine light weight roofs on ten suffer from D3 and W1. D2 finally is a flaw without consequences as soon as the vapor retarder gets short-circuited by leaks.

Table 2 Design flaws

n^r	**Flaw (D) or imperfection (W)**
D1.	Vapor and air flow retarding layer not included in the roof section
D2.	Vapor resistance of the retarder too low for the conditions in the building
D3.	Poor detailing of the vapor and air flow retarder
W1.	Lazy mounting of the retarder without attention for joints and overlaps

5 Probability

Even when the flaws and the one imperfection of table 2 are committed in any case, still the probability interstitial condensation will develop is not 1. It depends on the indoor climate, the inside-outside air pressure difference and the vapor resistance of the layers above the thermal insulation. Climate measurements in a vast number of schools, dwellings and offices and a campaign in swimming pools delivered the vapor pressure statistics for that type of buildings, see table 3.

Table 3 Indoor climate in dwellings, schools, offices and swimming pools (add the amplitude for january, subtract for july)

Percentile	**Δp_{ie} in dwellings, schools and offices (Pa)**			**Δp_{ie} in Swimming pools (Pa)**		
	Annual Mean	**Stand. Deviat.**	**Annual Ampl.**	**Annual Mean**	**Stand. Deviat.**	**Annual Ampl.**
0.5%/*5%*	65	78	65	*370*	377	177
50%	270		210	1000		177
95%	400		210	1630		177

6 Two examples from practice

6.1 Roof above a school building

The roof under consideration covered the atrium of a kindergarten. Its surface totaled 293.5 m² (27.43x10.7 m). The load bearing system consisted of a bowed central steel girder HEB 240, spanning 27.4 m, with perpendicular girders IPE 160 1.4 m apart. Original section: (1) Ceiling in perforated aluminum sheets, (2) 4 cm mineral fiber, (3) PE vapor and airflow barrier, 0.2 mm, installed between the girders, (4) glass wool, 240 mm, installed between the girders, (5) aluminum roof cover (See e.g. [2],[3]). Shortly after the building was occupied, the director complained about dripping moisture. A first investigation learned that the contractor forgot the PE-foil. Before decommissioning however he corrected that flaw by adhering a new retarder below the finished ceil-

ing and adding a duplicate of mineral fiber and the ceiling. The discussion therefore turned to the question what solution should have been most reliable in minimizing condensation risk: the original design or the solution the contractor implemented. We looked for an answer by judging four situations: no vapor retarder, perfectly installed vapor retarder, original design, corrected construction. The air permeance's K_a and the vapor resistance's Z of the different layers are summarized in table 4. A tracer gas test proved that on the average air exfiltrated through the roof, while laboratory testing learned that dripping only became active at a condensation quantity above 300 g/m².

Tabel 4 Air permeance and vapor resistance of the layers (values taken from literature)

Layer	Thickness m	Density kg/m³	Z x 10^8 m/s	Air permeance K_a (=aΔP_a^{b-1}) A Kg/(m².s.Pa^b)	b-1 -
Ceiling			0.35	0.19	-0.5
Mineral fiber	0.04	145	2.60	2.86 10^{-4}	0
Glass wool	0.24	16	15.7	5.05 10^{-4}	0
Roofing			1730	6.73 10^{-5}	0.1

6.1.1 Results (cold week with θ_e=-5°C and ϕ_e close to 95%)

No vapor retarder The roof accumulated 0.18+0.1ΔP_a kg of condensate per m² at the 50% indoor vapor pressure percentile (ΔP_a: difference in inside-outside air pressure in Pa). The 0.5% percentile gave 0.015 ΔP_a. This result shows that the last case, dripping will only start if the weekly mean inside-outside air pressure difference passes 20 Pa (exfiltration rate of 3.0 m³/(m².h)), a situation unlikely to happen. At the 50% percentile, 1.2 Pa and an exfiltration rate of 0.2 m³/(m².h) suffice, a situation with probability 1. Or, at the 0.5% percentile, the risk is zero, while at the 50% percentile, it touches 0.5. In global, we may conclude that the overall risk on dripping moisture is situated between 0.5 and 0.995%. A full analysis gave a risk of 85%, i.e. quite high.

Perfect vapor retarder Accumulation dropped to 0.0013 kg/m² at the 0.5%, 0.0065 kg/m² at the 50% and 0.001 kg/m² at the 95% indoor vapor pressure. Dripping in that case is excluded, i.e. a risk zero

Original design Did not guarantee airtightness. In fact, the PE-foil was designed to be mounted between the girders which means that per girder two open joint were left, i.e. flaw D3. In that case, 0.1ΔP_a kg of condensate got accumulated per m² at the 50% vapor pressure percentile and 0.015 ΔP_a at the 0.5% percentile, i.e. hardly any difference with the situation without vapor retarder, i.e. a risk of 85%!

Corrected construction Here a field control eliminated two unknown: the indoor climate and the air permeance. The measurements gave: Δp_{ie}=146 Pa in winter for a temperature of 19.4°C (close to a 6% percentile), G_a= 9.7 $10^{-4}\Delta P_a^{0.525}$

$m^3/(m^2.s)$. Apparently, the corrected roof was even more permeable than table 4 may suggest for the roof as designed. Hundreds of screws perforated the retarder. The edges were not sealed and the aluminum cover was more air permeable than assumed in table 4. A detailed tracer gas analysis though learned that exfiltration and wind washing were both active, in a ratio 1 to 0.48 near the edges and 1 to 1.24 in the center. A condensation analysis gave an annual maximum of 0.23 kg/m^2 moisture without wind washing. With, the total went down to 0.1 kg/m^2. Both numbers suggest a dripping risk close to zero.

6.1.2 Solution

Although the roof was an exemplary case of flaw D3 and imperfection W4, the zero risk made a repair superfluous. One question however remained: why moisture dripped down shortly after completion? The answer is simple. The first months built in moisture shifted the indoor climate from a 6% percentile to a value closer to a 50% percentile.

6.2 Roof above a swimming pool

A large tropical swimming pool was covered with a pyramidal roof of 4064 m^2. The roof section consisted of: (1) timber lath ceiling, (2) vapor and airflow retarder with a vapor resistance of $5.4\ 10^{11}$ m/s, (3) 16 cm mineral fiber between the joists, (4) overlapping perforated underlay foil, (5) laths, (6) steel tiles. (See e.g. [3]). Already the first winter the users complained about dripping. A neutral investigation revealed interstitial condensation to accumulate below the underlay and the tiles. At first sight, the designer could not be blamed. He specified the vapor retarder correctly, while the drawings included several details how to fix and tighten it. However, one important aspect of buildability was overlooked. The thin retarder had to be mounted on the timber laths before the joist were fixed. So, craftsman moved on it and screws perforated the retarder at 1777 locations. The result was a roof without air tightness, as proved by a laboratory test on the section, including three joists. We measured an air permeance close to 10^{-4} $kg/(m^2.s.Pa)$. A control of the indoor climate gave θ_i=30°C, Δp_{ie}=1400 Pa, a 86% percentile for swimming pools, which means that 14 on 100 pools have a more severe climate. The consequences for condensation were a disaster.

6.2.1 Results (reference year for cold week with θ_e=-5°C and ϕ_e close to 95%)

Perfect vapor retarder, as intended by the designer

In that case, no problem. Some condensation takes place below the underlay with 5 g/m^2 as a maximum at the end of the winter. More moisture condenses below the steel tiles. Accumulation on annual basis however does not happen and the maximum even does not attain 50 g/m^2. Dripping consequently is not possible.

Leaky vapor retarder

The dramatic change in condensation response is documented in figure 1. An amazing amount of water condenses below the underlay. Self drainage balances part of it, leading to a permanent run off of water on

the underlay. The condensation underneath the steel tiles only increases that run off. What is left below the underlay finds its way to the vapor retarder where it drips inside through the leaks. The risk this will happen in the case being was one.

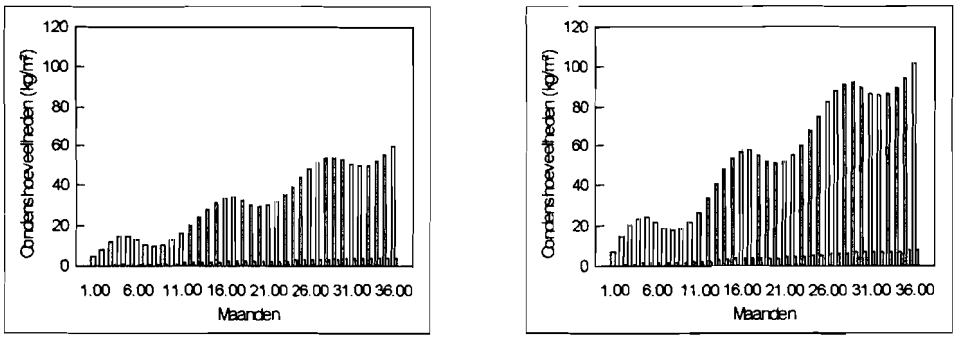

Fig. 1 Vapor retarder leaky. Accumulation of condensate 2.25 m above the neutral plane and 5.85 m above it. The highest values concern the underlay, the lowest the tiles.

6.2.2 Solution

Contrary to the school building were no risk was noted, a risk one obliged to retrofit the existing roof with inclusion of a thick bituminous vapor and air flow retarder with self healing properties, a vapor permeable underlay and a system of counter-laths and laths.

7 Conclusion

Risk analysis may be a useful tool in judging buildability of a roof during service life. The two examples prove that decisions in relation to repair in case of malfunction may be quite different when risk is taken into account. The roof above the school building was not upgraded, while the roof above the tropical swimming pool got a complete retrofit. In the first case, dripping moisture was a transient with a risk close to zero once the building was dry. In the second case a permanent risk with a value close to 1 existed.

References

[1] Hens H., The performance concept, a way to innovation in construction, Proceedings of the CIB-ASTM-ISO-RILEM Conference on the Applications of the Performance Concept in Buildings, Vol 2, p 5.1-5.-12. Tel Aviv, 1997

[2] Janssens A., Reliable Control of Interstitial Condensation in Lightweight Roof Systems, Doctoral Thesis, K.U.Leuven, 1998, 217 p.

[3] Laboratory of Building Physics, Tropisch zwembad Herford, dakproblemen (Tropical swimming pool Herford, roof problems), report 98/6, 21 p.

[4] Laboratory of Building Physics, Vochtproblemen in het aluminium dak van de vrije basisschool te Essene, deel 1 (Moisture problems in the aluminum roof of the primary school at Essene, part 1), report 98/2 (1), 8 p.

[5] Laboratory of Building Physics, Vochtproblemen in het aluminium dak van de vrije basisschool te Essene, deel 2 (Moisture problems in the aluminum roof of the primary school at Essene, part 2), report 98/2 (2), 11 p.

THE HYGROTHERMAL PERFORMANCE OF THE FLAT VENTILATED ROOF OF THE NON-HEATED BUILDING. CASE STUDY

O. Koronthályova, P. Matiasovesky

THE HYGROTHERMAL PERFORMANCE OF THE FLAT VENTILATED ROOF OF THE NON-HEATED BUILDING. CASE STUDY.

O. Koronthályová , P. Matiašovský

Institute of Construction and Architecture, Slovak Academy of Sciences, Dúbravská c. 9
842 20 Bratislava, Slovakia
E-mail: usarkoro@savba.sk, usarmat@savba.sk

Abstract

The factors causing the conditions of a condensation in ventilated flat roof of nonheated object have been analysed. The reults of numerical simulation have been compared with behaviour of real object.. The condensation occurs at sunny days. Ventilation regime in the roof cavity influences the type of this condensation.

Key words: Flat cold roof, air cavity, ventilation rate, condensation, thermal inertia

1 Introduction

At the design of flat cold roof the question of the optimum cavity ventilation is still of interest. The requirements of adequate ventilation with air barrier and/or water vapour barrier are commonly accepted in the case of the heated indoor space. In the case of the absence of heating it is considered that no condensation problems can occur because of no indoor moisture source. In spite of this experience there are some situations that occasional condensation takes place.

The aim of the study is to analyse the factors causing the conditions of such a condensation.

2 Description of the object

Flat cold roof of large garage object in Bratislava has been monitored in autumn 1996. The reason of the monitoring was regular occurrence of water dripping at the ceiling of the roof precast concrete slabs during sunny days spells.

The analysed roof has a shell precast concrete deck covered by bitumen felt (Tab. 1). The roof is ventilated by vents with total area 0.125 m^2. The roof area is 490 m^2. The volume of the roof cavity is 88 m^3. The indoor space volume is 1220 m^3. Mean ventilation rate of the garage is 5 h^{-1}. The garage is not heated. Thermal resistance of

external walls is 1.4 m^2.K/W. The loadbearing structures of the object are of reinforced concrete (200 kg/m^3 of enveloped space), with relatively high thermal inertia.

Tab.1. Composition and material properties of the evaluated roof

Layer	Thickness [m]	Mean density [kg/m^3]	Thermal conductivity [W/m.K]	Vapour resistance factor [-]
Bitumen felt	0.015	900	0.2	9400
Precast concrete deck	0.5	2 200	1.57	25
Ventilated air space	0.18	1.3	1.2	1
Mineral wool insulation	0.05	40	0.04	2
Hollow precast concrete slab	0.25	940	1.5	7

During the search indor and outdoor air temperatures and relative humidities as well as the temperature and relative humidity in the roof cavity have been measured. In the analysed object no damage of the roof membrane have been detected. Small exfiltration of air from the indoor to the roof cavity have been found. There are no internal water vapour sources in the object. Nevertheless increased water vapour pressure in the roof cavity by ca 400 Pa have been detected in the roof cavity. With the aim of further analysis the simulation of hygrothermal performence of the whole object have been carried out.

3 Numerical simulation of hygrothermal behaviour of the object

For the purpose of the simulation of heat and moisture transfer between the structures of the object - indoor space - roof cavity - outdoor environment 1D analog model have been created.

The 1D simulation of the heat and moisture transfer was based on the solution of two coupled equations for heat and moisture balance:

$$\frac{\partial\left(\rho_w \cdot \psi + \left(\psi_0 - \psi\right)\cdot \rho_v\right)}{\partial \tau} = \frac{\partial}{\partial x}\left(\rho_w \cdot D_w \cdot \frac{\partial \psi}{\partial \varphi}\cdot\frac{\partial \varphi}{\partial x}\right) + \\ + \frac{\partial}{\partial x}\cdot\left(\delta_p \cdot \left(p_{sat}\cdot\frac{\partial \varphi}{\partial x} + \varphi \cdot \frac{\partial p_{sat}}{\partial t}\cdot\frac{\partial t}{\partial x}\right)\right) + A_m \quad (1)$$

$$\frac{\partial}{\partial \tau}\cdot\left(\rho\cdot c\cdot t + \rho_w \cdot c_w \cdot \psi \cdot t + \left(\psi_0 - \psi\right)\cdot\rho_v \cdot c_v \cdot t\right) = \\ \frac{\partial}{\partial x}\left(\lambda\frac{\partial t}{\partial x}\right) + h_e \cdot \frac{\partial}{\partial x}\cdot\left(\delta_p \cdot \left(p_{sat}\cdot\frac{\partial \varphi}{\partial x} + \varphi\cdot\frac{\partial p_{sat}}{\partial t}\cdot\frac{\partial t}{\partial x}\right)\right) + A \quad (2)$$

where ρ_w is density of water [$kg.m^{-3}$], ψ is moisture content (volume by volume) [-], ψ_0 is open porosity [-], ρ_v is water vapour concentration [$kg.m^{-3}$], x is coordinate [m], D_w is moisture diffusivity [$m^2.s^{-1}$], φ is relative humidity [-], δ_p is vapour permeability [s], p_{sat} is saturation water vapour pressure [Pa], A_m is moisture gain (loss) caused by ventilation [$kg.m^{-3}.s^{-1}$], t is temperature [°C], ρ is density [$kg.m^{-3}$], λ is thermal conductivity [$W.m^{-1}.K^{-1}$], c is specific heat capacity [$J.kg^{-1}.K^{-1}$], h_e is specific enthalpy of evaporation [$J.kg^{-1}$], A is heat gain (loss) caused by ventilation [$W.m^{-3}$].

The moisture gain (loss) caused by ventilation was expressed by relation:

$$A_m = (\rho_{va} - \rho_{vx}).\ n / 3600 \qquad (3)$$

where ρ_{va} is water vapour concentration in ambient air [$kg.m^{-3}$], ρ_{vx} is water vapour concentration in ventilated air layer of construction [$kg.m^{-3}$], n is ventilation rate [h^{-1}].

The heat gain (loss) caused by ventilation was expressed as:

$$A = (t_a - t_x).\ \rho_a.c_a\ .\ n / 3600 \qquad (4)$$

where t_a is ambient air temperature [°C], t_x is temperature in ventilated air layer [°C], ρ_a is density of air [$kg.m^{-3}$], c_a is specific heat capacity of air [$J.kg^{-1}.K^{-1}$].

The boundary conditions were as follows:

$$q = \alpha.(t_a - t_s) + I\ .\ a - L\ .\ e\ .\ (1 - CC) \qquad (5)$$

$$\dot{m} = \beta \cdot (\rho_{va} - \rho_{vs}) \qquad (6)$$

where α is surface film coefficient for heat transfer [$W.m^{-2}.K^{-1}$], t_s is surface temperature [°C], I is global radiation [$W.m^{-2}$], a is absortivity of solar radiation [-], L is sky irradiation [$W.m^{-2}$], e is emissivity [-], CC is cloudiness [1/10], $\dot{m}$ is density of moisture flow [$kg.m^{-2}.s^{-1}$], ρ_{vs} is water vapour concentration on surface [$kg.m^{-3}$]. The calculated mean ventilation rate was 1.5 h^{-1} in roof cavity and 5 h^{-1} in indoor space. The air flow by convection is not taken into account in this model.

The system of coupled non-linear differential equations (1) and (2) is solved using the finite difference - Crank Nicholson scheme. The obtained system of nonlinear algebraic equations is solved using the Newton iterative method [1].

The simulation have been done for hourly climatic data set of year 1985 which have been chosen as 95% reliability critical year from the aspect of intersticial condensation.

4 Interpretation and discussion of the results

Numerical simulation of coupled heat and moisture transfer has not shown any explicite condensation in the roof. This result was caused by the fact that the simulation programme does not considere an air movement in the roof cavity. In real the conditions for natural convection presence are fulfilled during more than half year besides this fact also the cross ventilation flow through the air cavity enables warmer air penetration into colder higher mineral wool layers. If these phenomena are considered the condensation in the roof will occur at following situations:

- In the case when saturation pressure of water vapour at the bottom deck surface is lower than water vapour pressure in the cavity the condensation at the surface takes place.
- In the case when saturation pressure of water vapour in mineral wool is lower than water vapour pressure in the cavity the condensation in the mineral wool insulation takes place. The condensed water is drainaged at the top of the concrete slab and can penetrate to the ceiling which causes the observed water dripping.

According to calculation the conditions for condensation at bottom surface of the deck had fulfilled at 11 days of the considered year at nights of the sequence of cloudless days with sudden decrease of outdoor temperature.

The conditions for condensation in the thermal insulation layer had fulfilled at 48 days of the year at daytime during bright days with great sums of global solar radiation.

Both detected situations are in agreement with monitored occurrence of condensation in the evaluated object. In Fig. 1. both typical situations characterised by temperature and water vapour pressure courses are shown. The first situation occurs between 20:00 of the first day and 6:00 of the second day. The second situation occurs between 10:00 and 16:00 of the second day.

5 Conclusions

The risk of the water vapour condensation in the cold roof above non heated indoor space in the cases when contribution of the indoor moisture source is excluded occurs as the result of following factors interaction:
- the roof has great thermal inertia,
- the ventilation rate of the roof cavity is small,
- the condensation occurs at sunny days spells with great daily amplitudes of outdoor air temperature course,
- moisture content in the roof structures results from previous construction process or from higher outdoor air relative humidities in previous period.

For the evaluation of condensation in air cavity of the cold deck roof with slab with high thermal inertia the reference years focused to interstitial condensation risk assessment are not suitable. The evaluation of this problem needs calculation not for extremaly cold and moist year but for the year with extermaly high total solar radiation intensity.

Acknowledgment

The authors are grateful to VEGA (Grant No. 2/5105/99) for the supporting of this work.

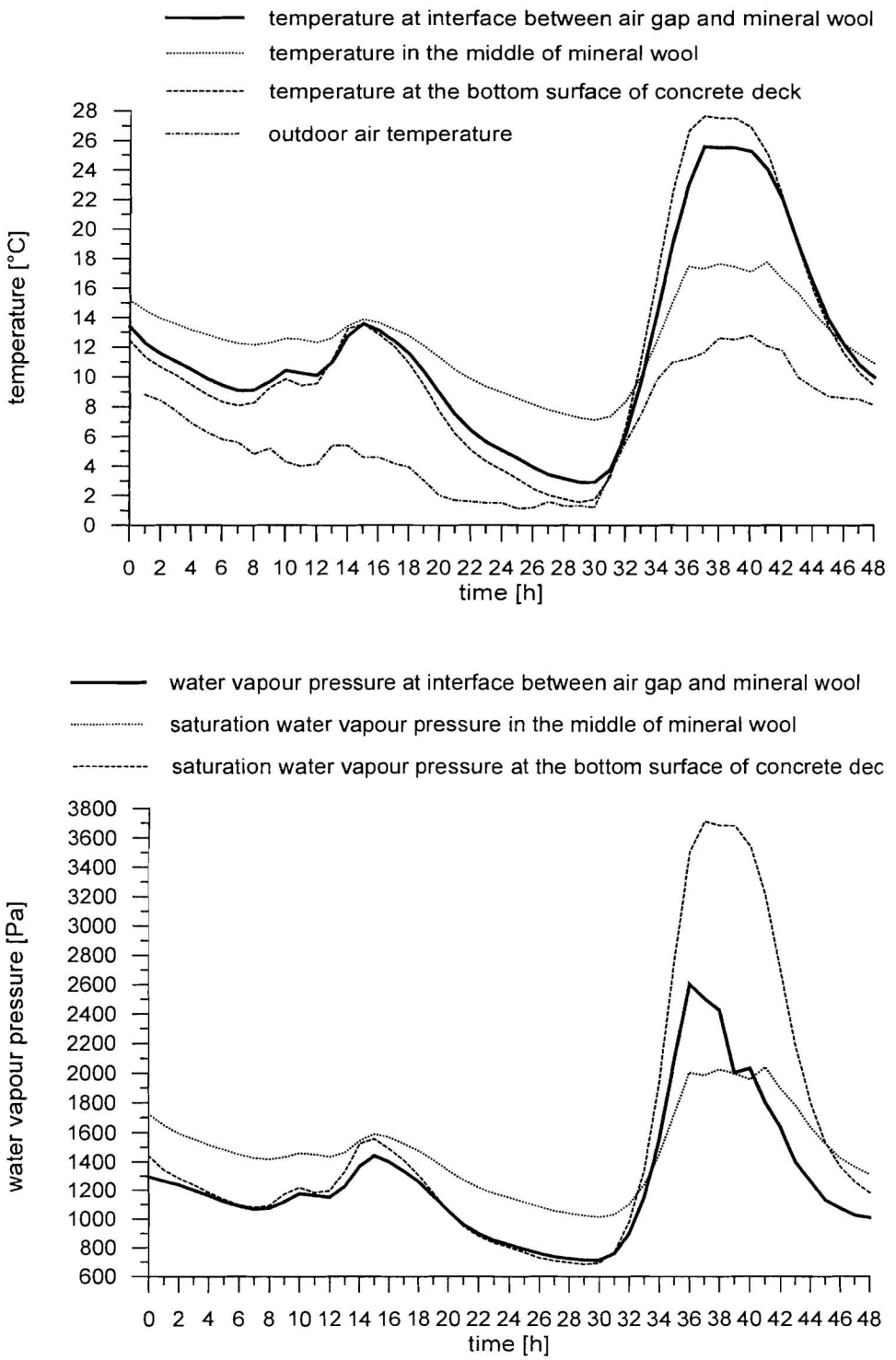

Fig. 1. Typical temperature and water vapour pressure courses characteristic for condensation occurence

References

1. Hens, H.: IEA ANNEX 24 Final Report. Vol. 1. Task 1: Modelling. Acco Leuven 1996.
2. Rode, C.: National construction. Denmark: Flat roofs. IEA ANNEX 24 Internal Report T4-DK-95/01/.

THE HYGROTHERMAL ENVIRONMENT IN CRAWL SPACE OF RESIDENTIAL HOUSES IN JAPAN

A. Iwamae, M. Matsumoto, T. Matsushita, O. Matsumura

THE HYGRO-THERMAL ENVIRONMENT IN CRAWL SPACE OF RESIDENTIAL HOUSES IN JAPAN

A. Iwamae[1], M. Matsumoto[2], T. Matsushita[3] and O. Matsumura[4]

[1]Sekisui house Ltd., 6-6-1 Kabutodai Kizu Kyoto 619-0224, JAPAN, gantaro@mb.infoweb.ne.jp
[2]Osaka-sangyo University, 3-3-1 Nakagaito Daito Osaka 574-0013 JAPAN, m-matsu@edd.osaka-sandai.ac.jp
[3]Kobe University, Rokko-dai, Nada, Kobe 657-0013, JAPAN, matusita@kobe-u.ac.jp
[4]Government of Housing Loan Corp., 4-5-20 Minami-Hommachi Tyuou Osaka 541-8546, JAPAN

Abstract

We found many houses have condensation in the crawl space in summer. These houses have enough openings on the foundation to ventilate and vapor retarder at the ground surface for the recommend in the building code. The temperature and humidity in the crawl space have great influences to durability of the house. We made clear the annual variations of hygro-thermal environment of the crawl space by the field measurements and numerical analysis. We monitored the temperature and humidity variations of about 40 houses in Japan for 2 years. The numerical calculations based on the vertical 1 dimensional heat transfer model represented the monitored results. The results show the houses in Japan normally have extremely high humidity in the crawl space in summer. The daily average of crawl space's vapor pressure is nearly equal to that of the outdoors. The thermal resistance of the floor and moisture of the ground do not have great effect on the crawl space humidity.

Keywords: Field measurement, Condensation, Ground heat, Ventilation, Outdoor condition

1 Introduction

We have reported that some Japanese houses have water pool in it's crawl space in summer. (Iwamae & Matsumoto 1997) In our study, the reason of the pool is condensation which is due to the high humidity of the outdoor air and the low temperature of the ground under the floor. From the point of view of building's durability, the condensation is considered as severe warning. It deduces the durability greatly. But if it is not so high that the condensation occurs, the high humidity without condensation also affect the durability. It helps the growth of the rot of wood and the

rust of iron. To estimate and lengthen the durability of house, we must know the real states of the hygro-thermal environment of the crawl space.

In order to more clarify the humidity variation in the crawl space, we monitored temperature and humidity variations of about 40 houses in Japan from summer of 1997 through fall of 1998. We think this number of the monitored houses is large enough to represent the average and general state. The monitored results tell us the real state, however, they do not tell the reason. The hygro-thermal environment looks to depend on the thermal profile of the ground, the insulation level of the house, the outdoor conditions and the degree of the air change rate between the crawl space and the outdoors, etc. To define the degree of the effect of these factors, we make the numerical model which is based on the vertical one dimensional heat transfer process. By this numerical model, we calculated the each effect of these factors.

2 Field research

Figure 1 shows the number and location of the monitored houses in the map of the entire country. From the northern area to southern area, the research area covers all over the country. Table 1 is the list of monitored houses. It tells the built year, floor area and state of soil cover under the floor etc. we monitored two points for each house. One is the crawl space and the other is the outdoors. The measurement interval is one hour.

Figure 2 shows the distribution of the monthly average of the monitored temperature and humidity of outdoors. The figure also shows the standard value which has been measured by official weather station. These are the average values of past 30 years. Our results show good agreement with the standard values. This fact says that our research is not affected by the abnormal weather.

Figure 3 shows the annual variations of the monthly average of the crawl space humidity. As we described in the former report, many researchers in Japan had focused on the winter environment in the crawl space. According to our literature survey, this figure is the first result of annual variation of the crawl space. It is obvious that the relative humidity of the crawl space is high in summer. Many houses have more than 80% humidity. This figure also shows the dryness in winter.

Figure 4 shows the relation between the monthly average and the degree of high humidity. The vertical axis is the rate that the measured value exceeds 80% RH (white circle) or 90% RH (gray square). Figures 3 and 4 show that the humidity of the crawl in many houses is extremely high in summer, which is enough high to deduce the durability of the house if the members have not been antisepticized.

Figure 5 shows the relation between the monthly average specific humidity of the outdoors and the crawl space. We use two types of symbols to distinguish the results of covered cases and that of uncovered cases of soil under the floor. The crawl spaces of uncovered soil are higher than the outdoors. In contrast with this, the spaces of covered soil are nearly equal to the outdoors. This fact has great influence on the hygro-thermal estimation of the crawl space, it simplifies the treatment of transfer process of humidity. We can merely set the crawl space humidity as equal to the specific humidity of the outdoors.

Figure 6 shows the relation between the degree of the thermal resistance of the floor and the average humidity in summer. Some people say that the advance of insulation

level of the house makes big the degree of condensation of the crawl space. This is right theoretically, but this figure shows the thermal resistance of the house has little effect on the crawl space humidity.

All the residents of the monitored house do not think that the crawl space under them is very humid in summer, since the daily life have not been in contact with the crawl space.

3 Numerical analysis

Figure 7 shows the basic concept of the numerical model which is based on the vertical one dimensional heat transfer process. According to the measurement results, the specific humidity in the crawl space is equal to the outdoors. In comparison with 1D and 3D model, we confirm that the horizontal heat transfer in the ground has not so large to effects the crawl space temperature.

We do not consider the effect of the solar heat, sky radiation and the evaporation heat the earth surface, since the solar heat is nealy equal to the sum of latter two factors.(Iwamae and Matsumoto 1986)

The governing equations for the upper room, the crawl space and the ground are as follows respectively.

$$C\gamma_a \frac{dT_{room}}{dt} = \frac{\tilde{Q}_{room} + Q_U A_{floor}}{V_{room}} \quad [1]$$

$$C\gamma_a \frac{dT_{crawl}}{dt} = \frac{Q_D - Q_U}{H_{crawl}} + C\gamma_a Cc_{crawl}(T_{out} - T_{crawl}) \quad [2]$$

$$C\gamma_s \frac{\partial T_s}{\partial t} = \lambda_s \nabla^2 T_s \quad [3]$$

Here,

$$\tilde{Q}_{room} = (K_{roof} A_{roof} + K_{wall} A_{wall} + C\gamma_a Cc_{room} V_{room})(T_{out} - T_{room}) \quad [4]$$

$$Q_U = K_{floor}(T_{room} - T_{crawl}) \quad [5]$$

$$Q_D = \alpha_c(T_{crawl} - T_{surf}) \quad [6]$$

We use the measured data at Osaka 1997 for the annual weather variations. The heat conductivity of the ground soil is 1.16 J/msK which means that the soil has much water in it. The standard value of the air change rate of crawl space to the outdoors is 7 times/hour. The insulation thickness of the floor is 0.05m.

Figure 8(a) and (b) show the variations of the temperature and humidity of the crawl space in one week of summer. The calculated results show good agreement with the measured data.

Figure 9 shows the results of various air change rates. The values are monthly average. The air change rate of 3 times to the standard makes the temperature 4 degree higher, and makes 15% lower the relative humidity. But the frequency of the high humidity in summer is not small. It is difficult that we determine the select of forced ventilation to solve this humid problem.

Figure 10 shows the results of various heat conductivity of the soil. The bigger value means that the ground has more water in it, the smaller value means the ground is dry. In Japan, some people often say the reason of humid crawl space is due to the humid

soil. But this figure shows they are not correct. The water content of the soil has not great effects on the crawl space humidity.

Figure 11 shows the results of various thermal resistance of the floor. The horizontal axis shows the thickness of the insulation. As mentioned former section, the thermal resistance also has little effect on the space humidity. These small differences do not reflect the measurement data.

4 Conclusion

According to our research and calculation, it is normal that the humidity of the crawl space in summer is extremely high. The most valuable information is that the humidity is equal to out-door specific humidity.

As described in former report, Japanese are fond of the air ventilation between the room and the outdoors. Our estimation shows this is not always correct. Our another study shows better result for the basement insulation house. We must estimate the effects of various factors quantitatively, especially for the traditional technique.

Symbols

	Temperature [K]	$C\gamma$	Heat capacity [J/m^{3}K]
λ	Thermal conductivity [J/msK]	Q	Heat flux [J/m^{2}s]
C_c	Air ventilation times[times/s]	α_c	heat transfer coefficient [J/m^{2}sK]
K	Thermal conductance [J/m^{2}sK]	V	Volume of space [m^3]
A	Area [m^2]	H	Height [m]

Script *s* soil *a* air *room* the upper room *crawl* the crawl space *out* outdoors, *surf Soil surface*

References

[1] Iwamae A and M. Matsumoto et al. 1997, Condensation in crawl space of dwelling house in Japan, proceedings of CIB-W40 in Kyoto, pp.301-312

[2] Matsumoto M. and A. Iwamae 1988, An analysis of temperature and moisture variations in the ground under natural climatic conditions, Energy and Buildings, Vol. 11, pp.221-237

Table 1 the list of monitored houses

Code	Built year	Floor area	Type of soil cover	Insulation type	Interval of ventilation hole
Sendai-A	83	53.0	Uncovered	FP A4 16	4.3
Sendai-B	78	41.2	Uncovered	FP A4 16	5.0
Sendai-C	91	32.0	Uncovered	GW 50	5.0
Sendai-D	93	68.2	VR + sand	FP B3 57	5.0
Sendai-E	95	64.5	VR	FP B3 57	4.7
Sendai-F	-	59.2	Uncovered	None	5.0
Ibaragi-A	91	65.8	VR	FP A4 30	5.0
Ibaragi-B	82	96.0	VR + sand	GW 50	-
Ibaragi-C	95	73.6	Concrete	FP A4 102	4.6
Ibaragi-D	92	67.5	VR	FP A4 30	4.1

Ibaragi-E	94	60.8	VR	FP A4 30	5.1
Ibaragi-F	90	45.5	Uncovered	GW 50	4.2
Ibaragi-G	95	70.0	Concrete	None	5.0
Kanazawa-A	95	270.7	VR + sand	FP A4 30	7.1
Kanazawa-B	93	64.5	VR + sand	FP A4 30	5.7
Kanazawa-C	93	73.9	VR + sand	FP A4 30	5.3
Kanazawa-D	97	148.7	Concrete	FP B3 57	4.2
Osaka-A	95	69.0	VR	FP A4 53	4.6
Osaka-B	92	97.3	VR + sand	FP A4 45	5.9
Osaka-C	96	87.0	Concrete	FP B3 57	10.3
Osaka-D	94	63.0	VR	FP A4 16	4.3
Osaka-E	95	72.1	VR	FP B3 57	6.0
Osaka-F	86	75.5	Asphalt	FP A4 30	3.4
Osaka-G	89	54.2	Uncovered	GW 50	5.5
Osaka-H	81	58.3	Uncovered	FP A4 20	3.6
Osaka-I	72	123.5	Uncovered	None	3.8
Hiroshima-A	85	67.5	VR + sand	FP A4 16	4.9
Hiroshima-B	85	79.5	Uncovered	FP A4 16	4.2
Hiroshima-C	85	57.9	VR	FP A4 16	4.4
Hiroshima-D	88	76.3	VR + sand	FP A4 16	4.4
Hiroshima-E	74	50.0	Uncovered	None	5.0
Fukuoka-A	92	82.5	Concrete	FP A4 16	4.3
Fukuoka-B	93	126.7	VR	FP A4 16	3.6
Fukuoka-C	95	73.1	Concrete	FP A4 53	4.1
Fukuoka-D	92	87.5	VR	FP A4 45	5.9
Fukuoka-E	96	89.8	Concrete	FP A4 53	3.6

Type of soil cover: VR□plastics sheet
Insulation type: FP Formed polystyren, GW Grass wool

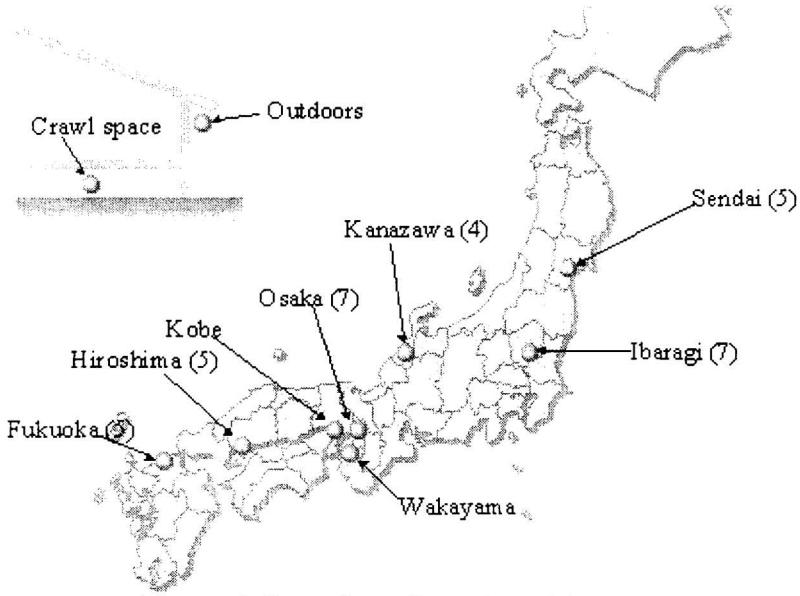

Figure 1. Location of monitored houses

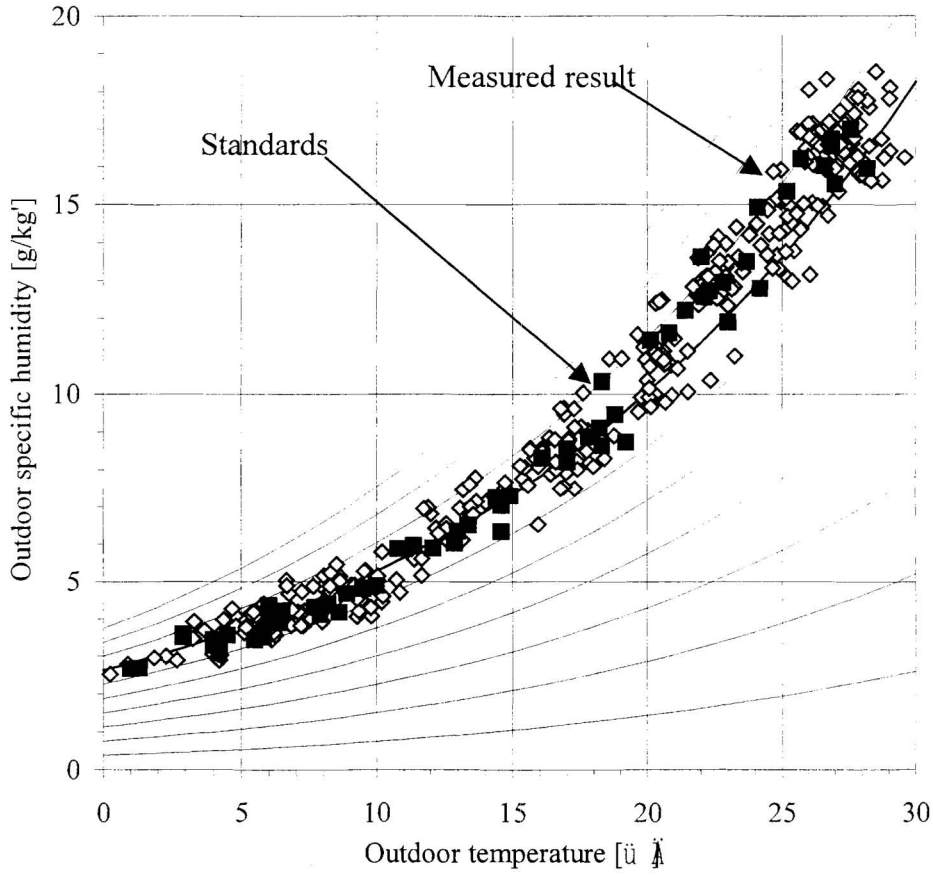

Figure 2. Distribution of the monthly average of the temperature and humidity of outdoor air

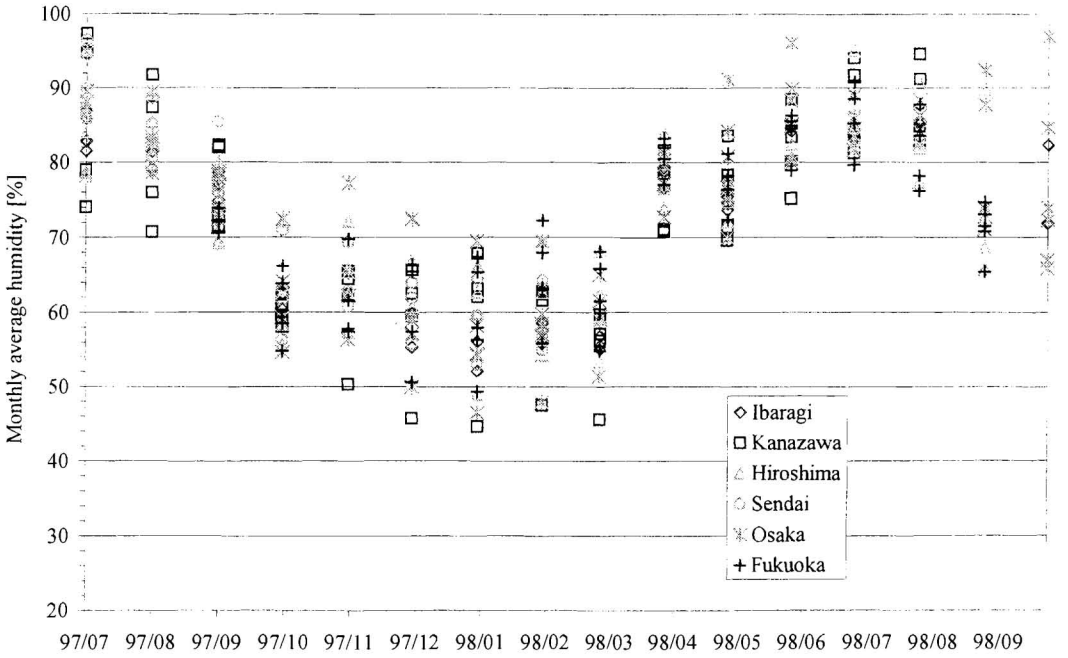

Figure 3. Annual variation of the monthly avergae of relative humidity of the crawl space

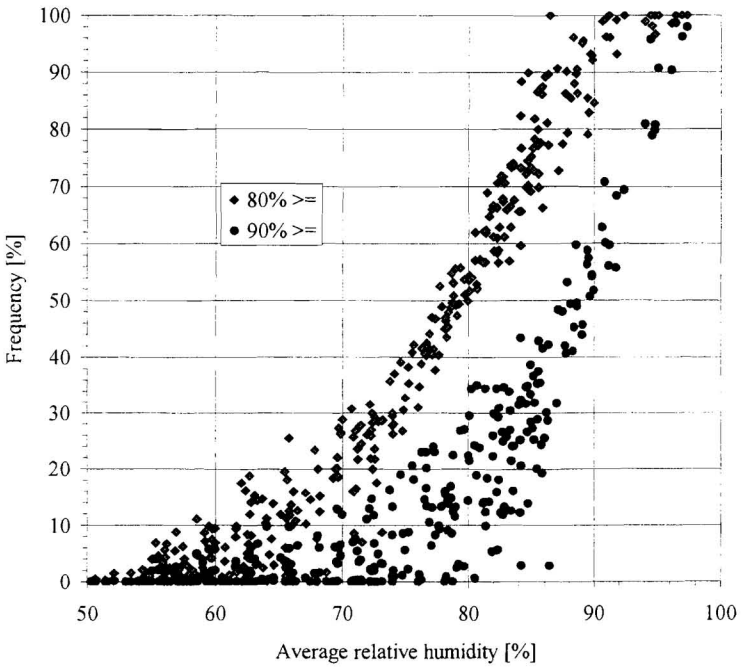

Figure 4. The relation between the monthly avergae humidity and degree of high humidity

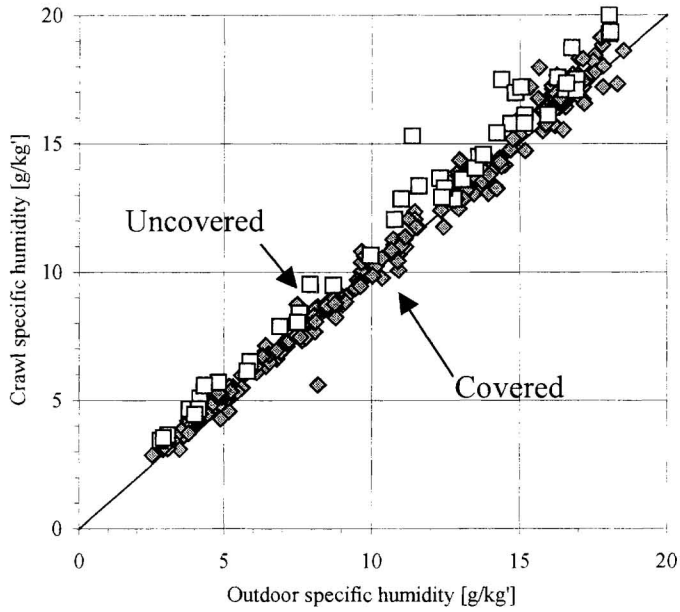

Figure 5. The relation between specific humidity of the outdoors and the crawl space

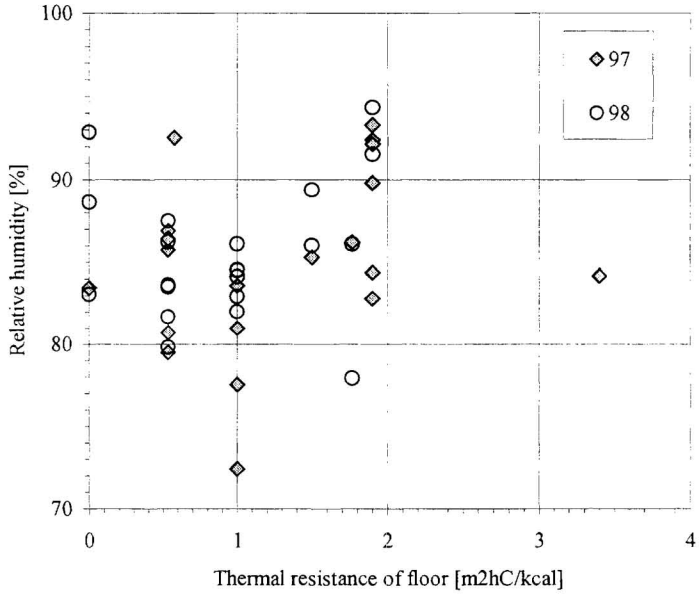

Figure 6. The relation between thermal resistance of the floor and space humidity

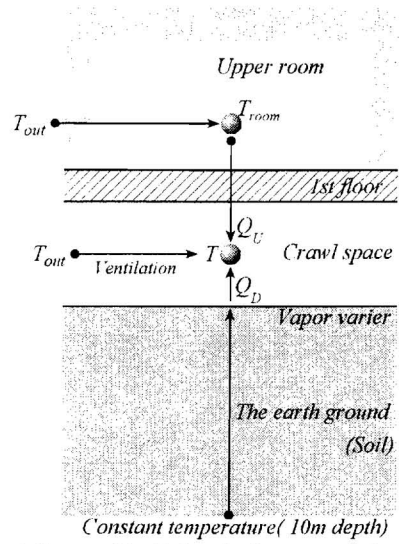

Figure 7. Calculation model

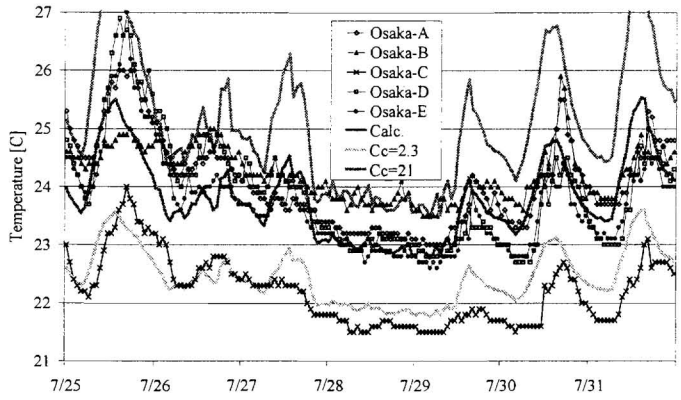

Figure 8(a). Calculation temperature in comparison with measurement results

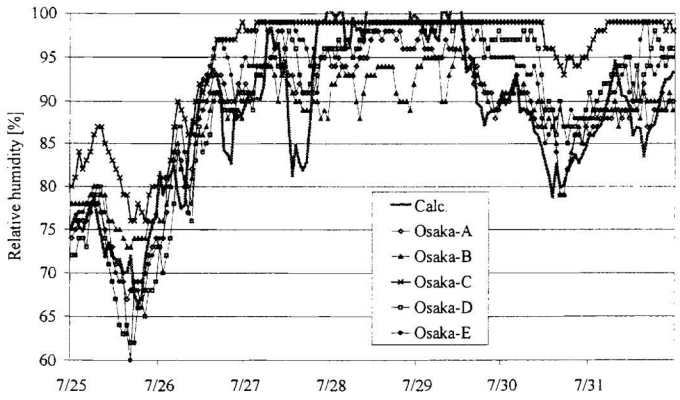

Figure 8(b). Calculation humidity in comparison with measurement result

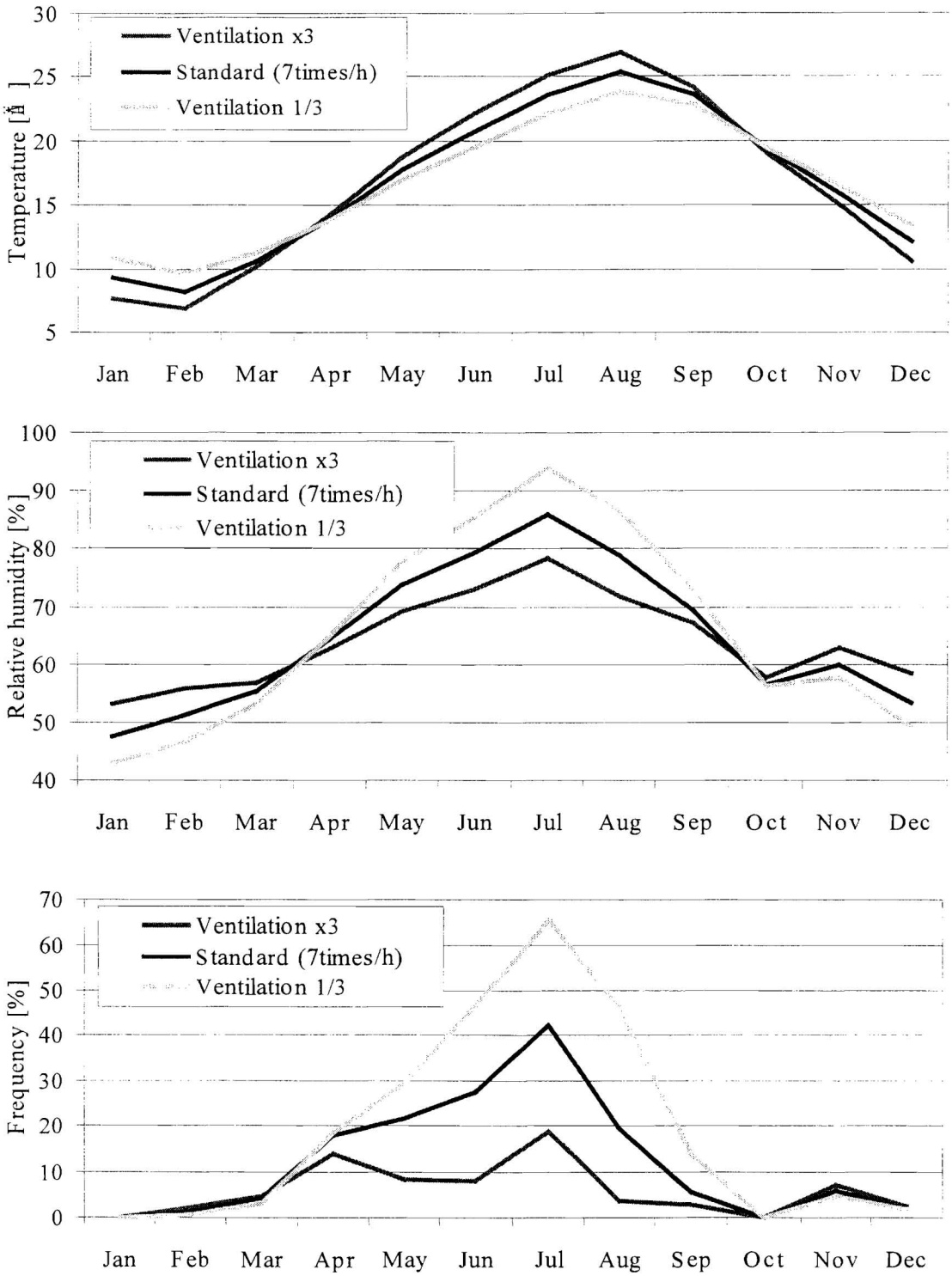

Figure 9. Calculated results of various air ventilation rate

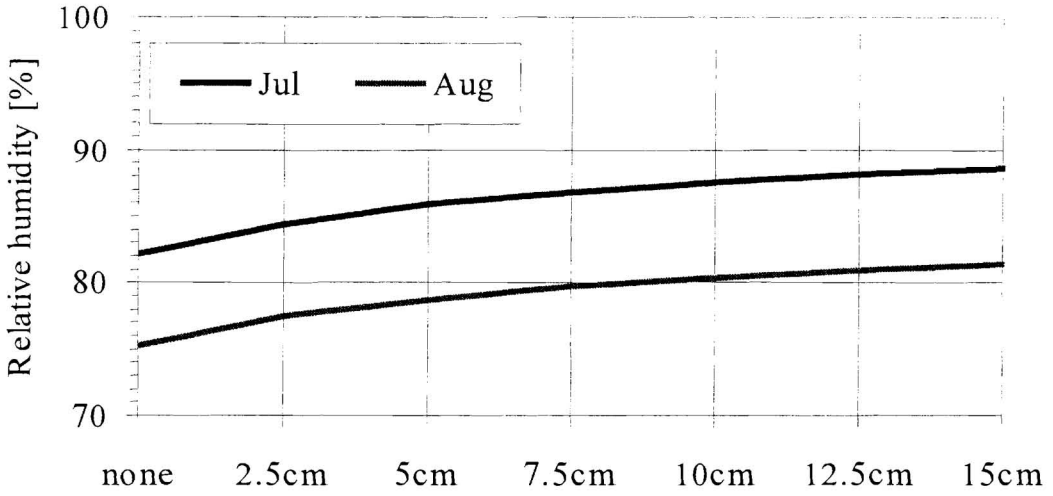

Figure 10. Calculated results of various thickness of floor insulation

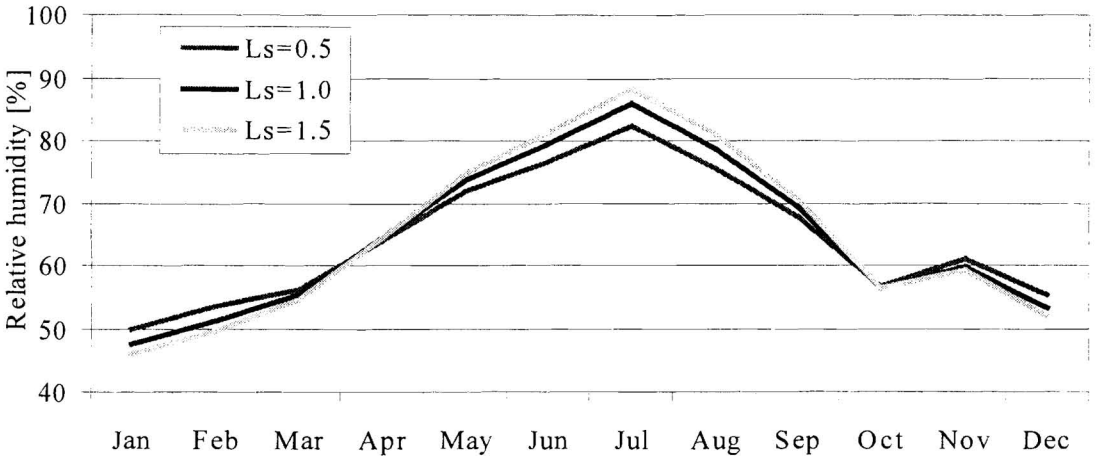

Figure 11. Calculated results of various thermal conductivity of the soil

CONVERSION OF A BUILDING TO ACHIEVE A GOOD INDOOR ENVIRONMENT – THE HEALTHY OFFICE

I. Samuelson

CONVERSION OF A BUILDING TO ACHIEVE A GOOD INDOOR ENVIRONMENT - THE HEALTHY OFFICE

Ingemar Samuelson

SP, Swedish National Testing and Research Institute, ingemar.samuelson@sp.se

Abstract

This paper describes how building physics can be employed in order to achieve a good indoor environment. By bringing all those involved in the building process together, they can improve their understanding of each other's requirements and reduce the risk of making wrong decisions. Quality assurance means that SP is involved right from the initial specification of requirements for a good indoor environment, through inspection of the building documents and workmanship to final operation, care and cleaning of the finished office. Faults could be avoided as no designs or materials could be chosen without SP approving the choice from an indoor environmental point of view.

Keywords Indoor environment, Healthy building, Quality Assurance

Background

Relating the importance of the indoor environment to health is a challenge for science. Hopefully, improved knowledge of the relationships between a building, its indoor environment and health can help to reduce the increase in allergies and other hyper-sensitivities.

When converting a building to produce new office premises in Stockholm, a special effort was made to produce a healthy building. SP - the Swedish National Testing and Research Institute - was involved in specifying requirements in respect of moisture resistance, ventilation, noise, selection of materials and so on, and also inspected the work while it was in progress and monitored the end result. The project is an example of how building physics knowledge can be applied to practical work. Proper protection against moisture is a prerequisite for healthy building, and has formed an important part of the project.

Constructing healthy buildings requires cooperation between all parties, from scientists and public authorities to designers, contractors, administrators and users. All need to listen to each other and learn from each other if what we know about healthy building is actual to result in healthy buildings. It was against this background that the

'Healthy Office' conversion project was started, and has in Sweden become a reference building for tomorrow's workplaces.

What is a healthy indoor environment in an office?

The way in which we experience the indoor environment is concerned not only with physically measurable quantities, such as temperature, draughts, ventilation air flow rates, noise, air quality or light, but also with æsthetic factors such as layout, light, colours, space, materials and so on. To these must be added other factors such as job satisfaction and good relationships with superiors and colleagues. A healthy office has all these.

Healthy indoor environments are created as the result of realisational creativity, planning and layout design, choice of materials, technical designs and systems for heating, ventilation and electricity and water supply. SP and the purchaser have drawn up requirements relating to measurable parameters for the healthy office that affect the impression of the indoor environment. The recommended values are based on those suggested by a Nordic working party that has produced criteria for healthy materials and designs.

Table 1 Advice and recommendations for the conversion

Function or parameter	Recommendation	Comments
Indoor temperature	20 - 24 °C	Temperatures below 20 °C feel cold and fingers become stiff. Occupants become tired at temperatures above 24 °C. Most people think that a temperature of 22 °C is just right.
Air velocity	< 0,15 m/s	Higher air velocities are experienced as draughts.
Air flow rates	Outdoor air flow rate > 7 l/s per person, with ability to be boosted	Necessary air change rates depend on the emission load from building materials, furnishings and occupants. Conference and board rooms normally have low flow rates, but which can be boosted.
Ventilation noise	LpA < 35 dB LpC < 50 dB	Measured values in conference rooms are below the recommended values (LpA = 31, LpC = 49).
Noise from neighbouring offices	$R'_{w,8}$ > 48 dB (Building Regulations requirements $R'_{w,8}$ > 44 dB)	After rebuilding a wall, we obtained $R'_{w,8}$ > 47 dB.
Damp	All moisture damage to be rectified.	Inspection during the conversion found damp coming through an exterior wall. This was corrected.
Relative humidity	Indoor RH not to result in water vapour difference greater than	Indoor relative humidity depends on outdoor RH and indoor temperature.

Function or parameter	Recommendation	Comments
	2,0 g/m^3.	
Emissions from materials and furnishings	Contents declarations and emission declarations required for all materials and furnishing used.	Materials in each group have been selected for non-hazardous contents and low emission.
Cleaning	Methods of cleaning, and cleaning chemicals, to be chosen so as to ensure a good indoor environment.	Working methods and chemicals have been selected in conjunction with the cleaning contractor for best results, with the choice being determined by the end results and any effects of chemicals on the indoor environment.
Operation and care	Procedures and working methods to be defined for all who, in any way, look after or use the premises: users, cleaners and administrators.	

Quality assurance through P-marking

P-marking provides a quality assurance system for the entire process, from planning and design, through the building work to final use and administration. It is intended to ensure that the conversion work fulfils the requirements set out in legislation, standards or generally employed codes of practice. In conjunction with SP, the purchaser has in this case set further, more demanding, requirements, in respect of elimination of allergy risks in connection with the choice of materials, designs and - in particular - cleaning methods and materials used for cleaning. SP has made measurements and checked to ensure that the requirements have been met. While the work was in progress, SP has also maintained frequent contact with the architect, as well as with the designers and contractors. SP has assisted in deciding on materials and designs, and has recommended suitable methods of cleaning and choice of materials. Physical measurements have shown that the performance requirements have been met.

Existing walls, floors and ceilings were inspected before the design work started, looking for **damp**, moisture damage, odours and the presence of micro-organisms. Radon concentrations were also measured.

Good air quality was also ensured during the design and building phases by providing an adequate **air flow rate** and by selecting materials having low emissions. Good ventilation is needed in order to remove pollutants such as moisture, odour and carbon dioxide from occupants, emissions from office equipment and those from building materials and furniture.

Surface coverings such as flooring materials, carpets, ceiling tiles and paints, as well as formless materials such as adhesives, filler and mastics were selected after due consideration of their performance, their contents and their claimed **low emission**.

A good **noise environment** has been ensured by the provision of adequate acoustic insulation (e.g. through additional insulation in the wall with the neighbouring property), low-noise building services systems (ventilation systems etc.), correct room acoustic attenuation and design and the selection of furniture that does not contribute to unnecessary noise generation or reflection.

Good **lighting conditions** have been chosen in order to assist good working performance and concentration.

Good **thermal comfort** has been ensured, even at the design outdoor temperature.

Measurements of **electric and magnetic fields** have shown low values, except in the vicinity of certain items of apparatus.

Complaints about the indoor environment from staff, visitors etc. when the building is in use will be documented. Details must be noted of how the complaint has been dealt with, e.g. whether checks have been made or what has been done about the problem. The purpose of this is that staff or others should know that there is a system for dealing with such matters, and that there should be early warning of what might be incipient problems.

Clear and easily understood **operating and care instructions** for the premises are a prerequisite for continued good air quality. The various documents need to be matched to the needs of the target personnel concerned, i.e. perhaps to the building operator's staff, to cleaners or to occupants and users. There are instructions for cleaning, and chemicals to be used have been selected to suit the surfaces to be cleaned, the job to be done and the need for good indoor air quality. The instructions for the heating and ventilating systems provide details of such aspects as the maximum number of persons based on the capabilities of the systems, work being carried out in the building and so on.

The building process

The project was planned and designed between January and April 1997. The building and installation work ran from May until August, with the final inspection being carried out on 15th August 1997.

It has been important that all parties should understand the objective of creating a healthy office. There has therefore been intensive liaison throughout the conversion work, with weekly site meetings conducted by the administrator's project manager. No changes were allowed to the documents without the approval of the project manager, the architect and SP. There was frequent contact with SP, and decisions were made at short notice. SP's wide range of expertise has been utilised for dealing with problems of emissions, noise, odour, ventilation, instrumentation etc.

The occupants moved into the new premises - the healthy office - on 22nd August. The work had been somewhat delayed, due to delivery delays during the summer. However, rather more serious was the fact that inspection found that a number of faults had been built in, as a result of failing to follow drawings in all respects. It was necessary, for example, to move a number of measuring devices and fittings, and to take

down a number of false ceilings in order to increase the number of cleaning access points for the ventilation system.

Display

A display panel has been installed so that the occupants of the building and visitors to it can see exactly what the indoor conditions are at any time. Values for a number of climate parameters are displayed: outdoor conditions, and indoor conditions in the conference rooms and the boardroom, two ordinary office rooms and the common area. A green signal with each parameter value indicates whether it is within the recommended limits. The display also scrolls the values for the last seven days for one climate parameter at a time.

During the use phase

Temperature, relative humidity and carbon dioxide concentration in the conference rooms and some of the office rooms are continuously measured and shown on a display in the entry hall. The values are not used by any control system: in the event of serious departures from the desired values, it is necessary to contact the operating personnel.

Complaints about the indoor environment from occupants, visitors etc. must be documented. The details must show how the complaint has been dealt with, e.g. whether checks have been made or what has been done about the problem. The purpose of this is that staff or others should know that there is a system for dealing with complaints, and that there should be early warning of what might be incipient problems.

Clear and easily understood **operating and care instructions** for the premises have been prepared in order to ensure continued good air quality. There are instructions for cleaning, and chemicals to be used have been selected to suit the surfaces to be cleaned, the job to be done and the need for good indoor air quality. The instructions for the heating and ventilating systems provide details of such aspects as the maximum number of persons based on the capabilities of the systems, work being carried out in the building and so on.

Validity of the P-marking

Check measurements of the indoor environment will be made once a year, with operation and care also being checked at the same time. The P-marking of the various systems will be renewed as appropriate.

Experience

The following experience of the healthy office building has so far been acquired:

- The subjective impression of a good indoor environment is closely linked to layout, colours, lighting conditions and the choice of materials. However, it is also necessary to achieve the recommended values of a number of physical parameters.
- It is important that all parties involved should be engaged in the entire process. Although the building, ventilation and electrical consultants were involved more or less from the start, the cleaning contractors were not brought in until a late stage. Their requirements in respect of materials and their 'cleanability' should have been allowed for from the planning stage.
- Frequent contacts between the parties are important, both during the planning stage and while the actual work is being carried out. A dedicated architect and a responsible project manager have been important figures: without them, it would not have been possible to operate the project towards its clear objective of a healthy office.
- The basic conditions of the building itself are favourable: a concrete building, with a massive structure and an attractive exterior. However, it was sometimes difficult to run the necessary pipes, ducts and wires: it was necessary at times to modify their intended arrangements.
- SP's participation in the project was initially regarded by some parties with some scepticism. The quality assurance work seemed to cause more bother than benefit, but it and SP's role were gradually accepted as the work proceeded.
- The display in the entry hall makes occupants and visitors aware of the special emphasis on good indoor environment.

HOW WELL SHOULD ONE KNOW THE HYGROTHERMAL PROPERTIES OF BUILDING MATERIALS

K. Kumaran, J. Wang

HOW WELL SHOULD ONE KNOW THE HYGROTHERMAL PROPERTIES OF BUILDING MATERIALS?

Kumar Kumaran and Jinkai Wang

Building Envelope and Structure, Institute for Research in Construction, National Research Council of Canada, Ottawa K1A 0R6, Canada
E-mail: kumar.kumaran@nrc.ca, jinkai.wang@nrc.ca

Abstract

Hygrothermal models enable us to analyze the hygrothermal behaviour of building envelope components. Knowledge on several hygrothermal properties is a prerequisite for the application of such models. Often the question is asked: How well should one know the properties? This paper makes an attempt to provide some facts that may assist one to answer the question. A well-controlled drying experiment was conducted on a cement board used as exterior sheathing member in North America. All hygrothermal properties of the material have been determined through well known test procedures. The experimental data were used to benchmark an advanced hygrothermal model. The model was subsequently used to conduct a parametric analysis of the drying behaviour of the cement board. In the analysis, three hygrothermal properties that affect the drying process were systematically varied. These properties are: sorption/suction isotherm, water vapour permeability and moisture diffusivity. The results show that the sorption/suction isotherm has to be determined as precisely as possible according to current procedures. A 50 % variation in the vapour permeability has noticeable effect on the drying behaviour of the cement board. But a 50 % variation in the moisture diffusivity has insignificant effect on the drying details.

Key words: drying, vapour permeability, sorption/suction isotherm, moisture diffusivity, hygrothermal models.

1 Introduction

Heat, air and moisture transport models[1] are powerful tools in the hands of building practitioners. These models can assess the long-term hygrothermal performance of a given building envelope assembly that operates in a specific geographic location and provides a specific indoor environment. The models shall include all the known aspects of building physics and the numerical techniques used shall be reliable. In addition, the following hygrothermal properties of various materials in the assembly shall be representative of current products: **thermal conductivity** as a function of temperature and moisture content, **heat capacity** as a function of temperature and moisture content, **equilibrium moisture content** as a function of relative humidity, **water vapour permeability** as a function of relative humidity, **moisture diffusivity** as a function of moisture content, **water absorption coefficient** and **air permeabilty** as a function of pressure difference and moisture content.

Determination of these properties is a challenging task due to a variety of uncertainties and practical difficulties. Some are inherent to the procedures. The others are induced by the material non-homogeneity and product variability. To give an example, ten plywood products were subjected to the cup measurements to determine their water vapour permeabilities at a mean RH equal to 86 %. The deviation of the results from an average value of 9.5E-12 kg m^{-1} s^{-1} Pa^{-1} was 28 %. So, how well one has to know the above properties to make acceptable predictions? Results from systematic parametric analyses using reliable hygrothermal models that have been properly benchmarked may answer this question.

2 A drying experiment to benchmark models

Three 30 cm X 30 cm test specimens were cut from a cement board that is used as a sheathing member in walls in North America. The average thickness of the product is 12.5 mm. The hygrothermal properties of the product determined at the Institute for Research in Construction in an earlier investigation are listed in Table 1.

The specimens with edges sealed using a mixture of waxes impermeable to moisture were saturated by keeping under water for 24 h. The initial increases in weight were recorded and the specimens were vertically placed on one of their edges in a chamber maintained at 25 °C and 70 % RH. Air was circulated over the major surfaces with velocities between 0.1 and 0.3 m/s. The specimens were periodically removed from the chamber and the decrease in weight recorded until equilibrium was attained. The average drying curve for the three test specimens is given in Table 2.

Table 1. Hygrothermal properties of the cement board.

Density = 1130 kg m^{-3} Heat capacity = 840 J kg^{-1} K^{-1}
Thermal conductivity = 0.25 W m^{-1} K^{-1}

Sorption/suction curve		Moisture diffusivity		Vapour permeability	
RH (Fraction)	Moisture content (kg/kg)	Moisture (kg/kg)	Diffusivity (m^2/s)	RH (Fraction)	permeability (kg $m^{-1}.Pa^{-1}.s^{-1}$)
0.02	8.77E-03	0.00	1.00E-13	0.00	7.80E-12
0.14	1.21E-02	0.02	1.00E-13	0.12	8.09E-12
0.26	1.44E-02	0.03	1.00E-13	0.24	8.40E-12
0.38	1.67E-02	0.05	5.00E-12	0.37	8.78E-12
0.50	1.94E-02	0.06	8.55E-10	0.49	9.32E-12
0.52	2.00E-02	0.06	8.89E-10	0.51	9.43E-12
0.64	2.37E-02	0.08	1.15E-09	0.63	1.04E-11
0.76	2.93E-02	0.09	1.60E-09	0.76	1.22E-11
0.88	4.03E-02	0.11	2.68E-09	0.88	1.76E-11
1.00	1.25E-01	0.13	9.14E-09	1.00	2.68E-11

Table 2. The average drying curve for the three test specimens

Time, h	Moisture content, g	Time, h	Moisture content, g
0	189.90	11.5	80.09
1	177.85	23.75	46.90
2	166.41	28.5	42.93
3	154.38	29.5	40.21
4	143.22	33.4	38.13
5.5	127.79	47.75	34.00
6.5	116.02	51.5	33.02
7.5	108.47	58.15	32.16
8.5	99.67	73.9	31.61
9.55	91.00	100	30.37
10.5	85.31	123.5	29.84

3 Results from a simulation of the drying process

An advanced hygrothermal model developed at the Institute was used to simulate the drying experiment exactly. Since the specimens were immersed in water for 24 h, it was assumed that they were at a uniform initial RH =100 %. The results from the simulation are compared with the measurements in Figure 1.

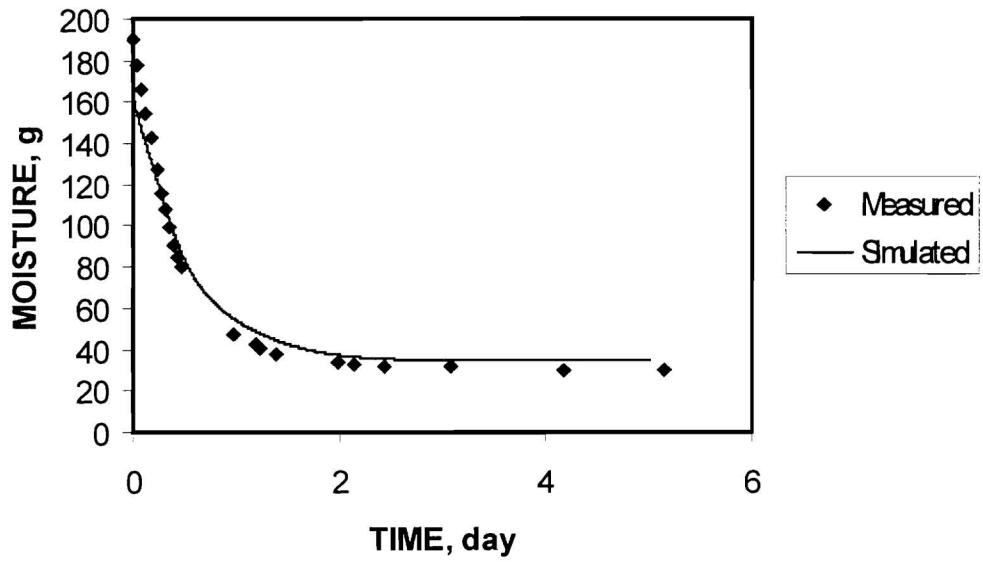

Figure 1. Comparison of the simulated and measured drying curves.

Though the measured initial moisture content was slightly higher than the simulated, the overall agreement between the measured and simulated drying curves is acceptable in terms of the duration of the process and the shape of the drying curve.

4 Parametric analysis and discussion

The hygrothermal properties as listed in Table 1 were used in the original simulation referred to in Figure 1. Eight other simulations were carried out as coded below, by systematically varying three hygric properties: sorption/suction curve, vapour permeability and moisture diffusivity.

Code	Variation from the properties listed in Table 1
vap 50	The vapour permeability was reduced by 50 % of the original
vap 150	The vapour permeability was increased by 50 % of the original
dfl 50	The moisture diffusivity was reduced by 50 % of the original
dfl 150	The moisture diffusivity was increased by 50 % of the original
sorp 50	The sorption curve was reduced by 50 % of the original
sorp 150	The sorption curve was increased by 50 % of the original
all 50	All three properties were reduced by 50 % of the original
all 150	All three properties were increased by 50 % of the original

Figure 2 compares the results from these simulations with the original drying curve shown in Figure 1. The moisture contents are normalized against the initial moisture content. There is very little difference among the results for the initial part of the drying curve, until the moisture content reaches 50 % of the initial value.

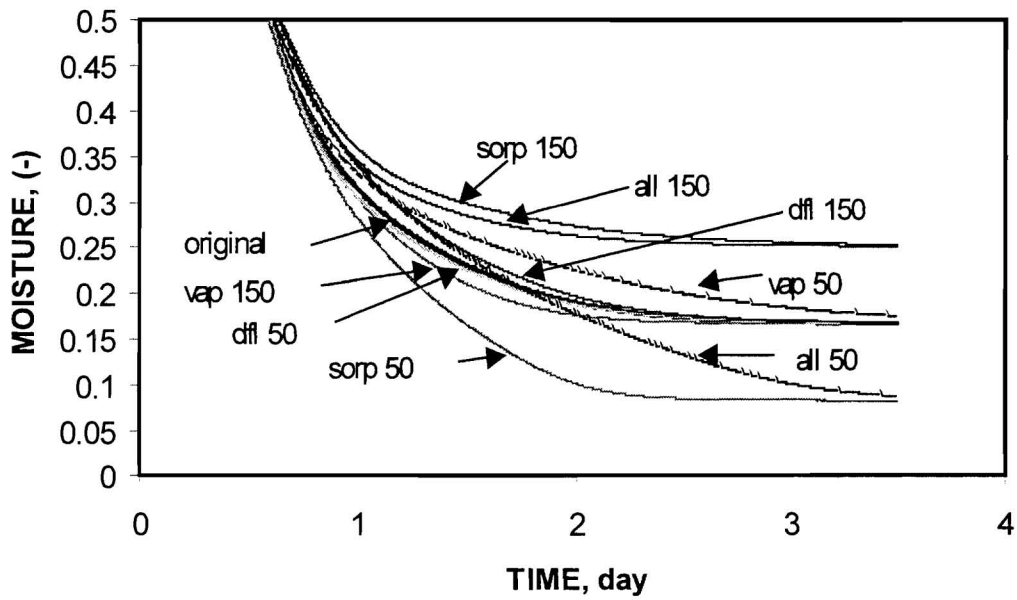

Figure 2. Results from the parametric analysis compared with the original drying curve

A 50 % uncertainty in moisture diffusivity alone has insignificant effect on the details of the drying curve. A 50 % uncertainty in the vapour permeability changes the

shape of the curve by affecting the duration of the process, especially when it is underestimated. A 50 % uncertainty in the sorption curve, as one would expect, affects the shape of the drying curve significantly. The reason for this is that all model calculations assume local equilibrium at all time. 50% uncertainties in all three properties will result is very erroneous results, in terms of the shape of the drying curve as well as the duration of the process.

4 Concluding remarks

Comparison of the simulated and measured drying curves in this investigation confirms that the physics of the drying process is captured well by the hygrothermal model developed at the Institute. Also the numerical techniques used are sound. The properties of the material being well determined, the agreement between the two drying curves is acceptable in terms of the shape and time frame.

Parametric analysis of the drying process investigated here leads to the following remarks. A proper knowledge of the order of magnitude of the moisture diffusivity may give acceptable drying curves. It is desirable that the vapour permeability is known at least within 20 % of the actual value. However, the sorption curve has to be known rather well, maybe within 5 %.

Reference

[1] Hens, H., Heat, Air and Moisture Transport, Final Report, Volume 1, Task 1: Modelling, International Energy Agency Annex 24, Laboratorium Bouwfysica, K. U.-Leuven, Belgium, 1996.

TOWARDS A UNIFIED METHODOLOY FOR DURABILITY PREDICTION

M. Bomberg, K. Kumaran

TOWARDS A UNIFIED METHODOLOGY FOR DURABILITY PREDICTION (EXEMPLIFIED BY FREEZE-THAW RESISTANCE OF CLAY-BRICKS)

Mark Bomberg* and Kumar Kumaran*
*Institute for Research in Construction, National Research Council of Canada, Ottawa, ON, Canada, K1A OR6, E-mail: Mark.Bomberg@nrc.ca

ABSTRACT

Recent advances in modeling of two-dimensional, simultaneous, coupled, heat, air and moisture flows permit predicting moisture content profiles in many wall systems exposed to defined climate and service conditions. The input needed for such a calculation is complex and includes conditions of driving rain, solar and air temperatures, typical rates of cooling, frequency and duration of the freezing temperatures. Establishing a probability of the moisture content profile at a prescribed time e.g., at the start of freezing enhances the evaluation of the long-term performance of building envelopes.

To predict the service life of a building component means to quantify the response of the building envelope to the environment and to define conditions at the onset of the damage. Currently the damage process is introduced through an experiment that seldom relates environmental forces and the damage process in analytical terms.

In this paper a unified methodology that extrapolates the limit states analysis to assessment of durability processes quantifies the relation of the damage process to the environmental forces. This approach is exemplified by the limiting (critical) moisture content of clay-brick with regard to freezing. Yet, the limit states concepts cannot be applied in the practice. The limiting moisture content with regard to freezing can not be compared with "characteristic moisture contents" of clay-brick. Neither can the moisture potential (energy of the pore-water) be established for these moisture contents.

It appears that the research on moisture movement through porous materials such as clay bricks has been dedicated just to the calculation of moisture content. While a few effects of moisture e.g., fungal defacement can be related to the moisture content alone, other durability considerations require the knowledge of the energy of the pore water. This is a serious gap. If a consensus can be reached within CIB W-40 committee, a small group could undertake a comparative study to define the range of moisture contents associated with the capillary saturation and extension of that knowledge to predict durability.

Key words: building envelope design, limit states method, long-term performance, serviceability, durability, service life, damage functions, life cycle cost, evaluation, environmental control, check list, functional analysis.

1. INTRODUCTION

In Canada, the limit states (LS) method is used for evaluation of structural performance. CSA S478 standard, which guides the durability assessment, also implies LS principles. With this in mind, Bomberg and Allen (1996) and Allen and Bomberg (1997) expanded the use of limit states to durability evaluation.

2. THE LIMIT STATE METHOD

The generalized limit states[1] method is based on the condition of failure[2]. Table 1 categorizes the limit states criteria[3] in terms of safety, function (serviceability) or

[1] The term "generalized" is omitted to highlight that the same method covers structural and durability considerations.

appearance. Requirements (a) and (b) are related to safety; others to the loss of function or appearance (Vanier and Lacasse, 1996). The sequence of LS method application is listed in Table 2.

Table 1. Different requirements of the limit states (LS) method

(a) instability e.g., overturning
(b) strength (shear, bending, buckling), i.e., insufficient structural capacity to resist loads
(c) unacceptable deflection or vibration
(d) surface damage or discoloration, as it relates to appearance
(e) local damage (loss of function), e.g., delamination of concrete cover,
(f) property falls below a prescribed threshold, e.g., reduction of wall thermal resistance

Table 2. Limit States evaluation of the building envelope for durability

STEP	Limit States method
1	Select loads applied to the building envelope
2	Establish loads acting on and within the component
3	Select the performance aspect and the performance indicator that relates deterioration or damage process to the service time
4	Establish the maximum value of the performance indicator, S_i, during the design life by application of the damage function
5	Establish the performance limit, R_i, at the onset of failure, (testing/modeling).
6	Check the limit state criterion, $S_i < R_i$. If the predicted performance indicator exceeds the performance limit, changes must be made.

The LS method starts with the analysis of loads (Table 3). One can, then, select one aspect of performance and for the actual environmental conditions, calculate (or establish otherwise) the performance indicator during the design life and compare it with the performance limit.

2.1 Loads in the Limit States method

Loads include forces, movements, structural and environmental loads (Table 3). This term replaces such terms as "actions" or "environmental agents" to describe factors defining the microenvironment (temperature, humidity, presence of hyposulphite ions, etc.) that affect the process of material deterioration. In the structural analysis, all loads are considered external to the structure. With the durability analysis, loads are either external or internal (environment acting on or within the building envelope). Internal loads were sometimes called load effects[4], since they are actually determined by the external environmental loads and the construction itself. For instance, in the case of brick veneer ties, the temperature and humidity of air in the cavity between the brick veneer and the main part of the wall determine on the rate of corrosion of the metal ties.

[2] A feature of the deterioration or damage process which describes the onset of functional failure of component or subsystem, such as exceeding the strength of a material (loss of strength in brick ties caused by corrosion), onset of instability due to force, or reaching an excessive deflection of a component.

[3] The limit states criterion, for a particular performance aspect, compares the value of the performance indicator during the whole design life with its limiting value.

[4] We do not use the name "load effects" to avoid confusion with performance indicators which relate the deterioration / damage process to either internal or external loads.

Table 3. Examples of loads used in the Limit States method

EXTERNAL LOADS	INTERNAL LOADS
Ambient or surface temperature	Temperature, thermal gradient
Radiation: IR, UV	IR, UV
Moisture: rainfall, snowfall, ice	condensation, moisture content
Contaminants: Cl, SO_2, NO_2, Fungi, CO_2 (carbonation)	Cl^- in water, fungal growth, CO_2 in air or water
Structural loads: wind, snow, seismic, impact (accidental)	Forces, stress, strain, deflection, movements,

The microenvironment inside the building envelope is shaped by the indoor and outdoor conditions and the response of the subsystem. The internal loads may be calculated by using information on external loads and a model of heat, air and moisture flows.

2.2 The performance indicator

The limit states method defines conditions when the component fails to perform the required function. To quantify these relationships we use the concept of damage functions (Grondin, 1993). The damage function is a simple mathematical model of the deterioration/damage process relating service life to the environmental loads acting on the analyzed component or subsystem. Typically, damage functions incorporate parameters such as maximum stress or strain, number of stress cycles, area reduction, loss of mass during material deterioration or cumulative exposure time. Using the damage function for each performance aspect, either an extreme or a cumulative performance indicator, S_i, provides a measure of performance (or, conversely, damage) during as well as at the end of the design life. There are two types of performance indicators, either physical characteristics (e.g., stress, strain, deflection, loss of mass or area, thermal or noise resistance) or an aggregate performance indicator called the cumulative exposure time. As the performance indicator is a function of time and environmental factors it may vary, in which case the extreme value is used for durability evaluation.

The cumulative exposure time (CET) was postulated by Bomberg and Shirtliffe (1994). CET is defined as a sum of the intervals of time when the actual moisture content is equal to (or higher than) the critical moisture content times the degree of severity of this exposure, namely:

$$CET = \Sigma (I \bullet F_{ex}) \qquad (1)$$

where

I = the interval during which moisture content is equal to or higher than the critical moisture content; F_{ex} = the severity factor during this exposure.

Typically, I is the interval in which the deterioration process takes place and F_{ex} describes the contribution of the actual environment to the rate with which this process takes place. For instance, the rate of corrosion of metals exposed to air depends on temperature and humidity at the surface. Corrosion may start, say, at room temperature at 90% RH, but will proceed faster at a higher relative humidity and the same temperature. Therefore, for a given temperature range, one may define $F_{ex} = 0$ at 90% and $F_{ex} = 1$ at 99.0%. The severity factor could be greater than one in the presence of other agents e.g., contaminants that lower pH.

Use of the CET provides an alternative approach to deterioration or damage processes. For instance, a performance indicator for delamination of concrete caused by corrosion of reinforced steel is the tensile stress in concrete and the performance limit is the tensile stress during delamination (Genge, 19994). Using this performance indicator would require statistical analysis, which given the uncertainty involved in service conditions, may give a large standard error. One may prefer to calculate CET on the

basis of the information from several failures (the design and material used, the period to each failure and environmental conditions in each case). Since CET retains the critical features of the deterioration/damage process and the failure mechanism is taken into account in the choice of the performance limit (LCET is defined below), using computer modeling one may predict CET for another set of environmental conditions.

Note that the "time of wetness", previously used in the durability assessment is replaced by the CET. The fact that CET includes a varying severity factor does not complicate calculations. Becker (1985), Kashiwagi (1995), and others showed that large errors are allowed in weighing factors for multiple regression or for fuzzy logic schemes, when such evaluations involve many aspects of performance. In effect, a linear approximation of the severity factor will suffice for most cases.

2.3 The performance limit

R_i is the value of the performance indicator at the onset of failure. Like the performance indicator, this criterion is either a physical property (e.g. limit on force, stress, strain and deflection or number of stress cycles) or the limit of the exposure period (limit of the cumulative exposure time, LCET). Typically, the LCET criterion may be used for delamination of concrete under chloride attack, fracture of pre-stressed reinforcement, or spalling on the exposed masonry surface.

2.4 The limit state criterion: $S_i < R_i$

For a particular performance aspect, one checks if the performance indicator is greater than the performance limit during the design life.

If the deterioration process is cumulative in nature, the initial performance indicator equals zero. With time, and in accordance with the damage function, the performance indicator increases until it reaches the performance limit. At this stage the limit states has been reached and the service life ended (with regard to the analyzed performance aspect). The main question is whether this happens before or after the design life of the component.

If the limit state criterion is not satisfied, (service life was shorter than the required design life), one can either alter the design or modify the design life of the component. Otherwise, one continues to examine other performance aspects for the same design or returns to a general evaluation.

3. AN EXAMPLE: ONE STEP FREEZE-THAW DAMAGE FUNCTION

The concept of limiting moisture content or limiting degree of saturation[5] with respect to freeze-thaw can be exemplified by tests performed by Fagerlund (1970) and discussed by Bomberg and Shirtliffe (1994). The limiting degree of saturation is the highest degree of saturation, which may be found in a specimen without it becoming damaged under freeze-thaw process. The discussed example made it clear that at a certain degree of moisture saturation, any freezing, either a single or multiple freeze-thaw cycling[6], will cause a freeze-thaw damage. In the discussed case, the damage was characterized by a dramatic reduction in the residual dynamic modulus (the dynamic Young's modulus divided by the modulus determined on the undisturbed specimen). Effectively, in this somewhat simplified methodology, the limiting degree of saturation is independent of the test method, and therefore may be used as a limit states criterion for this type of material.

---

[5] The central issue of our discussion (see later text) is how to define the "maximum" moisture content to which the actual moisture content is related.

[6] Identical results are obtained with different numbers of freeze-thaw cycles or one-step freezing.

The above example illustrates the process of evaluating the probability of frost damage in the material. The limiting degree of saturation for the specific material (product) is determined[7] and compared with the actual degree of saturation predicted from the model that is applied for the given climate. Hence, frost damage is expected to occur during the period of sub-zero temperatures when the S exceeds the R_s.

4. WHAT IS THE MAXIMUM MOISTURE CONTENT UNDER CAPILLARY FORCES ALONE?

It is widely recognized that using a degree of saturation instead of moisture content reduces the scatter of experimental data (Hedenblad and Nilsson, 1985). It has also been recognized that using maximum moisture content attainable under maximum driving forces (vacuum saturation, boiling water etc) as the reference moisture content does not focus attention on the capillary forces alone (Krus, 1996).

The goal is to measure the maximum moisture content that would be obtained when water has filled all the pores that are accessible for ingress due to capillary forces alone. The importance of this point (see thesis by: Brocken, 1998; Descamp, 1997; Wessman L., 1997; Pel 1995) may be inferred from the following set of hypotheses[8]:

- One may assume that when the system of coupled and simultaneous HAM transfer equations is congruent with the material characteristics used in this system, it does not matter whether this system is based on single-phase or lumped moisture potentials (though the numerical precision may be locally affected)
- Material characteristics should be determined in the vicinity of characteristic moisture contents to be both reliable and precise
- Calculations of capillary moisture flows, either in wetting or in drying, should be related to the zero capillary suction
- The condition of zero capillary suction may correspond to the whole range of moisture contents, particularly when the wetting rate varies or when an incomplete wetting and drying runs follow each other
- The entrapment of air in the liquid phase, as well as its diffusion in and out the pore water, may have an insignificant effect on the energy status of pore water but a significant effect on the moisture content
- To calculate stress-strain relations during the freezing process, one must account for capillary, osmotic, freezing and other pressure sources acting on the pore water. To this end one must know the range of moisture content where the capillary potential (capillary suction) is equal to zero[9].

Traditionally, the knick-point in the plot of one-dimensional water intake versus square root of time has been thought to indicate moisture content that correspond to zero capillary suction. This is, however, a crude approximation. Different moisture contents at the knick point can be obtained if the rate of water supply is limited, material is partly wet or flow of air at the other boundary is restricted.

5. PROPOSED SCOPE OF COMPARATIVE STUDY

Any detailed analysis of freeze-thaw resistance is likely to involve a separate equation for air diffusion through the liquid water. It is advisable to establish the range in which the air entrapment can be replaced by water without changing its capillary potential (suction). Knowing this range is also critical for handling the moisture hysteresis in HAM models.

---

[7]The test must involve REV, uniform temperature and moisture content. The test may be based on either dilatometry or non-destructive measurements of mechanical properties.

[8] This conference paper being restricted to six pages allows merely listing the hypothesis for discussion.

[9] We shall denote the range of moisture contents that correspond to such a definition as the capillary saturation range

To establish such a range one may consider some of the experimental set-ups for water immersion:

- Minimum moisture content (maximum air entrapment) could be obtained when a 50 mm cube is immersed 75 mm into 100-mm deep water tank to undergo 3-D intake process.
- Maximum moisture content (minimum air entrapment) can be obtained when a 50 mm cube with four surfaces waterproofed, one provided with a ceramic filter and immersed 25 mm is immersed into water. The water intake rate is slowed clown by the filter and the other material surface is exposed to air. Alternatively, one may consider a process of 1-D water intake with prolonged interruptions.

6. C LOSING REMARKS

The method for durability evaluation, presented in this paper, is based on the limit states method. Even this method is widely used in the structural design, design for durability has traditionally been performed in an unstructured manner. Because of the iterative nature of the design process and the complexity of the issues, the introduction of LS method enhances the use of HAM models for the prediction of loads.

Using an example of freeze-thaw durability, the paper identifies an existing gap in research and proposes a new project.

REFERENCES

Allen D. E. and M. T. Bomberg, 1997, Limits states design for durability, 7th Conf. on Bld. Sci. and Technology, Toronto

Becker R., 1985, "A method for the generation of weighing factors for performance evaluation systems", Building and Environment, Vol. 20. No. 4, pp.195-200

Bomberg M. and D. Allen, Use of generalized limit states method for design of building envelopes for durability, J. Thermal Insul. and Bldg. Envs., Vol. 20, pp.18-39

Bomberg M and C. J. Shirtliffe, 1994,"A conceptual system of moisture performance analysis", ch. 26, ASTM MNL 18, Manual on Moisture Control in Bldgs, pp.453-461

Brocken H. J. P.,1998, Moisture transport in brick masonry: the gray area between bricks, U of Eindhoven

Descamps F., 1997, "Continuum and discrete modeling of isothermal water and air transfer in porous media", U. of Leuven

Genge G.R., 1994, "Cost-effective/affordable repairs", Sem. on cost-effective concrete repairs, CMHC/NRC.

Grodin, G.Y., 1993, "Damage functions for service life prediction of zinc and steel components", Internal report No. 647, Institute for Research in Construction NRC.

Hedenblad G. and L. O. Nilsson, 1985, Degree of capillary saturation, CIB W-40 Holzkirchen meeting

Kashiwagi D. T , 1995,"Performance based procurement system for roofing", J. Thermal Insul. and Bldg. Envs., Vol. 19, pp.49-58

Krus M, 1996, Moisture transport and storage coefficients of porous mineral bldg. mat., Fraunhofer IRB Verlag

Pel L.,1995, Moisture transport in porous building materials, Eindhoven U of Technology,

Vanier D. J.and M. A. Lacasse, 1996, "BELCAM project: "Service life, durability and asset management research", 7th Int. Conf. on Durability of Building Materials and Components, Stockholm

Wessman L., 1997, Studies on the frost resistance of natural stone, Lund University

REDUCTION OF ENERGY CONSUMPTION INTO NO INDOORS BY USING INFRA HEATERS

M. Korenská, L. Pazdera, J. Smutny

REDUCTION OF ENERGY CONSUMPTION INTO NO INDOORS BY USING INFRA HEATERS

Marta Korenska[1], Lubos Pazdera[1], Jaroslav Smutny[2]

[1] Department of Physics, Faculty of Civil Engineering, Technical University of Brno, Zizkova 17, 602 00 Brno, Czech Republic

[2] Department of Railway Construction and Structures, Faculty of Civil Engineering, Technical University of Brno, Veveri 95, 662 37 Brno, Czech Republic

E-mail: marta@dp.fce.vutbr.cz, fypaz@fce.vutbr.cz, zksmu@fce.vutbr.cz

Abstract

New conception heating large-space objects recede from central boiler-room, divorce hot waters if need be vapour in industrial works and advise their heating by gas infrared radiator. Heating radiation system with infra heater presents energy economic system, handling proper unobjectionable micro-climatic conditions at workspace and notably with share on improvement life environment thereby, that burning gas is optimal from views protection life environment.

Key words: energy, infra heater, heat, humidity, industrial hall

1 Introduction

Energy obtaining is one of most important factor for society existence. Process of rationalisation economy with fuels and energies is impossible to comprehend only like run to economies of consume energy, but also like efficient exploitation reasonable primary energy sources. Question protection life environment presents pivotal problem for healthy development our society extant, which is pollution especially manufacture heat for purposes of heating. Limitation of fuel consumption of poor quality kind of unyielding fuel is the most significant steps for improvement life environment, especially brown coal and enhancement power effectively at production and supplies heat. Enhancement technical level heating systems, improvement thermal insulating quality of building, production and finality hall and object they can notably reduce fuel consumption.

This research has been supported by research project *CEZ J22/98 No.~261100007.*

2 Thermal equilibrium of the interior with radiation heating.

We must determine thermal energy input Q_p, by theoretic solution of the house heating. It is necessary for assurance of interior calculation heat of the air t_i. It must act satisfy the demand of the heat cosiness for human being by select norm calculation exterior heat t_e.

The thermal energy input Q_p usually calculates from equations of thermal equilibrium of the heating interior in the steady state. It is necessary to differentiate fundamentally the convection or panel heating by the evaluation. The convection storage heater realises heater transfer mainly with the convection and the panel storage heater realises the heater transfer mainly with the radiant heat transmission.

3 Convection heating

Heat flow inducted into interior by storage heater is from it educated one into neighbouring space or exterior to single building construction by convection and heat transfer on exteriorly building structure. Conduction and heat transfer of heat flow for j building construction Q_{EJ} is given as sum of convection for this building construction (Q_{KJ}) and radiation building construction from the others building constructions of interior Q_{SJ} by Fig. 1, so that heat equilibrium equation for arbitrary j construction is defined by

$$Q_{ej} = Q_{kj} + \sum Q_{sj} \tag{1}$$

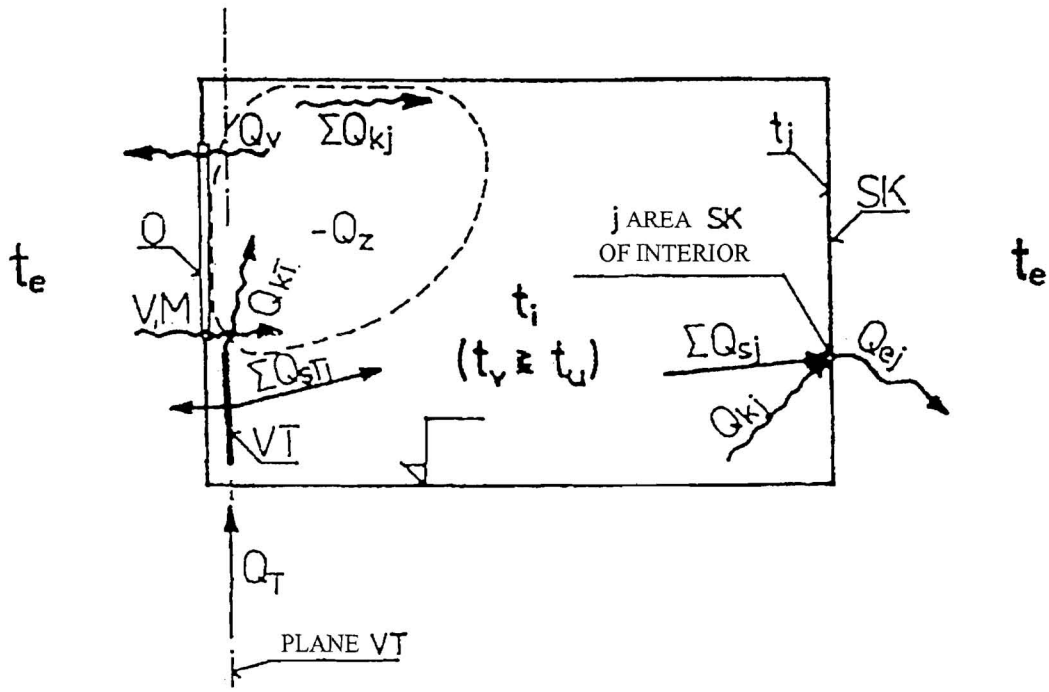

Fig. 1 Thermal equilibrium of interior to convection heating

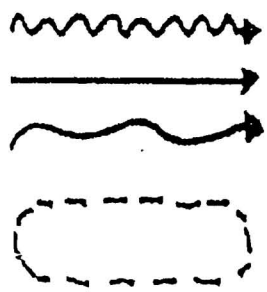

VT - convection storage heater, *SK* - building construction, *O* - window construction, *V*- volumetric infiltration air flow, *M* - weigh volumetric infiltration air flow, Q_{kt} – heat which is transmitted to interior by convection, Q_v- heat losing by aeration, Q_z- convection heat gain, ΣQ_{sTj}- heat, which is transmitted by radiation to *j*-th construction, t_e- exterior temperature, t_i- interior temperature, t_u- active temperature of cool areas, t_v- temperature in interior, *P* - radiation storage area

Fig. 2 Notation for Fig. 1 and Fig. 3.

4 Radiation heating

Heat flow bring up into interior with from it lead off into neighbouring space by radiation heating surface or into exterior of single building construction by conduction and heat transfer on exteriorly building construction. Conduction heat flow and heat transfer Q_{EJ} for j building construction is given by difference total radiation heat flow incident on j-those building construction Q_{SJ} and convention heat flow Q_{KJ} (interior air take away heat from heating radiation *j* of that surface) by Fig. 3, so that heat equilibrium equation for arbitrary *j* those building construction will be done

$$Q_{ej} = \sum Q_{sj} - Q_{kj} \tag{2}$$

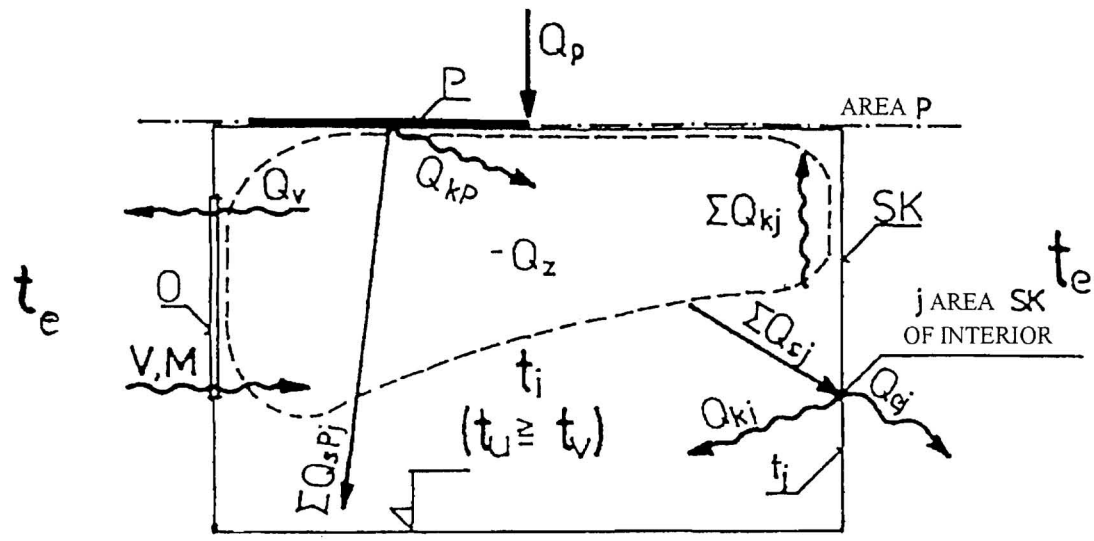

Fig. 3 Thermal equilibrium of interior to panel heating

5 Heating systems

Heating high industrial and workshop hall is very problematic. Heating air fly up. Bottom working section, where workers are situated and where heat needful is situated, air is warming less. Warming-up of big quantity of air in hall by classical method (e.g. air heating) is not only slow, but in the first place uneconomical (see Fig. 4.).

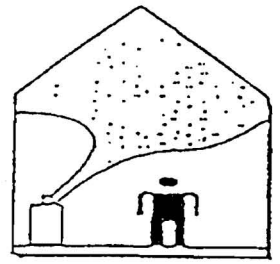

Usually system

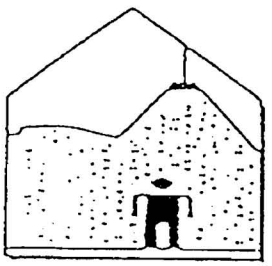

Infra heater system

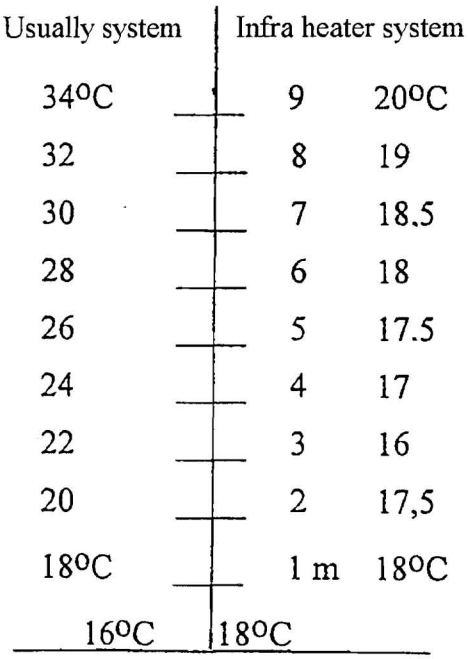

Fig. 4 Confrontation of usually and infra heater systems

6 Conclusion

Heating of big halls by gas infra heater is exceedingly economical. Big advantage is, that fall off tempering before working hours. Effect heating infra heater is appreciable almost instantly after switch on heating arrangement. Effect heating infra heater with appreciable almost instantly after switch on heating arrangement. Infra heaters can heat local, then only there, where it is necessary. It is eliminated to heat of places where workers are occurred minimum or at all.

References

[1] Kalus D.: *Gas infra incandescent radiators*, Bratislava 1996

[2] Literature of firm DIFOTTERM, Prague 1996

HYGROTHERMAL ANALYSIS FOR ENERGY CONSERVATION IN BUILDINGS WITH HISTORICAL VALUE

A. Radu, C. Georghu, P. Stefanescu

HYGROTHERMAL ANALYSIS FOR ENERGY CONSERVATION IN BUILDINGS WITH HISTORICAL VALUE

A. Radu, C. Gheorghiu, P. Stefanescu

Civil Engineering Department, Faculty of Construction and Architecture, Bd. D. Mangeron 43, Iasi 6600 Romania

Abstract

In the case of buildings with historical value, the thermal rehabilitation measures for energy conservation are possible only by adding an insulation layer over the internal side of the external walls. Structural interventions for consolidation, with reinforced concrete could also be made and, in order to avoid any undesirable condensation phenomena, a bidirectional analysis of the vapor diffusion field should be made. Despite its limited capacity, the 1-D Glaser method is recommended by today's technical codes. Some typical cases have been studied assuming the same principles and using for the 2-D diffusion field analysis the same software as for the 2-D thermal field exploration. As a result, the necessity of prolonging the thermal insulation on the lateral partition elements has been established.

Key words: historical buildings, energy conservation, heat and mass transfer, numerical simulation

1. Introduction

The most efficient way of improving the thermal protection capacity of the building external walls is to add an outside insulation layer on the frontages. However this is not admissible in the case of old buildings having architectural and cultural value (museums, schools, churches, and dwellings). Therefore, in such cases the intervention must be located on the inner face of the external walls. A reinforced concrete element (lintel, pillar, tie beam or coating) is often necessary to satisfy today's safety requirements against the seismic action.

A complex local heat and mass transfer bridge is created and a condensation risk could often occur at the junction between the external wall and the internal partition elements (walls and floors): see fig. 1.

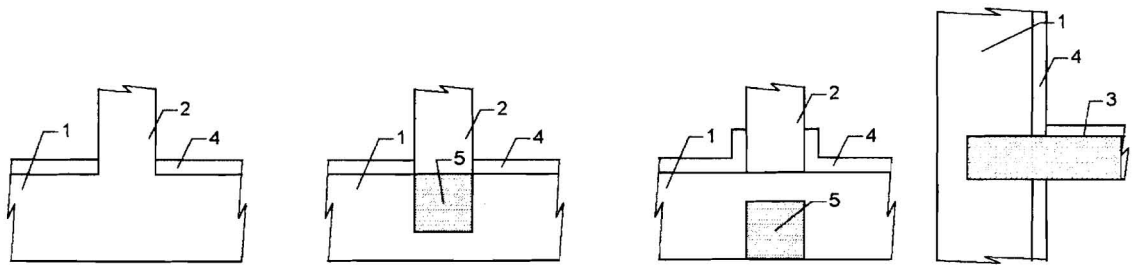

Fig.1 Heat and mass transfer bridges at the junction between the external and internal building elements: 1- masonry external wall; 2- masonry internal wall; 3- reinforced concrete floor; 4- additional thermal insulation layer; 5- reinforced concrete element

To control and prevent condensation phenomena, a bidirectional (2-D) analysis of the heat and vapor diffusion is necessary. The classical Glaser method [1] has a limited capacity, by solving only 1-D problems in steady state regime and neglecting some connected liquid or pellicular moisture transfer and the influence of changing the material humidity on the thermal conductivity and vapor permeability. However, the Glaser method is recommended by the technical codes and used in design practice giving good, conservative results. Attempts to solve the 2-D transfer, based on the Glaser assumptions and using electrical models or numerical simulations with finite and boundary elements have been realized before [2,3,4,5]. A computer software WUFI has also been developed for simultaneous complex heat and moisture transport by M. Kunzel [6]. Their utilization in design practice is quite difficult. Assuming that the moisture transport is driven by the vapor diffusion alone, the present research has been realized using the same finite elements computer software for both thermal and diffusion field analysis in steady state regime. This possibility has been mentioned by G.T .Dow [7].

2. Mathematical and physical background

The mathematical model for heat transfer and vapor diffusion is presented in tab. 1.

Tab. 1 Mathematical model

-Heat transfer by conduction-		-Vapor migration by diffusion-	
$\frac{\partial}{\partial x}\left(\lambda\frac{\partial\theta}{\partial x}\right)+\frac{\partial}{\partial y}\left(\lambda\frac{\partial\theta}{\partial y}\right)+I=0$	(1)	$\frac{\partial}{\partial x}\left(\mu\frac{\partial p_v}{\partial x}\right)+\frac{\partial}{\partial y}\left(\mu\frac{\partial p_v}{\partial y}\right)+I=0$	(1')
$\theta=\theta(x,y)$	(2)	$p_v=p_v(x,y)$	(2')
$\lambda\frac{\partial\theta}{\partial n}=\alpha(\theta_i-\theta_e)$	(3)	$\mu\frac{\partial p_v}{\partial n}=\beta(p_{vi}-p_{ve})$	(3')
$\lambda_1\left\|\frac{\partial\theta}{\partial n}\right\|_1=\lambda_2\left\|\frac{\partial\theta}{\partial n}\right\|_2$	(4)	$\mu_1\left\|\frac{\partial p_v}{\partial n}\right\|_1=\mu_2\left\|\frac{\partial p_v}{\partial n}\right\|_2$	(4')

It can be easily observed that the mathematical models for heat transfer by conduction and vapor diffusion are of identical form. Therefore any available software for heat transfer analysis can also be used for the vapor diffusion field analysis. However there are also differences:

$$p_v \le p_s \qquad (5)$$

$$\beta_i = \beta_e = \infty \qquad (6)$$

3. Numerical simulation

Let us consider the case of an intersection between the external wall and internal wall, presented in fig. 2. The thermophysical characteristics of the building materials are presented in tab. 2.

Tab. 2 Thermophysical characteristics

Name of building material	Density ρ [kg/m^3]	Thermal cond. λ [W/mK]	Vapor permeability μ [g/m h mmHg]
Ceramic brick masonry	1800	0.8	14
Expanded polystirene	20	0.03	-
Reinforced concrete	2500	1.74	5

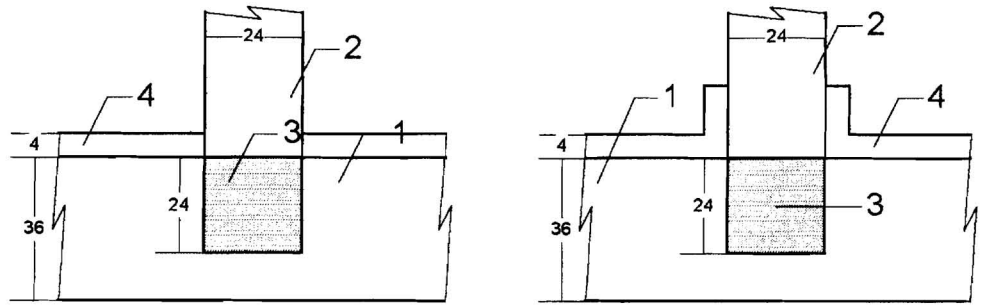

Fig. 1 Junction between the internal and external walls: a- thermal insulation only at the exterior wall, b- added thermal insulation at the interior wall; 1- masonry external wall, 2- masonry internal wall, 3- reinforced concrete pillar, 4- additional insulation layer

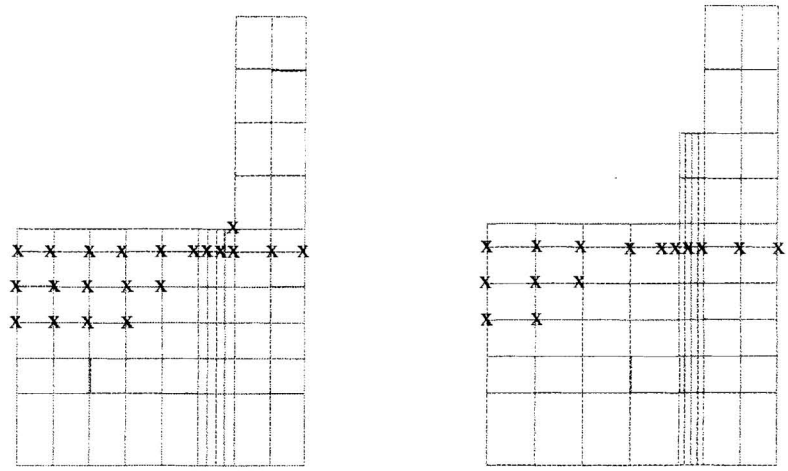

Fig. 2 Discretization used in finite element analysis, considering half of the model because of symmetry; the marked points represent the real condensation zone

The finite element discretization (fig. 2) has been made using a rectangular mesh with variable dimensions: Δx=1...6cm, Δy=4...12cm. The finest mesh has been used for the most susceptible condensation areas (e.g. the inner corner between the exterior and interior walls).

The steps involved in simulation analysis are shown in fig. 3.

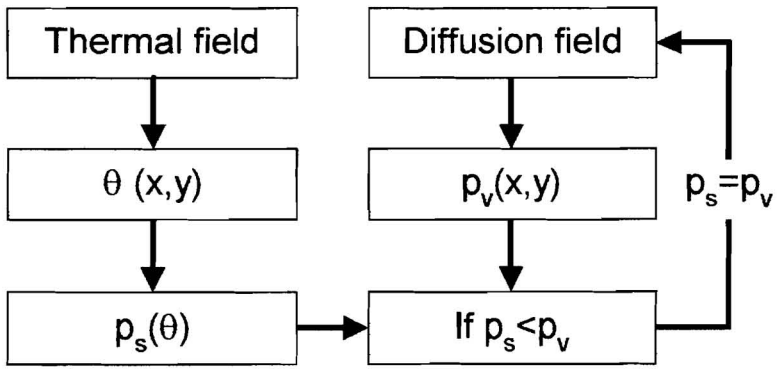

Fig. 3 Flowchart of the simulation analysis

The first simulation concerns the thermal field analysis. Through this analysis the temperatures for each point in the mesh has been obtained (fig. 3). Then, the saturation

Acknowledgments

The financial support for the described research investigation was provided by the INCO-COPERNICUS programme and the Technical University of Iaşi. The authors would like to express their gratitude for the support received.

References

1. Glaser, G., Graphisches Verfahren zur Untersuchung vom Diffusionsvorgangen, Kaltetechnik, 11, Heft 10, 1959.
2. Radu, A., Representation analogique des champs thermique et de diffusion pour l'etude de la condensation dans les elements de construction, Ann. Int. pour le calcul analogique, 2, 1968.
3. Radu, a., Biborosch, L., Elektrische Analogieverfahren von Diffusionsvorgangen in Wanden mit Warmerbrucken bei Ausscheidung von Wasser, Kaltetechnik, 1, 1968.
4. Radu, A., Vornicu, T., Zweidimensionale Berechung der Warmeleit- und Wasserdampfvorgangen in aussenbauteilen, Bauphysik, 10, H-1, 1988.
5. Stefanescu, D., Determining water vapor diffusion field in boundary element method, Bul. I.P.I, t.XLIII (XLVII) 3-4, 1997.
6. Kunzel, H.M., Verfahren zur ein- und zweidimensionalen Berechnung des gekoppelten Warme- und Feutchtetransports in Bauteilen mit Kennwerten. Diss. Univ. Stuttgart, 1994.
7. Dow, G., Effect of repeated thermal and moisture bridges on the steady state calculation of interstitial condensation, CIB W40 Meeting "Heat and Moisture Transfer in Buildings" Kyoto, Japan, 1997.

MOISTURE MOVEMENT IN CLOTHING UNDER GRAVITY

S. Takada, S. Hokoi, M.K. Kumaran

MOISTURE MOVEMENT IN CLOTHING UNDER GRAVITY

S. Takada[1], S. Hokoi[1], M. K. Kumaran[2]

[1]Department of Architecture and Environmental Design, Graduate School of Engineering, Kyoto University, Yoshidahonmachi, Sakyo-ku, Kyoto, 606-8501 Japan
[2]Building Envelope and Structure, Institute for Research in Construction, National Research Council, Canada, Ottawa, Ontario, K1A 0R6 Canada

E-mail: satoruta@archi.kyoto-u.ac.jp, hokoi@archi.kyoto-u.ac.jp, kumar.kumaran@nrc.ca

Abstract

A model of the liquid moisture movement under gravity in cloth is investigated in this paper. Firstly, the moisture diffusivity is determined from the experiment on the moisture absorption process in the horizontal direction where the gravity does not have influence on the moisture movement. Secondly the moisture absorption process in the vertical upward direction where the gravity has influence on the movement is analyzed with the use of the moisture diffusivity determined above. The validity of the parameter related to the gravity effect (the gradient of the equilibrium relationship) is investigated by comparing the result of the numerical calculation with that of the experiment using a gamma-spectrometer for the same kind of cloth. In conclusion, since they agree as a whole, the model proposed here can be used.

Key words: moisture diffusivity, equilibrium relationship, gamma-spectrometer, clothing, sweat, thermophysiology

1 Introduction

In order to realize healthy and comfortable air-conditioning, it is important to grasp the thermophysiological response of human body to the thermal and hygric environment. Especially under an environment where regulatory sweating occurs intensively, most of the liquid moisture as sweat is once absorbed into the clothing, then accumulates in it, and at last, evaporates at the outer surface of the clothing. In such a situation, the rate of evaporation from the clothing surface, which is a function of the moisture content of the clothing surface, will have a significant influence on the body temperature regulation system [1]. Therefore it is important how the moisture absorbed into the clothing diffuses in the clothing. From such a viewpoint, the authors have been studying the liquid moisture movement in cloth and have shown the moisture movement in the horizontal direction can be described with a diffusion model [2]. In this paper, the moisture movement under gravity is investigated based on the water content measurement using gamma-spectrometer. With the use of the model described in section 2, this measurement is analyzed numerically.

2 Basic equations

The moisture flux in a porous material under gravity is expressed in two ways as follows for vertical coordinate z, where the direction of gravity is taken as negative [3].

$$q_w = -D_w \frac{\partial w}{\partial z} - \lambda'_\mu g \quad \text{or} \quad q_w = -\lambda'_\mu \left(\frac{\partial \mu}{\partial z} + g\right) \qquad \text{(1-a, 1-b)}$$

where, q_w : moisture flux [kg/{(cm)^2□s}], w : volumetric water content [(cm)^3/(cm)^3],
D_w: moisture diffusivity due to w gradient [kg/(cm□s)], z : coordinate [cm],
μ : water chemical potential [J/kg], g : gravity acceleration [cm/s^2],
λ'_μ : moisture conductivity due to μ gradient [kg/{(J/kg)□cm□s}].
Now the equilibrium relationship (sorption isotherm) of cloth is written as equation (2).

$$\mu = f(w, T) \qquad (2)$$

$$\frac{\partial \mu}{\partial z} = \frac{\partial \mu}{\partial w}\frac{\partial w}{\partial z} + \frac{\partial \mu}{\partial T}\frac{\partial T}{\partial z} \qquad (3)$$

where, f : equilibrium relationship [J/kg], T : temperature [K].
By neglecting the effect of temperature on the equilibrium relationship [4], the second term on the right-hand side of equation (3) becomes zero, and by comparing equations (1-a) and (1-b), equation (4) is obtained, which describes the relationship among three variables: 1) moisture diffusivity D_w, 2) gradient of equilibrium relationship to moisture content $\partial\mu/\partial w$, 3) moisture conductivity due to water chemical potential λ'_μ.

$$D_w = \lambda'_\mu \frac{\partial \mu}{\partial w} \qquad (4)$$

The moisture balance equation in the cloth is written as equation (5), when the liquid moisture transfer is superior to vapor one. In equation (5), the evaporation on the surface of the cloth is taken into account.

$$\frac{\partial u}{\partial t} = -\frac{\partial}{\partial z}\left[-D\frac{\partial u}{\partial z} - \frac{1}{a\rho_w}\cdot\lambda'_\mu g\right] - \frac{1}{a\rho_w}\cdot\frac{E}{l} \qquad (5)$$

where, u : degree of saturation($= w/a$), t : time [s], a : porosity of cloth [(cm)^3/(cm)^3],
ρ_w : density of water [kg/(cm)^3], l : thickness of cloth [cm],
E : evaporation rate at cloth surface [kg/{(cm)^2□s}], and $D = D_w/\rho_w$.
Though equation (5) can also be written with the use of water chemical potential, the measurement of it is difficult. Therefore the expression using moisture content is adopted here.

In the following section, the experiments are conducted on the moisture movement in the direction perpendicular to the gravity (horizontal direction) and the moisture diffusivity D is determined by analyzing it. Then in section 4, the experiments on the moisture movement under gravity are conducted and analyzed numerically using the moisture diffusivity determined in section 3.

3 Moisture movement in horizontal direction [2]

3.1 Experiment

A strip of cotton broadcloth (size: 30*200*0.25 [mm]) is put on the frame made of fishing line and one of the edges of the strip is dipped into the water at t=0. The

moisture content distribution is measured gravimetrically by cutting the specimen at an interval of 1 [cm]. The distribution is measured five times at t=100, 200, 300, 400, 600 [s]. The result is shown in Fig. 1 along with the computational results.

3.2 Analysis

Equation (5) is solved numerically, where the gravity acceleration is put at zero and the vertical coordinate z is replaced with the horizontal coordinate x. The direction of the moisture movement from the water reservoir is taken as positive. For the boundary condition at x=0 (just near the water reservoir), the measured values are used. The moisture diffusivity D is determined so that the calculated moisture content distribution agrees with the experimental. The determined D is given by equation (6) and the calculated result using it is shown in Fig. 1. The calculated and experimental results agree well.

$$D = 4.0\times10^{-5}\cdot\exp(9u) \quad [(cm)^2/s] \quad (u \le 0.7)$$
$$= 0.02 \quad [(cm)^2/s] \quad (u > 0.7) \tag{6}$$

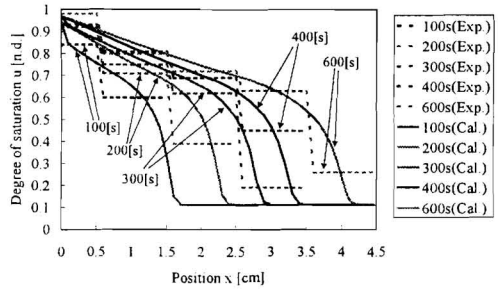

Fig. 1 Distribution of u (Moisture movement in horizontal direction)

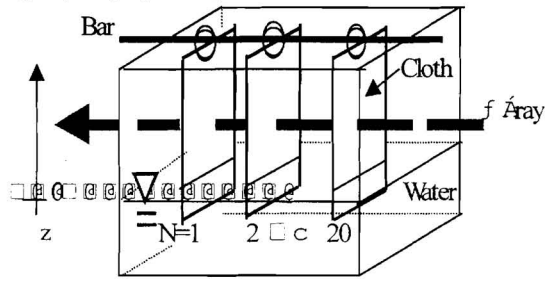

Fig. 2 Experimental setup (Moisture movement in vertical direction)

4 Moisture movement in vertical direction

4.1 Experiment

In section 3, the moisture content during the water absorption process in the horizontal direction was measured gravimetrically. In this section, the process under gravity is measured with the use of the gamma-spectrometer in National Research Council, Canada. The experimental setup is shown schematically in Fig. 2. One hundred and fifty [ml] of distilled water is in a box made of plexiglass (size: 308*165*153 [mm]), and at t=0, twenty sheets of broadcloth specimen (size: 40*100*0.25 [mm]) hung on a bar are immersed 1 [cm] into the water. This measurement is based on sensing the gamma-ray absorption by the moisture contained in the specimen [5]. The gamma-ray absorption by only one or two sheets of cloth is too small to measure accurately, and from the preparatory test, twenty was found to be enough. Separators are attached between the sheets on the bar lest they should contact each other. In this way, the variation of the moisture content is measured at seven heights (z=0.8, 1.3, 1.8, 2.3, 2.8, 3.3, 3.8 [cm]; The origin of coordinate z is set at the water surface shown as in Fig. 2.) In obtaining every datum, gamma-ray beam is radiated for ca. 30 [s] at the point. The interval of the measurement is ca. 45 [s].

The results are shown along with the calculated results in Fig. 5 and 6. The range of the fluctuation in the measured values of the degree of saturation reaches 0.1 at the maximum, and it is not so small. However, since the fluctuation is random, the averaged data can be used.

4.2 Analysis

Based on equations (5) and (6), the distribution of degree of saturation at each time is calculated numerically. The boundary condition at z=0 is given as saturation, that is u=1. The equilibrium relationship, whose gradient is related to the effect that the gravity has on the moisture movement, is determined as follows.

4.2.1 Equilibrium relationship

In the field of textile, there are several measurements on the equilibrium relationship of cloth. Very few data, however, are obtained just near saturation, the important region in the present analysis. In this study, the equilibrium relationship near saturation is decided from the moisture content distribution in equilibrium state. In an equilibrium state, the water chemical potential is a function of position as follows.

$$\mu = -g z \tag{7}$$

Here, based on the moisture content distribution measured during t=76 to 109 [min], when the distribution is nearly stationary, the equilibrium relationship was decided. It is shown in Fig. 3, along with the approximation function. In a strict sense, the distribution is not in an equilibrium state, since the moisture evaporation continues on the surface. In this study, however, it is assumed that the influence of the evaporation can be neglected and that the moisture distribution equilibrates. Using the gradient of the approximation function in Fig. 3, the moisture conductivity λ'_μ is obtained from equation (4). The parameters determined through these procedures are shown in Fig. 4.

4.2.2 Comparison with experiment

As shown in Fig. 5, the calculated values agree well with the measured results during t=0 to 20 [min]. As for z=0.8 [cm], the calculated values are smaller as a whole and it seems that there is still some room for improvement in determining the parameters for the higher moisture content region. On the other hand, the calculated values are too lower after t=20 [min] at the points far from the water surface. This seems to be due to the overestimation of the evaporation on the surface. In the current calculation, the humidity ratio of the ambient air is given as constant, while in reality the humidity ratio around the cloth seems to have increased owing to the evaporated moisture in the course of time. The result of a calculation in which the evaporation is neglected is shown in Fig. 6. Even at the point far from the water surface, the calculated values agree well with the measured after t=50 [min]. Therefore if the humidity ratio of the ambient air were given properly, the measured values would coincide with the calculated. Thus it can be said that the assumptions and parameters used in this investigation are valid as a whole.

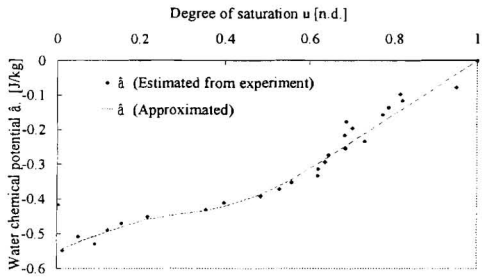

Fig. 3 Equilibrium relationship

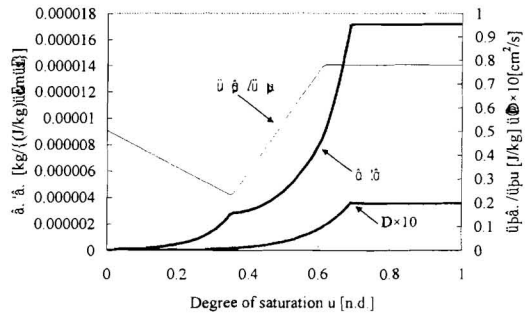

Fig. 4 Parameters used in calculation

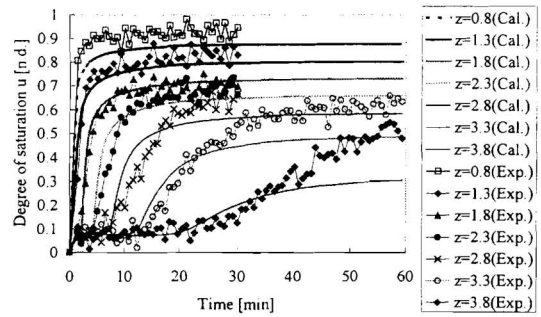

Fig. 5 Variation in u (z in [cm], Evaporation is considered in the calculation.)

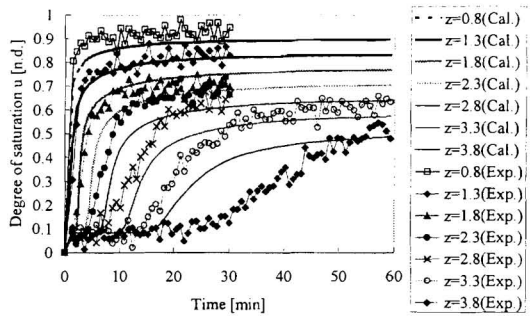

Fig. 6 Variation in u (Evaporation is neglected in the calculation.)

4.2.3 Width of gamma-ray beam passing through specimen

If a gamma-ray beam radiated from the source propagated exactly horizontally, the distance between the specimen and the source would have nothing to do with the measured amount of gamma-ray which reaches the detector. However, the locus of the gamma-ray beam is not usually horizontal and the gamma-ray diffuses gradually as it propagates. In other words, the scanned area in the specimen changes depending on the distance between the gamma-ray source and the specimen. Fig. 7 shows the schematics of the process. In measuring a specimen whose absorption coefficient distribution is homogeneous or changes linearly in the direction of scanning, the difference between the measured values and the true values at the center point of the measured area will be very little. On the other hand, for a specimen with a non-linearly distributing absorptivity, the distance between the source and the specimen will have a significant influence on the results.

The relationship between the distance from the source and the width of the beam is estimated from another experiment (detection of water surface with the distance varied). As the result, the width is 0.52[cm] at the minimum (Sheet No.20 in Fig. 7) to 1.07[cm] at the maximum (Sheet No.1). The obtained data must be the summation of every sheet whose scanned width is a function of distance from the gamma-ray source. Using the relationship, the calculated results in Fig. 6 is modified in order to correspond to the measured results. It is shown in Fig. 8. 'Fig.6' in legend is the same data as in Fig. 6 (not modified), and 'Mod.' means the modified data. Although they differs slightly at the points far from the water surface in the early stages of the moisture absorption, the difference is small as a whole, which means the distribution of moisture content is

almost linear.

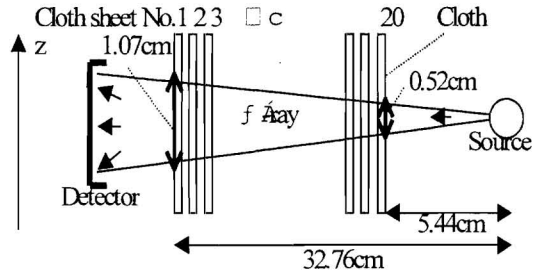

Fig. 7 Schematics of gamma-ray diffusion

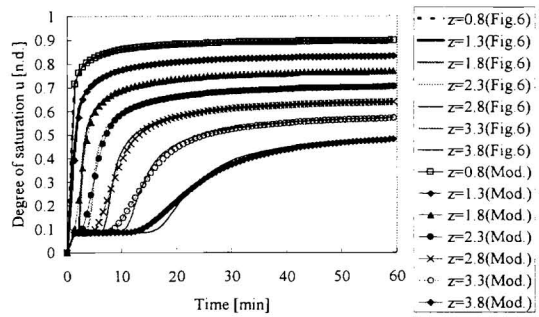

Fig. 8 Variation in u (calculated)

5 Conclusions

The liquid moisture movement in the cloth is investigated for broadcloth made of cotton. The obtained conclusions are as follows.

a) The moisture diffusivity is determined based on the experiment of water absorption process for cloth supported horizontally.
b) The water absorption in the opposite direction with the gravity is measured with the use of the gamma-spectrometer, and the result is analyzed with the diffusion model considering the gravity effect. The calculated results agree with the experimental results as a whole. The proposed model can be used.

Acknowledgement

This research was partially supported by the Ministry of Education, Science, Sports and Culture of Japan, Grant-in-Aid for Encouragement of Young Scientists, 10750438, 1998, and by The Kyoto University Foundation. Thanks are offered to Mr. R. Marchand, Dr. M. Nafal and Mr. J. Lackey for help with the measurement using gamma-spectrometer at National Research Council, Canada.

References

[1] S.Takada, S.Hokoi, N.Kawakami and M.Kudo; Experimental Study on Thermo-physiological Response of Clothed Subjects Exposed to Thermal Transients - Sweating and Evaporation Process -, Journal of the Human-Environment System 2,1, pp.57-67, 1999.
[2] S.Takada, S.Hokoi and T.Umeno; Heat and Moisture Movement in Clothes, Proceedings of CIB W40 meeting, Kyoto, Japan, pp.277-290, 1997.
[3] M.Matsumoto, S.Hokoi, M.Yamamoto; Summaries of Technical Papers of Annual Meeting, Architectural Institute of Japan D, pp.889-890, 1985. (in Japanese)
[4] M.Matsumoto, Shin-kenchikugaku taikei 10, Shoukokusha, 1984. (in Japanese)
[5] M.K.Kumaran and M.Bomberg; A gamma-spectrometer for determination of density distribution and moisture distribution in building materials, Proceedings of the International Symposium on Moisture and Humidity, Washington, D.C., 485-489, 1985.

MOISTURE PENETRATION DEPTH FOR PERIODICALLY VARYING RELATIVE HUMIDITY AT THE BOUNDARY

J. Arfvidsson

MOISTURE PENETRATION DEPTH FOR PERIODICALLY VARYING RELATIVE HUMIDITY AT THE BOUNDARY.

Jesper Arfvidsson
Lund University, Dept of Building Physics, Box 118, 221 00 Lund, Sweden
jeper.arfvidsson@byggtek.lth.se

Abstract
The paper presents a method to calculate the moisture penetration depth and the undisturbed moisture level, inside the region of periodic variation, in a porous material subjected to a periodic relative humidity variation at the boundary. The moisture properties may be highly non-linear. The method is strictly valid for a semi-infinite material. The theory to determine the undisturbed moisture level is given in detail, and a calculation method to determine the penetration depth is presented. Results for three different building materials subjected to daily and annual periodic relative humidity at the boundary are given.

Keywords: penetration depth, moisture flow, Kirchhoff potential

1 Introduction

A building material is normally exposed to moisture conditions that are variable with time. Natural variations in moisture state can often be described as a periodic variation. A material exposed to such periodic moisture conditions during a long time will take up or loose humidity in a periodic way.

Figure 1 illustrates the solution for a periodic variation at the boundary. The relative humidity varies between a maximum (70%) and a minimum value (30%) during the period time t_p (24hours). The curves in the figure are the moisture distribution at different times (t_p, $t_p/4$, $t_p/2$, $3t_p/4$) during the time period t_p. The dotted curves show the maximum and minimum values at different depths in the material. We see how the range of relative humidity variation decreases with the depth. Let x_p be the point where the relative humidity variation is equal to 1%. We define this point x_p as the *penetration depth*, see Figure 1.

In moisture calculations a complication is the non-linear behaviour. The mean value of the surrounding relative humidity is not the same as the value of the relative humidity in the material at the penetration depth and inwards. We define this value as the *undisturbed relative humidity*, φ_{und}. See Figure 1. Here the mean value for the surrounding relative humidity is 50% but the undisturbed value deep in the material becomes 56%. The variation of the relative humidity is, due to non-linearity, not symmetric.

The method presented below determines the moisture penetration depth and the undisturbed relative humidity in a material subjected to a variable surrounding relative humidity. The model determines a single value, which in a correct way represent a variable boundary condition in a material, taking non-linear effects into account. This

value is valid from the penetration depth and further into the material. The method is strictly valid for a semi-infinite material.

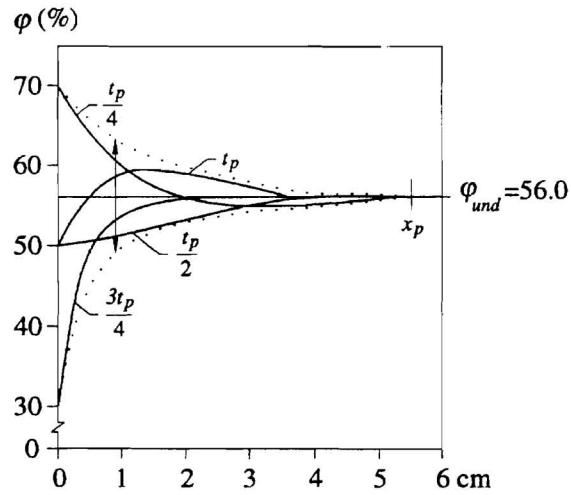

Fig. 1. The moisture distribution at different times during the period time t_p due to a periodic boundary condition at the boundary. The amplitude of the variation (dotted lines) decreases with the depth. The penetration depth for the variation is marked x_p.

2 Calculation model

The model presented uses the Kirchhoff potentials to describe the moisture transport. This simplifies the model considerably. A short description of the Kirchhoff potentials is given in the next section.

2.1 Kirchhoff potential

Let g denote the moisture flow and ϕ any moisture flow potential. In the one-dimensional case we have, when temperature effects and hysteresis are neglected:

$$g = -D_\phi(\phi)\frac{\partial \phi}{\partial x} \tag{1}$$

Here ϕ may denote relative humidity φ, absolute humidity v or water vapour pressure p in gas phases, pore water pressure $P_{p.w.}$ chemical potential μ_w for water or moisture content w. The flow coefficient D_ϕ depends on ϕ. Kirchhoff originally introduced Kirchhoff's flow potential, when the flow coefficient is a function of the state [1]. This potential is defined by:

$$\psi(\phi) = \psi_{ref} + \int_{\phi_{ref}}^{\phi} D_\phi(\phi)\, d\phi \tag{2}$$

It is a function of ϕ for each material: $\psi = \psi(\phi)$. The flow potential ψ is independent of which ϕ and D_ϕ one chooses to use. The reference values ϕ_{ref} and ψ_{ref} can be chosen arbitrarily for each material. We normally, by convenience, put the value of ψ to zero for a reference level ϕ_{ref} for the material: $\psi(\phi_{ref}) = 0$

The moisture flow equation (1) becomes:

$$\vec{g} = -\nabla\psi \tag{3}$$

The formulation using Kirchhoff potentials are further investigated and explained in [2].

2.2 Mathematical problem

We have the following mathematical problem. The moisture balance equation, using the Kirchhoff potential, is in the one-dimensional case:

$$\frac{\partial w}{\partial t} = \frac{\partial^2 \psi}{\partial x^2} \qquad w = w(\psi) \tag{4}$$

The boundary moisture state varies periodically:

$$w(0, t + t_p) = w(0,t) \tag{5}$$

We seek the truly periodic solution:

$$w(x, t + t_p) = w(x,t) \tag{6}$$

$$\psi(x, t + t_p) = \psi(x,t) \tag{7}$$

It is obtained for example by starting with a constant value for $w(x,0)$, $0<x<\infty$, and continuing the calculations for many periods until the above periodic conditions for $\psi(x,t)$ and $w(x,t)$ are attained.

2.3 Theory for undisturbed moisture values during a periodic process

The undisturbed moisture level φ_{und}, ψ_{und} etc. of the periodic process at depth $x \geq x_p$ inside the material is of great interest. The convergence to truly periodic conditions is much more rapid if we start with this undisturbed value in the material. The technique to determine the undisturbed value is presented below.

Consider a periodic process with a period time t_p , and boundary condition according to (5). Then w and ψ vary periodically (6) and (7). The moisture balance equation is integrated in time over a whole period t_p. The left hand side of the equation (4) then becomes zero:

$$\int_t^{t+t_p} \frac{\partial w(x,t)}{\partial t} dt = w(x, t + t_p) - w(x,t) = 0 \tag{8}$$

The right hand side of the equation becomes:

$$0 = \int_t^{t+t_p} \frac{\partial \psi^2(x,t)}{\partial x^2} dt = \frac{\partial}{\partial x^2} \left(\int_t^{t+t_p} \psi(x,t)\, dt \right) \tag{9}$$

Let $\psi_m(x)$ be the mean value of ψ at the depth x during the period:

$$\psi_m(x) = \frac{1}{t_p} \int_t^{t+t_p} \psi(x,t) dt \tag{10}$$

Then we have, according to equation (9) that $\psi_m(x)$ is linear in x:

$$\frac{d^2}{dx^2}(\psi_m(x)) = 0 \quad \Rightarrow \quad \psi_m(x) = A \cdot x + B \qquad 0 < x < \infty \tag{11}$$

In the limit $x \to \infty$, we have:

$$\psi_m(\infty) = A \cdot \infty + B \tag{12}$$

Because ψ_m is limited A=0. This means that ψ_m will be independent of x:

$$\psi_m(x) = B = \psi_m(0) \tag{13}$$

We have the result that the mean value of $\psi(x,t)$ over a time period is equal to the average value of ψ at the boundary $x=0$. By calculating $\psi_m(0)$ from the periodical

boundary condition the mean value for all x is obtained. For large values of x, where the variation is completely reduced. We know the ψ-value. So we have:

$$\psi_{und} = \psi_m(x \geq x_p) = \psi_m(0) \qquad (14)$$

From the material data relations we also know the corresponding relative humidity, φ, and the moisture content, w.

2.4 Determination of the penetration depth

When the undisturbed value for the relative humidity in the material is known for a specific periodical variation of the relative humidity on the boundary, the penetration depth can be calculated using a one- dimensional moisture calculation program. We define the amplitude as the difference between the maximum and minimum value of the relative humidity in the material at each point x. The amplitude is the dotted line in Figure 1. This amplitude will decrease with the distance from the exposed boundary. . Let x_p be the point where the relative humidity variation is equal to 1%. We define this point as the penetration depth, see Figure 1.

Consider a sufficiently thick piece of material. As initial relative humidity we put the undisturbed relative humidity φ_{und}, determined with the above shown technique. This relative humidity is also put as boundary condition on one side of the material. On the other side we have the periodical boundary condition. Then we calculate the moisture distribution in the material during that number of periods necessary to get identical solutions during one period and another.

The solution is found faster putting this undisturbed relative humidity φ_{und} as initial condition in the calculation. Any other value would require longer calculation time to obtain the right solution.

2.5 Computer program JAM-P

A computer program (JAM-P), especially designed to perform this kind of calculations, has been developed. An explicit forward difference method is used to solve the moisture balance equation (4). The numerical calculations involve two steps. The spatial distribution of ψ at a certain time-step determines the moisture flows and hence the net accumulation of moisture in each calculation cell. Thus, the new moisture distribution at the following time-step is known from the relation between ψ and w. A full description of the used numerical technique is found in Arfvidsson and Claesson, 1998.

The program needs material data where the relation between moisture content w, relative humidity φ, and Kirchhoff potential ψ is specified for the actual interval in relative humidity. The working procedure for the program JAM-P is:

- The cyclic boundary condition is given as two levels of relative humidity φ_1 and φ_2, valid during the times t_1 and t_2, respectively.
- ψ_{und} is determined for the actual moisture variation at the boundary
- The corresponding value φ_{und} (from material data) is given as initial condition in the calculation.
- The boundary condition φ_{und} is put on one side and the actual variable boundary condition on the other.
- A one-dimensional transient moisture flow calculation is made for five period times.
- The result is presented graphically. Curves for the maximum and the minimum relative humidity from the boundary and inwards to the undisturbed constant value are shown.

2.6 Calculation on four materials

The program JAM-P has been used to calculate penetration depths and relative humidity levels in different materials subjected to periodic variations of relative humidity with different period time. Four building materials is chosen; spruce, brick, lightweight concrete, and concrete with water cement ratio 0.7.

Two different cyclic boundary conditions are chosen. The relative humidity varies between two constant values 50% and 90% in both cases. They represent a climatic variation over 24-hours and over a year.

All used material data except brick is from steady-state measurements presented by Hedenblad [3]. Brick is from Andersson [4].

3 Results and Discussion

The result, using the described method, is shown in figure 2. The penetration depth x_p and the undisturbed relative humidity in the material φ_{und} are summarised in Table 1. It should be noticed that the mean value of the relative humidity of the boundary is 72.5%.

We start with the results from the calculations with a period time of 24 hours. The result shows that we can group the tested materials into two groups. The two qualities of concrete and wood have a diurnal penetration depth of about 1cm. Lightweight concrete, brick and sandstone have a diurnal penetration depth of 5 to 8 cm.

In the calculation results with a period time of one year we find the same two groups of materials again. Wood and concrete have an annual penetration depth of 10 to 15 cm and the other materials more than 70 cm.

The undisturbed relative humidity φ_{und} differs in the materials. Concrete with W_0/C=0.7 have the highest value, φ_{und} =88%. Lightweight concrete, and brink have lower values on the undisturbed relative humidity. The values are closer to the average relative humidity at the boundary. Wood shows a value in-between.

Table 1. Undisturbed relative humidity φ_{und} and moisture penetration depth for the two cyclic conditions (table 2) and six materials.

Material	φ_{und} (%)	x_p (cm) 24h	x_p (cm) 1 year
Concrete W_0/C=0.7	88	1	12
Lightweight concrete	77	6	72
Brick	77	8	94
Spruce (tangential)	83	1	15

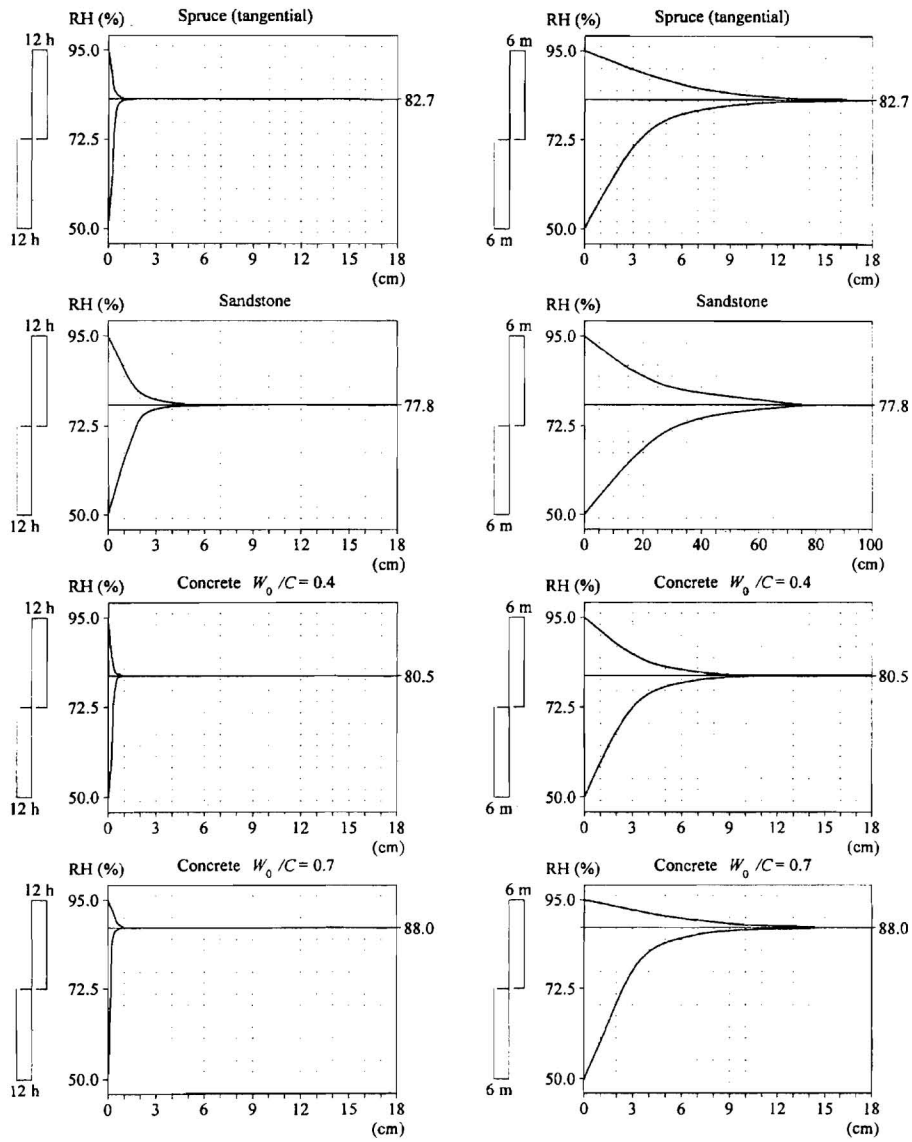

Fig. 2 Result for Diurnal (left) and annual (right) variation of relative humidity at the boundary for three materials.

References

1. Carslaw, H. and J.C. Jaeger, 1959. *Conduction of Heat in Solids*, pp. 8-13, 2:nd ed., Oxford University Press, Oxford.
2. Arfvidsson , J and Claesson, 1998. *Moisture Transport Calculation in Building Materials using Kirchhoff Potentials*. Accepted for publication in Building and Environment.
3. Hedenblad, G. 1996. *Material data for Moisture Transport Calculation.* (In Swedish) T19:1996, Byggforskningsrådet, Stockholm.
4. Andersson, A-C. 1985. *Verification of Calculation Methods for Moisture Transport in Porous Building Materials.* Document D6:1985, Swedish Council for Building Research, Stockholm, Sweden.

" *theory*, ASHRAE Transactions, Vol 96, Part 1, pp. 447-454, 1990.

FREEZING-THAWING PROCESSES IN BUILDING WALLS

FREEZING-THAWING PROCESSIS OF GLASS FIBER BOARD

S. Hokoi, M. Hatano, M. Matsumoto, M.K. Kumaran

FREEZING-THAWING PROCESSES IN BUILDING WALLS
- Freezing-Thawing Processes of Glass Fiber Board -

S. Hokoi[1], M. Hatano[2], M. Matsumoto[3], M.K. Kumaran[4]

[1]Professor, Graduate School of Engineering, Kyoto University, Japan, Dr. Eng.
[2]Government of Housing Loan Corporation, Japan, Mr. Eng.
[3]Professor, Faculty of Engineering, Osaka Sangyo University, Japan, Dr. Eng.
[4]National Research Council, Canada, Ph.D.

Abstract

For the prevention of vapor condensation and damage by it in cold regions, behaviors of water and ice in porous materials should be understood. In this study, experiments on the freezing-thawing processes of a glass fiber board, which is a typical insulation, are conducted. The freezing-thawing processes are analyzed with the use of simultaneous heat and moisture transfer equations that take into account the existence of ice.

The result of the analysis agrees with that of the experiment on the whole. In materials with large pores such as glass fiber board, the moisture transfers mainly in gaseous phase. As a result, the maximum ice content is found at the colder boundary of the wall, which differs from the result in our previous investigation [3] for the soil (Leda Clay) whose pores are much smaller.

Keywords: Vapor condensation, Heat and moisture transfer, Freezing-thawing, Transport properties, Glass fiber

1. Introduction

While vapor condensation on an inner wall surface has been decreasing due to appropriate thermal insulation and designs aimed at preventing condensation damage, the possibility of condensation inside the wall may be increasing. Especially in cold regions, liquid water may freeze in porous building materials and cause serious damage. In order to avoid condensation damage, the transient state of the water and ice in materials should be predicted. From such a point of view, a basic theory on freezing-thawing processes has been proposed and analytical examples with respect to soil and snow have been shown [1][2].

In our previous paper [3], the freezing-thawing processes in a wall made of soil (Leda Clay) were analyzed. The present paper reports the experimental results on freezing-thawing processes in glass fiber board, a typical insulation material. The results are analyzed by making use of simultaneous heat and moisture transfer equations that take into account the existence of ice. Since the glass fiber board has large pores, and thus moisture moves mainly in gaseous form up until high moisture content, different

thermal and hygric behaviors from the wall made of soil are expected. Furthermore, the influence that the material properties have on the freezing process is examined.

2. Freezing-Thawing Experiments on Glass Fiber Board

2.1 Freezing process

The experiment was conducted at N.R.C.C. (National Research Council, Canada). The test piece is a 10cm×10cm×10cm glass fiber board with the density of 48 [kg/m^3]. The side of the sample was made vapor-tight by acrylic plates, while the bottom by aluminum foil as shown in Figure 1. The side of the sample was also insulated by 30mm thick styro-foam plates. The upper side faces the ambient air of temperature 20□ and R.H.60%.

From time 0, cold refrigerant with a constant temperature of −10□ was flowed through the water bath under the sample. Water vapor flows into the sample from the ambient air through the upper surface and condenses near the bottom, a part of it freezes there. The moisture content distribution was measured by a gamma-ray spectrometer at 2mm interval.

Figure 2 shows the measured total moisture (liquid water and ice) content in glass fiber board. The moisture content increases from the bottom side with time. After 500 hours, a characteristic kink appears in the moisture content profile at 9mm to 15mm from the bottom.

The measured temperature distribution is shown in Figure 3. As the freezing proceeds, the temperature decreases. The profile is convex upward as a whole. The temperature gradient near the bottom is gradual compared with those in other regions and the temperature increases after

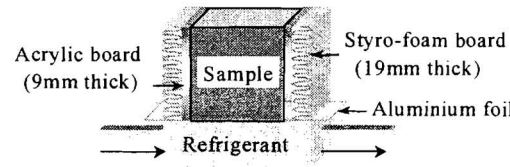

Fig.1 Schematic of experimental setup.

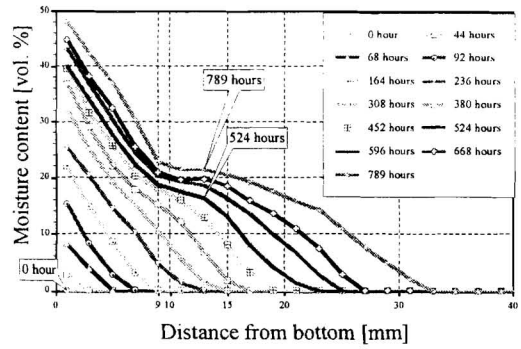

Fig.2 Measured total moisture (liquid water + ice) content distribution during freezing process.

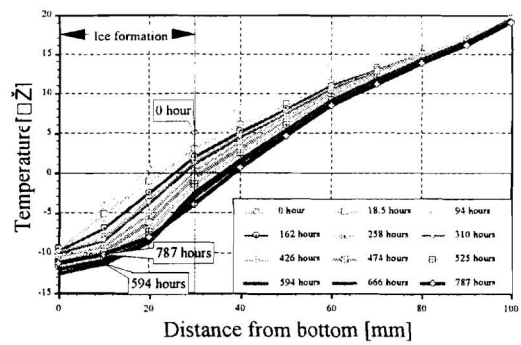

Fig.3 Measured temperature distribution during freezing process.

594 hours (about 25 days). This is probably due to the decrease in thermal resistance in the bottom region with the freezing process.

2-2. Thawing process

The thawing experiment was started after the freezing experiment by heating the refrigerant up to 32□. Figure 4 shows the measured distribution of the moisture content during the thawing process. As the ice evaporates, total amount of moisture decreases.

The measured temperature distribution is shown in Figure 5. In a region 10 to 20mm from the bottom, the temperature lower than 0 □ is kept for a long time. This mean is that the ice remained there longer than any other region. After one and a half hours, the temperature becomes higher than 0 □ everywhere. The thawing rate is high compared with that of the freezing.

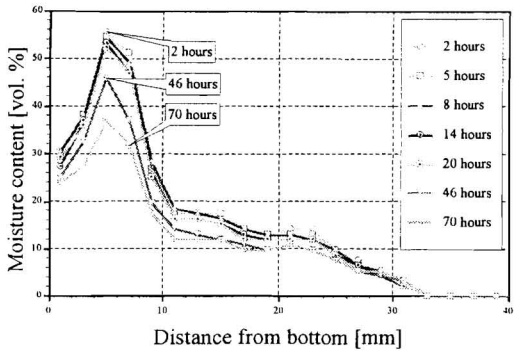

Fig.4 Measured total moisture (liquid water + ice) content distribution during thawing process.

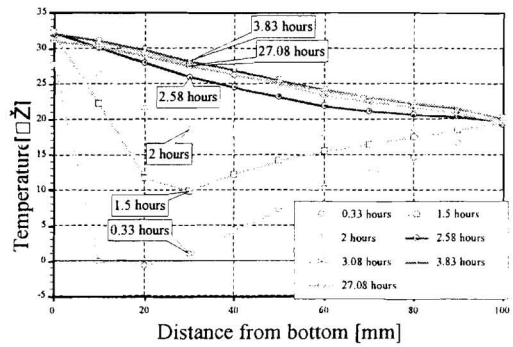

Fig.5 Measured temperature distribution during thawing process.

3. Analysis of Freezing-Thawing Processes

The experiment was analyzed by making use of the governing equations used in the previous paper [3]. Freezing-thawing processes are dealt with as a three-phase system including gaseous, liquid and solid phases. Heat and moisture flow through the sample is regarded as two-dimensional, where the heat flux through the side surfaces of the sample is taken into account.

3-1. System analyzed and method of analysis

A sample of 10cm×10cm glass fiber is analyzed. Heat and moisture flow in the sample is regarded as two-dimensional both in the vertical and horizontal directions. No moisture flow is assumed through the bottom and the side surfaces. The third kind boundary condition is used on the upper surface. The governing equations are solved by an explicit finite difference method. The sample is divided into 25 slices with thickness of 4mm in the vertical direction, while divided into 5 slices (×2) of 10mm thickness horizontally by taking into account the symmetry. The physical properties of glass fiber board in reference [4] are used. However, the calculated ice content became quite high in the cold regions when the original vapor permeability was used. Thus, the value was adjusted as shown in Figure 6 so that the calculated results agreed with the measured ones.

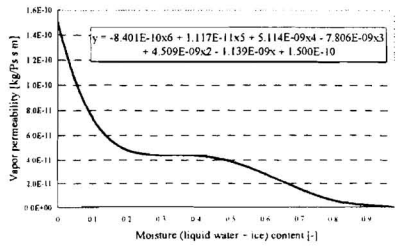

Fig.6 Vapor permeability and moisture content

3-2□Analysis of Freezing Process

(1) Computational conditions

The bottom surface temperature falls from 5□ to −10□ in 60 minutes, while the temperature and chemical potential of the ambient air are kept constant. The relative humidity of the air is 60%. As initial conditions, the temperatures on the upper and bottom surfaces are set at 20□ and 0□, respectively. A linear temperature profile is assumed between the two surfaces. Uniform distribution is used in the horizontal direction.

The side of the sample was made impermeable and insulated by 2cm thick styro-foam board. However, the thermal resistance appears adjusted to a larger value □r = 2.03 [m^2K/W]□ in order to obtain a better agreement with the measured results. The heat transfer coefficient at the bottom surface is set at 23.3 [W/m^2K].

(2) Results and discussions

Figure 7 shows the calculated total moisture content distribution. Whereas it differs slightly from the measured result in Figure 2, it can express such characteristics that the freezing propagates from the bottom and that there is a kink in the moisture profile.

The freezing mainly occurs in a region near the bottom. The reason is as follows: the moisture moves mainly in gaseous phase up to high moisture content since the porosity of the glass fiber is very large, 98%. As a result, no concentration of freezing occurs at the region where the temperature is nearly 0□ (30mm from the bottom). This is completely different from the previous result in the case of the wall made of soil [3].

Since the vapor permeability shown in Figure 6 is used in the calculation, the moisture does not concentrate only near the bottom but distributes over the sample. Judging from a good agreement with the measured result, the assumption that the vapor permeability decreases with moisture content should be reasonable.

Figure 8 gives the time history of the temperature distribution. The features of the measured result such as convex upward and flat near the bottom are well predicted. The

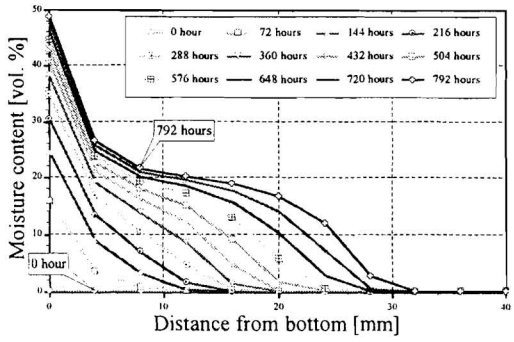

Fig.7 Calculated total moisture (liquid water + ice) content distribution during freezing process.

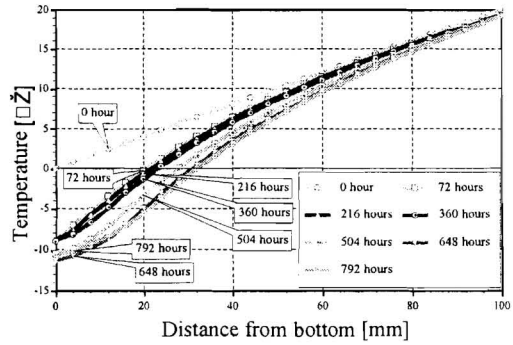

Fig.8 Calculated temperature distribution during freezing process.

convex temperature distribution is partly because of the latent heat of phase change, however, the heat flux from the lateral direction is the main reason. This is demonstrated by the fact that the temperature distribution obtained by the present two-

dimensional calculation agrees well with the measured result while the one-dimensional calculation (not shown here) gives an almost linear distribution. On the other hand, the temperature distribution convex downward near the bottom region is caused by the increasė in thermal conductivity with the amount of the frozen moisture. This also causes the enlargement of the frozen region and the temperature increase in the region, which agree well with the measured results in Figure 3.

3-3. Analysis of thawing process after freezing (one-dimensional analysis)

As a preliminary study, the thawing process was analyzed by a one-dimensional calculation. After the freezing process, the bottom temperature is raised to 32□ and then kept at the temperature. The calculated total moisture content and temperature distributions are shown in Figures 9 and 10, respectively. By raising the temperature of the circulating refrigerant, the ice melts and evaporates from the bottom surface. The calculated moisture content agrees with the measured result in that the moisture content in the bottom region decreases much faster than any other.

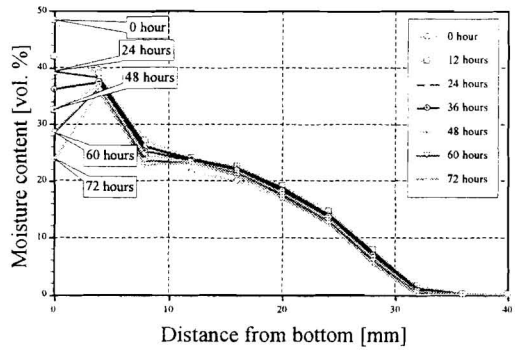

Fig.9 Calculated total moisture (liquid water + ice) content distribution during thawing process.

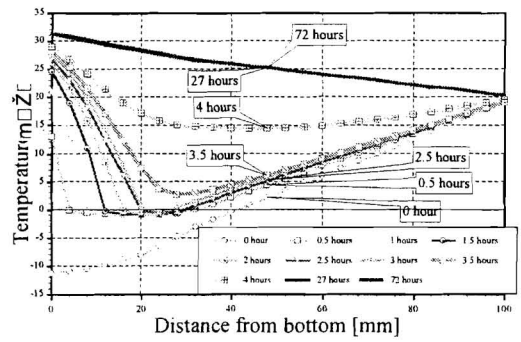

Fig.10 Calculated temperature distribution during thawing process.

The calculated temperature agrees fairly well with the measured result. It remains below 0□ where the ice is found, and it increases from the bottom in sequence. However The time required for thawing is longer than that in the experiment, partly because that the acrylic plates work as heat bridge is not taken into account [4].

4□Influence of Transport Properties on Freezing Process

The ice content distributions under freezing conditions are shown in Figure 11 for several materials. These are the results calculated under a constant temperature. The wall made of glass fiber has the maximum value at the cold side where the temperature is far below 0□. On the other hand, the peaks of the ice content are found at the regions where the temperature is nearly 0□ in the walls made of ALC and soil.

Table 1 shows the relationship between the material properties and the place where the peak occurs in the ice content distribution. The peak position evidently depends on whether the moisture moves mainly in gaseous or liquid phase.

Table 1. Effect of material properties on location of the maximum ice content

	ALC Wall	Soil Wall (Leda Clay)	Glass Fiber Board
Porosity	70□	37.5□	98□
moisture transfer	mainly in liquid phase		mainly in gaseous phase
position of maximum ice content	temperature □□		cold edge

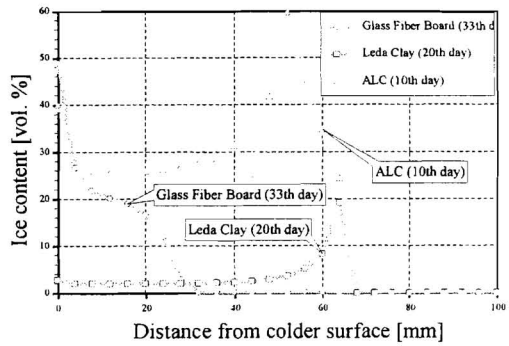

Fig.11 Ice content distribution for various materials.

5. Conclusions

The experiment was carried out on the freezing-thawing processes occurring in walls made of glass fiber. The thermal and hygric behaviors were clarified. The freezing process was analyzed by using the two-dimensional equations of simultaneous heat and moisture transfer. The calculated distributions of the temperature and moisture content showed good agreement with the measured results. Thawing after the freezing process occurs from the cold boundary and its rate is faster than that of freezing. The transport properties have a significant influence on the freezing process.

Acknowledgement

This research was partially supported by the Ministry of Education, Science, Sports and Culture of Japan, Grant-in-Aid for Scientific Research (B), 11450216, 1999.

Thanks are offered to Mr. R. Marchand for help with the measurement using gamma-spectrometer at National Research Council, Canada.

References

[1] M.Matsumoto and S.Ma: A Numerical Analysis for the Freezing-Melting Processes of Soils, J. Archi. Planning Envi. Eng., AIJ, No.482, pp.25-34, Apr., 1996.

[2] A.Iwamae and M.Matsumoto: A Study on Thermal and Hygric Behavior of Snowpacks Based on Field Measurements, J. Archi. Planning Envi. Eng., AIJ, No.468, pp.17-25, Feb., 1995.

[3] M.Hatano, S.Hokoi and M.Matsumoto: An Analysis of Freezing-thawing Processes in Building Walls, Proc. of CIB W40 meeting, Kyoto, Japan, pp.141-158, 1997.

[4] M. Ohuchi: An Identification of Thermal and Hygric Properties of Building Material, Master thesis, Graduate School of Natural Science, Kobe University, 1996.

INFLUENCE OF CRACK ON HEAT AND MOISTURE TRANSFER IN CONCRETE WALL

Y. Kishimoto, S. Hokoi, S. Takada, M. Matsumoto, J. Toman, R. Czerny

INFLUENCE OF CRACK ON HEAT AND MOISTURE TRANSFER IN CONCRETE WALL

Y. Kishimoto[1], S. Hokoi[1], S. Takada[1], M. Matsumoto[2], J. Toman[3], R. Černý[4]

[1]Department of Architecture and Environmental Design, Graduate School of Engineering, Kyoto University, Yoshidahonmachi, Sakyo-ku, Kyoto, 606-8501 Japan
[2]Department of Environmental Design, School of Engineering, Osaka-sangyo University, 3-1-1 Nakagaito, Daito, Osaka, Japan
[3]Department of Physics, Faculty of Civil Engineering, Czech Technical University, Thákurova 7, 166 29 Prague 6, Czech Republic
[4]Department of Structural Mechanics, Faculty of Civil Engineering, Czech Technical University, Thákurova 7, 166 29 Prague 6, Czech Republic
E-mail: be.kishi@archi.kyoto-u.ac.jp, hokoi@archi.kyoto-u.ac.jp, satoruta@archi.kyoto-u.ac.jp, m-matsu@edd.osaka-sandai.ac.jp, cernyr@fsv.cvut.cz

Abstract

Cracks caused by drying shrinkage and thermal expansion increase the air and water permeabilities of concrete wall, and as a result, affect the durability of the building walls significantly. The present paper numerically investigates the influence that the cracks have on the heat and moisture transfer in a concrete wall during drying process. First, an isothermal system is analyzed, and the influence of the crack on the moisture transfer is shown. It becomes smaller as the distance from the material surface becomes larger. The moisture content in the region back of crack changes a lot compared with the case without crack. Secondly a non-isothermal system, where the humidity ratio of ambient air is the same as in the isothermal case, is investigated. In this case, the difference in total evaporation rate between with and without a crack is rather small, and the influence of the crack on the temperature distribution is also small enough. On the other hand, the difference in the distribution of moisture content is larger.

Key words: crack, concrete, heat and moisture transfer, durability, drying

1 Introduction

Various dynamic loads on building components, temperature difference due to solar radiation, and drying shrinkage resulting from the evaporation of working water cause stress in the material, deformation of the material, and even cracks in serious cases. When a crack is generated, the characteristics of the moisture transfer around the crack may differ significantly from that far from the crack, especially in the case of the material which has small moisture conductivity like concrete [1][2]. Thus, the cracks can accelerate penetration of rainwater, alkali-aggregate reaction, corrosion of reinforcement, and so on. These affect the durability of the building elements significantly [3]. But in most studies on heat and moisture transfer in building materials, the problem of cracks has not been investigated thoroughly.

The purpose of this study is to investigate numerically the influence that the cracks have on the heat and moisture transfer in a concrete wall. A surface region of the concrete wall with a crack is analyzed during drying process. By comparing the result with that in the case of no crack, the effect of cracks on the moisture transfer in the material is clarified.

2 Method of analysis

The analyzed wall is a 30mm thick layer of concrete wall shown schematically in Fig. 1. The analyzed two dimensional area ranges 30mm in x direction (the crack depth direction) from the material surface, and 20mm in y direction from the center of the crack. The crack depth from the material surface is changed at three levels, that is 0mm, 10mm and 20mm, and the width is set at 0.2mm.

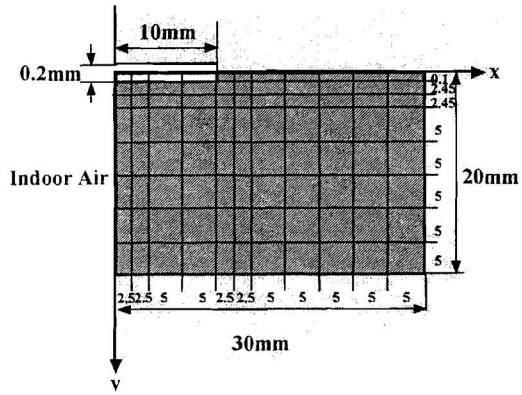

Fig.1 Analyzed model (crack depth=10mm)

In the crack, only conduction of heat and diffusion of water vapor are taken into account. In the concrete, simultaneous heat and moisture transfer model described by equations (1) and (2) is used. Equations (1) and (2) are solved by a finite difference method of Crank-Nicolson type. Basically, the width of control volume is set at 5mm both in x and y directions. Near the material surface and the crack, the width of 2.5mm is used. The analyzed width of the crack is set at 0.1mm in y direction by making use of symmetry condition. The time increment is 10 seconds. Table 1 shows the physical properties of a concrete used in the calculation. Other transport properties are referenced from [4].

Tab. 1 Physical properties

	Density [kg/m^3]	Specific heat [J/kgK]	Thermal conductivity [W/mK]	Vapor diffusion coefficient [m^2/s]
Concrete	2300	0.93	1.624	
Crack(still air)	1.205	1.00	0.024	0.22

As an initial condition, the temperature and relative humidity are set at 20□ and 95% (humidity ratio is 13.95kg/kg'). Indoor air temperature and relative humidity are kept constant at 20□□60% (humidity ratio is 8.81kg/kg':isothermal case) and 23□□49% (the same humidity ratio:non-isothermal case). The heat transfer coefficient on the material surface is 9.28 [W/m^{2}K], 4.64 [W/m^{2}K] for convection and 4.64 [W/m^{2}K] for radiation. The moisture transfer coefficient is 0.004 [kg/m^{2}s(kg/kg')]. On the surfaces at y=0mm and 20mm, heat and moisture fluxes are set at zero due to symmetry. At x=30mm, the constant values same as the initial conditions are given to the temperature and humidity ratio. A simulation for 15 days is performed.

Energy balance

$$c\rho\frac{\partial T}{\partial t}=\nabla\cdot\left\{\left(\lambda+R\cdot\lambda'_{Tg}\right)\nabla T\right\}+\nabla\cdot\left(R\cdot\lambda'_{\mu g}\nabla\mu\right) \qquad (1)$$

Moisture balance

$$\rho_w\left(\frac{\partial\psi_w}{\partial\mu}\right)\frac{\partial\mu}{\partial t}=\nabla\cdot\left(\lambda'_{\mu}\nabla\mu\right)+\nabla\cdot\left(\lambda'_{T}\nabla T\right) \qquad (2)$$

where,

T :Temperature [K], μ :Water chemical potential (relative to free water) [J/kg],
c :Specific heat [J/kgK], ρ,ρ$_w$:Densities of concrete and water, respectively [kg/m^3],
ψ_w :Volumetric water content [m^3/m^3], R :Latent heat of vaporization [J/kg],
λ :Thermal conductivity [W/mK],
λ'_T :Moisture conductivity due to temperature gradient [kg/msK],
λ'_{Tg} :Moisture conductivity in gas phase due to temperature gradient [kg/msK],
λ'_{μ} :Moisture conductivity due to water chemical potential gradient [kg/ms(J/kg)],
$\lambda'_{\mu g}$:Moisture transfer in gas phase due to water chemical potential gradient [kg/ms(J/kg)].

3 Results and discussions

3.1 Isothermal case

3.1.1 Distribution of humidity ratio in crack

The moisture transfer in concrete wall with crack is influenced by the faster vapor transfer in crack air than in concrete. Fig. 2 shows the time history of humidity ratio distribution at y=0mm in the case of (a) no crack, (b) crack depth of 10mm, and (c) crack depth of 20mm.

In the case with no crack, a remarkable decrease in humidity ratio can be seen only in a narrow region of x<5mm until the 15th day and x<10mm even after 100 days.

In the case of 10mm deep crack, the humidity ratio distribution on the 1st day is already similar to that on the 100th day in the case with no crack. Besides, a linear distribution of the humidity ratio is formed between x=0mm and 10mm in the crack. After that, the humidity decreases further in the back region on the crack.

In the case of the 20mm deep crack, the humidity ratio distribution on the 1st day is quite similar to the case of 10mm crack. After that, in the region from x=0mm to x=10mm, the decrease in humidity ratio is slower than that in the case of 10mm crack, while in the region deeper than x=10mm, it is fast compared with the case of the 10mm crack.

3.1.2 Drying rate and moisture content distribution

Fig. 3 shows the variation in drying rate and the amount of the water evaporated. The latter is calculated based on the evaporation velocity from the surface (x=0, 0<y<20).

As time passes, the drying rate decreases in every case. The drying of water in the cases with a crack is faster than that in the case with no crack. The drying rate in the case of the 20mm crack is slightly larger than that in the case of the 10mm crack, although the difference is very small. The

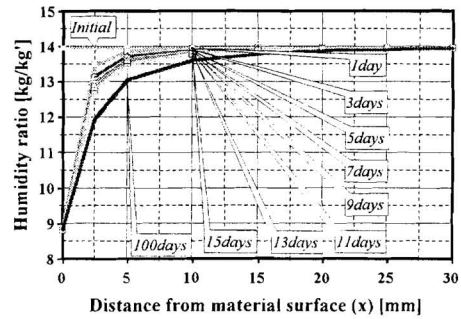

(a) No crack

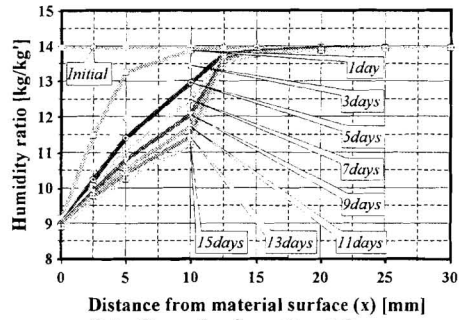

(b) Crack depth=10mm

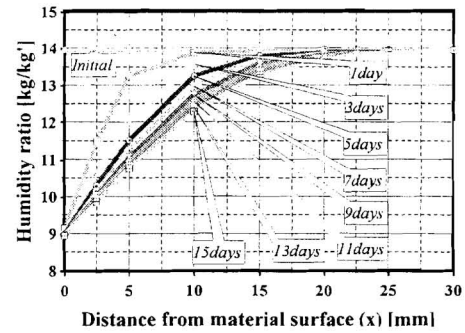

(c) Crack depth=20mm

Fig. 2 Humidity ratio distribution (y=0)

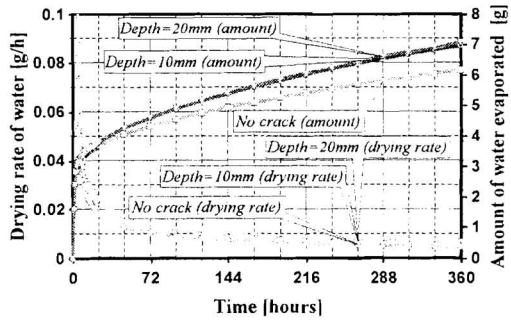

Fig. 3 History of drying rate and amount of water evaporated

amount of water evaporated in the cases with a crack is 15% larger than that in the case with no crack on the 15th day (360 hours).

Fig. 4 shows the distribution of the volumetric moisture content (a) on the 15th day and (b) the 100th day in the case with no crack, (c) in the case of 10mm crack, and (d) 20mm crack on the 15th day.

As shown in Fig. 4(c), the distribution is two-dimensional in the case of 10mm crack. In the region far from the crack (y>10mm), the distribution of the moisture content is almost one-dimensional, and it is almost the same as that in the case without crack shown in Fig. 4(a). The distribution of the moisture content at y=5mm is very close to that on the 100th day in the case with no crack shown in Fig. 4(b). It can be said the influence of crack is significant in this region (y<5mm).

It can be seen that the moisture transfer from concrete to the air in the crack is slower than that from concrete to the indoor air, since the gradient of the moisture content near the material surface is steeper than that near the crack as shown in Fig. 4(c) and 4(d). This is partly because the convection is taken into account at the material surface, while not at the surfaces in the crack. In this study, the air in the crack is assumed to be stationary, since the crack is very narrow (0.2mm).

In order to investigate the influence of the crack depth, the moisture content in the case of 20mm depth in Fig 4(d) is compared with that in the case of 10mm depth in Fig 4(c). In the region from x=0mm to x=10mm, the difference in the distribution is very small. In the region x>10mm and 0<y<10mm, the moisture content in the case of the 20mm depth falls more, although the difference is not so large. The drying progresses faster than that on the 100th day in the case with no crack shown in Fig 4(b).

The crack accelerates drying around the crack. This effect becomes smaller as the position in a crack is deeper. The influence of the depth of crack appears more in x direction.

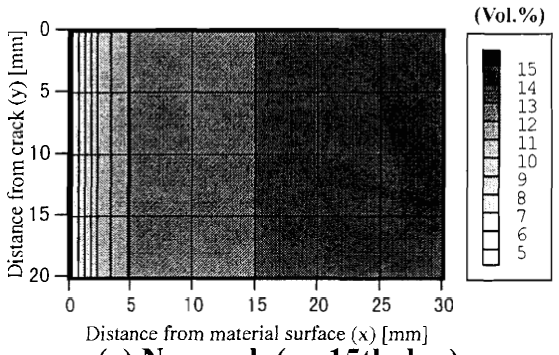

(a) No crack (on 15th day)

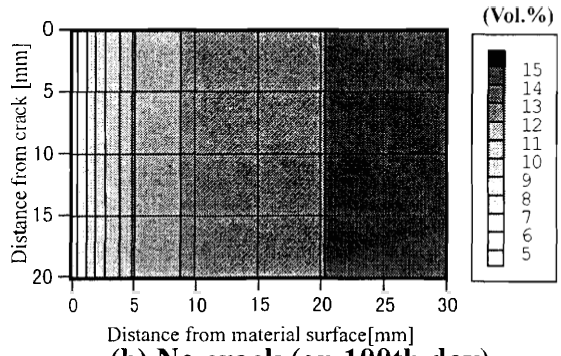

(b) No crack (on 100th day)

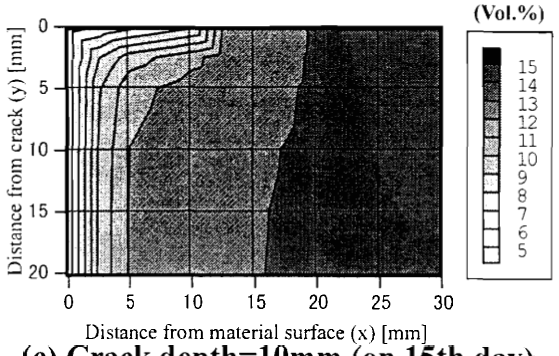

(c) Crack depth=10mm (on 15th day)

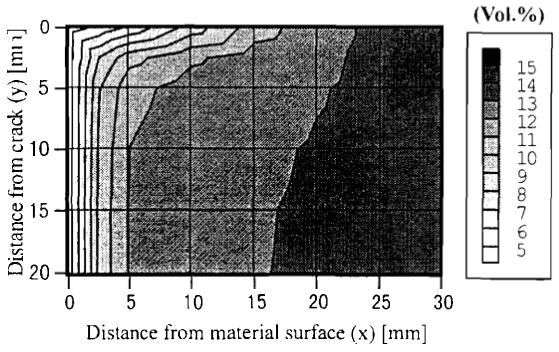

(d) Crack depth=20mm (on 15th day)

Fig.4 Distribution of volumetric moisture content (Vol.%)

3.2 Non-isothermal case

The calculations so far are for an isothermal system (20□). In this section, the influence of temperature gradient is investigated.

Temperature gradient in the material affects the moisture transfer, especially the vapor transfer.

The indoor air temperature is changed from 20□ to 23□ at time 0 in the calculation. The humidity ratio is set at the same value as the isothermal case (8.81 kg/kg').

Fig. 5 shows the variation in the drying rate and the amount of water evaporated. The drying rate is much larger than that in the isothermal case. However, the difference due to the crack is not so large compared with that in the isothermal case. The amount of water evaporated in the cases with a crack is 0.1% larger than that in the case with no crack on the 15th day (360 hours).

Fig. 6 shows the distribution of the volumetric moisture content on the 15th day (a) in the case with no crack, in the cases of (b) the 10mm crack depth, and (c) the 20mm crack depth.

The moisture transfer is faster and the two dimensional distribution of the moisture content is more evident than the isothermal case.

In both crack depths of 10mm and 20mm, the region where the moisture content decreases due to the crack is 5mm in y direction. Compared with the isothermal case, the difference of the moisture content between in y<5mm and y>5mm is large and thus, the influence of the crack on the moisture content is significant in y direction.

The temperature distribution is almost one-dimensional and the influence of the crack cannot be seen in the temperature distribution as shown in Fig. 7. It can be said that the effect of the crack on heat transfer is negligible.

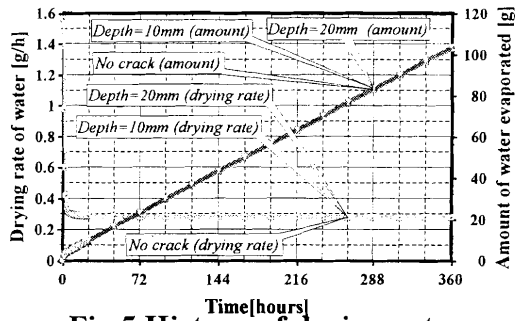

Fig.5 History of drying rate and amount of water evaporeted

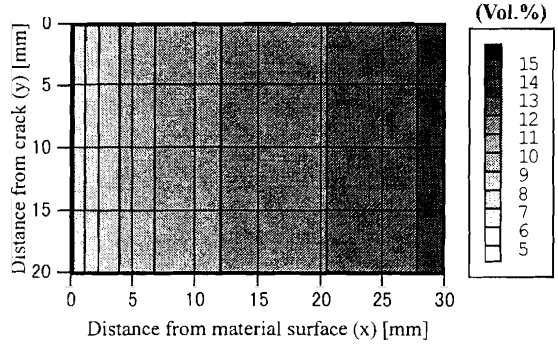

(a) No crack

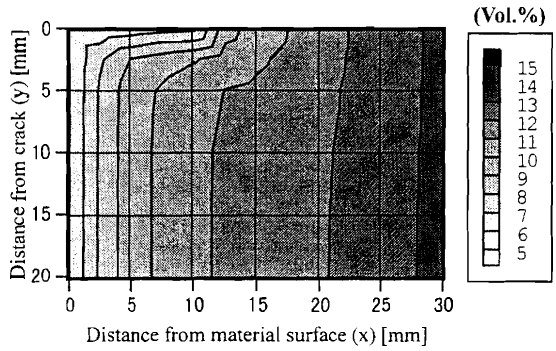

(b) Crack depth=10mm

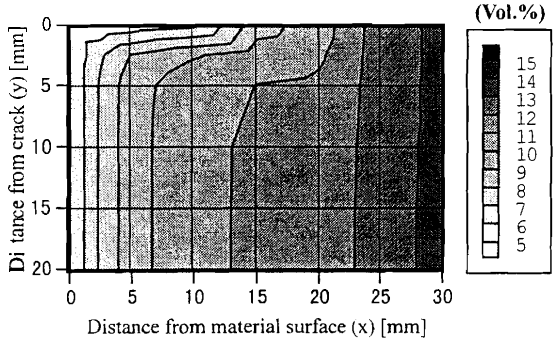

(c) Crack depth=20mm

Fig.6 Distribution of moisture content on 15th day (Vol.%)

4. Conclusions

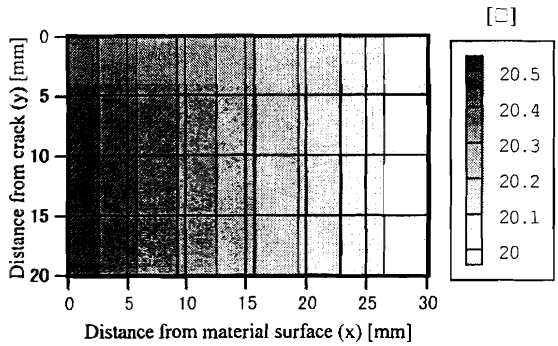

Fig.7 Temperature distribution on 15th day [□]

In order to investigate the influence of cracks on the moisture transfer in walls quantitatively, the thermal and hygric behaviors around a crack is analyzed numerically. The surface region of a concrete wall with a crack (0.2mm in width, 10mm or 20mm in depth) is focused on. The results on drying process are as follows.

1) In an isothermal case, the influence of a crack on the moisture transfer in a concrete wall reaches 5mm from the crack in the direction of the crack width in the case of 20mm deep crack. The moisture distribution at the point 5mm from the crack on the 15th day is similar to the distribution on the 100th day in the case with no crack. The influence will be more significant if the cracks distribute more densely.

2) An analysis with a temperature gradient is conducted under the condition that the humidity ratio of the ambient air is the same as the isothermal analysis. The moisture transfer is faster as a whole, and the difference between with and without a crack is smaller.

Acknowledgement

This research was partially supported by the Ministry of Education, Science, Sports and Culture of Japan, Grant-in-Aid for Scientific Research (B), 11450216, 1999, TOSTEM Foundation for Construction Materials Industry Promotion, and Sougou-kenkyu shoureikai.

References

[1] R.Cerny et al.: Thermal and Hygric Properties of Building materials under Nonstandard Conditions, 1998 (private communication).

[2] M. Yanagida et al.: Experimental Study of Moisture Diffusivity - Measurement of Moisture Diffusivity of Wood Part 2 -,Summaries of Technical Papers of Annual Meeting, Architectural Institute of Japan D, pp.1407-1408, 1989. (in Japanese)

[3] K. Otsuka et al.: Concrete Engineering, Asakura Books, The 1st edition, Oct., 1992. (in Japanese)

[4] M. Matsumoto and D. Ogura: An Analysis of Heat and Moisture Behavior in Underground Space by Quasilinearized Method, Proc. of CIB W40 meeting, Kyoto, Japan, pp.313-328, 1997.

A PHASE DIVIDING FUNCTION FOR DESCRIPTION OF THE NON-ISOTHERMAL MOISTURE TRANSPORT IN POROUS MATERIALS

J. Grunewald, R. Plagge, P. Haupl

A PHASE DIVIDING FUNCTION FOR DESCRIPTION OF THE NON-ISOTHERMAL MOISTURE TRANSPORT IN POROUS MATERIALS

J. Grunewald, R. Plagge, P. Häupl

Institute of Building Climatology, Faculty of Architecture, Technical University of Dresden, Zellescher Weg 17, 03069 Dresden, Germany, e-mail: grunewald@ibk.arch.tu-dresden.de

Abstract

The application of a general thermodynamical mass and energy transport model to the coupled heat, air, moisture and salt transfer in porous materials results in a balance equation system and the related constitutive equations for the considered quantities. The constitutive equations describe a phase-divided moisture transport leading into phase-divided hygric transport coefficients (advective transport coefficients for the liquid and the gaseous phase, vapour diffusion coefficients).
Since phase-divided hygric transport coefficients are not directly measurable, but moisture transport coefficients in distinct moisture ranges, moisture conductivities and a phase dividing function are introduced. The moisture conductivities include liquid water and vapour transport. For a known phase dividing function, the phase-divided hygric transport coefficients of the balance equation system can be calculated from the measured moisture conductivities.

Keywords: constitutive equations, hygric transport coefficients, moisture conductivities, phase dividing function

1 Balance equations

A general thermodynamical model including the constitutive equations, derived in [2], can be applied to the coupled heat, air, moisture and salt transfer in porous building materials. The resulting balance equation system and the constitutive equations for the considered quantities are established. For the description of heat, air, moisture and salt transport in porous building materials, the phase system is considered as consisting of three phases, a solid (m), a liquid (l) and a gaseous (g) phase. General mass balance equations are applied to the total precipitated salt (p), to the components of the liquid phase: liquid water (w) and total dissolved salt (s) and to the components of the gaseous phase: dry air (a) and vapour (v). Eliminating the rates of phase change, the liquid water and the vapour balance are added which results in the moisture balance, and the precipitated and dissolved salt balance are added into one salt mass balance. Furthermore, a balance equation of internal energy is used to describe the thermal behaviour of the system.
The modelling can be simplified, if some assumptions are accepted and a number of less important effects are neglected. The gaseous phase is considered as a binary system consisting of dry air and vapour, where the partial pressures of dry air and vapour form the gas pressure $p_g = p_a + p_v$. Gravitation is the only volumetric force taken into account, and the mass production terms contain only phase changes. Since only one salt mass balance is established, the mass

concentration of salt in the liquid phase and the precipitated salt content are regarded as total quantities according to the different salt species. In the balance equation of internal energy, the production of internal energy by compression and friction is not taken into account, because their contribution is assumed to be negligible.
The necessary transition from the microscopic balance equations to the macroscopic scale causes further terms: the dispersive fluxes of the components in flowing fluid phases. The dispersive flux is considered for salt and water transport in the liquid phase, not for vapour and air transport in the gaseous phase. For the above assumptions, the four macroscopic balance equations, the moisture mass balance *(1)*, the air mass balance *(2)*, the salt mass balance *(3)* and the internal energy balance *(4)*, can be written in local formulation.

$$\frac{\partial}{\partial t}[\rho_w\theta_l + \rho_v\theta]_g = -\frac{\partial}{\partial x_k}[(\rho_w v_k^{m_l} - j_{k,disp}^{m_s} - j_{k,diff}^{m_s})\theta_l + (\rho_v v_k^{m_g} + j_{k,diff}^{m_v})\theta]_g \qquad (1)$$

$$\frac{\partial}{\partial t}[\rho_a\theta]_g = -\frac{\partial}{\partial x_k}[(\rho_a v_k^{m_g} - j_{k,diff}^{m_v})\theta]_g \qquad (2)$$

$$\frac{\partial}{\partial t}[\rho_s\theta_l + \rho_p\theta]_p = -\frac{\partial}{\partial x_k}[(\rho_s v_k^{m_l} + j_{k,disp}^{m_s} + j_{k,diff}^{m_s})\theta]_l \qquad (3)$$

$$\frac{\partial}{\partial t}[\rho_m u_m + \rho_p u_p\theta_p + \rho_l u_l\theta_l + (\rho_v u_v + \rho_a u_a)\theta]_g = -\frac{\partial}{\partial x_k}[\rho_l u_l v_k^{m_l}\theta_l + (\rho_v u_v + \rho_a u_a)v_k^{m_g}\theta]_g \qquad (4)$$

$$-\frac{\partial}{\partial x_k}[j_{k,diff}^{Q} + (h_s - h_w)(j_{k,disp}^{m_s} + j_{k,diff}^{m_s})\theta_l + (h_v - h_a)j_{k,diff}^{m_v}\theta]_g$$

The l.h.s. of the balance equation system *(1)* - *(4)* describes the storage of moisture, air, salt and internal energy, and the terms at the r.h.s. of *(1)* - *(4)* present the divergences of the total flux of these quantities.

2 Transport coefficients

The balance equations *(1)* - *(4)* contain six independent flux expressions, which can be formulated using the general constitutive equations derived in [2]. According to the considered quantities, one gets the advective liquid water flux *(5)*, the advective flux of the gaseous phase *(6)*, the vapour diffusion *(7)*, the salt diffusion *(9)*, the salt dispersion *(9)* and the reduced heat flux *(10)*.

$$\rho_l v_k^{m_l} = -K_l\left[\frac{\partial p_l}{\partial x_k} + \rho_l g_k\right] \qquad \textit{Advective flux of the liquid phase} \qquad (5)$$

$$\rho_g v_k^{m_g} = -K_g\left[\frac{\partial p_g}{\partial x_k} + \rho_g g_k\right] \qquad \textit{Advective flux of the gaseous phase} \qquad (6)$$

$$j_{k,diff}^{m_v} = -\rho_g D_{vn}\frac{\partial c_v}{\partial x_k} - \frac{D_{vp}}{R_g T}\frac{\partial p_g}{\partial x_k} \qquad \textit{Vapour diffusion} \qquad (7)$$

$$j_{k,diff}^{m_s} = -\rho_l D_{sn}\frac{\partial c_s}{\partial x_k} - \rho_l\beta_l D_{sp}\frac{\partial p_l}{\partial x_k} \qquad \textit{Salt diffusion} \qquad (8)$$

$$j_{k,disp}^{m_s} = -\left|\frac{v_k^{m_l}}{\theta_l}\right| D_{sd}\frac{\partial c_s}{\partial x_k} \qquad \textit{Salt dispersion} \qquad (9)$$

$$j_{k,diff}^{Q} = -\lambda\frac{\partial T}{\partial x_k} \qquad \textit{Reduced heat flux} \qquad (10)$$

The hygric transport coefficients K_l, D_{vn} and D_{vp} are not exactly measurable according to their definitions, and should not be regarded as material properties. The hygric transport coefficients are phase-divided defined, but according to the state-of-the-art in moisture transport measurement technics, a phase-divided measurement of moisture flux is impossible. Therefore, this problem is further discussed introducing a phase dividing function and moisture conductivities.

3 Phase dividing function

The phase-divided experimental determination of liquid water transport coefficients and vapour diffusion coefficients of porous building materials caused always difficulties in the past. Vapour diffusion coefficients are determined affected by the movement of liquid water leading to the well known different interpretations of the moisture dependence of the vapour diffusivity [3, 4, 5, 6]. On the other hand, the determination of liquid water transport coefficients in the unsaturated moisture range is not possible without being influenced by the moisture transport in the gaseous phase. This leads to the conclusion, that a phase-divided definition of hygric transport coefficients is not meaningful because their experimental determination cannot be practically realised.
The total moisture flux should be written in terms of four independent forces (vapour pressure gradient or capillary pressure gradient alternatively, temperature gradient, gas pressure gradient and gravity). These forces result from the governing thermodynamic potentials used in the constitutive equations. Then, the different parts of moisture flux can be determined according to their driving forces, since isothermal and isobar conditions can be experimentally realised. Using the constitutive equations *(5)-(7)*, the mass flux of liquid and gaseous water read as *(11)* and *(12)*.

$$\rho_l v_k^{m_l} = -K_l\left[\frac{\partial p_l}{\partial x_k} + \rho_l g_k\right] \qquad (11)$$

$$j_k^{m_v} = -\frac{\rho_v}{\rho_g}K_g\left[\frac{\partial p_g}{\partial x_k} + \rho_g g_k\right] - \rho_g D_{vn}\frac{\partial c_v}{\partial x_k} - \frac{D_{vp}}{R_g T}\frac{\partial p_g}{\partial x_k} \qquad (12)$$

The macroscopic capillary pressure can be introduced as difference pressure between the liquid and the gaseous phase $p_l = p_c + p_g$ (see [1]), and the gradient of the vapour mass concentration is replaced by the vapour pressure gradient and the gas pressure gradient. Employing

$$\frac{\partial c_v}{\partial x_k} = \frac{p_g}{p^2}\frac{\partial p_v}{\partial x_k} - \frac{p_v}{p^2}\frac{\partial p_g}{\partial x_k} \qquad \frac{1}{p^2} = \frac{R_v R_a}{[p_g R_v + p_v(R_a - R_v)]^2}$$

with

$$R_v^* = \frac{p^2}{p_g^2}R_g \qquad R_g^* = \frac{p^2}{p_v p_g}R_g \qquad R_g = \frac{p_g R_v R_a}{(p_g - p_v)R_v + p_v R_a},$$

the liquid and gaseous water flux can be written as *(13)* and *(14)*. In order to get an convenient formulation, the underlined terms have been complemented.

$$\rho_l v_k^{m_l} = -[K]_l\left(\frac{\partial p_c}{\partial x_k} + \rho_l g_k\right) - [K]_l\frac{\partial p_g}{\partial x_k} \qquad (13)$$

$$j_k^{m_v} = -\left[\frac{D_{vn}}{R_v^* T}\right]\left(\frac{\partial p_v}{\partial x_k} + \underline{\rho_v g_k}\right) - \left[\frac{D_{vp}}{R_g T} - \frac{D_{vn}}{R_g^* T} + \frac{\rho_v}{\rho_g}K_g\right]\frac{\partial p_g}{\partial x_k} - \left[K_g - \frac{\underline{D_{vn}}}{R_v^* T}\right]\rho_v g_k \qquad (14)$$

The capillary pressure is related to the relative humidity and to the vapour pressure by the well known Kelvin-equation $p_c = \rho_l R_v T \ln(\varphi)$. The vapour pressure gradient can be expressed by the gradients of capillary pressure and temperature.

$$\frac{\partial p_v}{\partial x_k} = \frac{\rho_v}{\rho_l}\frac{\partial p_c}{\partial x_k} + \frac{\partial p_v}{\partial T}\frac{\partial T}{\partial x_k} \qquad (15)$$

Replacing the capillary pressure gradient and the vapour pressure gradient in *(14)* by the above relation *(15)*, the alternative formulations *(16)* and *(17)* of liquid and gaseous water flux are obtained.

$$\rho_l v_k^{m_l} = -\left[K_l \frac{\rho_l}{\rho_v}\right]\left(\frac{\partial p_v}{\partial x_k} + \rho_v g_k\right) - [K_l]\frac{\partial p_g}{\partial x_k} + \left[K_l \frac{\rho_l}{\rho_v}\frac{\partial p_v}{\partial T}\right]\frac{\partial T}{\partial x_k} \qquad (16)$$

$$j_k^{m_v} = -\left[\frac{D_{vn}}{R_v^* T}\frac{\rho_v}{\rho_l}\right]\left(\frac{\partial p_c}{\partial x_k} + \rho_l g_k\right) - \left[\frac{D_{vp}}{R_g T} - \frac{D_{vn}}{R_g^* T} + \frac{\rho_v}{\rho_g}K_g\right]\frac{\partial p_g}{\partial x_k} - \left[\frac{D_{vn}}{R_v^* T}\frac{\partial p_v}{\partial T}\right]\frac{\partial T}{\partial x_k} - \left[K_g - \frac{D_{vn}}{R_v^* T}\right]\rho_v g_k \qquad (17)$$

The total moisture flux is the sum of the volumetric content-weighed mass fluxes of liquid and gaseous water, $j_k^{m_w} = \rho_l v_k^{m_l}\theta_l + j_k^{m_v}\theta_g$. The addition of the expressions *(13)*, *(17)*, *(14)* and *(16)*, containing the same driving forces, yields the total moisture flux *(18)*. From equation *(18)* follows, that the moisture movement through a porous medium for non-isothermal and non-isobar conditions is caused by the gradients of capillary pressure (or vapour pressure), gas pressure, temperature and the gravity force.

$$j_k^{m_w} = -K_c\left(\frac{\partial p_c}{\partial x_k} + \rho_l g_k\right) - K_p\frac{\partial p_g}{\partial x_k} - \left[\frac{D_{vn}}{R_v^* T}\frac{\partial p_v}{\partial T}\theta_g\right]\frac{\partial T}{\partial x_k} - \left[K_g\theta_g - \frac{D_{vn}}{R_v^* T}\theta_g\right]\rho_v g_k \qquad (18)$$

$$= -K_h\left(\frac{\partial p_v}{\partial x_k} + \rho_v g_k\right) - K_p\frac{\partial p_g}{\partial x_k} + \left[K_l\frac{\rho_l}{\rho_v}\frac{\partial p_v}{\partial T}\theta_l\right]\frac{\partial T}{\partial x_k} - \left[K_g\theta_g - \frac{D_{vn}}{R_v^* T}\theta_g\right]\rho_v g_k$$

According to the driving forces, moisture conductivities can be introduced. These are the capillary moisture conductivity $K_c(\theta_l, c_s\ T)$ due to the capillary pressure gradient, the hygroscopic moisture conductivity $K_h(\theta_l, c_s\ T)$ due to the vapour pressure gradient and the moisture conductivity $K_p(\theta_l, c_s\ T)$ due to the gas pressure gradient. The latter moisture conductivity is not regarded as material function. An estimation for $K_p(\theta_l, c_s\ T)$ will be discussed below.

$$K_c(\theta_l, c_s\ T) = \underbrace{K_l\theta_l}_{f_{lg}K_c} + \underbrace{\frac{D_{vn}}{R_v^* T}\frac{\rho_v}{\rho_l}\theta_g}_{(1-f_{lg})K_c} \qquad \textit{Capillary moisture conductivity} \qquad (19)$$

$$K_h(\theta_l, c_s\ T) = \underbrace{K_l\frac{\rho_l}{\rho_v}\theta_l}_{f_{lg}K_h} + \underbrace{\frac{D_{vn}}{R_v^* T}\theta_g}_{(1-f_{lg})K_h} \qquad \textit{Hygroscopic moisture conductivity} \qquad (20)$$

$$K_p(\theta_l, c_s\ T) = K_l\theta_l + \left(\frac{D_{vp}}{R_g T} - \frac{D_{vn}}{R_g^* T}\right)\theta_g + \frac{\rho_v}{\rho_g}K_g\theta_g \qquad (21)$$

The moisture flux for isothermal and isobar conditions can be alternatively described by the moisture conductivities $K_h(\theta_l, c_s\ T)$ in the hygroscopic moisture range and $K_c(\theta_l, c_s\ T)$ in the overhygroscopic moisture range. The fourth term in *(18)* is assumed to be small compared to the other terms and can be neglected.

$$(j_k^{m_w})_{p_g,T} = \begin{cases} -K_h(\theta_l, c_s\ T)\left[\dfrac{\partial p_v}{\partial x_k} + \rho_v g_k\right] & 0 \le \theta_l \le \theta_{Hyg} \\ -K_c(\theta_l, c_s\ T)\left[\dfrac{\partial p_c}{\partial x_k} + \rho_l g_k\right] & \theta_{Hyg} < \theta_l \le \theta_{Sat} \end{cases} \qquad (22)$$

For solving the above balance equation system *(1) - (4)*, the phase-divided hygric transport coefficients K_l, D_{vn} and D_{vp} have to be known. In order to express these coefficients by the defined moisture conductivities, K_c and K_h, the liquid water and vapour parts of the isothermal-isobar moisture flux have to be expressed. This requires the introduction of a phase dividing function $f_{lg}(\theta_l, T)$ as shown in *(19)* and *(20)* (see [1]). The phase dividing function describes the liquid water and vapour flux percentages of the moisture flux depending on the moisture content. From *(19) - (21)*, one gets directly the transport coefficients of the balance equation system for liquid water flux and vapour diffusion expressed by introduced the moisture conductivities and the phase dividing function.

$$K_l\theta_l = f_{lg}(\theta_l, T)K_c(\theta_l, c_s\ T) \qquad (23)$$

$$D_{vn}\theta_g = [1 - f_{lg}(\theta_l, T)]\ K_h(\theta_l, c_s\ T)R_v^* T \qquad (24)$$

$$D_{vp}\theta_g = \left(K_p(\theta_l, c_s\ T) - K_l\theta_l - \frac{\rho_v}{\rho_g}K_g\theta_g + \frac{D_{vn}}{R_g^* T}\theta_g\right)R_g T \qquad (25)$$

The defined moisture conductivities (see [7] for the capillary moisture conductivity) are measurable quantities as follows:

$K_c(\theta_{Sat}, c_s\ T) = K_{Sat}(c_s, T)$ $(0°C \le T \le 50°C,\ 0 \le c_s \le c_{Sat})$ *Saturated moisture conductivity*

$\dfrac{K_h(\theta_l, c_s\ T)}{K_{Sat}(c_s, T)} = K_{h,r}(\theta_l)$ $(0 \le \theta_l < \theta_{Hyg})$ *Relative hygroscopic moisture conductivity*

$\dfrac{K_c(\theta_l, c_s\ T)}{K_{Sat}(c_s, T)} = K_{c,r}(\theta_l)$ $(\theta_{Hyg} \le \theta_l \le \theta_{Sat})$ *Relative capillary moisture conductivity*

The moisture conductivity K_p was not introduced as a material function and has to be estimated. From *(19)* and *(21)* follows, that K_p is equal to K_c at saturation $(\theta_l = \theta_{Sat}, \theta_g = 0)$. In the overhygroscopic moisture range, the liquid water flux prevails the vapour diffusion, and the second term of *(21)* can be neglected by $D_{vp}/(R_g T) = D_{vn}/(R_g^* T)$. The gradient of the capillary pressure is about $\rho_l/\rho_v = 10^5 \ldots 10^6$ times greater than the vapour pressure gradient. The capillary moisture conductivity K_c is by the same factor smaller than the hygroscopic moisture conductivity K_h. The vapour pressure gradient has the same order of magnitude as the gas pressure gradient in the hygroscopic range, and K_p has the same order of magnitude as K_c. It can be concluded, that the moisture movement in the hygroscopic range due to the gas pressure gradient (except the vapour advection) is much smaller compared to the moisture movement due to the vapour pressure gradient. Thus, omitting of the second term in *(21)* is also justified in hygroscopic moisture range. For these assumptions, *(21)* and *(25)* simplify to *(26)*.

$$K_p(\theta_l, c_s\ T) = K_l\theta_l + \frac{\rho_v}{\rho_g}K_g\theta_g \qquad D_{vp} = D_{vn}\frac{R_g}{R_g^*} \qquad (26)$$

The remaining task is the determination of the moisture conductivities $K_{Sat}(c_s, T)$, $K_{h,r}(\theta_l)$, $K_{c,r}(\theta_l)$ and the determination of the phase dividing function $f_{lg}(\theta_l, T)$. It is important to know, that for isothermal conditions the phase dividing function does not influence the moisture mass

balance. But a "false" phase dividing function would lead to errors in non-isothermal moisture transport calculations because of its effect on the part of the vapour diffusion due to the temperature gradient. The different energy states of liquid water and vapour cause a dependence of the energy balance on the phase dividing function. The determination of the "correct" phase dividing function is also very important for the salt mass balance and the air mass balance. Thus, the phase dividing function have to be found by non-isothermal moisture and energy transport experiments.

List of Symbols

c_m	J/kgK	*Specific heat capacity dry material*
c_s	kg/kg	*Salt concentration liquid phase*
D_{vn}, D_{vp}	m^2/s	*Vapour diffusion coefficients*
D_{sn}, D_{sp}	m^2/s	*Salt diffusion coefficients*
D_{sd}	m^2/s	*Salt dispersion coefficient*
f_{lg}	–	*Phase dividing function*
g_k, g	m/s^2	*Gravity acceleration*
K_c, $K_{c,r}$	s, –	*Capillary moisture conductivity*
K_{Sat}	s	*Saturated moisture conductivity*
K_h, $K_{h,r}$	s, –	*Hygroscopic moisture conductivity*
K_p	s	*Moisture conductivity due to the gas pressure gradient*
p_g	Pa	*Pressure of the gaseous phase*
p_v	Pa	*Partial vapour pressure*
p_{vs}	Pa	*Saturation vapour pressure*
p_a	Pa	*Partial air pressure*
R_v	J/kgK	*Specific gas constant of vapour*
R_a	J/kgK	*Specific gas constant of dry air*
R_g	J/kgK	*Specific gas constant gaseous phase*
R_v^*	J/kgK	*„Changed" specific gas constant of vapour*
R_g^*	J/kgK	*„Changed" specific gas constant of gaseous phase*
T	K	*Temperature*
t	s	*Time*
u_m	J/kg	*Specific internal energy of solid material*
u_p	J/kg	*Specific internal energy of precipitated salt*
u_l	J/kg	*Specific internal energy of liquid phase*
u_w	J/kg	*Specific internal energy of liquid water*
u_v	J/kg	*Specific internal energy of vapour*
u_a	J/kg	*Specific internal energy of dry air*
x_k	m	*Spatial vector*

References

[1] Grunewald, J. 1997. *Konvektiver und diffusiver Stoff- und Energietransport in kapillarporösen Baustoffen.* Dissertation an der TU Dresden, Fakultät Bauingenieurwesen.

[2] Grunewald, J. 1999. *Mass and Energy Transport in Porous Media – I. Thermodynamical Identification of Driving Potentials.* Recent Research Developments in Heat, Mass & Momentum Transfer. Research Signpost, Trivandrum, India. (in Press)

[3] Häupl, P.; Stopp, H. 1987. *Feuchtetransport in Baustoffen und Bauwerksteilen.* Dissertation B, TU Dresden.

[4] Kießl, K. 1983. *Kapillarer und dampfförmiger Feuchtetransport in mehrschichtigen Bauteilen –Rechnerische Erfassung und bauphysikalische Anwendung.* Dissertation, Universität-Gesamthochschule Essen.

[5] Krischer, O. 1942. *Der Wärme- und Stoffaustausch im Trocknungsgut.* VDI-Forschungsheft, 415, 1-22.

[6] Neiß, J. 1982. *Numerische Simulation des Wärme- und Feuchtetransports und der Eisbildung in Böden.* Fortschritt-Berichte der VDI-Zeitschriften, Reihe 3, Nr. 73, VDI-Verlag.

[7] Plagge, R. 1991. *Bestimmung der ungesättigten hydraulischen Leitfähigkeit im Boden.* Dissertation an der TU Berlin, Fachgebiet Bodenkunde.

A NUMERICAL ANALYSIS OF ANNUAL BEHAVIOUR OF MOISTURE CONTENT IN A WELL INSULATED AND AIRTIGHT ENVELOPE

(THE EVALUATION OF SHRINKAGE OF A WOODEN STUD)

M. Sato

A NUMERICAL ANALYSIS OF ANNUAL BEHAVIOR OF MOISTURE CONTENT IN A WELL INSULATED AND AIRTIGHT ENVELOPE (THE EVALUATION OF SHRINKAGE OF A WOODEN STUD)

Manami Sato

Department of Architecture, Faculty of Engineering, Osaka Institute of Technology, Omiya 5-16-1, Asahi-ku, Osaka,535-8585, Japan, E-mail: sato@archi.oit.ac.jp

Abstract

Recently, many well insulated and airtight houses have been built building, even in a mild climate such as Japan. These houses consist of pre-fabricated wooden stud envelopes which are designed to enhance energy conservation and thermal comfort for persons in a cold climate. It have been reported that internal moisture condensation in a envelope mentioned above occurs in summer, in Japan.

It have been known that moisture adsorption of a yard lumber can control air humidity in a room. Moisture content of the yard lumber varies annually in a building envelope. The increase in moisture content increases expansion of the yard lumber. Conversely, the decrease in moisture content increases the shrinkage. The behavior of expansion/shrinkage repeats many times annually. In order to avoid the decrease in durability (for example : the warp, the crock, the twist and the split etc.) ,it is important to expect the behavior of moisture content.

In this paper, a numerical analysis of relative humidity (temperature and moisture content) in a wooden stud envelope which is a well insulated and airtight wall, is shown. For the stud in the wall, the behavior of expansion/shrinkage caused by moisture adsorption is evaluated as compared with experimental data.

Key words: well insulated and airtight envelope, variation of relative humidity, shrinkage of a yard lumber

1 Introduction

It has known that a yard lumber is of well adsorption of water vapor. The houses which are considered with moisture adsorption of a yard lumber, have been constructing in hot and humid climate as Japan. The surfaces of yard lumber which was used in these houses, faced ambient air generally. It has been known that the moisture content of yard lumber varies around a equilibrium steady state annually because of the moisture adsorption.

Now the constructive industry intercepts a yard lumber to be exposed to ambient air. Many well insulated and airtight houses which were developed in Northern Europe or in Canada and Northern America, have been built in Japan. It is expected that an excess of fiber saturated point of a yard lumber ensures from the accumulation of moisture

content caused by adsorption and that the evaporation of water vapor encourages the yard lumber to be dry exceedingly. The yard lumber expands/shrinks corresponding with the variation and distribution of moisture content (relative humidity). A decrease in durability will ensure from shrinkage of the yard lumber .

In this paper, I show a numerical analysis of moisture content in a wooden stud envelope which is well insulated and airtight. For a stud which is made from Douglas fir in the wall, the behavior of expansion/shrinkage caused by the annual variation of moisture content is evaluated as compared with experimental data.

2 Governing equations[1)] and calculation methods

The governing equations are as follows. These are conservation equations for a porous material which consists of a solid, water in a liquid state, water in a vapor and humid air. It is assumed that the liquid phase diffusion can be disregarded. Moisture transfer in material is described by diffusion of the water vapor and moisture content in material is described by accumulation of the liquid water.

moisture: $(\frac{\Phi}{R_v \cdot T}+\kappa)\frac{\partial P_v}{\partial t}+(\Phi\frac{\partial \rho_v}{\partial T}+v)\frac{\partial T}{\partial t}=\nabla(\lambda'_{P_v}\nabla P_v)$ (1)

energy : $(c\rho - r\cdot v)\frac{\partial T}{\partial t}+(-r\cdot\kappa)\frac{\partial P_v}{\partial t}=\nabla(\lambda\nabla T)$ □□ (2)□

$$\kappa=\rho_w\frac{\partial\phi}{\partial X}\ (3),\quad v=-\rho_w\frac{\partial\phi}{\partial T}\ (4)$$

In this moisture balance equation, moisture diffusive flow caused by the temperature gradient of the material is almost negligible. □ is an adsorptive coefficient corresponding to the variation in water vapor pressure in the material. □is an adsorptive coefficient corresponding to the variation in temperature.

moisture boundary equation: $-\lambda'_{P_v}\frac{\partial P_v}{\partial n}=\alpha'_{P_v}(P_v0-P_v)$ (5)

energy boundary equation : $-\lambda\frac{\partial T}{\partial n}=\alpha(T0-T)$ □ (6)

c□: thermal capacity of humid material(J/Kg/K), n: normal direction on the wall surface(m), r: phase change enthalpy of vapor water adsorbed(J/Kg), P_v: vapor pressure(pa), P_v0: vapor pressure of room air(pa), t: time(s), T: temperature(K),T0: temperature of room air(K),□: true porosity (vol/vol),□: moisture content(vol/vol),$□_v$: vapor density(Kg/m^3),□: thermal conductivity(W/m/K),$□'_{Pv}$: moisture conductivity(Kg/m/s/pa), □: coefficient of heat transfer(W/m^2/K),$□_{Pv}$: coefficient of moisture transfer(Kg/m^2/s/pa□

The geometry considered is a two-dimensional well insulated and airtight envelope (Fig. 1).

Thermal and moisture properties of the materials in the envelope are shown in Table 1,Table 2 and Table 3.

Generally, it is expected that the variable range of moisture content in a yard lumber is wide because it is well adsorptive material. Moisture conductivity of the yard lumber is variable with moisture accumulation. Though very little data of moisture conductivity

have been measured. I assume that moisture conductivity of a plywood is similar to property of a fiberboard as shown in Fig.2. I assume that moisture conductivity of a stud (Douglas fir) is approximation as shown in Fig.3.

The equilibrium moisture content relations which were evaluated experimentally, are shown in Figs. 4 and 5.

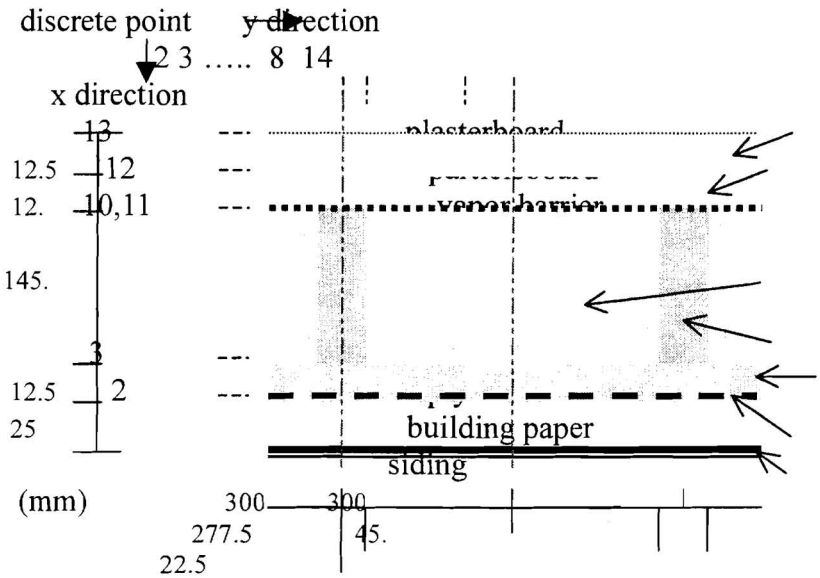

Figure 1 Geometry of a two-dimensional well insulated and airtight envelope

Table 1[2),3)]

material	plywood	rock wool	stud (*1)	□articleboa □d	Plasterboa□d
Density(Kg/cubic meters)	547	100	430	682	963
Specific heat (J/Kg/K)	1298.9	838	1295.8	1298.9	838
heat conductivity (W/m/K)	0.151	0.038	0.116	0.151	0.616
Moisture conductivity *E-10 (Kg/m/Pa/s)	(Fig.2)	□1.46	(Fig.3)	0.033	0.27

*1: Douglas fir

Material	moisture permeant resistance (□sPa/K)
building paper	5.55E+07
vapor barrier	2.16E+11
vinyl cloth	1.70E+09

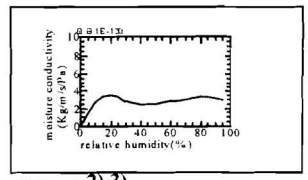

Table 2[2),3)]

Figure 2[3)]

Table 3

	coefficient of heat transfer	Coefficient of moisture transfer
Inner surface	9.3(W/□/K)	4.99E-08(Kg/□/s/Pa)
Outer surface	23.26(W/□/K)	15.0E-08(Kg/□/s/Pa)

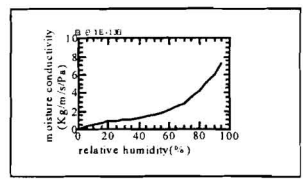

Figure 3[3)]

For boundary condition, room air temperature is constant (25□) during a year. Relative humidity is 50% from November to March. It is 60% in other months. I assume that temperature and relative humidity in a airway are similar to outdoor conditions. The variations of temperature and relative humidity in the airway are approximated in one term of sinusoidal wave considering with annual weather conditions of Osaka.

The governing equations (1)□(6) were analyzed using the finite difference method. I could solve the equations using one second discrete time certainly when a least discrete distance was 6.0 mm.

For the sake of certification, I analyzed the periodic steady state distributions of temperature and relative humidity in the envelope considering experimental boundary conditions during a week in summer. Results from numerical analysis simulated the experimental distribution of temperature .

3 Results of calculation

3.1 Thermal and moisture behavior in a well insulated and airtight envelope

In this section, annual relative humidity variations in the well insulated and airtight envelope are shown in Figus.6 and 7. Initial condition of this analysis is as follows. This envelope was equilibrated to ambient air at May. The equilibrium relative humidity for a plywood and a stud was 90%. The initial moisture content of stud (Douglas fir) corresponded to the relative humidity was 14.8wt% (5.0 vol%). Usually, the moisture content value is approved to build a house. The remaining material in the envelope was 60% relative humidity.

The numerical results on discrete point 8 of y direction(Fig.1) are shown in Fig. 6. It can be seen that the variation of relative humidity at 13 of x direction(Fig.1) which faces room, is distinctly because of the adsorption. The maximum relative humidity is about 80% in summer. And the minimum value is about 30% in winter. The increase in moisture accumulation at 10 of x direction(Fig.1) where is a boundary between vapor barrier and rock wool, occurs during summer. The phenomenon has been known the internal moisture condensation of summer. It can been seen that the layer of rock wool has dried to be less than 30% relative humidity during winter. The relative humidity at 3 of x direction(Fig.1) where is a boundary between plywood and rock wool, decreases from 90% to 60%, during a year.

The numerical results on discrete points 2 and 3 of y direction are shown in Fig.7.

On discrete point 3 of y direction , it can be seen that the stud affect the variations of relative humidity in plasterboard and particleboard slightly. The relative humidity on the boundary between stud and vapor barrier decreases in winter as shown in Fig. 7. It indicates that the stud dries up in winter.

On discrete point 2 of y direction, relative humidity on the surface of plasterboard(at 13 of x direction) decreases monotonously. It is more than 70% during a year. On the boundary between stud and vapor barrier, the relative humidity varies slightly because of the adsorption of stud (Douglas fir). It can be seen that relative humidity in the whole stud has been more

than 60% during a year. The effects of stud on the thermal and moisture behavior in the envelope are observed distinctly. The decrease/increase in relative humidity at the edge of stud exceeds the behavior at the core.

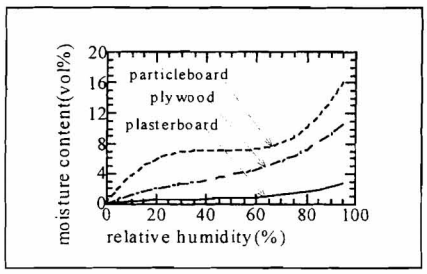

Figure 4

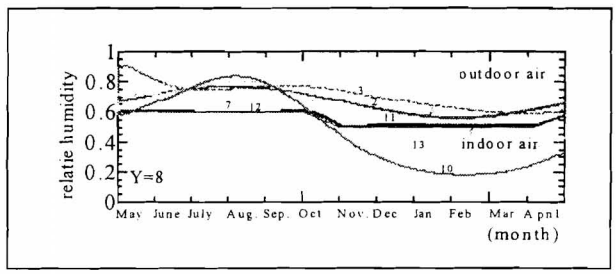

Figure 6

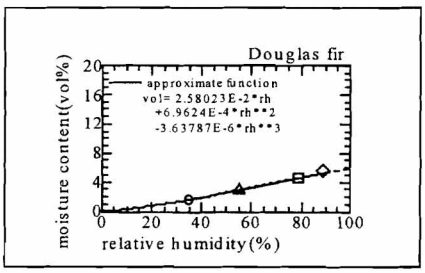

Figure 5

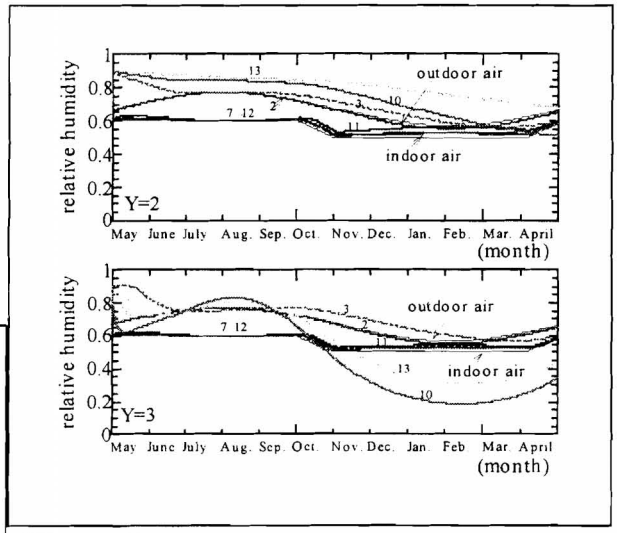

Figure 7

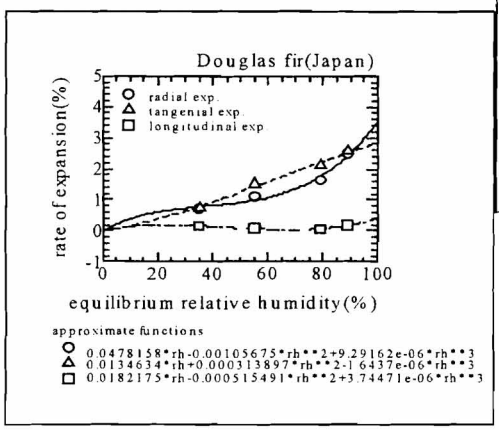

Figure 8

3.2 Evaluation of shrinkage of a stud

Figure 8 is shown the rate of expansion of a Douglas fir which is obtained experimentally. A method of the experiment is shown as follows. I provided some cube pieces of the Douglas fir (30x30x30 mm^3) which were the state of oven-dry. They were equilibrated to ambient humid air individually. The expansion caused by moisture accumulation was evaluated to measure length of the cube piece. It is observed that the tangential expansion and the radial expansion caused by moisture accumulation are larger than the longitudinal expansion.

The distribution of expansible rate at each discrete point in the stud are shown in Figures 9 and 10. Very little shrinkage is observed on the core of stud as shown in Figure 9. The shrinkage is observed distinctly on the edge of stud as shown in Figure

10. The maximum rate of shrinkage is 2.5% on the boundary between stud and vapor barrier, during a year.

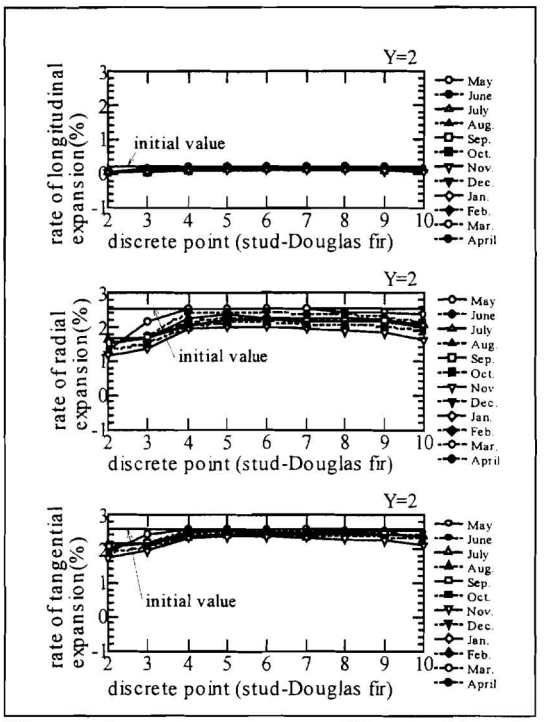

Figure 9

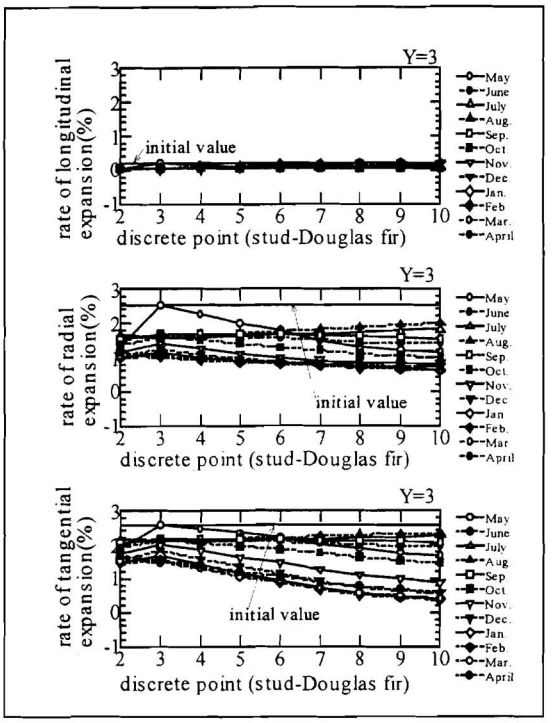

Figure 10

4 Conclusions

Annual thermal and moisture variations in a well insulated and airtight envelope are analyzed. The effect of moisture adsorption and thermal resistance of the stud on thermal and moisture behavior in the envelope are evaluated.

It is observed that the increase in relative humidity caused by internal moisture condensation occurs on vapor barrier in summer. The increase in moisture content of the core of stud is caused by internal moisture condensation in summer. The relative humidity of the core is more than 60% during a year because the decrease in moisture content caused by moisture evaporation is slightly. It is indicated that the edge of stud dries up exceedingly in winter.

The shrunken rate distribution of stud in the envelope is evaluated. It is expected that a maximum rate of shrinkage caused by decrease in moisture content is 2.5% on the edge of stud. When constructing a well insulated and airtight house, the transform of the stud caused by becoming dry or moisture accumulation should be dealt with cautiously.

REFERENCE

1.M. Matsumoto,Humidity, Building Environmental Physics Series of Building Science, No.10, Shyokokusya, Tokyo, 1984.

2.ASHRAE:Handbook of Fundamental,1972

3.SHASE:Handbook I,Maruzen,Tokyo,1967

THE TEMPERATURE DEPENDENCE OF MOISTURE PERMEABILITY

G.H. Galbraith, J.S. Guo, R.C. McLean, C.K. Lee, D.J. Kelly

THE TEMPERATURE DEPENDENCE OF MOISTURE PERMEABILITY

G H Galbraith[1], J S Guo[1], R C McLean[2], C K Lee[2], D J Kelly[1]

[1] Department of Building & Surveying, Glasgow Caledonian University, City Campus, Cowcaddens Road, Glasgow G4 0BA, Scotland
[2] Department of Mechanical Engineering, James Weir Building, University of Strathclyde, 75 Montrose Street, Glasgow G1 1XJ, Scotland
E-mail: ghga@gcal.ac.uk, j.guo@gcal.ac.uk, rmclean@mecheng.strath.ac.uk, ckl@mecheng.strath.ac.uk, d.kelly@gcal.ac.uk,

Abstract

This paper reports on an investigation into the effect of temperature on the moisture permeability of two hygroscopic building materials. The materials were tested at a minimum of three different temperatures. At each temperature, four humidity gradients were applied to enable the variation of permeability to be described mathematically using the concept of differential permeability. Results indicate that the temperature influence on permeability is related to the relative humidity, with significant differences being observed in the critical high humidity (liquid flow) regime.

Keywords: Moisture, permeability, temperature, building materials.

1 Introduction

In recent years, a considerable amount of research has taken place into the development of computer-based simulation tools to describe the phenomenon of combined heat and mass transfer through building envelopes [1]. The reliability of these models is highly dependent upon the measured moisture permeabilities of materials, which are used as a fundamental input parameter. The European Measurement Standard [2] for the determination of permeability requires measurements at a single test temperature of 23°C, which is hardly representative of the exposure conditions of construction materials in practice. This would not be considered important, except that little experimental information is available on the influence of temperature on the values of moisture permeability obtained.

This paper reports the results of isothermal permeability measurements on two hygroscopic building materials at different levels of temperature to examine the dependence of moisture permeability on temperature. This work forms part of an extensive research programme being undertaken by the Authors into temperature gradient effects on moisture movement in porous building materials.

2 The Flux Equations

The total moisture flux through a porous media, g_{tot}, can be expressed in terms of vapour and liquid flow components as [3]:

$$g_{tot} = -D_v \nabla p_v - D_L \nabla p_L \tag{1}$$

where p_v is the vapour pressure, p_L is the liquid pressure, and D_v and D_L are the respective vapour and liquid transfer coefficients. Taking p_L as a function of p_v and temperature T, the liquid pressure gradient in equation (1) becomes:

$$\nabla p_L = \frac{\partial p_L}{\partial p_v} \nabla p_v + \frac{\partial p_L}{\partial T} \nabla T \tag{2}$$

Using Kelvin's equation, the partial differentials can be expressed as:

$$\frac{\partial p_L}{\partial p_v} = R\, T\, \rho_L \frac{1}{p_v} \tag{3}$$

$$\frac{\partial p_L}{\partial T} = \frac{\partial (R\, T\, \rho_L \ln \phi)}{\partial T} = R\, \rho_L \ln \phi - R\, T\, \rho_L \frac{dp_s}{p_s\, dT} \tag{4}$$

where p_s is the saturation vapour pressure and ϕ is the relative humidity. Applying the Clausius-Clapeyron and ideal-gas equations, equation (4) becomes:

$$\frac{\partial p_L}{\partial T} = R\, \rho_L \ln \phi - \frac{h_v}{T v_L} \tag{5}$$

and the gradient of p_L can be written as:

$$\nabla p_L = \frac{R\, T\, \rho_L}{p_v} \nabla p_v + (R\, \rho_L \ln \phi - \frac{h_v}{T v_L}) \nabla T \tag{6}$$

Substituting this expression for ∇p_L into equation (1) gives:

$$g_{tot} = -D_v \nabla p_v - D_L (\frac{R\, T\, \rho_L}{p_v} \nabla p_v + (R\, \rho_L \ln \phi - \frac{h_v}{T v_L}) \nabla T) \tag{7}$$

This equation provides a description of moisture flow using vapour pressure and temperature as independent variables. Under isothermal conditions, it simplifies to:

$$g_{tot} = -(D_v + D_L \frac{R\, T\, \rho_L}{p_v}) \nabla p_v = -\mu \nabla p_v \tag{8}$$

where μ is the differential permeability:

$$\mu = D_v + D_L \frac{R\, T\, \rho_L}{p_v} \tag{9}$$

The strong dependence of D_L on material moisture content results in μ being a non-linear function of relative humidity.

For one-dimensional flow, the total moisture flux can be expressed as:

$$g_{tot} = -\mu \frac{dp_v}{dx} = -\frac{p_s}{L}\int_{\phi_1}^{\phi_2} \mu \, d\phi$$

$$= -\frac{p_s(\phi_2 - \phi_1)}{L}\,\bar{\mu} = \frac{(p_{v1} - p_{v2})}{L}\,\bar{\mu} \qquad (10)$$

where $\bar{\mu}$ is the average permeability over the thickness L of the specimen and p_{v1} and p_{v2} are the boundary vapour pressures.

The differential permeability function $\mu(\phi)$ can be generated from values of $\bar{\mu}$ measured from a series of cup tests covering the whole humidity range [4]. It has been shown [5] [6] that the best basis for the description of this function is the form:

$$\mu = A + B\,\phi^C \qquad (11)$$

The average and differential permeability are related by

$$\bar{\mu} = \frac{1}{\phi_2 - \phi_1}\int_{\phi_1}^{\phi_2} \mu \, d\phi$$

and integrating the above equation thus gives:

$$\bar{\mu} = A + \frac{B\,(\phi_2^{C+1} - \phi_1^{C+1})}{(C+1)\,(\phi_2 - \phi_1)} \qquad (12)$$

where A, B and C are constants determined by using nonlinear regression.

3 Experimental Investigation

The experimental investigation involved moisture permeability measurements on 18mm plywood (7-ply Indonesian, 604 kg/m^3) and 18mm medium density fibreboard (Sonaepan, 692 kg/m^3) under at least three different temperatures. The experiments were carried out using conventional gravimetric cup tests in conformity with the general recommendations contained in the European Standard prEN/ISO 12572 [2]. The test cup used accommodated circular samples of approximately 94mm diameter and produced a measurement area of 65cm^2. The tests were carried out within an Environmental Chamber which maintained a relative humidity of 60% at the exposed sample surfaces. At each temperature, measurements were made using four different vapour pressure regulators within the test cups: calcium chloride desiccant (0%), saturated solutions of ammonium chloride (80%) and ammonium dihydrogen orthophosphate (93%), and distilled water (100%). Six samples of each material were tested for each vapour pressure regulator. The daily weight

change for each cup was measured using a balance with an accuracy of ± 0.001g. After equilibrium was attained (i.e. a linear weight change with time), weighing was continued over a period of at least five days. Based on the measured mass flow rates and the monitored test conditions, the average permeability was then determined using equation (10).

4 Results

Table 1 gives the calculated average permeability values and corresponding standard deviations for the four test materials. From a statistical viewpoint, it can be concluded that the experimental results are highly reliable, because in almost all cases they show very low values of standard deviation. The data in this table has been analysed to determine the differential permeability coefficients A, B and C for each material at each test temperature. The results are presented in Table 2. The differential permeability curves generated from the calculated values of A, B and C are shown in Figures 1 and 2.

Table 1: Test Conditions and Measured Average Permeabilities

MATERIAL	T	MEASURED PERMEABILITY (kgm/Ns) x10^{-12}							
		0 - 60%		60 - 80%		60 - 93%		60 - 100%	
	(°C)	Mean	SD	Mean	SD	Mean	SD	Mean	SD
Plywood	10.5	1.430	0.150	2.091	0.209	2.541	0.178	2.989	0.394
	20.5	1.438	0.108	2.237	0.299	2.747	0.103	3.396	0.471
	26	1.491	0.163	2.298	0.241	3.293	0.343	4.215	0.076
	30	1.525	0.117	2.332	0.168	3.435	0.241	4.434	0.113
MDF	10	7.357	0.209	8.060	0.505	7.853	0.442	8.336	0.115
	20	7.295	0.198	8.085	0.548	8.744	0.318	9.029	0.188
	30	7.159	0.397	7.840	0.191	8.381	0.420	9.044	0.184

Table 2: Determined Differential Permeability Coefficients

MATERIAL	T (°C)	A (kgm/Ns) x10^{-12}	B (kgm/Ns) x10^{-12}	C	R^2
Plywood	10.5	1.39	4.19	5.22	0.998
	20.5	1.39	5.23	5.75	0.994
	26	1.46	9.02	7.06	0.999
	30	1.49	9.94	7.32	0.999
MDF	10	7.29	1.75	3.00	0.864
	20	7.21	4.36	4.52	0.995
	30	7.13	5.73	6.29	0.996

In the low humidity region below about 60% relative humidity, in which the moisture transfer process is dominated by vapour diffusion, the differential permeability values at each temperature remain essentially constant. Little temperature effect is evident. The maximum differences in differential permeability at 60% relative humidity are only 6.7% for plywood and 2.0% for MDF. These results indicate the weak dependence of vapour transport on the levels of test temperature adopted. Such variations are also well within the limits of accuracy expected from such measurements in practice [7].

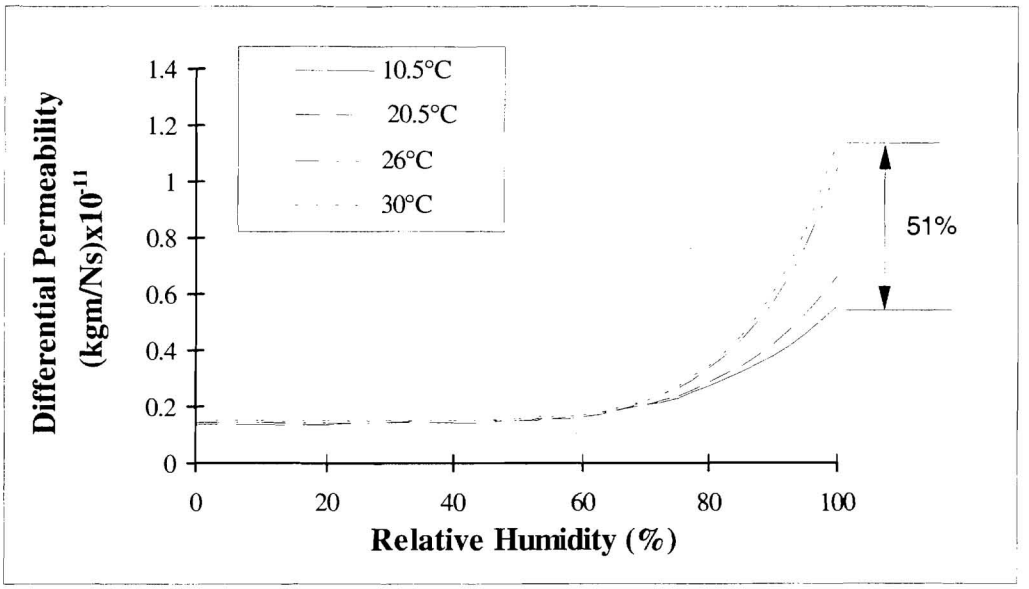

Figure 1: Differential Permeability Curves for Plywood at Different Temperatures

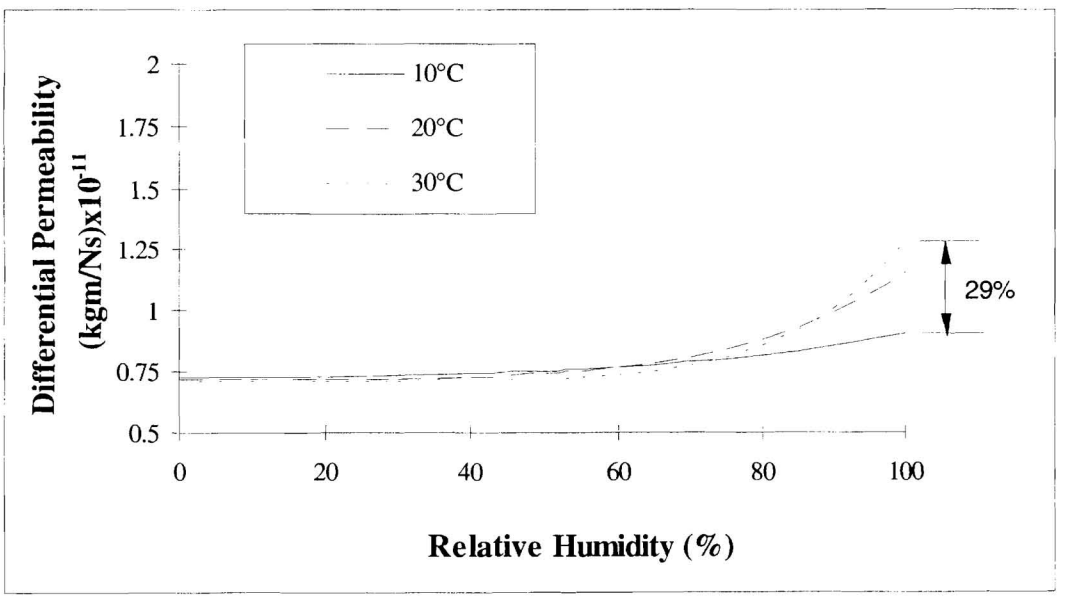

Figure 2: Differential Permeability Curves for MDF at Different Temperatures

As the relative humidity increases above about 60% to 70%, the differential permeability values exhibit a continuous increase. This can be attributed to the progressive initiation of capillary condensation, from small size pores to larger ones, and the increasing contribution of liquid water flow. In this liquid-dominated region, a significant and consistent temperature effect is obvious. At a given relative humidity, the permeability increases with increasing temperature. Near 100% relative humidity, plywood exhibits a 51% difference in differential permeability value between 10°C and 30°C, while MDF shows a 29% variation. It is interesting to note that these experimental results differ from the behavioural pattern proposed by Kunzel [8], which suggests that the moisture flux related to a vapour pressure difference would be expected to decrease with increasing temperature.

5 Conclusions

This experimental investigation leads to the following conclusions:

- The influence of temperature on water vapour diffusion in the low humidity regime is negligible for the two materials investigated. It is anticipated that this result might well be valid for most, if not all, building materials.
- The two materials display a measurable and significant temperature effect in the high humidity, liquid flow regime. The experimental results presented here are clearly inadequate to enable the generation of an universal mathematical model for the inclusion of this effect within the differential permeability procedure. An extension of these experiments to a wider range of wood-based and masonry materials is now being undertaken by the Authors which aims to produce a mathematical description of this effect which can be reliably applied in the future.

References

1. International Energy Agency Annex 24 (1996), Final Report Volume 1.
2. prEN/ISO 12572 (1998), 'Hygrothermal performance of building materials and products-Determination of water vapour transmission properties'.
3. Galbraith, G.H, (1992), 'Heat and moisture transfer within building materials' Ph.D. thesis. University of Strathclyde.
4. McLean, R.C, Galbraith, G.H, and Sanders, C.H, (1990), 'Moisture transmission testing of building materials and the presentation of vapour permeability values' Building Research & Practice, 2, 82-91.
5. Galbraith, G.H, McLean, R.C and Guo, J.S, (1998), 'Moisture permeability data: Mathematical presentation', Building Services Engineering Research & Technology, Vol.19, No.1, 31-36.
6. Galbraith, G.H, McLean, R.C and Guo, J.S, (1998) 'Moisture permeability data presented as a mathematical relationship', Building Research & Information, 26(3), 157-168.
7. Galbraith, G.H, McLean, R.C, Tao, Z and Kang, N, (1992), 'The comparability of water vapour permeability measurements', Building Research & Information, Vol.20, No.6, 364-372.
8. Kunzel H M (1995), One and two-dimensional calculation of the simultaneous heat and moisture transport in building components using simple parameters, IBP-Bericht FtB-39e/1995.

ANISOTROPY OF LIQUID MOISTURE TRANSFER IN BUILDING MATERIALS

J. Drchalová, R. Czerny, J. Havrda

ANISOTROPY OF LIQUID MOISTURE TRANSFER IN BUILDING MATERIALS

J. Drchalová[1], R. Černý[2], J. Havrda[3]

[1]Department of Physics, Faculty of Civil Engineering, Czech Technical University, Thákurova 7, 166 29 Prague 6, Czech Republic
[2]Department of Structural Mechanics, Faculty of Civil Engineering, Czech Technical University, Thákurova 7, 166 29 Prague 6, Czech Republic
[3]Institute of Chemical Technology, Department of Glass and Ceramics, Technická 5, 16628 Praha 6, Czech Republic
EMail: drchalov@fsv.cvut.cz, cernyr@fsv.cvut.cz

Abstract

The anisotropy in moisture transfer is studied on two typical fibre containing plate building materials produced in the Czech Republic, Dekalux and Dekalit P, using a simple method for determining moisture diffusivity κ on the basis of the total mass of water penetrating into the material during a specified time interval at one-sided moistening. The results obtained by this method, called "method with constant κ", are verified by a comparison with the well established Matano method for rod samples but this comparison does not give any unambiguous conclusion due to the inhomogeneity of the studied materials. Therefore, another verification is performed with a well homogeneous ceramic material. Here, the comparison with two commonly used methods for determining κ shows that the method with piecewise constant κ exhibits a relatively good agreement with both Matano and double integration method in the range of high moistures, and therefore it can be considered as a simple and effective tool for identifying the anisotropy in moisture transfer; for low moistures the method can not be used in its current formulation.

Key words: moisture diffusivity, anisotropy, building materials

1 Introduction

Moisture transfer in porous materials is modelled under assumption of an isotropic medium in most cases (e.g. [1]-[3]). This assumption is quite logical and pragmatic because the moisture diffusivity κ is measured practically on rod samples only and its orientation dependence is neglected by the most experimentalists.

The practical problem in determining the possible anisotropy in these materials consists in the fact that classical methods for measuring κ (e.g. [4]–[7]) are suitable for measurements on rod samples only, and for instance in the case of plate materials they fail because in the direction across the plate, it is not feasible to determine moisture content in a sufficient number of points. Therefore, we have developed a simple method which needs only measuring of the time history of the water content

in the sample. This method is applicable for measurements in directions both along and across the plate.

In this paper, we study experimentally the anisotropy of moisture transfer in two lining materials, commonly employed in building structures in the Czech Republic, Dekalit P and Dekalux. Then, we analyze the accuracy of particular methods for determining the moisture diffusivity using experimental results with a relatively well homogeneous material, an extruded porcelain mixture.

2 Methods for measuring moisture diffusivity

Based on the previous analysis of methods for determining moisture diffusivity [8], we will restrict ourselves to just two methods for rod samples, the Matano method [4] which is probably the most frequently used in the practice, and the double integration method [7] which is the most accurate and most reliable one. We will not repeat here the derivation of both methods as it has been done before, the reader can find it in [7].

For the plate materials in the direction across the plate, we will introduce our method with piecewise-constant κ (PCK). The method consists in the assumption that the moisture diffusivity κ can be considered as piecewise constant with respect to the moisture density. Then, the diffusion equation with Dirichlet boundary conditions and constant initial conditions can be solved analytically.

Using the measured total mass of water m_m which penetrated into the sample during the time interval $[0, \tau]$, we get the following transcendent equation for κ

$$m_m(\tau) - S(\rho_1 - \rho_2)\frac{d}{2} + \frac{2dS}{\pi^2}(\rho_1 - \rho_2)\sum_{n=1}^{\infty}\frac{1}{n^2}(1 - \cos(n\pi)) \cdot \exp\left(-\frac{\kappa n^2 \pi^2 \tau}{d^2}\right) = 0, \quad (1)$$

where ρ_2 is the initial moisture density (i.e., the mass of liquid moisture per unit volume) in the sample, ρ_1 is the maximum moisture density which can be achieved in the material (one side of the sample is in direct contact with water during the moistening process), d is the length of the sample in the direction of the moisture transfer, S is the cross section of the sample in the direction perpendicular to the moisture transfer.

Eq. (1) can be solved by some of the iterative methods, such as the Newton method.

The value of κ determined by the solution of (1) we award to a characteristic average value of the moisture density in the time interval $[0, \tau]$,

$$\rho_{m,c} = \frac{m_m(\tau)}{2Sd} + \frac{\rho_1 + \rho_2}{2}. \quad (2)$$

In practical measurements we perform the experiment with a set of samples with various values of the initial moisture density ρ_2, and determine the corresponding set of values of the moisture diffusivity $\kappa(\rho_{m,c})$. In this way we obtain a pointwise given $\kappa(\rho_m)$ function, i.e., the dependence of moisture diffusivity on moisture density.

3 Materials and samples

The experimental work has been done on two typical building materials, Dekalux and Dekalit P.

Dekalux is an environmental friendly cellulose-based replacement material for the asbestos-cement products, designated for heat-insulating external linings, internal-wall- and lower-ceiling linings, and wood- and steel-structure facings. Dekalux is produced by EZA umperk, Czech Republic, and contains cement, organic and inorganic fibre and silicate-based additives. The volume mass of the material is 1750 kgm^{-3}, the material plates are produced in thicknesses of 5 mm to 12 mm.

Dekalit P is another replacement material for the asbestos-cement products of the same producer. The difference between Dekalux and Dekalit P is in the technology of production and in the ratio between the components. Dekalit P contains less organic substances, has a lower volume mass (900 kgm^{-3}), and is designated for increasing the fire-protection properties of building structures as internal lining. The material plates are produced in thicknesses of 6 mm to 15 mm.

The dimensions of the samples were 10 x 40 x 200 mm for the Matano method, for the method with piecewise constant κ then 10 x 60 x 60 mm for the direction along the plate, and 80 x 100 x 10 mm for the direction across the plate.

4 Experimental setup

In the practical measurements, standard experimental setup was employed (see e.g. [7]). One of the 10 x 40, 10 x 60 mm, or 80 x 100 mm surfaces was in direct contact with water, the second one was left in free contact with the surrounding air, the lateral area of the samples was water- and vapor-proof insulated. The mass of the moistened specimens was continuously measured as function of time, in the case of the Matano method, the $\rho_m(x, t_o)$ function (t_o is a specified time) was determined by the gravimetric method.

5 Experimental results

In evaluating the measured results, we calculated the moisture diffusivities in dependence on the relative moisture content u which is more frequently used in the building practice than the moisture density ρ_m applied throughout the first part of the paper, and is defined as

$$u = \frac{\rho_m}{\rho_d}, \tag{3}$$

where ρ_d is the volume mass of the dried specimen.

The results are summarized in Figs 1a,b. For Dekalux, no anisotropy was observed; the differences between κ determined in three perpendicular directions were within the limits of the experimental uncertainty. In the case of Dekalit P which is lighter and contains more pores, relatively, than Dekalux, the anisotropy was clearly distinguished. While for the two perpendicular directions along the plate no differ-

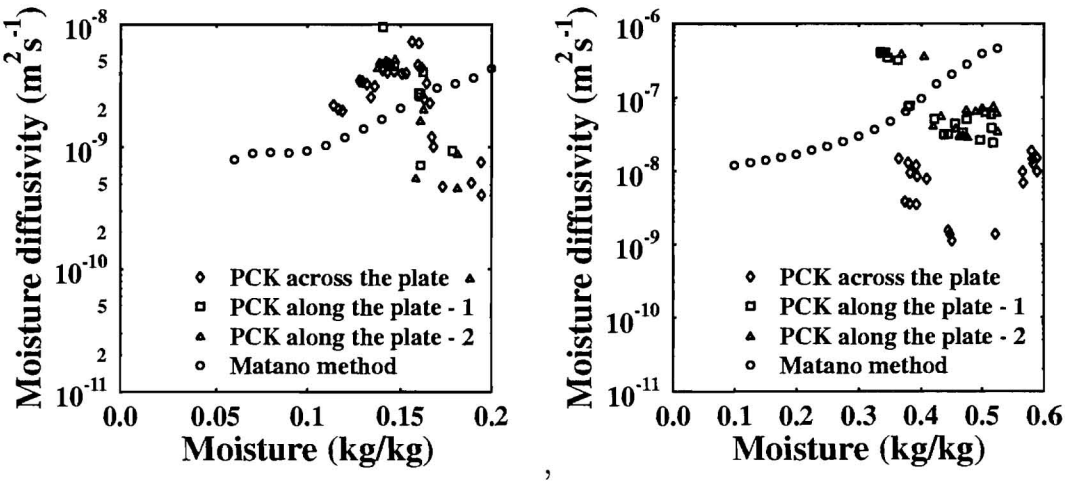

Fig.1 Moisture diffusivity of a) Dekalux, b) Dekalit P

ences in κ were observed, κ in the direction across the plate was at least one order of magnitude lower than in the direction along the plate.

6 Discussion

The results of measuring anisotropy in moisture transfer from the previous Section look very promising. Apparently, the method with piecewise constant κ is sensitive enough to distinguish between the moisture diffusivities in two basic orientations of plate materials with a high content of fibers such as Dekalit P. However, we did not find any anisotropy for Dekalux which is heavier, contains more cement, and therefore the influence of fibres is not that important.

We compared the results obtained with PCK to those determined by the classical Matano method on rod samples cut from the plate. Figs. 1a,b show that the agreement was not very good, in general. The results obtained by the two methods agreed well in the range of 60–80% of maximum water saturation only, otherwise marked differences were observed, and even the character of the $\kappa(u)$ curves was different.

Due to the inhomogeneity of the studied materials, it is practically impossible to identify exactly the reason of the differences. From the analysis by Černý et al. [8] we know that the Matano method achieves a lower precision in the region of both very high and very low moistures but the mentioned inhomogeneity prevent us from awarding the differences only to this factor in this case.

The most reasonable way how to analyze these differences more exactly is to perform measurements of $\kappa(u)$ with a more homogeneous material. As probably no such materials can be found among usual building materials, we have chosen a ceramic material which exhibits according to its producers from the Institute of Chemical Technology in Prague relatively very good homogeneity, namely an extruded porcelain mixture containing kaolin, clay, feldspar and Al_2O_3 which after

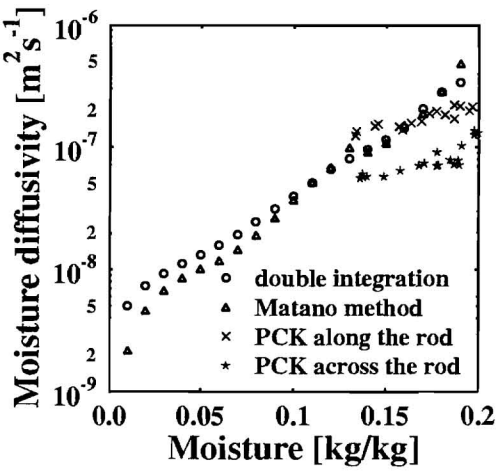

Fig. 2 Comparison of $\kappa(u)$ functions for the extruded porcelain mixture calculated by various methods

drying was burned at the temperature 750°C.

In the experimental tests, we have determined the $\kappa(u)$ functions from the measured $u(x)$ curves by the Matano method, the double integration method and the method of piecewise-constant κ. For the Matano method and the double integration method, the dimensions of the samples were 260 x 40 x 12 mm, for the method of piecewise constant κ then 40 x 40 x 12 mm. The method with piecewise constant κ was also employed for measuring κ in the direction perpendicular to the axis of the sample on 60 x 40 x 12 mm plates cut from the original rods. The measured results are presented in Fig. 2.

These results can be summarized as follows:

- the double integration method and the Matano method showed a very good agreement in all the range of moisture content,
- the method with piecewise constant κ showed a relatively good agreement with both Matano and double integration method in the range of high moistures, for low moistures it can not be used in its current formulation,
- the measurements of κ in two perpendicular directions using the method with piecewise-constant κ showed that despite its relatively good homogeneity the studied ceramic material exhibits anisotropy in moisture transfer.

7 Conclusions

The method with piecewise-constant κ was shown to be well suitable for determination of anisotropy in moisture transfer in the case when material possesses a clearly oriented structure. Therefore, the anisotropy can be measured for instance on fibered materials with a high content of pores with a sufficient accuracy. For heavier materials with a less obvious anisotropy, this method cannot be used as due to the inhomogeneity of the measured samples and the uncertainty of the measuring

technique, the differences in κ are within the errorbar of experimental measurements.

Acknowledgement

This research has been supported by the Grant Agency of the Czech Republic, under grants # 103/97/0094 and # 103/97/K003.

References

[1] P. Häupl, H. Fechner, J. Grunewald, H. Stopp, The Thermohygric Performance of Insulated Building Structures under Conditions of Use. Proc. of "Insulation Materials. Testing and Applications". R.S. Graves, R.R. Zarr (eds.), pp. 426–441. ASTM, West Conshohocken 1997.

[2] A.V. Luikov, Heat and Mass Transfer in Capillary-Porous Bodies. Pergamon Press, Oxford 1966.

[3] O. Krischer, W. Kast, Die wissenschaftlichen Grundlagen der Trocknungstechnik, 3. Auflage. Springer, Heidelberg 1993.

[4] C. Matano, On the Relation between the Diffusion Coefficient and Concentration of Solid Metals, Jap. J. Phys. 8 (1933), 109.

[5] P. Häupl and H. Stopp, Ein Beitrag zum Feuchtigkeitstransport in Bauwerksteilen. Schriftenreihe der Sektion Architektur der TU Dresden 16 (1980), 93.

[6] I. Kašpar, Moisture Transport in Building Materials (in Czech). DrSc. Thesis, CTU Prague, 1984.

[7] J. Drchalová and R. Černý, Non-Steady-State Methods for Determining the Moisture Diffusivity of Porous Materials, Int. Comm. Heat and Mass Transfer 25 (1998), 109.

[8] R. Černý, J. Drchalová, Š. Hošková, J. Toman, Inverse Problems of Moisture Transport in Porous Materials. Proc. of Second ECCOMAS Conf. on Numerical Methods in Engineering, J.A. Desidri, P. Le Tallec, E. Onate, J. Priaux, E. Stein (eds.), pp. 664-670. John Wiley and Sons, Chichester 1996.

WATER VAPOR PERMEABILITY AND HYGROSCOPIC SORPTION CURVES FOR VARIOUS BUILDING MATERIALS

S. Geving, B. Time, P.J. Hovde

WATER VAPOUR PERMEABILITY AND HYGROSCOPIC SORPTION CURVES FOR VARIOUS BUILDING MATERIALS

Stig Geving[1], Berit Time[1], Per Jostein Hovde[2]

[1] Norwegian Building Research Institute, Trondheim Department, Høgskoleringen 7, N-7491 Trondheim, Norway.
[2] Norwegian University of Science and Technology (NTNU), Department of Building and Construction Engineering, N-7491 Trondheim, Norway.
EMail: stig.geving@byggforsk.no, berit.time@byggforsk.no, per.hovde@bygg.ntnu.no

Abstract

Water vapour permeability has been measured for aerated concrete, porous asphalt impregnated wood fibre board, wood fibre board (hardboard), exterior grade gypsum board, plywood, polyethylene film (vapour barrier), polypropylene film (wind barrier), spunbonded polyethylene film (wind barrier), PVC roofing membrane and spruce. Sorption curves were measured for aerated concrete, plywood, spruce, wood chipboard (particle board) and wood fibre board (hardboard).

Key words: water vapour permeability, sorption curve, building materials

1 Introduction

As a part of the research programme "Moisture in building materials and constructions" (1993-97), experiments were performed on different building envelope constructions at a test house in Trondheim, Norway. Besides evaluating the hygrothermal performance of the different constructions, one of the main purposes of the test house measurements was collecting data for comparison with computer simulations of transient moisture transfer in building constructions. To be able to simulate the hygrothermal conditions of the various constructions the material properties have to be known. The most important material properties in this context are probably the water vapour permeability and the hygroscopic sorption curves. These two properties have been measured for most of the materials used in the constructions in the test house, and the results are presented in this paper.

The measurements have been carried out in the laboratories of the Norwegian Building Research Institute (NBI) and Department of Building and Construction Engineering, NTNU, Trondheim, during the period 1995-97. A more detailed presentation of these measurements and results is given in [1].

2 Methods

2.1 Water vapour permeability

The method has mainly been based on a Nordtest Method [2]. In addition corrections for the effect of the masked edge, the vapour resistance of the air layer in the cup and the surface resistance above the specimen have been included. The effect of increasing thickness of the air layer in the cup caused by evaporation of the salt solution during the measurement period has also been taken into account.

The material to be tested is placed on top of a cup as a lid. With the aid of a saturated salt solution, a constant relative humidity (RH) is obtained in the cup. This constant RH is then different from the RH that is obtained outside the cup. This creates a vapour flow either into or out of the cup. The vapour flow, determined through regular weighings of the cup, gives a measure of the vapour transfer rate. Then, by calculation, water vapour permeance, diffusion resistance and permeability can be determined. The water vapour permeance of the specimen is given by:

$$W = \frac{g}{\Delta p_v} \tag{1}$$

where W is the vapour permeance ($kg \cdot m^{-2} \cdot Pa^{-1} \cdot s^{-1}$), g is the density of water vapour flow ($kg \cdot m^{-2} \cdot s^{-1}$) and Δp_v is the vapour pressure difference between the saturated salt solution in the cup and the air outside of the cup (Pa). The test was stopped when five successive determinations of change in mass per weighing interval for each test specimen were constant within ± 5 % of the mean value for that specimen.

2.2 Sorption curves

The procedure for determining sorption curves was in accordance with a draft European Standard [3]. Four specimens of each material were dried in an oven according to [4]. The drying temperature was 40 °C for the gypsum board and 70 °C for the rest of the materials. When the dry mass of the specimens had been determined, the specimens were subsequently placed in the sorption apparatus at increasing RH levels to determine the adsorption curve and then at decreasing RH levels to determine the desorption curve. At every RH level the specimen was weighed until it was in equilibrium with the environment (constant mass). Constant mass was reached when the change of mass between two consecutive weighings made 24 hours apart was less than 0.1 % of the total mass.

For the adsorption curve six RH levels were used, obtained with the following salt solutions; $MgCl_2$, $MgNO_3$, NaCl, KBr, KNO_3 and K_2SO_4. The starting point of the desorption curve was the last point on the adsorption curve (K_2SO_4). For the desorption curve four RH levels were used, obtained with the following salt solutions; NaCl, $MgNO_3$, $MgCl_2$ and LiCl. The highest value on the adsorption curve for the different materials is not necessarily the final moisture equilibrium as we had to stop the experiment at the 97 % level after approximately 700 hours because of mould growth.

3 Materials and test equipment

2.1 Water vapour permeability

For the measurements, five specimens for each of the investigated materials were sealed at the top of the permeability cups made of aluminium, see Figure 1. It should be noted that the spruce specimens were mounted on somewhat different permeability cups, see [5]. The cups were placed in a room with a constant relative humidity of 50 ± 2 % RH and a temperature of 23 ± 1 °C. The "wet-cup" method was applied for all materials. The salt solution used in the cups was KNO_3, which yields a relative humidity of 94.0 ± 0.6 % at a temperature of 23 °C [3]. The average relative humidity across the test specimen was therefore approximately 72 % RH. The spruce was also measured at two other average RH-levels, i.e. 31 % and 63%. The salt solutions that were used were then respectively LiCl and NaCl.

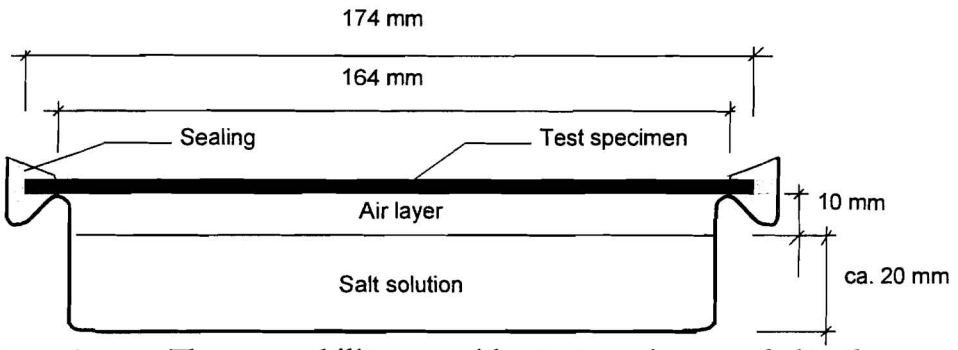

Figure 1 The permeability cup with a test specimen sealed to the cup.

2.2 Sorption curves

Between four and ten specimens of each of the five materials were prepared with a length and height of 70 mm and 50 mm, respectively. The thickness of the specimens equalled the thickness of the different board materials, however the specimens of aerated concrete and plywood were given a thickness of 40 mm and 9 mm, respectively. The thickness of spruce specimens varied between 2 mm and 10 mm. On each specimen a stainless steel hook was screwed approximately 2 mm into the specimen.

The sorption apparatus, which is a thin walled cylindrical polyethylene vessel with a top construction, is shown in Figure 2. The top construction includes a fan, a balance and the test specimens. The top construction can easily be moved from one vessel to another, so that the specimens quickly get into the next humidity level. The wanted RH-level is provided with shallow trays that are containing saturated salt solutions in the bottom of the vessels. The vessels are placed in a room with a fixed temperature at 23 ± 1 °C. Each vessel has six measuring points for temperature and three points for relative humidity. These values are logged every 30 minutes.

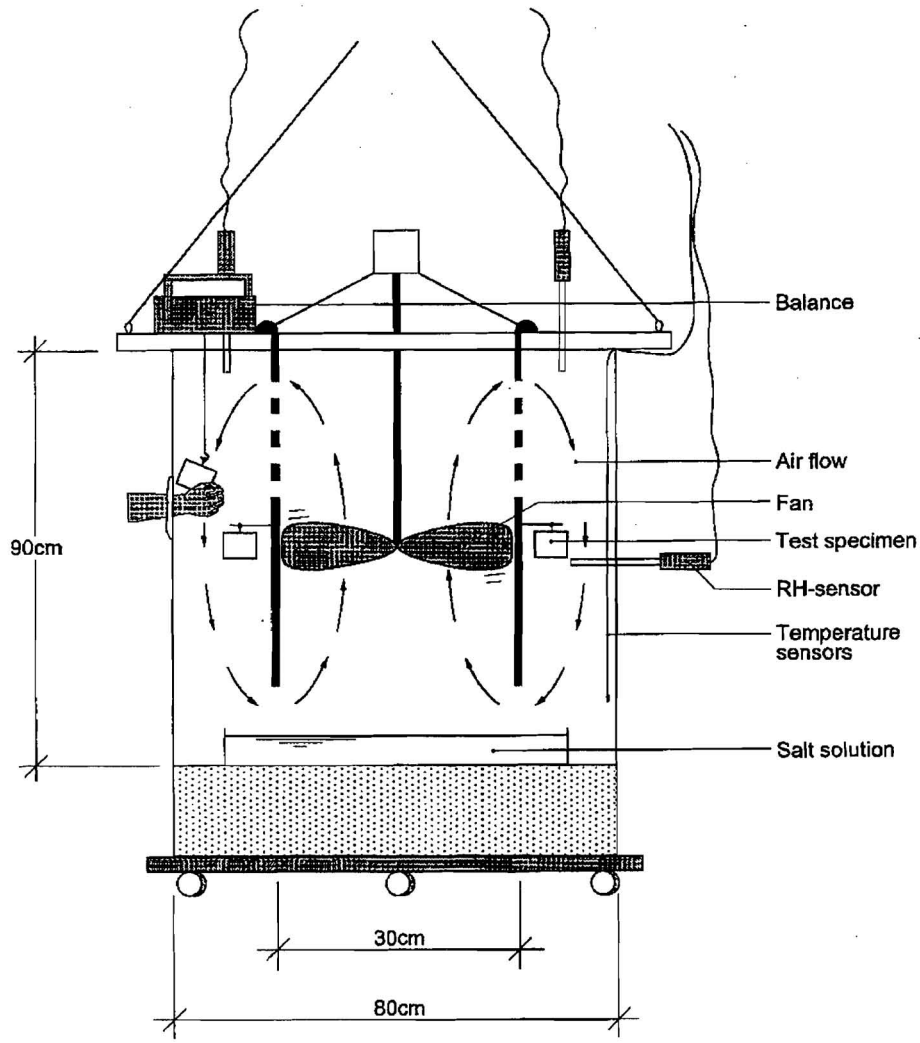

Figure 2 Cross section of the sorption apparatus.

4 Results

Table 1 Water vapour permeability for spruce measured in the transverse direction, i.e. a combined radial/tangential direction, for various RH-levels (with standard deviation σ). The values represent a mean value for thickness ranging from 2.4 mm to 10 mm.

Material	Density $kg \cdot m^{-3}$	Water vapour permeability ± σ ($10^{-12} \cdot kg \cdot m^{-1} \cdot Pa^{-1} \cdot s^{-1}$)		
		$\overline{RH}$: 31%	63%	72%
Spruce *	350-380	1.75 ± 0.34	6.01 ± 0.51	
Spruce *	440-465		3.94 ± 0.09	7.23 ± 0.26

* The measurements of the vapour permeability of spruce are more thoroughly reported in [5]. It should be noted that the procedures of those measurements may deviate to some extent from the procedures and methods described in the present paper.

Table 2 Measured water vapour permeance (with standard deviation σ). Average RH-level is 72 %.

Material	Thickn. mm	Density kg/m^3	Water vapour permeance ± σ (10^{-12}·kg·m^{-2}·Pa^{-1}·s^{-1})
Aerated concrete	21	474	1180 ± 70
Asphalt impregnated wood fibre board, porous	12	251	845 ± 264
Gypsum board, exterior grade	9	757	2430 ± 80
Plywood	22	411	145 ± 10
Polyethylene foil, vapour barrier	0.15		3.09 ± 0.57
Polypropylene foil, wind barrier	0,27		44.1 ± 3.3
PVC roofing membrane	1.3		15.0 ± 1.1
Spunbonded polyethylene foil, wind barrier	0.14		9720 ± 760
Wood fibre board, high density	11	803	371 ± 25

Table 3 Measured equilibrium moisture contents (weight-%) for adsorption and desorption curves.

	Wood chipboard		Wood fibre board (hardboard)		Plywood		Aerated concrete		Spruce	
RH (%)	Ads.	Des.	Ads.	Des.	Ads.	Des.	Ads.	Des.	Ads.	Des.
11.3	-	-	-	3.4	-	3.8	-	1.01	-	3.1
32.9	5.7	-	5.1	7.2	6.8	8.3	0.23	1.40	7.2	7.8
53.5	7.7	-	7.0	8.8	8.9	10.3	0.44	1.59	9.6	10.0
75.4	10.6	-	9.6	12.1	12.2	14.8	0.93	1.89	13.2	14.7
81.2	11.5	-	10.5	-	13.2	-	1.21	-	14.1	-
94	15.6	-	13.7	-	17.8	-	1.88	-	18.6	-
97.4	-	-	16.0	16.0	18.9	18.9	2.43	2.43	21.0	21.0

5 Discussion and conclusions

The measurements were compared with similar measurements documented in the literature, mainly from [6]. The results of the water vapour permeability measurements agree well with these previous measurements.

The measured results for sorption curves for different materials presented in this paper are however deviating more from results given in the literature. The following observations have been made:

- For the aerated concrete the difference in moisture content between the adsorption curve and the desorption curve is larger for all relative humidities in this report than in the corresponding measurements reported in [6]. This could imply that the final equilibrium values have not been attained, neither in adsorption nor desorption. However, the equilibrium criterion according to [3] has been fulfilled. The same effect has previously been observed for measurements on loose fill lightweight

expanded clay aggregates [7]. This equilibrium criterion might therefore not be suitable for materials that absorbs only small amounts of water (e.g. below 3 % by weight), and when the absorption and desorption processes are slow.

- For the wood based materials there are also significant deviations between the present results and other reported results. At the same time there are also significant deviations between the results from different laboratories, as reported in [6]. The moisture content of the wood fibreboard at the higher relative humidity levels are below values reported in the literature, a result which might imply that final equilibrium has not been attained. On the other hand, this is not the case for wood chipboard and plywood. The sorption curves reported for spruce, and the desorption isotherm in particular, are also relatively low compared to similar results reported in the literature. However, is known that measurements on sorption curves for spruce and pine vary quite a lot. A thorough comparison of sorption curves for spruce can be found in [5].

References

[1] E. Bergheim, S. Geving, B. Time. Hygroscopic material properties - Water vapour permeability and hygroscopic sorption curves for materials used in a test house. Project report 234, Norwegian Building Research Institute, Oslo, Norway, 1998.

[2] Building materials: Water vapour transfer rate, permeance and diffusion resistance. Nordtest Method NT Build 130 Edition 2, Nordtest, Espoo, Finland, 1990.

[3] Building materials - Determination of hygroscopic sorption curves. Working draft European Standard CEN/TC 89/WG 10 N 104, 1995

[4] Building materials - Determination of moisture content by drying at elevated temperature. Draft European Standard CEN/TC 89 N 338 E rev, 1995.

[5] B. Time. Hygroscopic Moisture Transport in Wood. Ph.D. Thesis. Norwegian University of Science and Technology (NTNU), Trondheim, Norway, 1998.

[6] M.K. Kumaran. Final Report Task 3: Material properties. IEA, Annex 24 HAMTIE. Laboratorium Bouwfysica, K.U.-Leuven, Belgium, 1996.

RAPID EXPERIMENTAL EVALUATION OF MATERIAL TRANSFER COEFFICIENTS FOR USE IN MOISTURE SIMULATION MODELS

G.H. Galbraith, J.S. Guo, D.J. Kelly, R.C. McLean

RAPID EXPERIMENTAL EVALUATION OF MATERIAL TRANSFER COEFFICIENTS FOR USE IN MOISTURE SIMULATION MODELS

G H Galbraith[1], J Guo[1], D J Kelly[1], R C McLean[2]

[1] Department of Building & Surveying, Glasgow Caledonian University, City Campus, Cowcaddens Road, Glasgow G4 0BA, Scotland
[2] Department of Mechanical Engineering, James Weir Building, University of Strathclyde, 75 Montrose Street, Glasgow G1 1XJ, Scotland
E-mail: ghga@gcal.ac.uk, j.guo@gcal.ac.uk, d.kelly@gcal.ac.uk, rmclean@mecheng.strath.ac.uk

Abstract

In order to validate and successfully apply moisture simulation models to building envelopes, the experimental evaluation of material transport data is required. Conducting standard permeability tests under reduced barometric pressures provides a rapid means of evaluating the separate vapour and liquid transfer coefficients. This paper describes an advanced experimental apparatus which can facilitate such tests. Test results are reported for a hygroscopic building material and their accuracy is compared with standard test methods.

Keywords: permeability, moisture, building materials, transfer coefficients

1 Introduction

The presence of excess moisture within a building can have serious implications with regard to health, safety and structural performance [1]. Consequently, a significant effort has been focused recently on the development of computer simulation models to predict the moisture characteristics of building envelopes. These models are based upon differential equations which describe the mechanisms of moisture transfer. The successful solution of these equations, and validation of the models, requires the experimental evaluation of material transfer coefficients.

The form moisture takes within a material depends on the prevailing environmental conditions and the material pore structure [2]. It is not unusual for the vapour and liquid phases to exist simultaneously. To overcome this problem, many prediction models assume that all moisture is transferred in the form of vapour below a relative humidity (RH) of 98% [3], at which the material becomes saturated with liquid water. It is known, however, that in porous building materials capillary condensation can occur at an RH of approximately 60% [4]. Moisture transfer at this stage cannot be described accurately as either vapour or liquid transfer, but as a combination of the two. Any prediction model which does not account for this two-phase transfer must be of questionable validity.

A previous conference presentation [5] described a test method which allows separate vapour and liquid transfer coefficients to be determined experimentally. The method involves carrying out standard permeability tests over a range of barometric pressures and results in the rapid attainment of test data. Since that time, the experimental apparatus has been substantially developed and further testing has taken place. These developments will be described in this paper and new results presented.

2 Theoretical Background

2.1 The Flux Equations

The derivation of the equations which describe the transfer of moisture in the vapour and liquid phases was fully covered in the previous presentation [5]. A repetitive derivation will not be given here. However, the prominent transfer equations do merit some comment.

It is accepted that moisture is transported through a porous building material in the form of both vapour and liquid [6]. The former can be expressed by a version of Fick's Law as [7]

$$j_v = -\upsilon a \frac{D}{R_v T} \nabla p_v \qquad (1)$$

where j_v is the vapour flux density (kg/m^2 s), R_v is the gas constant for water vapour (461. 52 J/kg K), T is the absolute temperature (K), p_v is the vapour pressure (Pa) and υ is the material tortuosity factor. D is the diffusion coefficient for water vapour in air (m^2/s), which is dependent upon temperature and inversely related to the total pressure, p_b. The volume fraction of air-filled pores, a, is dependent upon the relative humidity.

Equation (1) is often written as

$$j_v = -D_v \nabla p_v \qquad (2)$$

where D_v, the vapour permeability coefficient (kgm/Ns), is also dependent on temperature and inversely related to p_b.

The transfer of liquid through a porous material under isothermal conditions can be described in terms of a vapour pressure gradient via a form of the well-known Kelvin equation [8] as

$$j_l = -K_l \frac{R_v \rho_l T}{p_v} \nabla p_v = -K_l \frac{R_v \rho_l T}{\phi p_{vs}} \nabla p_v \qquad (3)$$

where ρ_l is the liquid density (kg/m^3), ϕ is the relative humidity, and p_{vs} is the saturation vapour pressure (Pa). The hydraulic conductivity, K_l (kgm/Ns), is governed by the material moisture content and decreases rapidly from a maximum at total saturation.

Equations (1) and (3) can be summed to give an expression for the total moisture flux,

$$j_{tot} = j_v + j_l = -(D_v + D_l) \nabla p_v = -\mu \nabla p_v \qquad (4)$$

where μ, the differential moisture permeability (kgm/Ns), is a highly non-linear function of RH for hygroscopic building materials. While the vapour coefficient D_v will be inversely proportional to the barometric pressure, the liquid permeability coefficient D_l is expected to be independent of it.

2.2 The Measurement of Moisture Permeability

The moisture permeability of a material sample is measured under isothermal conditions by means of the standard gravimetric cup technique [9]. This involves the determination of the total moisture flux across the sample for a known vapour pressure gradient. The average moisture permeability $\bar{\mu}$ can then be calculated using the following expression

$$j_{tot} = \frac{\bar{\mu}\left(p_{vi} - p_{vo}\right)}{l} \tag{5}$$

where l is the sample thickness (m) and p_{vi} and p_{vo} are the vapour pressures inside and outside of the cup respectively.

Using the data from standard tests covering the whole humidity range, it is possible to generate the differential permeability function $\mu(\phi)$[4]. This allows the accurate evaluation of permeability appropriate to the humidity conditions to which a material is subjected in practice. Galbraith *et al* [10] proposed that the most appropriate integral form of this function is

$$\bar{\mu} = \alpha + \frac{\beta}{\Delta\phi\,(\gamma+1)}\left(\phi_2^{\gamma+1} - \phi_1^{\gamma+1}\right) = D_v + \overline{D_l} \tag{6}$$

where α, β and γ are coefficients derived using statistical techniques[8][10] and $\overline{D_l}$ is the average liquid permeability corresponding to the relative humidity conditions maintained on either side of the sample.

3 The Low Pressure Tests

The experimental evaluation of separate vapour and liquid transfer coefficients is made possible by carrying out gravimetric cup tests under reduced barometric pressures and is based on the assumption that only the vapour transfer coefficient will be dependent upon the barometric pressure. This allows equations (5) and (6) to be re-expressed as

$$j_{tot} = \bar{\mu}\frac{\Delta p_v}{l} = \left(\frac{D_v'}{p_b} + \overline{D_l}\right)\frac{\Delta p_v}{l} \tag{7}$$

A graph of $\bar{\mu}$ plotted against $1/p_b$ should produce a straight line of gradient D_v' and intercept $\overline{D_l}$.

3.1 Low Pressure Test Procedure

The ability to carry out gravimetric cup tests under a range of barometric pressures requires specialised equipment. Based on the experienced gained in the initial investigations [5], a new test apparatus has been designed and built. This basically comprises of a pressure vessel, 600mm in diameter and 500mm in height.

In line with standard gravimetric cup test procedures, six cups should be tested simultaneously under identical test conditions. To overcome this problem within the low pressure environment, a remote measurement technique was devised in order to consecutively weigh each of the six cups at given time intervals. This came in the form of a computer- controlled carousel arrangement which allowed each cup to be rotated into position, before being lowered until it rests freely on the balance. The weight of each cup is logged by computer.

The pressure inside the vessel is maintained by a vacuum pump and is constantly monitored using a pressure transducer. The relative humidity is maintained at a constant 58% by a series of trays containing saturated solutions of sodium bromide. The temperature and relative humidity are monitored closely throughout the duration of the tests. A schematic diagram of the entire measurement apparatus is shown in Figure 1.

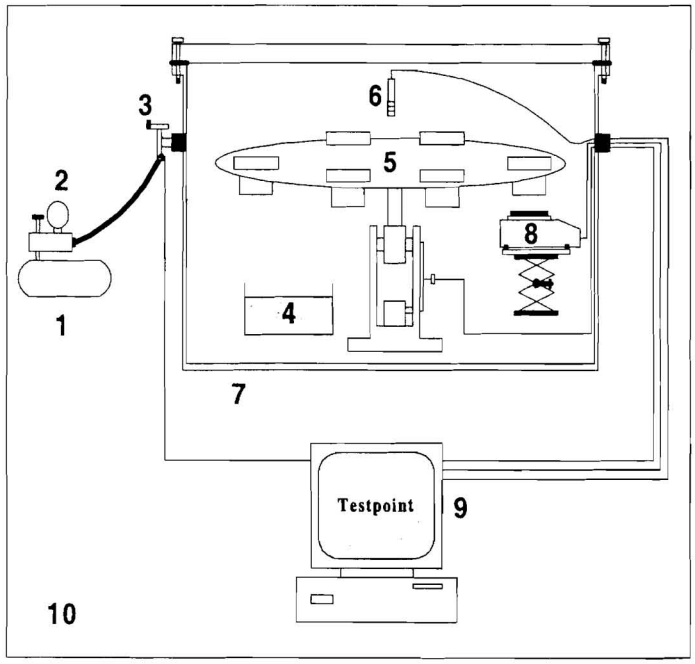

KEY :

1. vacuum pump
2. vacuum control switch
3. pressure transducer
4. vapour pressure regulator
5. carousel
6. RH and temperature sensor
7. pressure vessel
8. balance
9. computer
10. environmental chamber

Figure 1: Low Pressure Test Apparatus

At a selected test pressure, the weight change versus time graphs for each cup were produced and used to calculate the average permeability over the relative humidity range of the test. Results of several tests over identical RH conditions, but under different barometric pressures, were collated to produce plots of $\bar{\mu}$ against $1/p_b$.

3.2 Low Pressure Test Results and Comparison of Transfer Coefficients

The pressure test results for medium density fibreboard (MDF) are shown in Figure 2. The vapour pressure regulators used inside the cups were calcium chloride dessicant (3%RH), saturated solutions of ammonium chloride (80%RH) and ammonium dihydrogen orthophosphate (93%RH), and distilled water (100%RH). The temperature throughout the duration of the tests was maintained at 20°C.

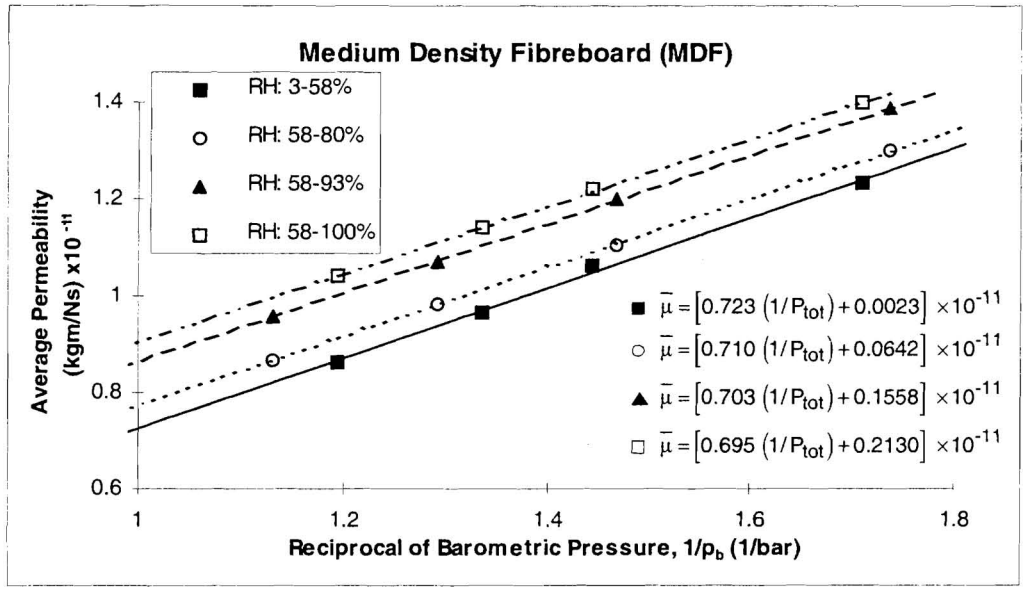

Figure 2: Pressure Test Results for MDF

Conventional gravimetric tests carried out on the test material yielded the following regression coefficients:

$$\alpha = 0.721 \times 10^{-11} \text{ kgm/Ns} \; ; \; \beta = 0.436 \times 10^{-11} \text{ kgm/Ns} \; ; \; \gamma = 0.452 \times 10^{-11}$$

The use of these values with equation (6) allows the determination of the vapour and liquid transport coefficients for the humidity conditions corresponding to those of the pressure tests. A comparison of vapour and liquid transfer coefficients, as evaluated using equation (6) and measured using the low pressure method are given in Table 1.

Table 1: Comparison of Transfer Coefficients

Test Conditions	Prediction Method			
	Conventional test		Pressure test	
RH	vapour $D'_v \times 10^{-11}$	liquid $\overline{D_l} \times 10^{-11}$	vapour $D'_v \times 10^{-11}$	liquid $\overline{D_l} \times 10^{-11}$
3 - 58%	0.721	0.007	0.723	0.002
58 - 80%	0.721	0.050	0.710	0.064
58 - 93%	0.721	0.140	0.703	0.156
58 - 100%	0.721	0.179	0.695	0.213

4 Discussion

An experimental procedure to measure material moisture permeability under reduced barometric pressure has been described and results from tests conducted on a hygroscopic building material have been reported. These results concur with previously reported low pressure measurements on particleboard [5] and current data being obtained for plasterboard.

The low pressure tests provide an experimental method to measure the individual transfer coefficients of vapour and liquid. The graphical representation of low pressure permeability data shows a reducing linear gradient as a function of increasing RH. This illustrates the reducing vapour transfer coefficient at RH values above 60%, shown in Table 1, where capillary condensation occurs. Although accepted as a theoretical description of the transfer process, the reduction in the vapour component has been unmeasurable until now.

Another feature of the low pressure test method is the rapid attainment of experimental results. The reduction in barometric pressure accelerates the equilibrium period by several orders of magnitude in some cases. This eliminates the lengthy test durations which are typical of standard gravimetric measurements, and reduces the probability of material degradation and/or inconsistent environmental test conditions.

The development of the low pressure technique is continuing and it is anticipated that a detailed theoretical analysis of the test procedure will be reported in the near future along with measurement data covering an extended range of common building materials.

References

[1] PEL L. 'Moisture Transport in Porous Building Materials', PhD Thesis, Technical University Eindhoven, 1995.

[2] ROSE D A. 'Water Movement in Porous Building Materials: Part 2 - The Separation of the Components of Water Movement', British Journal of Applied Physics, Vol. 14, 1963.

[3] GALBRAITH G H, McLEAN R C, TAO Z. 'Separation of Moisture Flow Through Porous Building Materials into Vapour and Liquid Components', Building Services Engineering Research and Technology, CIBSE Series A, Vol. 14, No. 3, 1993.

[4] McLEAN R C, GALBRAITH G H, SANDERS C. 'Moisture Transmission of Building Materials and the Presentation of Vapour Permeability Values', Building Research and Practice, Vol. 18, No. 2, 1990.

[5] GALBRAITH G H, McLEAN R C, KELLY D J. 'The Measurement of Moisture Permeability Under a Range of Total Pressures', CIBW40 Conference, Kyoto, Japan, 1997.

[6] ANDERSSON A C. 'Verification of Calculation Methods for Moisture Transport in Porous Building Materials', Swedish Council for Building Research, 1985.

[7] GALBRAITH G H. PhD Thesis, University of Strathclyde, 1992.

[8] GALBRAITH G H, McLEAN R C, GUO J. 'Moisture Permeability Data: a Mathematical Presentation', Building Services Engineering Research and Technology, CIBSE Series A, Vol. 19, No. 1, 1998.

[9] European Standard CEN/TC 89N. 'Thermal Performance of Buildings and Building Components: Determination of Water Vapour Transmission Properties', 1995.

[10] GALBRAITH G H, McLEAN R C, GUO J. 'Moisture Permeability Data Presented as a Mathematical Function Applicable to Heat and Moisture Transfer Models', Fifth International IBPSA Conference, Prague, 1997.

PROBLEMS OF MOISTURE MEASUREMENT WITH LOW RESOLUTION NMR

A.Y. Munsi, G.H. Galbraith, C.H. Sanders, R.C. McLean

PROBLEMS OF MOISTURE MEASUREMENT WITH LOW RESOLUTION NMR

A. Y. Munsi*, G. H. Galbraith*, C. H. Sanders, and R. C. McLean*****,

* Department of Building and Surveying, Glasgow Caledonian University, Glasgow, Scotland.
** Building Research Establishment (BRE), East Kilbride, Glasgow, Scotland.
*** Department of Mechanical Engineering, University of Strathclyde, Glasgow, Scotland.

Abstract

As moisture is a major problem for the durability of construction materials, it must be considered in building design for extended life of the structures. A Nuclear Magnetic Resonance (NMR) spectrometer is one method of measuring the moisture content in building materials. In this study, different parameters of a low resolution NMR spectrometer were investigated. The longitudinal spatial resolution was found to be wide spread. The effect of that may be a large error in the measurements where a short steep moisture gradient or variation in moisture gradient in a short distance is present. The signal distribution in the radial direction of the NMR was also found to be un-symmetrical, which made the situation worse. It is suggested that to minimise error in the measurements a standard sample prepared maintaining a close tolerance should be used and should be placed in the same position in the measurement area every time. The NMR signals were found to decrease due to increase in the sample temperature. To overcome the problem it is suggested that the measurement should be carried out in a very short time or the temperature effect should be considered.

Key words: Moisture Measurement, Building Materials, Nuclear Magnetic Resonance.

1. Introduction

Moisture is an important factor in most of the processes that cause deterioration of building materials, playing a dominant role in accelerating the degradation process[1]. The damage may be in several forms such as the decay of wood, swelling of materials leading to cracking, corrosion of metals, reduced frost resistance, freezing damage etc. Moisture also increases thermal conductivity of materials and hence increases the loss of energy from buildings. The cost of damage due to moisture is billions of pounds around the globe. Moisture can enter a structure by driving rain (which may be contaminated), flooding, condensation, run off from a roof and capillary rise of ground water. Water can transport contaminants such as soluble salts, which may remain in the structure on drying and cause structural damage, e.g. delamination, surface chipping or disintegration.

It has become generally accepted that the climate is changing due to greenhouse gas release and deforestation; besides increased temperatures and rising sea levels, both wind and rain are expected to increase in North west Europe, increasing the stress of driving rain on building facades[2].

Porous building materials are very vulnerable to moisture related damage since the pores allow water to enter into the structure. Many historical buildings and monuments in the UK are made of highly porous sandstone, where water can penetrate easily through the wall and make the building damp. If no measures are taken and the degradation continues then there is a possibility of collapse of the building structure and loss of lives.

Both the heat and moisture properties of the materials must be considered for effective building design. While the thermal properties of building materials have been determined by different researchers and considerable data are available, the equivalent moisture properties are absent. The data which are available are so scattered in different sources that any coherent conclusion cannot be made. An extensive study of moisture properties of different building materials, e.g. sandstone, mortar, brick, timber etc, is necessary to provide the relevant information.

There are a number of different methods to measure moisture in building materials including Nuclear Magnetic Resonance (NMR)[3,4], Neutron Radiography[5], Gamma ray[6,7] or X-ray abosrption, as well as the traditional oven drying. It has been demonstrated[3] that the moisture measurement using a NMR spectrometer is more effective than Neutron Radiography. This paper, part of a detailed study aimed at determining the different moisture properties of building materials investigates the importance of different parameters of the NMR spectrometer as a preliminary to the main investigation.

2. Description of Equipment

In this investigation a low resolution Nuclear Magnetic Resonance (NMR) spectrometer (manufactured by BRUKER ANALYTISCHE MESSTECHNIK, GMBH, Germany) was used to measure the moisture present in the specimens. The system is equipped with a permanent magnet with 125 mm pole-diameter, 50 mm airgap, the set frequency is 10 MHz (0.23 Tesla) with automatic field adjustment. No magnetic gradient is included to obtain a higher spatial resolution. The measurement position (situated in the airgap) is a cylindrical hole of diameter is 40 mm and the size of the probehead is 4 mm. The system operating temperature is 40 ^{0}C is maintained with a close tolerance.

The specimens are placed in the measurement position and the free induction decay (FID) signals from the hydrogen atoms present recorded. Since the investigation is aimed to determine the amount of moisture, i.e. the number of hydrogen atoms present in the specimen, the maximum intensity of the signals was taken. There are different settings in the spectrometer such as number of scans, recycled delay, analogue bandwidth, digital bandwidth, gain etc. Each of them was individually investigated to find out their effect on the signals (not shown here). The settings were optimised for the measurements and thereafter kept constant.

3. Experimental Procedure and Result

3.1 Investigation of Spatial Resolution in the Longitudinal Direction

The spatial distribution of the signals in the measurement position was determined using water samples or water saturated absorbent paper samples. To determine the spatial resolution in the longitudinal direction, a thin, absorbent paper sample 17 mm diameter and 0.912 mm thick, saturated with ~0.25 grams of water, was passed through the measurement position of the spectrometer held in a glass syringe. The experimental set-up for the investigation is shown in Figure 1.

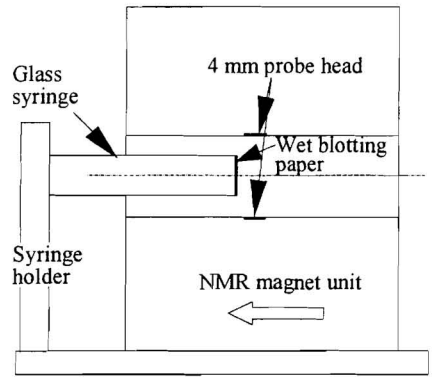

Figure 1 – Experimental set-up for determining the longitudinal sensitivity

The longitudinal spatial resolution was measured 4 times giving a similar pattern of signal distribution each time. One of the 4 measurements is presented here (Figure 2), where an exponential curve $y = \exp(-Ax^2)$ is fitted to the measured data.

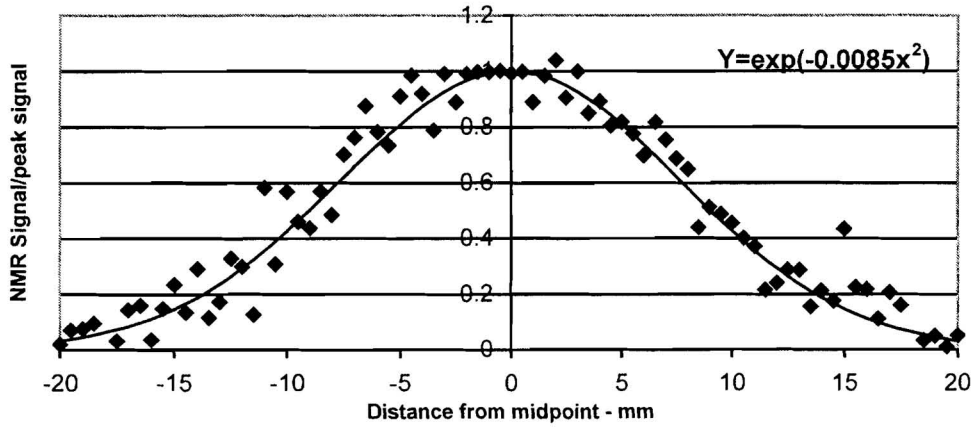

Figure 2 – Longitudinal resolution curve of the NMR spectrometer

The effective length of the NMR measurements were calculated by integrating the area under the fitted exponential curve and dividing the area by the maximum height. The effective lengths of the four different tests were 19.43mm, 19.34 mm, 19.89 mm, and 18.49 mm giving an average of 19.3 mm.

3.2 Investigation of Spatial Resolution in the Radial Direction

To determine the horizontal and vertical spatial resolution, a water filled glass tube, of 4 mm ID and 5 mm OD, was moved through the measured position vertically and horizontally as shown in the experimental set-up in Figures 3 and 4. The NMR signals were measured from two perpendicular radial lines: a horizontal line and a vertical line (shown in Figures 3 and 4).

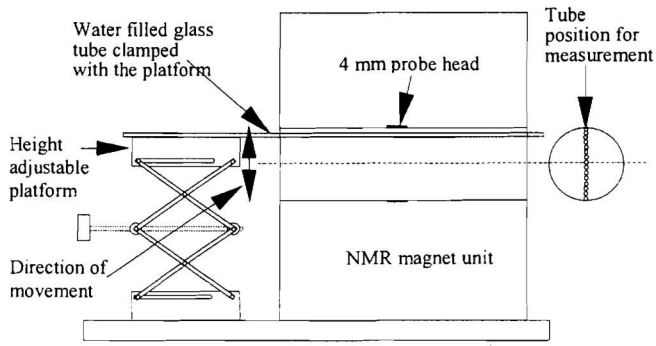

Figure 3 - Experimental set-up to determine radial distribution of NMR signals

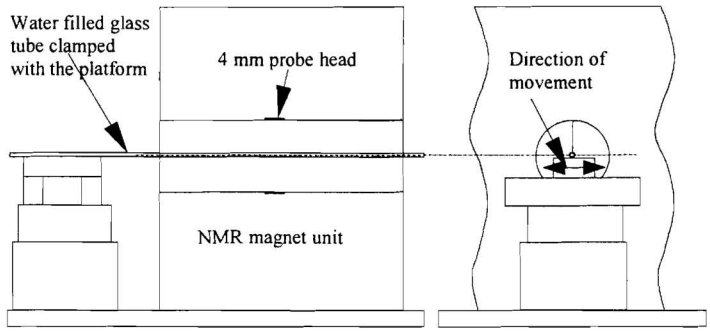

Figure 4 – Experimental set-up for horizontal sensitivity measurement

The signals were measured twice, in both measurements a similar pattern of signal distribution was found. The signals were plotted against the distance from the centre of the hole of the NMR (shown in Figure 5).

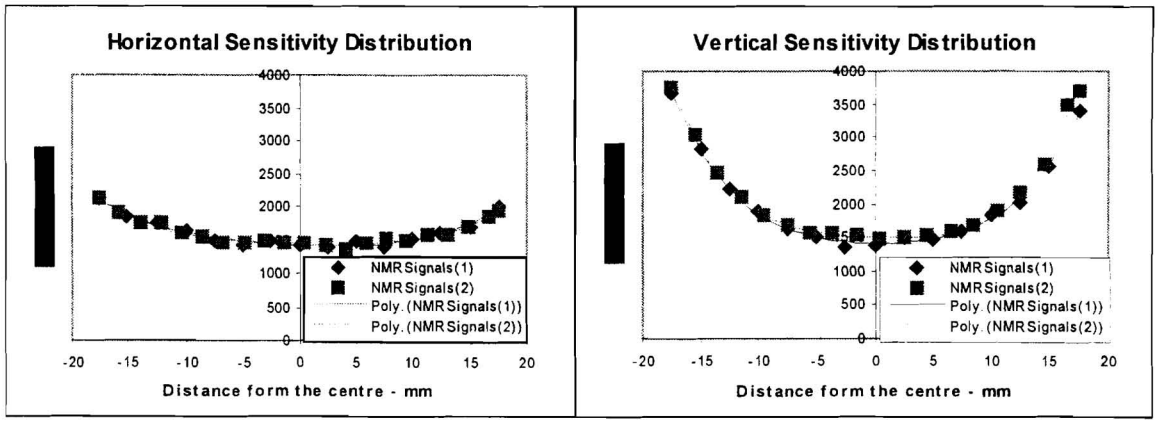

Figure 5 – Distribution of NMR signals in two perpendicular radial directions.

The signals were found to be a minimum at the centre of the measurement position increasing towards the wall. The distribution of the signals was symmetrical in both the horizontal direction and vertical directions but the variation was much higher in the vertical.

3.3 Investigation of Temperature Effect on the NMR Signals

The effect of sample temperature on the NMR measurements was also investigated. Samples of sandstone were crushed, saturated in water and placed in a sealed glass tube, heated to constant temperature in a water bath as shown in Figure 6.

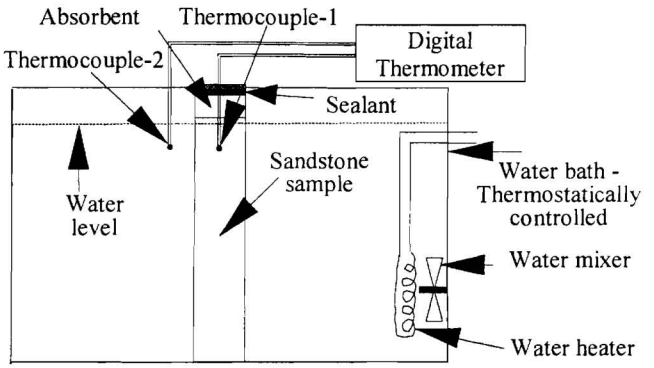

Figure 6 - Set-up for heating the sample at different levels of temperatures.

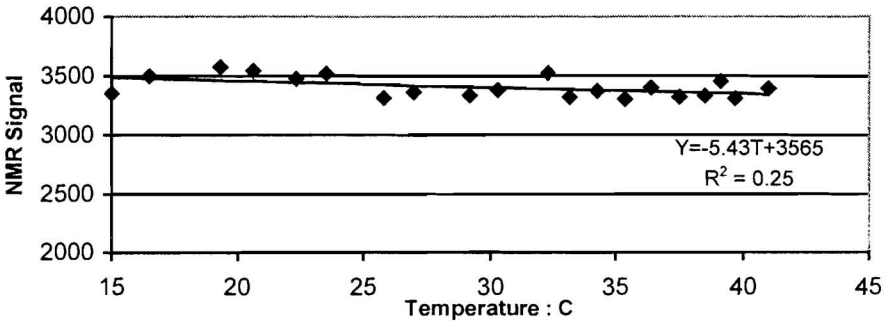

Figure 7 - NMR signals of wet crushed sandstone

The temperatures of the sample and water were measured and when the difference between the two temperatures was 0.1 ^{0}C or less the sample was taken out and the maximum NMR signal measured. The experiment was repeated giving similar results on each occasion. Figure 7 shows the result of one run.

Although there was a considerable amount of scatter the signals decreased as the temperature increased, with a gradient of -5.43 °C^{-1}. In contrast, a similar test with pure water gave a gradient of –22 °C^{-1}. This implies that there must be a relationship between the moisture content and decrease in signals due to temperature increase. However, when these changes are compared to NMR signal changes of about 1000 for a 1% (by mass) change in water content in sandstone samples observed previously[8], temperature effects can be considered negligible.

4. Conclusion

The longitudinal sensitivity of the machine is widespread (~38 mm), making it difficult to measure the distribution of moisture in a material with a gradient is present. A companion paper investigates the effect of this on the calculated liquid water diffusivity of typical building materials[9].

The sensitivity in the radial direction was found to be non-isotropic, with a much larger variation in the vertical compared to the horizontal direction. While this distribution does not cause any problems with samples that fill the measuring area, for the measurement of building materials where the specimens may be cut from a large sample, it may be difficult to prepare a sample of standard geometry. To minimise error the specimens should be prepared to certain geometry maintaining a very close tolerance.

The investigation of the temperature effect showed that signals from moisture decreases as the temperature of the sample increases. This does not cause any problem to the samples where very low moisture is present and measurement can be carried out in a very short period (2 to 3 minutes). For specimens with larger moisture content or if the measurement takes bit longer time the temperature effect may need to be considered. The solution of this problem is may be modifying the machine to operate at a lower constant temperature of say 20 ^{0}C and placing the system in an environmentally controlled chamber.

References

1. Hagentoft, C-E, The impact of heat, air and moisture transport on energy demand and durability, IEA Annex 24 Report 5: Performances and Practice, K-U Leuven 1998
2. Garvin, S.L., Phillipson, M.C., Sanders, C.H., Hayles, C.S. and Dow, G.T., Impact of climate change on building. BR349, BRE 1998.
3. Pel, L. Moisture Transport in Porous Building Materials, *PhD thesis*, Eindoven University of Technology 1995, The Netherlands.
4. Pel, L. et. al. Moisture Transport in Building Materials, *HERON*, Volume 41, No. 2, pp. 95-108, 1996.
5. Jutnes, H., Bryhn-Ingebrigsten, K. and Rosvold, G.O., Neutron radiography : an excellent method of measuring water penetration and moisture distribution in cementitious materials. Advances in Cement Research, 1994, 67-72.
6. Kumaran, M.K., Bomberg, M : A Gamma-Spectrometer for determination of density distribution and moisture distribution in building materials. Proc. of the International Symposium on Moisture and Humidity, Washington D.C. (1985), S 485-490.
7. Adan, O. C. G, Determination of Moisture Diffusivities in Gypsum Renders, *HERON*, Volume 40, No. 3, pp. 201-216, 1995.
8. Dow, G.T. et al Preliminary measurements of moisture in building materials using NMR spectroscopy. CIB W40 : Kyoto 1997.
9. Munsi, Y, Sanders C H, Galbraith, G.H. and McLean, R.C., The effect of instrument resolution on diffusion coefficients measured with NMR spectroscopy – to be published.

MEASUREMENTS OF PSYCHROMETRIC CONDITIONS IN DUST-MITE MICROENVIRONMENTS

M.J. Cunningham

MEASUREMENTS OF PSYCHROMETRIC CONDITIONS IN DUST-MITE MICROENVIRONMENTS

M J Cunningham

Building Research Association of New Zealand (BRANZ)
BRANZMJC@BRANZ.ORG.NZ

Abstract
A very small relative humidity sensor has been used to measure directly humidities in dust-mite microenvironments. Microhabitats examined were: bedding; furniture; and carpets with and without sub-carpet heating.

Bedding relative humidities showed complex behaviour according to the distance separation between the measuring point and the occupant. Immediately below the occupant, bed relative humidities *fell* when the person entered the bed. Similar behaviour is observed in a sofa.

In unheated carpets, humidities in the base were significantly higher than room humidities. In heated carpets temperatures became as high as 39 °C with corresponding relative humidities down to 24%.

Since it has been shown that dust mite microclimates can be very different from room conditions, reduction of dust mite numbers and allergen levels by the controlling of room humidities cannot be guaranteed to be successful without measuring and controlling microenvironmental conditions.

Keywords Indoor climate, microclimate, humidity, dust-mite, asthma

1. INTRODUCTION

There have been many studies examining the effectiveness of dust mite control by lowering room air relative humidity [1-7]. These studies have had mixed success. Failure to achieve sufficiently low relative humidities in the dust mites' microhabitat is one reason for these mixed results; changing room psychrometric conditions (temperatures and humidities) are only one factor determining psychrometric conditions in microhabitats such as bedding, the base of carpets, furniture etc.

1.1 Measurement of Microclimates

A new, very small, relative humidity sensor has been built capable of distinguishing relative humidity differences over distances of millimetres [8], e.g. between the top of a carpet and the base of the carpet pile. Results for bedding, furniture and carpeting and sub-carpet heating are reported here.

To acquire the bedding data, relative humidity sensors and thermistors were placed immediately under the bottom sheet and in several locations through the mattress. Only humidities under the bottom sheet are reported here. Sensors were placed just inside the lining of a sofa, to obtain the furniture data, and into the room air and the base of a carpet to obtain the carpet data.

One set of measurements was made in a living-room carpet with sub-carpet heating. The heating system consisted of plastic sheets with embedded electrical heating wire, the sheets being placed on the floor underneath the carpet. Data reported here was obtained from sensors placed at the base of the carpet pile.

2. RESULTS AND DISCUSSION

2.1 Carpets

Base-of-carpet results shown in Figure 1 are for 24 hours from midnight.

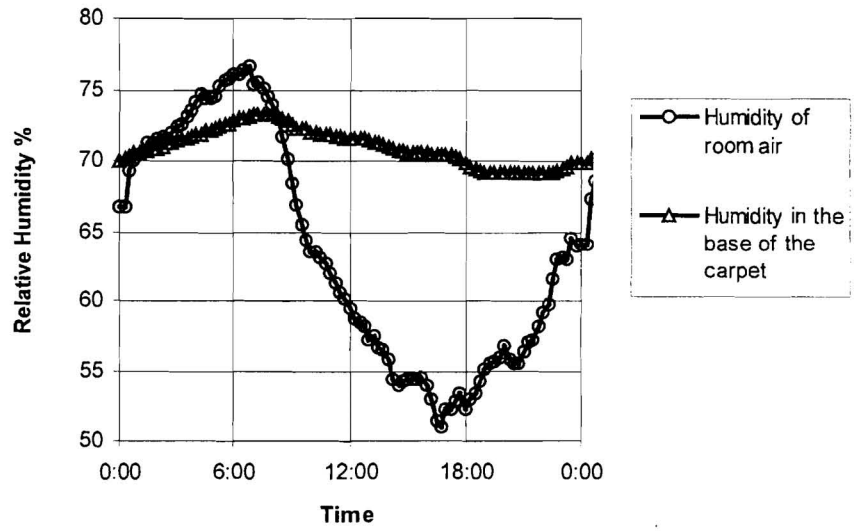

Figure 1: Measured base-of-carpet psychrometric conditions (unheated)

Significantly, it can be seen that the carpet is, on average, about 7% humidity above the room value. (See [9] for more discussion on this result.) The difference between the room air and carpet humidity values is important; although the room air humidity is possibly too low for mite survival, the value in the base of the carpet is not.

These results were obtained with the carpet on a suspended, uninsulated wooden floor. They are likely to be quite different for different flooring systems, such as concrete slabs, floors of non-ground stories, and floors with different sub-floor insulation detailing.

2.2 Sub-Carpet Heating

These results are for a different house than the one described above. Here a thermostated heating pad was laid on the floor under the carpet.

Measured humidities in the base of a carpet with thermostated sub-carpet heating over a period of 24 hours are shown in Figure 2. Temperatures in the base of the carpet rose to 39 °C. Under these conditions mites die only slowly [10,11].

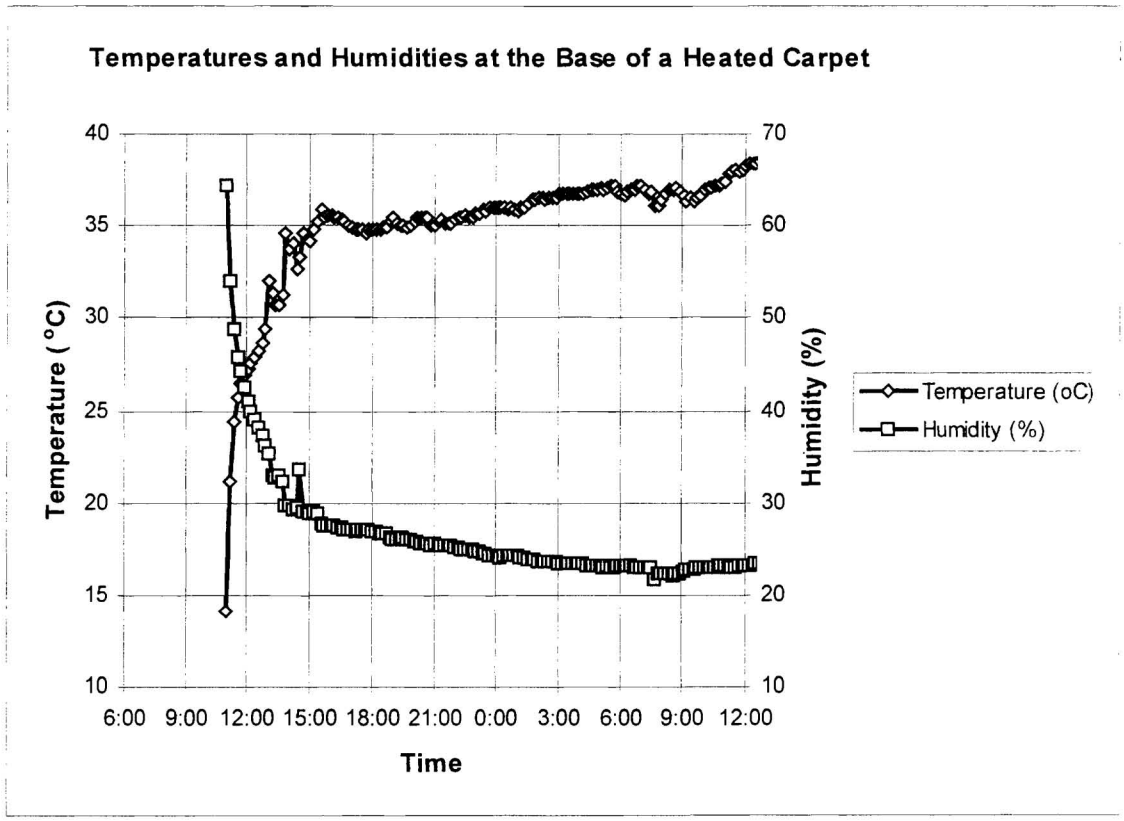

Figure 2: Carpet with sub-carpet heating – measured conditions in the base of the carpet

2.3 Bedding

Bedding humidities, directly under the lower sheet, are shown in Figure 3 for 24 hours from midnight.

During the period that the bed is occupied, the temperatures are high directly below the occupant, up to 36 °C, and the humidities are low, down to 45%. Contrary to expectations, the relative humidity *falls* when a bed is occupied. When the bed is occupied, temperatures and vapour pressures rise due to occupant body heat and moisture release; relative humidities are derived quantities in this case whose values are difficult to calculate *a priori*, see Cunningham [9].

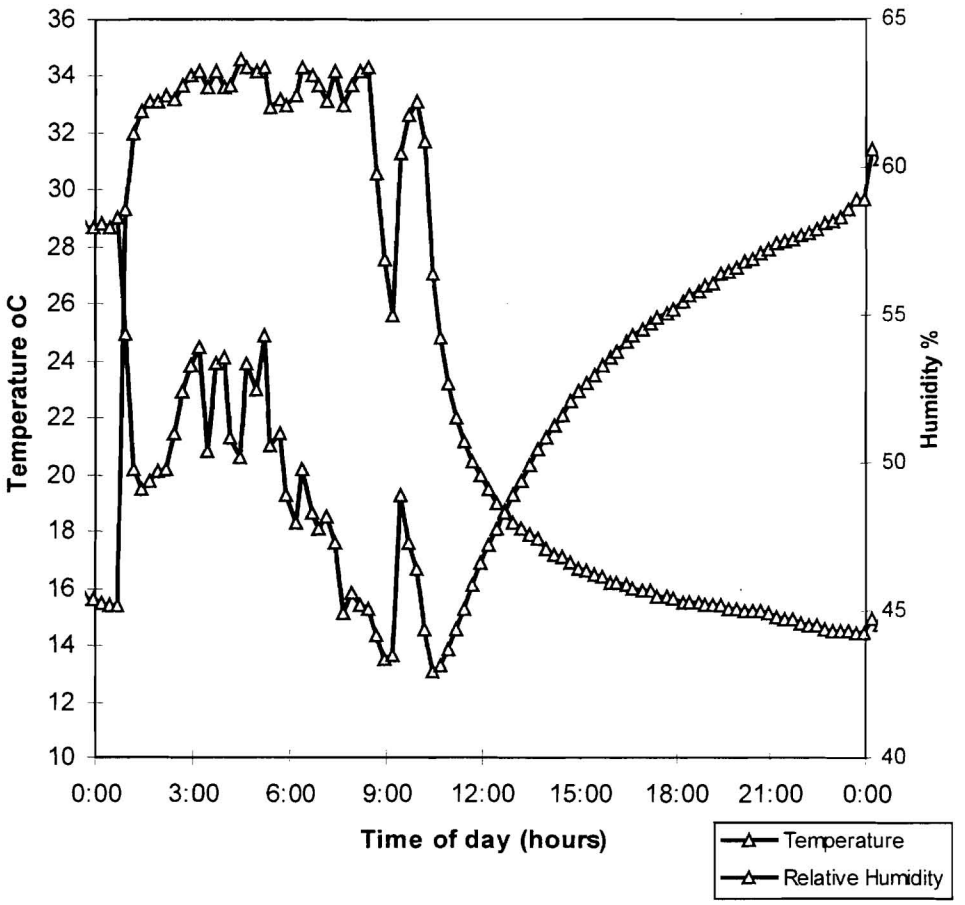

Figure 3: Measured bedding psychrometric conditions, directly under lower sheet

At first sight it appears the humidities under the sheet when the bed is occupied are easily low enough to kill mites. However, mite populations have been subjected to these bed conditions under controlled laboratory conditions and it has been found that these populations are quite viable [12].

2.4 Furniture

Measured humidities just under the surface of the back of a sofa are shown in Figure 4 for 48 hours from midnight.

The humidities and temperatures just under the fabric of the sofa show similar behaviour to those in bedding, i.e. when a person sits on the sofa relative humidities fall, because the temperature rise due to body heat contributes more to relative humidity fall than body moisture contributes to relative humidity rise.

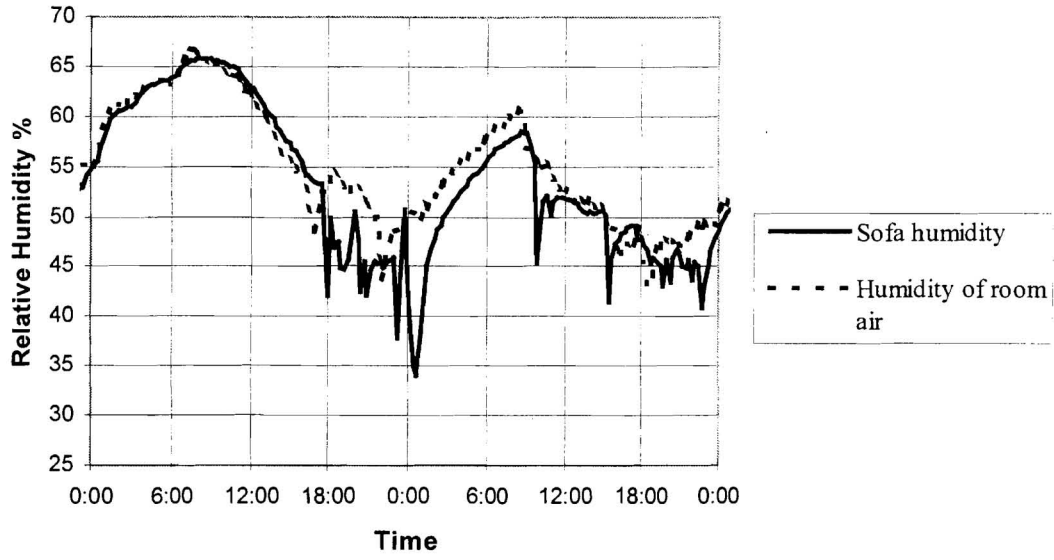

Figure 4: Measured humidities just under the surface of the back of a sofa

3. CONCLUSIONS

Results have been presented for microclimates in bedding, furniture, and carpets with and without sub-carpet heating. These measurements have been made with a very small relative humidity sensor capable of resolving humidity differences over a scale of millimetres. In some cases, particularly for bedding, the results were complex, and different from expectations. Experiments are in place measuring dust-mite viability in a controlled laboratory situation, using the real-world driving psychrometric conditions reported upon here.

4. ACKNOWLEDGEMENTS

The author wishes to thank Professor G. Tsongas, Portland State University, for directing him to the source of the humidity transducer that forms the basis of the device used in this work.

This research was funded by the New Zealand Building Research Levy and the Foundation for Research, Science and Technology's Public Good Science Fund (New Zealand).

5. REFERENCES

1. Korsgaard, J. 1983. Preventive measures in mite asthma. A controlled trial. *Allergy*, Vol. 38, pp. 93-102.
2. Walshaw, M. and Evans, C. 1990. Control of house dust mite antigen in bedding. *Lancet*, Vol. 335, p. 911.
3. Harving, H.; Korsgaard, J. and Dahl, R. 1988. Mechanical ventilation in dwellings as preventive measures in mite asthma. *Allergy Proc*, Vol. 9, p. 283.
4. Schober, G. 1988. Moisture and the production of household allergens. *Allergologie*, Vol. 11, p. 229.
5. Fletcher, A.; Custovic, A.; Kennaugh, J.; Taggart, S.; Pickering, A. and Woodcock, A. 1994. Dehumidification as a method of mite allergen avoidance in United Kingdom: can it work? *Mites, Asthma and Domestic Design, II.* Proc of 2nd Conf, Sydney, Nov, p. 101.
6. Cabrera, P.; Julia-Serda, G.; Rodriguez de Castro,F.; Caminero, J.; Barber, D. and Carrillo, T. 1995. Reduction of house dust mite allergen after dehumidifier use. *J Allergy & Clin Immunol,* Vol. 95, p. 635.
7. Hyndman, S.J.; Vickers, L.M.; Htut, T.; Maunder, J.W.; Peock, A. and Higenbottam T.W. 1997. A trial of dehumidification and ventilation behaviour in house dust mite control. *American Journal of Respiratory and Critical Care Medicine*, Vol. 155, No. 4: A940.
8. Cunningham, M.J. 1999. Development and performance of a small relative humidity sensor for indoor microclimate measurements. *Building and Environment*, Vol. 34, no 3, p. 349.
9. Cunningham, M.J. 1998. Direct measurement of temperature and humidity in the microhabitats of house dust mites *J Clinical & Exp Allergy*, Vol. 28, p. 1104.
10. Chang,J., Arlian,L., Dippold,J., Rapp,C., Vyszenski-Moher,D. 1998. Survival of the house dust mite Dermatophagoides farinae at high temperatures (40 - 80 oC) *Indoor Air*, volume 8, p34
11. Shibasaki,M., Takita,H. 1994. Effect of electric heating carpet on house dust-mites *Annals of Allergy*, volume 72, p541.
12. Cunningham, M.J.; Andrews, J.; Pyke, A. and Hearfield, M. 1999. *In preparation.*

HYGROTHERMAL MEASUREMENTS FROM A TEST HOUSE – A DATABASE FOR VERIFICATION OF HEAT-, AIR- AND MOISTURE TRANSFER MODELS

S. Geving, J.V. Thue, S.Uvslokk

HYGROTHERMAL MEASUREMENTS FROM A TEST HOUSE – A DATABASE FOR VERIFICATION OF HEAT-, AIR- AND MOISTURE TRANSFER MODELS

Stig Geving[1], Jan Vincent Thue[2], Sivert Uvsløkk[1]

[1] Norwegian Building Research Institute, Trondheim Department, Høgskoleringen 7, N-7491 Trondheim, Norway.
[2] Norwegian University of Science and Technology (NTNU), Department of Building and Construction Engineering, N-7491 Trondheim, Norway.
EMail: stig.geving@byggforsk.no, jan.thue@bygg.ntnu.no, sivert.uvslokk@byggforsk.no

Abstract

Hygrothermal measurements have been performed on different building envelope constructions at a test house in Trondheim, Norway. One of the main purposes of the test house measurements was collecting data for comparison with computer simulations of transient moisture transfer in building constructions. The measurement data from this test house are made available for research scientists who want to verify computer models for heat, air and moisture transfer through building structures.

This paper gives a short description of the data that are available for verification purposes from the test house. This includes a description of the test house, the wall and roof elements investigated, the instrumentation of the elements, boundary conditions, outdoor climatic parameters measured and measured material properties.

Key words: test house, database, verification, moisture transfer models

1 Introduction

As a part of the research programme "Moisture in building materials and constructions" (1993-97), experiments have been performed on different building envelope constructions at a test house in Trondheim, Norway. Most of the test elements were lightweight timber frame constructions. The roof elements were all horizontal with a high degree of one-dimensionality. The timber frame walls had different combinations of vapour retarders and wind barriers. The external surfaces were exposed to the ambient climate, while the indoor climate in the house was controlled at 23 °C and 50 % RH. The outdoor climate was monitored by an automatic weather station situated 10 meters from the test house. Moisture and temperature conditions in the elements were monitored continuously. The test house and the various measurements are thoroughly documented in [1].

2 Description of the test house

The roof and facades of the test house consist of prefabricated sections fixed to the outside of a steel frame structure. The test house is orientated in north-south direction and has the following indoor dimensions: length 10.7 m, width 3.45 m and height 3.5 m. The roof sections span from facade to facade, and have a 1:40 slope. All sections are 1,2 m wide and they are separated from each other regarding air and moisture transfer, by use of polyethylene foil. The sections may be changed individually without disturbing the neighbour sections. There are a total of 16 wall sections on the western and eastern facades and 8 roof sections. The test house is equipped with a low temperature electric heating system, balanced mechanical ventilation with heat recovery and an automatic air humidifying system. The test house is shown in Figure 1.

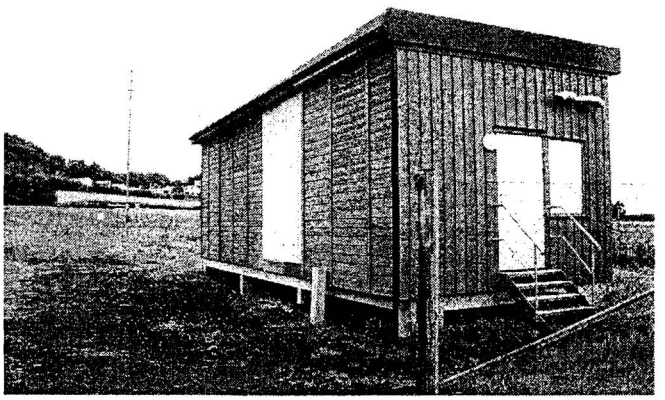

Figure 1 A south-west view of the test house.

3 Description of wall and roof sections

The wall sections are described in detail in Table 1. All the wood frame walls has 150 mm insulation, except of section E8 which has 300 mm insulation and a wood frame made of wooden I-joists instead of solid spruce. All the wall sections, except of sections W2, W5, E5 and E6, has a 23 mm ventilated air gap and 19 mm shiplap cladding outside of the wind barrier. Section W2 has 19 mm shiplap cladding but no air gap between the wind barrier and the cladding. Section W6 has noggings (with 0.8 m spacing) between the studs.

The wood frame roof sections (R1-R6) consists of the following materials from the interior; 12 mm chipboard, 0,15 mm polyethylene foil, 200 mm glass fibre (48x198 mm wooden beams), 22 mm plywood and 1,3 mm PVC roofing membrane. In two of the wood frame roof sections (R5 and R6) the beam spacing is 1.2 m, while the other four wood frame roofs (R1-R4) have a more normal 0.6 m spacing. In sections R5 and R6 the wooden beams are separated from the rest of the section with a polyethylene foil (see Figure 3). Four elements (R1, R6-R8) have a dark coloured roofing membrane

(emissivity ≈ 0.9), while the other four have a light coloured roofing membrane (emissivity ≈ 0.65). Section R7 and R8 consists of respectively 300 mm and 200 mm (+100 mm Rockwool) aerated concrete with PVC roofing membrane on the top.

Table 1 Description of materials used in the various wall sections. W1 and E1 denote section no. 1 on the western facade and eastern facade respectively. "Ratio" is the ratio between the water vapour resistance on the hot and on the cold side.

Sections	Internal lining	Vapour barrier	Wall construction/insulation	Wind barrier	Ratio (-)
W1	wood fibre board 12 mm	polypropylene foil (wind barrier)	wood frame wall (48x148 mm) / 150 mm glass fibre	wood fibre board 12 mm	35
W2* + W3	wood fibre board 12 mm	polypropylene foil (wind barrier)	wood frame wall (48x148 mm) / 150 mm glass fibre	gypsum board 9 mm	62
W4 + E4	wood fibre board 12 mm	-	wood frame wall (48x148 mm) / 150 mm glass fibre	gypsum board 9 mm	7
W5 + E5	-	-	LECA-block 250 mm/ 80 mm PUR-insulation in the middle	-	-
W6	gypsum board 9 mm	-	wood frame wall (48x148 mm) with noggings / 150 mm glass fibre	gypsum board 9 mm	1
W7 + W8	gypsum board 9 mm	-	wood frame wall (48x148 mm) / 150 mm glass fibre	gypsum board 9 mm	1
E1	wood fibre board 12 mm	polyethylene foil 0.15 mm	wood frame wall (48x148 mm) / 150 mm glass fibre	asphalt impr. wood fibre board, 12 mm	280
E2 **	wood fibre board 12 mm	polyethylene foil 0.15 mm	wood frame wall (48x148 mm) / 150 mm glass fibre	spunbonded polyethylene foil	3200
E3**	wood fibre board 12 mm	polyethylene foil 0.15 mm	wood frame wall (48x148 mm) / 150 mm glass fibre	polypropylene foil	14
E6 + E7	-	-	aerated concrete 300 mm	-	-
E8	wood fibre board 12 mm	-	wood frame wall (300 mm I-joists) / 300 mm glass fibre	gypsum board 9 mm	7

* No air gap between the wind barrier and the cladding.
** In September 1996 the wall sections E2 and E3 were modified. The wind barrier of section E3 was changed to 9 mm gypsum board. For both sections a horizontal 3 mm wide gap was sawn through the internal lining and vapour barrier near the bottom sill, and a similar gap through the wind barrier near the top sill at the external side.

4 Description of measurements

4.1 Hygrothermal measurements in wall and roof sections

The locations of the measuring devices for moisture content (MC) and temperature are shown in Figure 2. The logging system stores hourly mean values. The measurements started in October 1994 and lasted till June 1998. The moisture content of the timber frame members is measured by traditional pin electrode resistance measurements. The top plates, the bottom plates and the studs were instrumented for moisture measurements on the cold as well as warm side of the constructions. Corresponding temperature measurements were only employed for the studs. The MC electrodes intruded from the insulation cavity side until a depth so that the unprotected part of the

electrode was located 4-14 mm beneath the opposite wood surface. Surface temperatures were measured at the inside of the wind barrier and at the interior surface at the top and bottom section of the wall.
In September 1996 the wall sections E2 and E3 were modified to investigate the effect of forced convection, see Table 1. Relative humidity and temperature were then in a period measured at three heights in the middle of the insulation layer.

The locations of the measurement points in the roof sections are shown in Figure 3. Measurements were made in two different sections of the roof section, so every measurement location shown on the figure is represented by two parallel measurements. Relative humidity has been measured in three different depths in the roof and wall sections consisting of aerated concrete since February 1996.

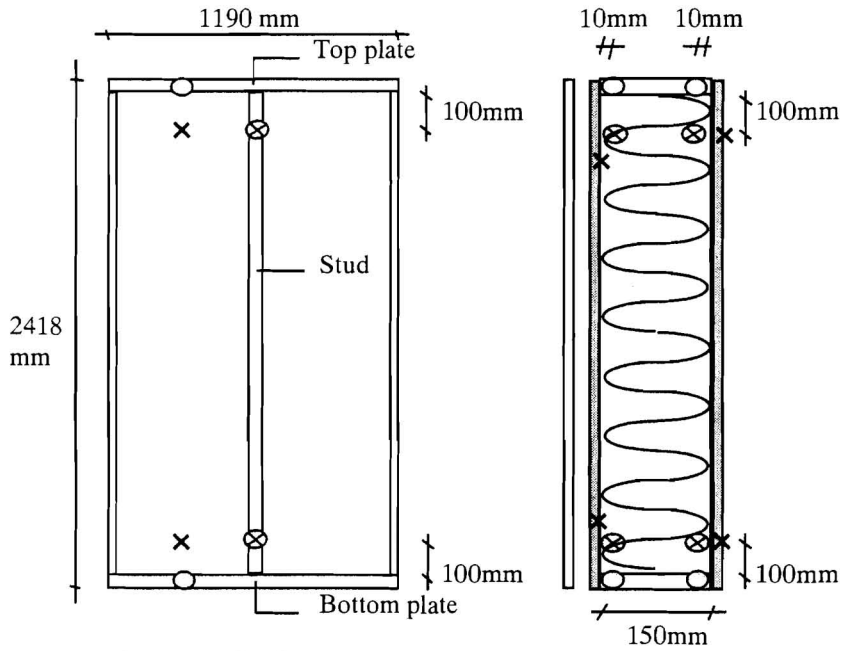

Figure 2 The framework of the wall test section, with measuring points.

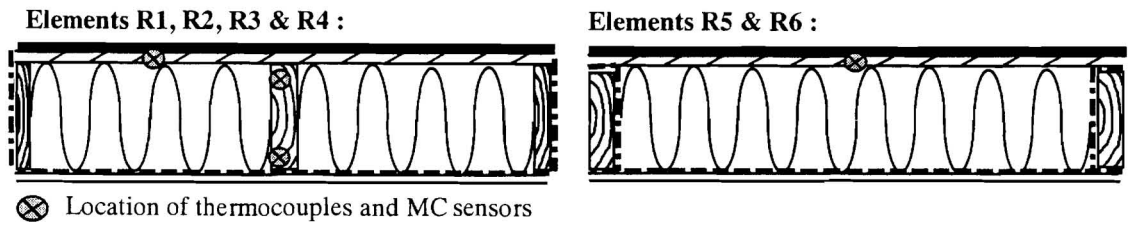

Figure 3 Measurement points in the roof sections, in wooden beams and plywood layer.

4.2 Other measurements

External climate data are measured with a Milos 500 Vaisala automatic weather station (AWS) placed 10 m to the south of the test house. Hourly averages of air temperature, relative humidity, air pressure, wind speed, wind direction, precipitation and global radiation are measured. In addition to the hourly average the maximum and the minimum minute average last hour is logged. The AWS has been operating since 15. March 1995. A program has been developed that estimate the hourly values of diffuse and direct solar radiation from global radiation.

Indoor air temperature and RH have been controlled at a constant level of 23°C and 50% RH, and are automatically logged every hour. The indoor air pressure was negative compared with outdoor pressure until April 1997, when it was turned to be positive by adjusting the ventilation system.

The water vapour permeability and hygroscopic sorption curves have been measured for most of the materials used in the test house. The measurements are documented in an accompanying paper [2]. Air permeability of same type glass fibre insulation has also been measured [3].

The air tightness of the wood frame wall sections have been measured on site. Data for air leakage through the sections, from one side to the other, have been estimated.

In December 1997 the shiplap cladding and the wind barrier on the wood frame walls were dismounted and imperfections regarding air gaps in the cavities were photographed and recorded. In addition the wood around two MC measurement point was sawn out of a section, in order to compare measurements made by the electrical resistance method and the gravimetric method.

5 Results and discussion

An example of measured moisture content of the sill- and top plate of section E1 is shown in Figure 4. The measurements show for most wall sections, a clear tendency of moisture redistribution in the winter, with moisture moving from the inner and lower parts of the timber framing members to the upper and outer parts. However in section E3 the highest moisture content is in the outer part of the sill plate. A rather high water vapour resistance and no hygroscopic capacity of the wind barrier probably caused this. Condensed water has probably run down along the wind barrier to the outer part of the sill plate during thawing periods in the winter. It was furthermore observed that some sections with an air gap between the insulation and the top plate got unexpected high moisture contents in the outer part of the top plate.

Several of the wall sections had no traditional vapour barrier and therefore relatively low water vapour resistance on the warm side of the insulation layer. This fact has however not led to dramatic high moisture contents. It was found that all sections got the highest measured moisture content during the period when the indoor air pressure was higher than the outdoor pressure.

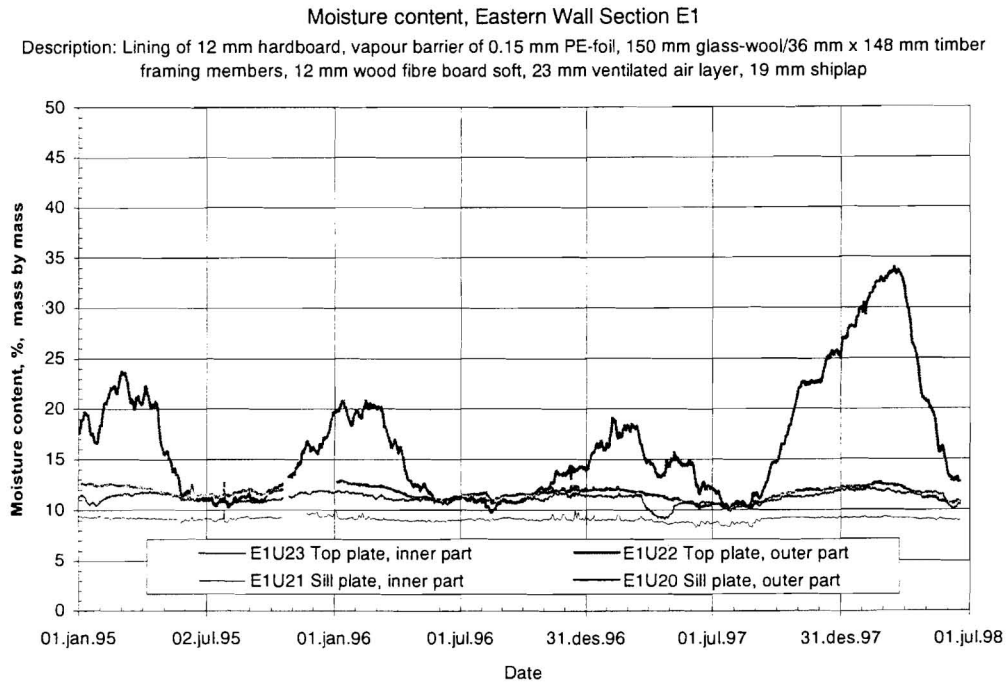

Figure 4 Measured moisture content of top- and sill plates in section E1.

6 Conclusion

Hygrothermal measurements have been performed on different building envelope constructions at a test house in Trondheim, Norway. The measurement data from this test house are made available for research scientists who want to verify computer models for heat, air and moisture transfer through building structures. The measurement data are well documented and available on various data formats. The data are well suited for verification purposes of one- (roof sections), two- and three-dimensional computer programs, modelling moisture transfer by water vapour diffusion, capillary suction and air convection. This paper gives a short description of the data that are available for verification purposes from the test house.

7 References

[1] S.Uvsløkk, S.Geving, H.B. Skogstad. Field measurements of moisture conditions in timber frame roof and wall structures. Description and results from a test house in Trondheim. Project report (to be published), Norwegian Building Research Institute, Oslo, 1999.

[2] S.Geving, B.Time, P.J.Hovde. Water vapour permeability and hygroscopic sorption curves for various building materials. Proc. of CIB W 40 Meeting, Aug. 30-Sep. 3, Prague, 1999.

[3] Ø.Økland. Convection in highly insulated structures. Ph.D. thesis, Norwegian University of Science and Technology, Trondheim, 1998.

THE INFLUENCE OF COMPRESSIVE STRESS ON THE THERMAL AND HYGRIC EXPANSION OF CONCRETE

J. Toman, R. Czerny, T. Klecka

THE INFLUENCE OF COMPRESSIVE STRESS ON THE THERMAL AND HYGRIC EXPANSION OF CONCRETE

J. Toman[1], R. Černý[2], T. Klečka[3]

[1]Department of Physics, Faculty of Civil Engineering, Czech Technical University, Thákurova 7, 166 29 Prague 6, Czech Republic
[2]Department of Structural Mechanics, Faculty of Civil Engineering, Czech Technical University, Thákurova 7, 166 29 Prague 6, Czech Republic
[3]Klokner Institute, Czech Technical University, Šolínova 7, 160 00 Prague 6, Czech Republic
EMail: toman@fsv.cvut.cz, cernyr@fsv.cvut.cz, klecka@vc.cvut.cz

Abstract

The linear thermal expansion coefficient α_T of cement mortar is measured in the temperature range of 20°C to 1000°C, the hygric expansion coefficient α_u is determined at room temperature. Both mechanically loaded samples (up to 70% of compressive strength) and samples without any load are studied. The experimental results show that samples $40 \times 40 \times 120$ mm exposed to the load in the standing position exhibit a significant difference in the $\alpha_T(T)$ function compared to the samples without any load while those exposed to the load in the flat position show a difference much lower. In measuring hygric expansion, although various regimes of moistening and drying are considered including full water saturation only little influence of external pressure on α_u is observed.

Keywords: thermal expansion, hygric expansion, high temperatures

1 Introduction

In the conditions of a fire, concrete structures undergo significant thermal stress which can result in a damage of the structure. However, thermal expansion of concrete is commonly measured at room temperature only, and high-temperature region is usually not very interesting for the engineers and designers. This may lead to bad mistakes in the evaluation of the structural response to a fire because for most materials, thermal expansion coefficient increases significantly with temperature and the resulting thermal stress is higher than expected from the room temperature data.

Length changes of porous materials can be affected not only by the change of temperature but also by the change of the moisture content [1]. Hygric expansion of concrete is usually not taken into account at all by the practice, although a higher content of moisture, particularly in the liquid state, can lead to hygric stresses which are at least comparable with the thermal ones [2].

Generally, the thermal and hygric expansion are measured in laboratory conditions only, and on the samples without any mechanical load. The possible structural

damage after load can, however, cause changes in these parameters which were not yet taken into account very frequently.

2 Thermal and hygric expansion parameters

The infinitesimal change of length due to the change of temperature is defined by

$$\mathrm{d}l_T = l_o \alpha_T \, \mathrm{d}T, \tag{1}$$

where l_o is the length at the reference temperature T_o, α_T is the linear thermal expansion coefficient. In an analogous way, the linear hygric expansion coefficient α_u can be defined

$$\mathrm{d}l_u = l_o \alpha_u \, \mathrm{d}u, \tag{2}$$

where

$$u = 100 \frac{m_m - m_d}{m_d} \tag{3}$$

is the moisture content in %, m_m is the mass of the moistened material, m_d the mass of the dried material.

Applying, in the first approximation, the superposition principle to the length changes due to temperature and moisture, we arrive at

$$\mathrm{d}l = \mathrm{d}l_T + \mathrm{d}l_u = l_o(\alpha_T \, \mathrm{d}T + \alpha_u \, \mathrm{d}u). \tag{4}$$

Defining the relative elongation ϵ as

$$\epsilon = \frac{\Delta l}{l} = \frac{1}{l_o} \int_{l_1}^{l_2} \mathrm{d}l, \tag{5}$$

we obtain

$$\epsilon(u,T) = \epsilon_T(u_o,T) + \epsilon_u(u,T_o) =$$

$$\int_{T_o}^{T} \left(\frac{\partial \epsilon}{\partial T}\right)_u \mathrm{d}T + \int_{u_o}^{u} \left(\frac{\partial \epsilon}{\partial u}\right)_T \mathrm{d}u = \int_{T_o}^{T} \alpha_T \, \mathrm{d}T + \int_{u_o}^{u} \alpha_u \, \mathrm{d}u. \tag{6}$$

3 Measuring the thermal and hygric expansion coefficients

Measuring the linear hygric expansion coefficient α_u at a constant temperature with the varying moisture content is relatively easy. On the contrary, the determination of α_T for porous materials is a little more complicated, since it is technically difficult to keep the absolute moisture content constant when the temperature is changing.

Therefore, in practical measurements [2] we first determine the dependence of the relative elongation on moisture at room temperature. The material is moistened either to the full water saturation or to the equilibrium moisture content, and then it is slowly dried with a simultaneous measurement of the length changes. Thus, a relation $\epsilon_u = \epsilon_u(u)$ is obtained over a wide range of moisture and at constant temperature. The function $\epsilon_u(u)$ is represented by point values. Therefore, a regression analysis is necessary to obtain a continuous function. In accordance with Eq. (6),

α_u is obtained as the first derivative of $\epsilon_u(u)$. Knowing the function $\alpha_u(u)$, we can continue with the temperature changes. Considering the superposition principle, we first measure the length changes caused by the changing temperature, and simultaneously determine the changes of moisture content. Then, these length changes are recalculated to the zero moisture content using the $\epsilon(u)$ functions which results in a pointwise given function $\epsilon_T = \epsilon_T(T)$ for a constant moisture ($u = 0$) as required by Eq. (6). Regression analysis and calculation of the first derivative of $\epsilon_T(T)$ with respect to T leads to the function $\alpha_T = \alpha_T(T)$.

4 Material samples

In practical experiments, we studied the samples of cement mortar. The composition of the mixture for one charge was the following: Portland cement ENV 197 - 1 CEM I 42.5 R (Kraluv Dvur, CZ) - 450 g, natural quartz sand with continuous granulometry I, II, III (the total screen residue on 1.6 mm 2%, on 1.0 mm 35%, on 0.50 mm 66%, on 0.16 mm 85%, on 0.08 mm 99.3%) - 1350 g, water - 225 g.

The mortar was prepared by mixing and compacting using mixing machine and vibrator. The dimensions of the samples were $40 \times 40 \times 120$ mm, the centers of the 40 $\times$ 40 mm faces were provided by contact seats for the use with contact comparator. The samples in moulds were left for the first 24 hours in a high relative humidity environment under wetted cloth. After mould removal, the time remaining to 28 days spent the samples in 20°C water and then they were put in protected external environment (a metal-sheet shed) with the relative humidity approximately 65%.

After 28 days, the compression strength was determined on selected samples (57.4 MPa). One part of the remaining samples was mechanically loaded, the other samples were left without any load.

5 Experimental procedure

In measuring the high-temperature linear thermal expansion of cement mortar, we employed the experimental device currently developed in our laboratory (see [3]). The device consists of a cylindrical, vertically placed electric furnace with two bar samples located in the furnace. The first sample is the measured material, the second sample is a reference material with the known dependence of the thermal expansion coefficient on temperature. The length changes of the samples are measured mechanically outside the furnace by thin ceramic rods which pass through the furnace cover and are fixed on the top side of the measured sample. These ceramic rods pass by an indefinite temperature field, therefore their elongation is not possible to be determined mathematically and a comparative method of determining the elongation of the rod is used.

In measuring hygric expansion, we have measured the length changes by the Carl Zeiss optical contact comparator with $\pm 1 \mu$m accuracy, the mass changes were determined by the electronic balance Sartorius with $\pm$1mg accuracy. The basic set of points $l_i(m_i, T_i)$ necessary for the determination of the $\alpha(u)$ function was obtained

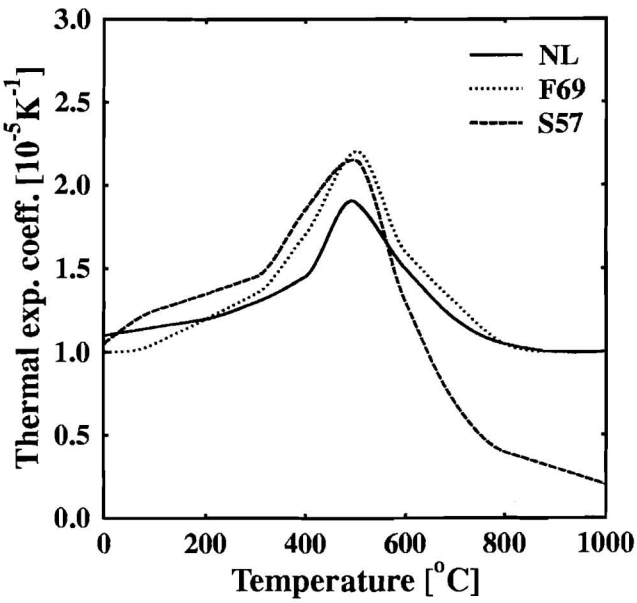

Fig. 1 Linear thermal expansion coefficient α_T of unloaded samples of cement mortar (NL) and those mechanically loaded to 69.5% of compressive strength in the flat position (F69) and to 57% of compressive strength in the standing position (S57)

in this way. The experiments were performed under isothermal conditions, with $T = (25.0 \pm 0.5)^o$C.

First, the dependence of the relative elongation on moisture content was determined. The samples were first dried in a hot-air dryer at $T = 110^o$C, then moistened in the environment with a known relative humidity of 40%, moistened to the full water saturation, and dried first in natural way in the laboratory and finally in hot-air dryer at $T = 110^o$C. Both length and mass changes were simultaneously measured during the moistening and drying processes.

6 Experimental results

The measurements of both linear thermal expansion and linear hygric expansion were performed on 12 samples each which were approximately 8 months old. One third of the samples was not exposed to any load (we will denote it NL in what follows), the second third was mechanically loaded to 69.5% of compressive strength flat (i.e. the load in the direction parallel to the 40 × 40 mm face, in the center of the 40 × 120 mm face - it will be denoted as F69), the final third to 57.3% of compressive strength standing (i.e. the load in the direction parallel to the 40 × 120 mm face, in the center of the 40 × 40 mm face - it will be denoted as S57).

Fig. 1 shows the dependence of the linear thermal coefficient α_T on temperature

Table 1 Hygric expansion coefficient of cement mortar in 10^5 $(\%kg/kg)^{-1}$ for various regimes of moistening and drying and various mechanical load

sample/region	FD4-0	M0-4	M4-8	ND8-6	ND6-4
NL	14.7	24.6	1.4	2.4	18.8
S57	19.0	25.1	2.80	2.5	27.0
F69	15.2	24.8	3.4	2.9	16.0

in the range of 20°C to 1000°C for the three mentioned cases. Generally, the character of all three curves in Fig. 1 remains similar, the $\alpha_T(T)$ functions increase up to 500°C and then decrease. This decrease is for the case of NL and F69 samples practically the same as the foregoing increase, and for 1000°C, the values of α_T are practically the same as for 20°C, but for S57 samples the $\alpha_T(T)$ function decreases much faster. This fact is most probably due to the character of the structural damage after mechanical load in the standing position where the microcracks have different orientation than for loading the sample in the flat position. The interesting moment is that the remarkable differences between $\alpha_T(T)$ functions of F69 and S57 appear in the higher temperature region only, $T > 500°C$. Practically it means that combination of damage due to the mechanical and thermal load was effective for the standing position of the sample and higher temperatures only, otherwise the thermal damage prevailed.

In measuring hygric expansion, several regions with abrupt changes of the first derivative with respect to moisture (i.e., of the hygric expansion coefficient) were identified, namely the forced drying from $u = 4\%$ to $u = 0$ (FD4-0 in what follows), the moistening on the air with 40% relative humidity (M0-4), the moistening in water (M4-8), natural drying from the full water saturation (ND8-6), and natural drying in the hygroscopic region (ND6-4). Table 1 shows the average values of α_u of samples mechanically loaded as defined before and in the mentioned regions of moistening and drying.

The results can be summarized as follows. The mechanical load before the measurements has a relatively little influence on the hygric expansion coefficient α_u. In general, for higher load higher values of α_u were observed; for the standing orientation of the sample higher α_u's compared to the flat orientation were measured.

The remarkable differences between α_u's (both at moistening and drying) in the hygroscopic and overhygroscopic regions can be explained by the mode of water penetration into the porous body in these two regimes. While in the hygroscopic region the most important way of the incorporation of the molecules of water into the porous structure is their absorption on the pore walls where first monomolecular and later polymolecular layers are formed (and the surface phase of water prevails the volume phase as a consequence), in the overhygroscopic region the water penetrates into the porous structure as a volume phase mostly and fills the inside of the pores as the pore walls are already covered by the surface phase of water.

The irreversible changes in the length of the sample following on one hand their saturation to the maximum water content and on the other their forced drying in

the hot-air dryer are most probably consequences of the late hydration of cement, ablation of macroparticles by water and removal of physically bonded water from the sample.

7 Conclusions

The linear thermal expansion coefficients of samples of cement mortar both mechanically unloaded and loaded in two different ways were determined in wide temperature range of 20°C to 1000°C. The low temperature data correspond well to the usual values of α_T for concrete. In the high temperature region, the $\alpha_T(T)$ functions have a maximum at approx. 500°C. The position of the $40 \times 40 \times 120$ mm samples during mechanical loading was found to have a remarkable influence on the values of α_T in the higher temperature region only, for $T > 500$°C. Generally, the effect of thermal load prevailed that of mechanical load in the studied situation.

The mechanical load up to 70% of the compressive strength was found to have a relatively low effect on the hygric expansion coefficient of cement mortar. On the other hand, the way of moistening and drying has appeared as a very remarkable influence which can result in variations as high as one order of magnitude in the hygric expansion coefficient. These variations are mainly due to the way of incorporation of water molecules into the porous structure (or water removal from it), and due to the late hydration processes caused by either full water saturation or by heating in the dryer.

Acknowledgement

This research has been supported by the Grant Agency of the Czech Republic, under grants # 103/97/0094 and # 103/97/K003.

References

[1] K. Schulgasser, Moisture and Thermal Expansion of Wood, Particle Board and Paper. Paper and Timber, No 6, 3 (1988).
[2] J. Toman, R. Černý, Coupled Thermal and Moisture Expansion of Porous Materials. Int. J. Thermophysics Vol. 17, 271 (1996).
[3] J. Toman, R. Černý, Measuring the Thermal Expansion of Building Materials at High Temperatures. Proceedings of the Seminar: Research Activities of Departments of Physics in Czech and Slovak Republic, p. 51. STU Bratislava, 1997 (in Czech).

INFERRING AIR-CHANGE RATES AND MOISTURE RELEASE RATES FROM PSYCHROMETRIC CONDITIONS IN DWELLINGS USING SYSTEM IDENTIFICATION TECHNIQUES

M.J. Cunningham

INFERRING AIR-CHANGE RATES AND MOISTURE RELEASE RATES FROM PSYCHROMETRIC CONDITIONS IN DWELLINGS USING SYSTEM IDENTIFICATION TECHNIQUES

M J Cunningham

Building Research Association of New Zealand (BRANZ)
BRANZMJC@BRANZ.ORG.NZ

Abstract
Theory is developed that shows how to infer, from psychrometric conditions alone, air-change rates and moisture release rates in dwellings.

The dwelling is modelled as a single zone and the dwelling hygroscopic materials are treated as a single lump. The corresponding differential equations are discretised and the coefficients compared to those derived from an ARX system identification model of the same system. Air-change rates and moisture release rates can be inferred from this comparison.

Moisture release rates and ventilation levels are measured and compared to the theoretical results. Results within 30% of measured values have been obtained, except for the case of moisture release rates under air-tight conditions where results seem unreliable.

Keywords System identification, infiltration, moisture, humidity, psychrometric conditions

1. INTRODUCTION

There are applications where it is desirable or necessary to know ventilation levels and moisture release rates over a large sample of houses, e.g. if assessing the level of mould and condensation across a large group of buildings, or surveying the relationships between socio-economic measures and housing measures such as indoor climate. Straightforward and quick techniques not utilising specialised, expensive and intrusive equipment are required for this kind of application. High accuracy is not required.

The author has shown how to infer ventilation rates, but not moisture release rates, from psychrometric data for the particular case of sinusoidal climate parameters [1], but

this is very much a special case that only exists approximately and irregularly in any psychrometric data set.

This work addresses this issue by using system identification techniques [2,3]. Such an approach has been widely for building thermal properties, [4-6], but not, to the author's knowledge, for building moisture properties.

2. THE PHYSICAL MODEL

The room or building of volume V_o (m^3) is modelled as a zone exchanging air with the outdoors, and with vapour pressure driven moisture transfer to and from the hygroscopic elements in the room. These hygroscopic elements are lumped as one node with an effective volume of V_h (m^3), an effective area for mass transfer with the room of A_h (m^2), and an effective surface mass transfer vapour resistance of r (N s kg^{-1}).

Conservation of moisture within the room gives

$$V_o \frac{\partial c_o}{\partial t} = V_o F(c_e - c_o) + \frac{A_h(p_h - p_o)}{r} + S \tag{1}$$

where S is the moisture source strength (kg s^{-1}) and F is the air-change rate (s^{-1}) and c_o and c_e are indoor and outdoor vapour concentrations respectively (kg m^{-3}). p_h and p_o are the water vapour pressures (Pa) in the hygroscopic lump and the room respectively. Mass interchange to the hygroscopic lump gives

$$V_h \frac{\partial m_h}{\partial t} = A_h \left(\frac{p_o - p_h}{r} \right) \tag{2}$$

where m_h is the moisture concentration in the hygroscopic lump. This is determined by the average sorption curve of the room's hygroscopic materials implying that

$$\frac{\partial m_h}{\partial t} = \frac{\partial m_h}{\partial \varphi} \frac{\partial \varphi}{\partial t} \tag{3}$$

where φ is the relative humidity in the hygroscopic lump and where $\frac{\partial m_h}{\partial \varphi}$ is the instantaneous slope of the sorption curve of the hygroscopic lump.

Two time constants t_1 and t_2 are now defined which characterise the hygroscopic properties of the room, viz.

$$t_1 = \frac{V_h r}{A_h p_{sat}} \frac{\partial m_h}{\partial \varphi} \quad \text{and} \quad t_2 = \frac{V_o W r}{A_h R T} \tag{4}$$

A further time is defined as

$$\frac{1}{t_3} = \frac{1}{p_{sat}} \frac{\partial p_{sat}}{\partial T} \frac{\partial T}{\partial t} \tag{5}$$

where p_{sat} is the saturated vapour pressure (Pa) in the hygroscopic lump.

Equations (1) and (2) become

$$\frac{\partial p_o}{\partial t} + \left(\frac{1}{t_2} + F \right) p_o - \frac{p_h}{t_2} = F p_e + \frac{S}{\gamma} \tag{6}$$

and

$$\frac{p_h}{\partial t} + \left(\frac{1}{t_1} - \frac{1}{t_3} \right) p_h - \frac{p_o}{t_1} = 0 \tag{7}$$

where

$$\gamma = \frac{W V_o}{RT}$$

and where W molecular weight of water (18 kg kmole-1) and R is the universal gas constant (8310 kg kmole-1).

3. SYSTEM IDENTIFICATION MODELS

3.1 Finding t_2 and ventilation rate - case with no moisture sources

We consider first the loose case (i.e. high ventilation levels) with no moisture sources, governed by equation (6) with $S = 0$.

The discrete form of equation (6) is

$$p_{oi} - \frac{p_{oi-1}}{\alpha \Delta t} = \frac{p_{hi}}{\alpha t_2} + \frac{F p_{ei}}{\alpha} \tag{8}$$

where

$$\alpha = \frac{1}{\Delta t} + \frac{1}{t_2} + F$$

Equation (8) is an ARX model, first order in the output variable p_o, and first order in the input variables p_e and p_h.

If the ARX model, equation (8), is written in the standard form [2,3]

$$p_{oi} + a_1 p_{oi-1} = b_1 p_{hi} + b_2 p_{ei} \tag{9}$$

then comparison between the coefficients of equation (8) and equation (9) gives

$$t_2 = -\frac{a_1}{b_1} \Delta t \quad \text{and} \quad F = -\frac{b_2}{a_1 \Delta t} \tag{10}$$

There exist standard algorithms for calculating the coefficients a_1 and b_1 and b_2 [2,3], so that t_2 and the ventilation level, F, can be found from equations (10).

3.2 Finding t_1 - tight case with no moisture sources

A similar process, starting from equation (6), in the approximate case of F≈0 yields an expression for t_1

$$t_1 = \frac{\Delta t}{\frac{1}{z_{pole}} - \frac{\Delta t}{t_2} - 1} \tag{11}$$

where z_{pole} is the value of the pole of the ARX model.

There exist standard algorithms for calculating the numerical value of the pole z_{pole} see for example [2,3], allowing the calculation of t_1 from equation (11).

4. AVERAGING

To find the moisture release rate S, an integral form of equation (6) is used – integrating equation (6) between $t = a$ and $t = b$ and rearranging gives

$$S = \left\{ \frac{\gamma}{\frac{1}{t_1} - \frac{1}{t_3}} \right\} \left\{ \left[\frac{1}{T} \left(\frac{\partial p_o}{\partial t} + \left(\frac{1}{t_1} + \frac{1}{t_2} - \frac{1}{t_3} \right) p_o - F p_e \right) \right]_a^b + F(\bar{p}_o - \bar{p}_e) \left(\frac{1}{t_1} - \frac{1}{t_3} \right) - \frac{\bar{p}_o}{t_2 t_3} \right\} \tag{12}$$

where $\bar{f} = \frac{\int_a^b f dx}{b-a}$ and $\left[G(p_o) \right]_a^b = G(p_o = b) - G(p_o = a)$ in the normal way.

5. EXPERIMENTAL

5.1 Description

This section describes the experiments undertaken to test the effectiveness of the system identification models developed above.

Various combinations of ventilation levels, moisture release rates and heating were realised in a bedroom and the indoor and outdoor temperatures and humidities measured with thermistors and capacitive humidity sensors. Moisture was released into the room in a controlled and measurable manner with a small open topped container on a hot plate turned to a very low heat. Heating was provided from a radiant thermostated electric heater.

Several experiments of a few hours duration were carried out, each aimed at finding different variables. Theoretical results were calculated using MATLAB© to calculate the

system model parameters followed by using and formulae (10), (11) and (12) to find t_1 , t_2 , F, and S.

6. RESULTS

As a typical example, Figure 1 shows data from Run 1 and Run 3.

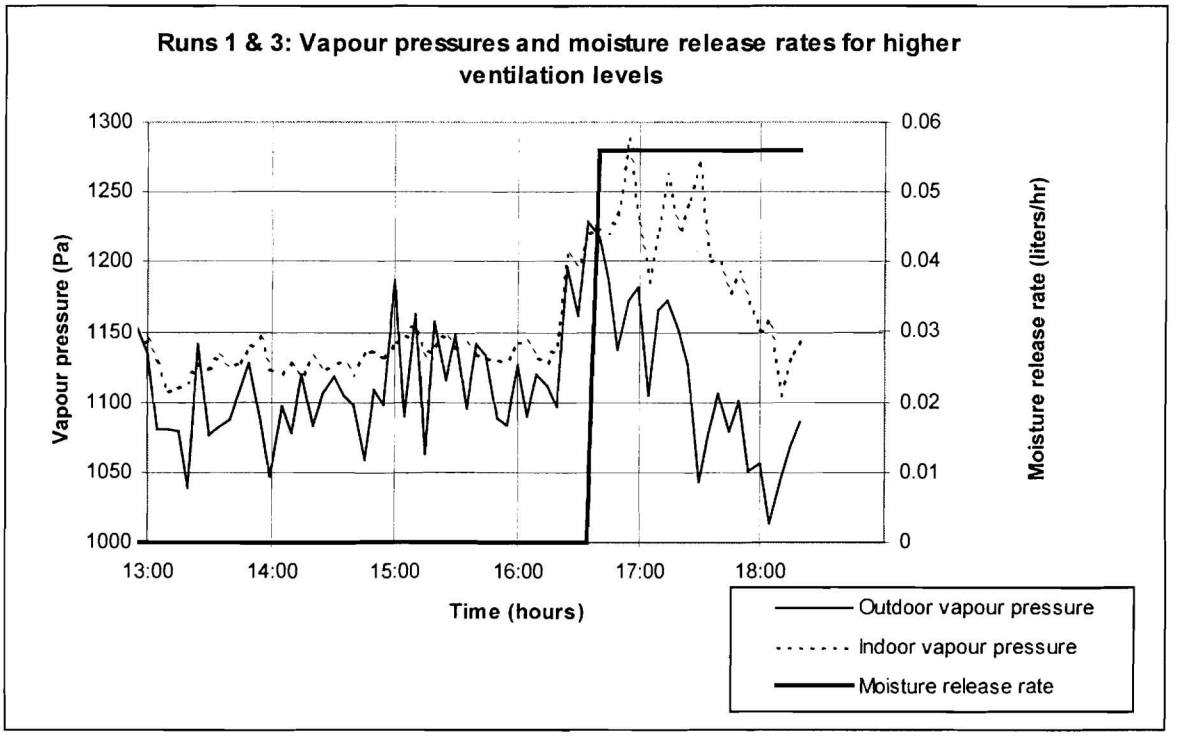

Figure 1: Run 1 and 3. Vapour pressure and moisture release rates at higher ventilation levels.

Table 1 gives the results for the various parameters calculated by the methods above, and compared to experimentally measured quantities.

Run number	Room hygroscopic parameter t_1	Room hygroscopic parameter t_2	Ventilation calculation	Ventilation experimental	Moisture release rate calculation	Moisture release rate experimental
1		0.28 hours	5.5 hour^{-1}	5.0 hour^{-1}		
2	0.46 hours					
3					0.072 L/hr	0.056 L/hr
4			1.3 hour^{-1}	1.0 hour^{-1}		
5					0.18 hour^{-1}	0.05 hour^{-1}

Table 1: Experimental and calculational results.

7. DISCUSSION AND CONCLUSIONS

Ventilation levels calculated at the higher air-change rates agree with measured values to within 10%, and at lower levels to within 30%. Moisture release rates agree to within 27% at higher air-change rates, but differ by more than a factor of 3 at lower air-change rates. In general it appears that the methods described in this work give useable results at higher ventilation levels for both air-exchange values and moisture release rates, and perhaps for air-exchange values at lower ventilation levels, but cannot predict well moisture release rates under air-tight conditions.

This lesser performance level for more air-tight rooms probably arises because, under these tight conditions, the room hygroscopic materials influence substantially the time dependency of the room relative humidity and vapour pressure. In order fully to model this hygroscopic influence a more accurate physical model than the one used here is clearly needed. Furthermore, it is unclear where in the room temperatures and humidities should be measured to fairly represent the room as one zone when, because of less external ventilation, room air circulation is lower.

8. REFERENCES

1. Cunningham, M.J. 1994. Using hygroscopic damping of relative humidity and vapour pressure fluctuations to measure room ventilation rates. *Building and Environment*, vol 29 (4), p501.

2. Söderström, T., Stoica, P. 1989. *System Identification*. Prentice-Hall International, London.

3. Ljung, L. 1993. *System Identification Toolbox for use with MATLAB©* The MathWorks Inc.

4. Baudier, M., Marchio, D. 1991. Dynamic model identification applied to the measuring of thermal characteristics of buildings. *Energy and Buildings*, vol 17 p21.

5. Coley, D., Penman, J. 1992. Second order system identification in the thermal response of real buildings. Paper II: recursive formulation for on-line building energy management and control. *Building and Environment*, vol 27 (3), p269.

6. Madsen, H., Holst, J. 1995. Estimation of continuous-time models for the heat dynamics of a building. *Energy & Buildings*, vol 22, p67.

TRANSIENT THERMAL BEHAVIOR OF LAYERED STRUCTURES

L. Vozár, W. Hohenauer, I. Stubna

TRANSIENT THERMAL BEHAVIOR OF LAYERED STRUCTURES

L. Vozár[1], W. Hohenauer[2], I. Štubňa[3]

[1]Department of Physics, Faculty of Natural Sciences, Constantine the Philosopher University, Tr. A. Hlinku 1, SK-94974 Nitra, Slovakia
[2] Department of Materials Technology, Austrian Research Centers, A-2444 Seibersdorf, Austria
[3]Department of Physics, The University of Trenčín, Študentská 2, SK-91101 Trenčín, Slovakia
Email: vozar@uvt.uniag.sk, wolfgang.hohenauer@arcs.ac.at, stubna@uniag.sk

Abstract

The use of layered materials has rapidly increased in a great number of applications - in case of building industry especially as thermal barriers, partially as electric insulation and wear, erosion and corrosion resistance protection. Because such structures are utilized under different transient thermal conditions it is of a great interest to study their transient thermal behavior.

The knowledge of thermophysical properties of these structures is the primary information needed for performing analytical as well as numerical analyses. One may study contact thermal resistance between layers that may indicate the quality of the layered composite. In situ measurement on layered systems allows testing whether and how thermophysical properties of layers differ from those values received for bulk materials. It has been shown that transient photothermal methods like the laser flash technique can be successfully utilized for a reliable estimation the thermal diffusivity and/or the thermal contact resistance.

The paper deals with an investigation of transient thermal behavior of layered systems. In case of analytical simulations the initial and boundary conditions corresponding to the laser flash experimental method are considered. The paper presents a draft of analytical theory and gives some results of an estimation of the thermal diffusivity of a composite consisted of a metallic and non-metallic two-layer.

Key words: layered structures, thermal diffusivity, thermal contact resistance

1 Introduction

Building constructions are frequently exposed on one side to variable weather conditions and on the other face enclosure an indoor space at a constant and uniform (room) temperature. The determination of the heat transfer through a wall is often treated as an example of the linear heat flow in a slab of finite thickness bounded by a pair of parallel planes of finite extent. They assume that each of the layers that compose the wall consists of a material of different thermal properties. The equation for the conduction in each layer of the wall is

$$\nabla.k\nabla T = c_p \rho \frac{\partial T}{\partial t}\ , \tag{1}$$

where k is the thermal conductivity - the basic thermophysical property used to relate heat fluxes to steady state temperature gradients, c_p is the specific heat at constant pressure and ρ the density.

For homogeneous isotropic materials whose thermal conductivity is independent on temperature and position the equation (1) can be rewritten as

$$\frac{\partial T}{\partial t} = \frac{k}{c_p \rho}\nabla^2 T = a\nabla^2 T\ . \tag{2}$$

Here the thermal diffusivity a represents the transport property that describes how quickly heat propagates through a material during a transient state.

If there occurs a temperature drop ΔT across the interface between two materials when analyzing a heat transfer through a layered composite the thermal contact resistance R should be considered. Then the heat flow q through the interface conforms to the equation [1]

$$q = \frac{\Delta T}{R}\ . \tag{3}$$

2 Theory and the laser flash method

In the flash method, the front face of a wall shaped sample is subjected to a pulse of radiant energy coming from a laser [2]. If material boundaries are flat and parallel to the sample front and rear surfaces and if there are no heat losses from the radial surface an one-dimensional heat transfer occurs across the sample. Analyzing the resulting temperature rise on the opposite (rear) face of the sample any thermophysical property value (the thermal diffusivity of one layer, or the thermal contact resistance) can be computed [3].

The analytical theory assumes one-dimensional heat flow across a wall composed from n layers. It considers the sample initials at constant equilibrium (zero) temperature. The front face of the wall is in the initial (zero) time uniformly subjected to the instantaneous heat pulse with the heat Q supplied to the unit area. In case of non-ideal experimental conditions - when heat losses from the front and rear face is not negligible, appropriate boundary conditions include heat flux term with the heat transfer coefficients at the front h_1 and rear face h_2. The expression for the transient temperature rise $T=T(x,t)$ in the sample can be received solving the heat conduction equation for each layer

$$\frac{\partial^2 T_i(x,t)}{\partial x^2} = \frac{1}{a_i}\frac{\partial T_i(x,t)}{\partial t}, \quad i=1,2,\ldots,n \tag{4}$$

with the initial

$$T_i(x,0) = 0 \tag{5}$$

and the boundary condition at the front and rear face as

$$-k_1 \frac{\partial T_1}{\partial x} = Q\delta(0) - h_1 T_1 \tag{6}$$

$$k_n \frac{\partial T_n}{\partial x} = -h_n T_n, \tag{7}$$

where $\delta(t)$ is the Dirac's delta function. The boundary conditions at the interface between the i^{th} and j^{th} layer describe the relations

$$k_i \frac{\partial T_i}{\partial x} = \frac{1}{R}\left(T_j - T_i\right) \tag{8}$$

$$k_i \frac{\partial T_i}{\partial x} = k_j \frac{\partial T_j}{\partial x} \tag{9}$$

The problem (equations 4-9) is negotiable using the Green's function approach as well as utilizing the Laplace transform technique [4]. Very efficient is to take the quadrupole formalism of the Laplace transform technique and the approach described in [5] that yields to simple expressions even though analyzing general complex cases.

3 Simulations

For a better understanding the phenomena a simple two-layered geometry is studied here. We consider to have sample that consists from 1.97 mm thick molybdenum and 0.21 mm ceramic layer with appropriate thermal properties as measured at 500 °C (molybdenum - k = 111.4 W/mK, a = 39.3.10^{-6} m^2/s, ceramic k = 6.09 W/mK, a = 2.83.10^{-6} m^2/s). From Fig 1 one can see, that thermal contact resistance below

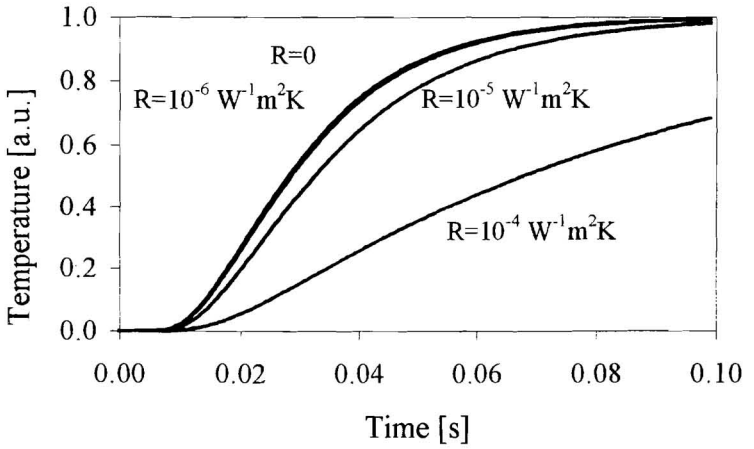

Fig. 1 Simulated rear face temperature rise vs. time curves calculated for various thermal contact resistance

10^{-6} $W^{-1}mK$ does not observably influence the temperature response investigated at the wall (sample) rear face. From the other point of view the result indicate the natural border of the thermal contact resistance estimation for the presented composite.

Fig 2 presents normalized sensitivity to thermal diffusivity of molybdenum Sa_{Mo}, to thermal diffusivity of ceramic Sa_{ceram}, to Biot number ($H = he/k$, where e is the sample (layer) thickness) S_H and sensitivity to thermal contact resistance S_R vs. time curves. We see that sensitivities to thermal diffusivity and sensitivity to thermal contact resistance have similar shape, what indicate that all these three parameters influence the temperature rise vs. time evolution in a similar and therefore they can not be estimated simultaneously.

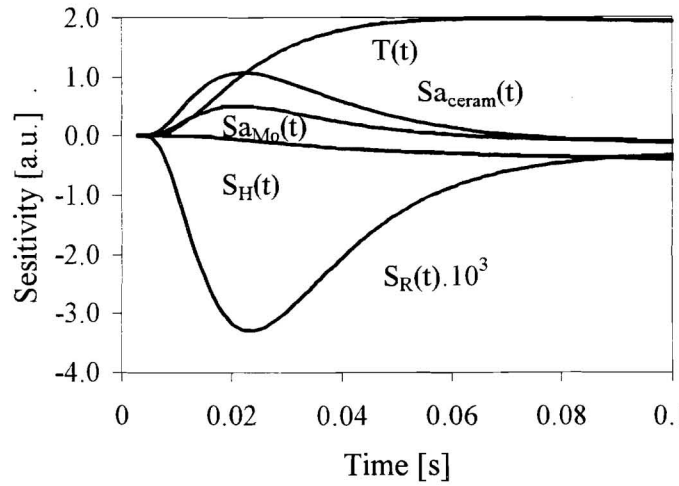

Fig. 2 Normalized sensitivities vs. time curves

Fig 3 presents a typical experimental temperature rise vs. time curve (No 1) and its least-squares-fit using the analytical model that considers the sample acting as a homogeneous medium (No 2) (here the unknown property is the 'apparent' thermal diffusivity). The curve No 3 considers a two layered Mo/ceramic sample with above mentioned thermal properties with non-zero thermal contact resistance - that is estimated here. The curve No 4 is based on an 'ideal two layered Mo/ceramic sample' model with zero thermal contact resistance - here the thermal diffusivity of ceramics is determined. We see that the case of an ideal two-layered composite suits the best to the experimental temperature rise vs. time evolution. Therefore a data reduction process based on the used analytical model can give a reliable data of thermal diffusivity of the ceramics material.

4 Measurement of thermal diffusivity

Fig 4 presents results of the thermal diffusivity estimation of the ceramic material on three samples of two-layered Mo/ceramic composite. The sample No 1 has 2.18 mm

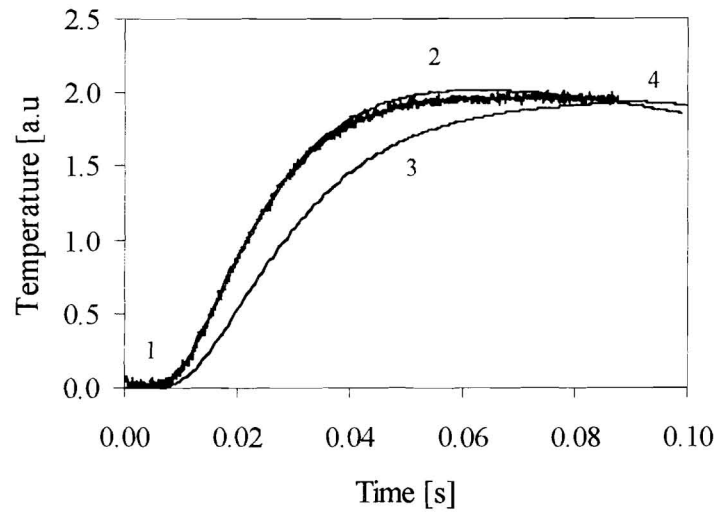

Fig 3 Experimental temperature rise vs. time data and its fit

thick ceramic layer and the thickness of molybdenum layer is 0.29 mm, the sample No 2 has layers thickness 2.31 mm and 0.35 mm; and No 3 - 2.295 mm and 0.329 mm. Acquired values are compared with those thermal diffusivities measured on a homogeneous ceramic samples. What can be seen is also for a thermophysical property measurement unusually high dispersion of result.

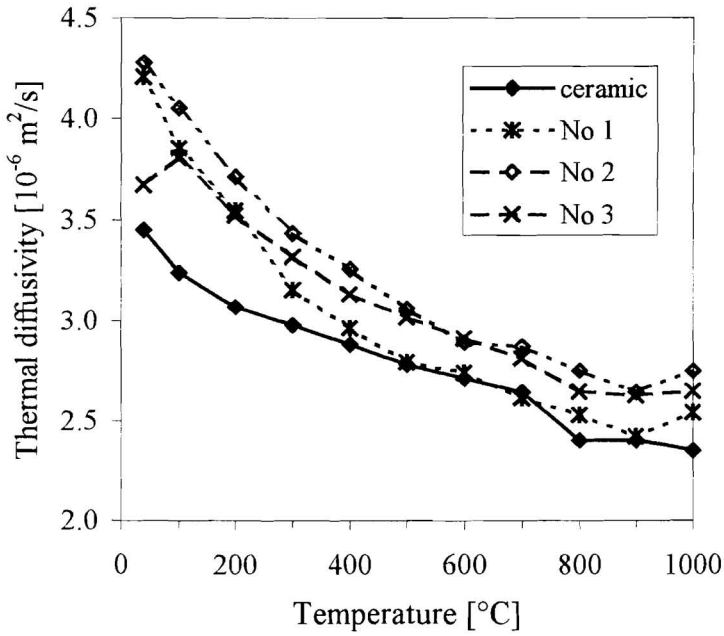

Fig 4 Thermal diffusivity of ceramic material

In fact an estimation of the thermal diffusivity from experimental data measured on a layered composite is a dependent measurement. The measurement of the thermal diffusivity of one layer requires besides the knowledge of other relevant properties (the density, the heat capacity and the thickness of both components) to know the thermal diffusivity of the remained layer. Errors in measurement of these additional parameters are propagated through the data reduction and result as inaccuracy of the thermal diffusivity determination. On the other hand physical borders limit the accuracy and the reproducibility of the method [3]. Therefore the flash method approach is not very suitable for a study of poor thermal conductive coatings on much better conductive substrate.

5 Conclusion

The paper shows that an experimental investigation of transient thermal behavior of a layered composite may be used as a suitable basis for measurement of a thermophysical property of a component. Because such measurement is a dependent measurement the accuracy of the required property estimation depends besides the accuracy of other relevant properties on an information that experimental data contains about the estimated property. This depends on the geometry and materials properties.

Acknowledgement

Authors wish to thank the Hertha Firnberg Foundation of the ARC Seibersdorf and the Slovak Science Grant Agency for the financial support.

References

[1] M.N. Özisik, Heat Transfer. A Basic Approach, McGraw-Hill Int. Editions, New York 1987.

[2] Parker W.J., Jenkins W.J., Butler C.P. and Abbott G.L., Flash Method of Determining Thermal Diffusivity, Heat Capacity and Thermal Conductivity, J. Appl. Phys. 32 (1961), 1679.

[3] W. Hohenauer and L. Vozár, An Estimation of Thermophysical Properties of Layered Materials using the Laser Flash Method, High Temp. - High Press (will be published)

[4] M.N.Özisik, Heat Conduction, John Wiley, New York 1980.

[5] A. Degiovanni, Conduction dans un 'mur' multicouche avec sources: extension de la notion de quadripole, Int. J. Heat Mass Transfer 31 (1988), 553.

APPLICATION OF ACOUSTIC EMISSION METHOD ON THE LOADED TIMBER WITH DIFFERENT HUMIDITY ANALYSED BY WIGNER SPECTRUM

M. Korenská, L. Pazdera, J. Smutny, Z. Weber

APPLICATION OF ACOUSTIC EMISSION METHOD ON THE LOADED TIMBER WITH DIFFERENT HUMIDITY ANALYSED BY WIGNER SPECTRUM

Marta Kořenská[1], Luboš Pazdera[1], Jaroslav Smutný[2], Zdeněk Weber[1]

[1] Department of Physics, Faculty of Civil Engineering, Technical University of Brno, Žižkova 17, 602 00 Brno, Czech Republic

[2] Department of Railway Construction and Structures, Faculty of Civil Engineering, Technical University of Brno, Veveří 95, 662 37 Brno, Czech Republic

E-mail: marta@dp.fce.vutbr.cz, fypaz@fce.vutbr.cz, zksmu@fce.vutbr.cz, weber@dp.fce.vutbr.cz

Abstract

An acoustic emission has been used to study the effects of low temperature gradients in standardised specimens of timber with variable humidity. Note that the acoustic emission method detects active defects into test structure. A part of the specimen was immersed into liquid nitrogen (-196 °C). The upper part of the specimen was exposed to the air whose room temperature was (about 20 °C). The timber specimens were blocks of dimensions 16 cm x 4 cm x 4 cm. Classification of acoustic emission sources were performed by using modern mathematical methods. The first series of measurements were carried out on dried-out specimens, the second series on specimens saturated with water.

Key words: acoustic emission, temperature gradient, non-destructive testing, mechanical wave, signal analysis, burst type signal

1 Introduction

The acoustic emission method is one of non-destructive testing techniques. A phenomenon of the acoustic emission is known as process rise and propagation of stress waves (acoustic photons) released for local dynamic dislocations of an inner solid structure. Defects into loaded structure generated the elastic waves. Sensors detect surface (Rayleigh) waves (Fig. 1). The defects are detectable only under activity. The inception of defect and its growth is concatenated with propagation of an accumulated energy. The sensor (usually piezoelectric transducer) converted mechanical wave into an electrical signal.

The humidity of building structures influences its strength. It was tested the defects under thermal load of the timber specimens. The acoustic emission method was used to determine phenomena over loaded time.

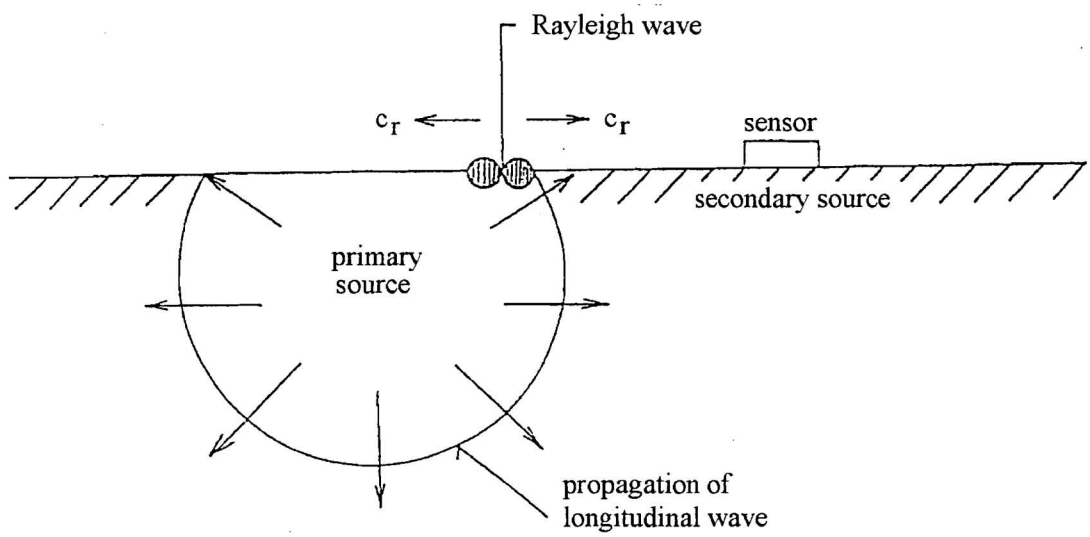

Fig. 1 Acoustic emission phenomena.

2 Experimental set-up

It was chosen specimens by dimension 16 cm x 4 cm x 4 cm. The timber specimens were included one end into bath with liquid nitrogen (the temperature –196°C) and other one in an air of laboratory (the temperature about 20°C) into polystyrene vessel (Fig. 3). A thermal gradient was over 200°C between the specimen ends.

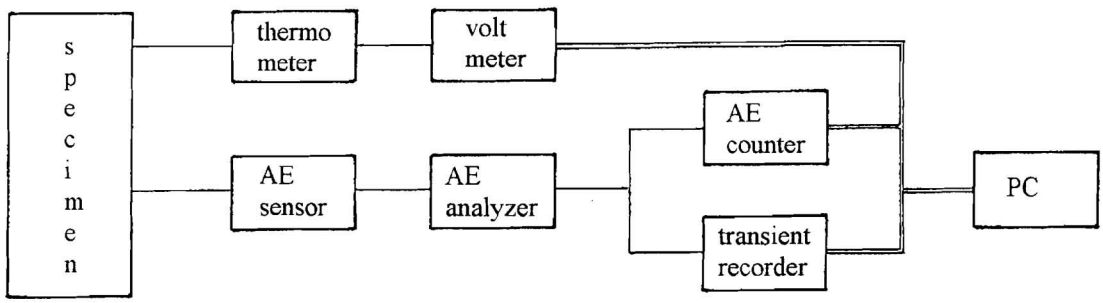

Fig. 2 Diagram of experiment.

The temperature was measured by an infra red thermometer on the air end of specimen. An acoustic emission sensor was contacted on the air end. The signal was

separated into two sections. A counter detected acoustic emission counts in the first side and some "big" burst type signals were recorded in the second side (Fig. 2).

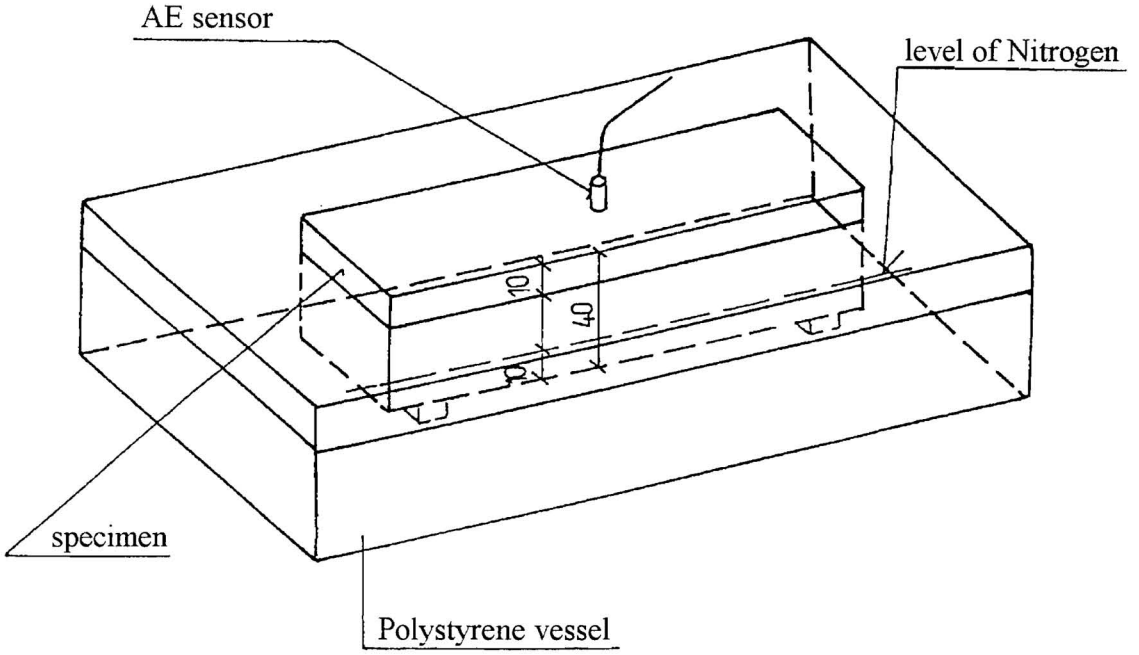

Fig. 3 Position of timber specimen into vessel.

The experimental conditions were temperature 20°C, relative humidity 30 % and atmospheric pressure 1.02×10^5 Pa.

3 Wigner spectrum

The recorded acoustic emission signals were analysed by Wigner spectrum. The Wigner spectrum is a combination of the Fourier transformation and the correlation calculation.

$$Ws(\tau, f) = \int x(t+\tau/2)\cdot x^*(t-\tau/2)\cdot \exp(-j2\pi f)\cdot dt\,,$$

where $x(t)$ is amplitude dependence on time of the recorded signal, τ is time parameter and f is frequency parameter. This is general time-frequency distribution which not using an analytical functions and in comparison with many other transformation it is not limited by Heisenberg's uncertainty. However, it requires large computation power, contains interference in discrete computing form and works in negative energy levels. The Wigner spectrum analyses with constant bandwidth.

The frequency analyses find average frequency spectrum of analysed signal, but the time-frequency techniques localise spectrum accurately in the time and the frequency. Notice, that the frequency axis is horizontal and the time axis is vertical and the values of spectrum are shown by contours.

4 Experimental results

The cumulative curve of an acoustic parameter shows that the test timbers with higher humidity have lower frequency of the parameter.

The time characteristic of the amplitude of the dry specimen (Fig. 4) shows a longer rise time the then of the wet specimen (Fig. 7). The frequency spectrum of the dry one (Fig. 5) contains a main frequencies on lower frequency then of the wet one (Fig. 8). A basically frequency is 80 kHz. The time-frequency spectrums (Fig. 6 and Fig. 9) show both time and frequency simultaneously. The contour diagrams plotted these spectrums. The high values of spectrums are seen on these diagrams. The fall of the amplitudes over 40 ms interval is better to see on time-frequency diagrams (Fig. 6 and Fig. 9) then on the time diagrams (Fig. 4 and Fig. 7). The damping of any frequencies is taken in time-frequency spectrums but it is not possible to find in the frequency spectrums (Fig. 8 and Fig. 5). The array of high spectrum values of the wet specimen is bigger then of the dry one.

5 Conclusion

The timber humidity considerably influences frequency of hits generated at low-temperature loading. The hit frequency is decreased with humidity increasing.

The time-frequency analysis shows difference spectrum between the specimens with variation humidity. Dried ones have single important frequency but wet ones have more then one frequency.

Acknowledgement

This research has been supported by the Grant Agency of the Czech Republic, under grants "Study, Analysis and Evaluation of Acoustic Emission Signals Applied on Thin-Wall Systems" GACR No.~103/97/P140 and under research project CEZ J22/98 No.~261100007.

References

[1] Šťastný F., Brablec A., Svobodová J., Teching of modern measurement methods, Proc. of SEFI-nWKG Seminar EMEPE'98 (Experiments and measurements in engineering physics education), Technical University, Brno, 15 - 17 October, 1998, p.53 - 56, ISBN 80-214-1223-2

[2] Brablec A., Trunec D., Šťastný F., Deconvolution of Spectral Line Profile, Europhysics Conference Abstracts, Vol. 20 E, Part B, ESCAMPIG 96, Poprad, Slovakia, p.237-238

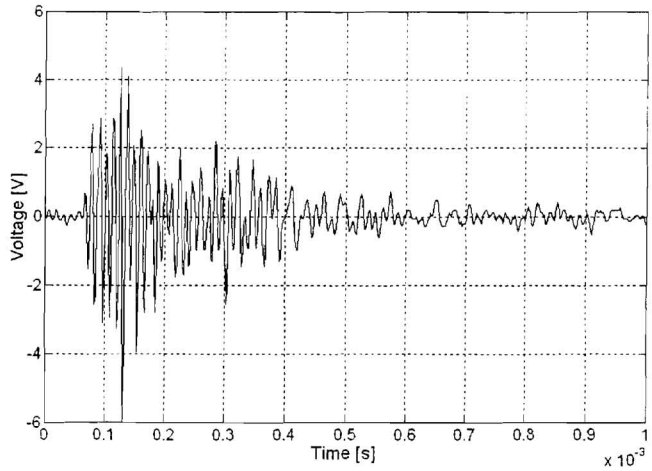

Fig. 4 Dry specimen

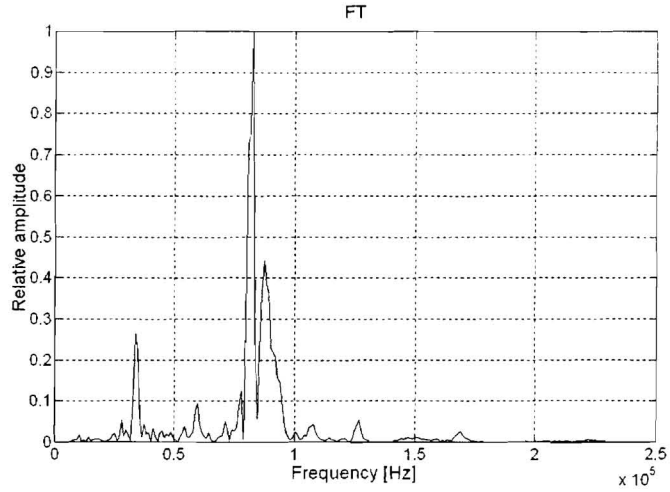

Fig. 5 Spectrum of Fig. 4

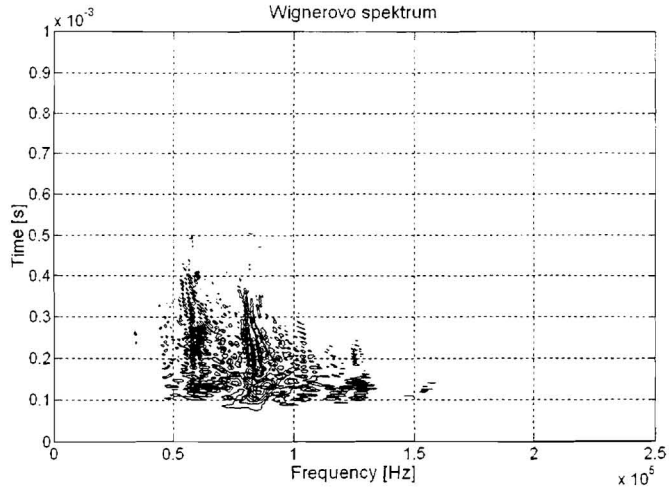

Fig. 6 Time-frequency spectrum of Fig. 4

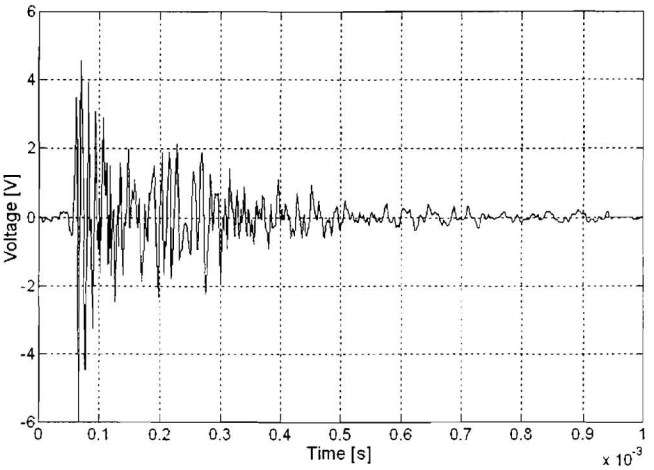

Fig. 7 Wet specimen

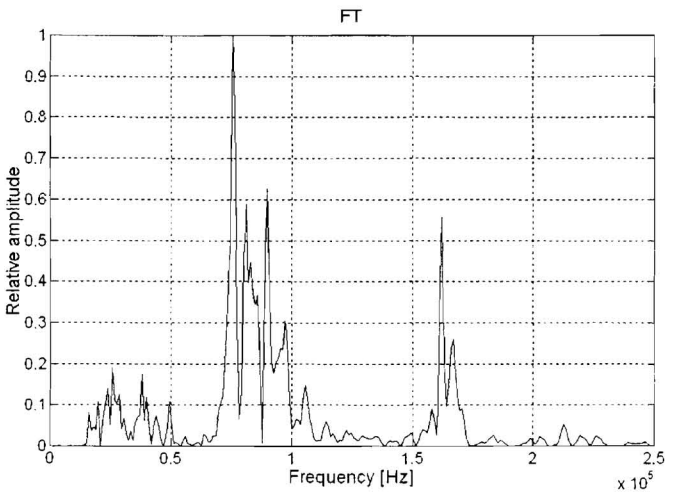

Fig. 8 Spectrum of Fig. 7

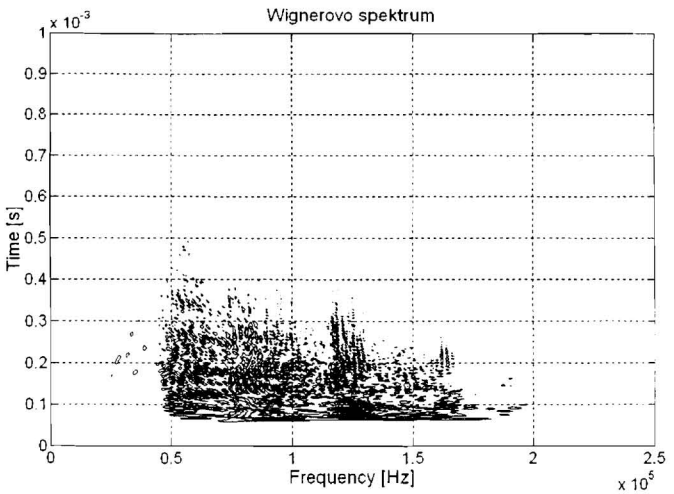

Fig. 9 Time-frequency spectrum of Fig. 7

AN ANALYSIS OF TEMPERATURE AND HUMIDITY VARIATIONS IN CRAWL

M. Matsumoto, X. Yanxiang

AN ANALYSIS OF TEMPERATURE AND HUMIDITY VARIATIONS IN CRAWL

Mamoru Matsumoto[1], Xia Yanxiang[2]

[1]Department of Environmental Design, School of Engineering, Osaka-sangyo University
3-1-1 Nakagaito Daito, Osaka JAPAN 574-8583
[2] Deapartment of Architecture and Civil Engineering, Fuculty of Engineering, Kobe university
1 Rokkodai, Nada, Kobe Japan 754-
E-mail m-matsu@edd.osaka-sandai.ac.jp

ABSTRACT

In crawl space, temperature and humidity are significantly effected by heat and moisture flow from/into earth ground contacted with crawl spaces. So, to analyze and simulate behavior of temperature and humidity in crawl, it must be account for theeffect of earth griound. There are many researchs for this problem as praatical problems. But, they did account insufficientlly for effects of earth ground as moisture source/sink, though account for heat capacity. To predict moisture in/out flow through earth ground surface, ground must be treated as fields of simultaneous heat and moisture transfer. In earth ground, moisture sources are water table under earth surface and water precipitation around building. We presented mathematical model to analyze those as simultaneous heat and moisture problems[1]. Using the model, measured results in small house are analyzed over year and presented [1]. In the paper, we analyzed and discussed annual behavior of temperature humidity. Detailed analysis of daily variations did not analyze. In this paper, we analyze not only annual variations but also daily variation, using measured values of outdoor temparature, humidity and rain precipitation etc. Results of analysis show thaat simulated results agree well with measured values. It is concluded that the mathematical model presented is valid to simulate thermal and hygric behavior in crawl space.

Key Words: Climate in Crawl, thermal and moisture effect of Earth Ground, Prevention of Moisture Damages, Heat and moisture Transfer

1 INTRODUCTION

Moisture problems occur frequently in crawl in Japan, especially during summer due to high humidity of outdoor air. There is no quantitative analysis of prediction on the problems, because of the significant effects of earth ground on crawl, of/on which heat and moisture flow were not accurately analyzed in building thermal environmental engineering. We have studied those problems by numerical simulations applying equations of coupled heat and moisture transfer. In porous media In those analyses, effects of amount of precipitation, location of water table, multi-dimensionality of the object field, air change rate of crawl and moisture barrier on the earth ground surface bounded crawl, have been discussed by numerical analysis[1,2]. A field measurement are performed over a year of a small test house built at Shiga, Japan[3,4]. In 1993, we presented mathematical model to analyze those as simultaneous heat and moisture problems[5]. Using the model, measured results in test house are analyzed over year and presented [5]. In the paper, we analyzed and discussed mainly annual behavior of temperature humidity. Detailed analysis of daily variations did not performed. In this study, using the measured data, measured every hour over a year, detailed analysis, not only annual variations but daily variations are done. Results of the numerical analysis are compared with the measured values and validity and accuracy of analyses are discussed. In addition to those, sensitivity analysis of several parameters are presented.

2 TEST HOUSE AND EXPERIMENT

Schematic diagram of the test house are shown in Fig.1. Plan of the test house is 4x4m. Height of crawl space(crawl) is 0.46m. Basement surrounded the crawl space is made of concrete wall(0.15m) without thermal insulation. On the basement, there are two small openings(0.1mx0.2m) which are for ventilation of the crawl space(in Japan, those openings are usually equipped and minimum total area of openings are regulated by regulation).

Floor slab of room above the underfloor space (i.e. ceiling of the crawl space) is made of a single layer of plywood (17.5mm) without thermal insulation. The room above the crawl space was usually not heated or cooled by artificial device, except for short period, that is almost under natural conditions during the experiment. Solar radiation radiated into the room through a windows (2mx2m). Temperature and humidity in the room were

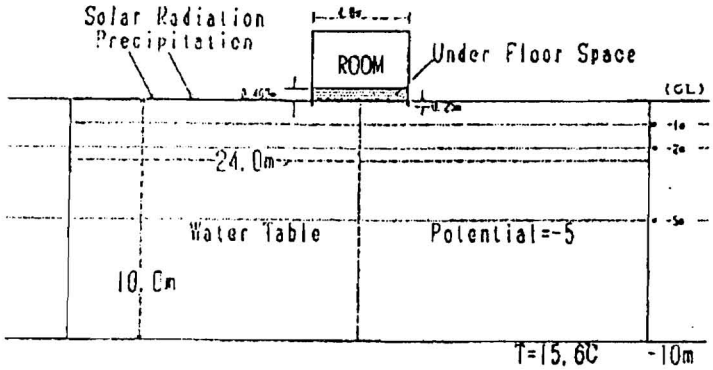

Figure 1 Schematic diagram of test house and domain of analysis

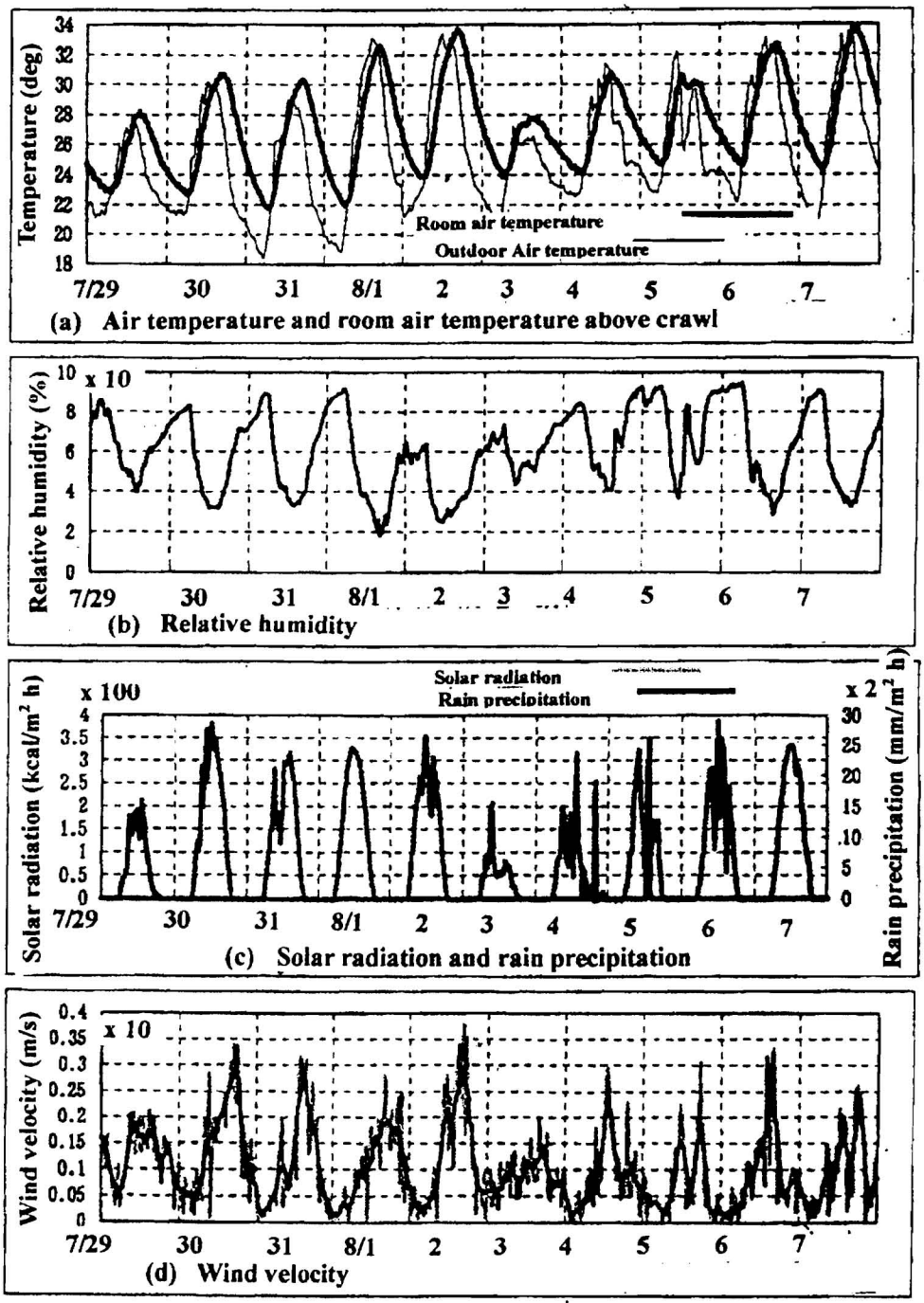

Figure 2 Measured values of outdoor climate (29th July-7th August)

continuously measured during the experiment. These measured values are used in the numerical simulations as the input data. All of input data such as outdoor air temperature, relative humidity, solar and longwave radiation, wind velocity and its direction etc. are continuously measured every hour or every 20min. during the entire experiment. Medium of the earth ground under the test house is sand. Of the test house, temperature and relative humidity in the crawl space are measured continuously over a year. And temperature and moisture content in/on the earth ground contacting with the crawl space are simultaneously measured.

3 ANALYSIS

In Fig.1, domain of analysis is shown. At the lower boundary of earth ground, temperature and moisture potential are specified. Vertical boundary of the earth ground is treated as surfaces of no flow of heat and moisture. Boundary conditions at earth ground surface contacted with outdoor air and crawl space are the third kind. At former surface, rain precipitation rate are accounted for as surface production of liquid water. And heat flow of solar radiation and long wave radiation are accounted for. Basement concrete slab and wooden floor of room are treated as pure heat conduction media.

Governing equations of the field are as follows

Heat balance equation of crawl space

$$c\gamma V\frac{dT_c}{dt}=2K_b(T_o-T_c)S_b+K_f(T_r-T_c)S_f+c\gamma\,NV(T_o-T_c)+\alpha_i\sum_{j=1}^{f}(T_j-T_c)S_j \qquad (1)$$

Moisture balance equation of crawl space

$$c'\gamma'V\frac{dP_c}{dt}=c'\gamma'NV(P_o-P_c)+\alpha'_i\sum_{j=1}^{f}(P_j-P_c)S_j \qquad (2)$$

Heat transfer equation in the earth ground

$$\frac{\partial T}{\partial t}(c_a\gamma_a T)=\nabla(\lambda+r\lambda'_{Tg})\nabla T+\nabla r\lambda'_{\mu g}(\nabla\mu-Fw) \qquad (3)$$

Moisture transfer equation in the earth ground

$$\rho_w(\frac{\partial\Psi}{\partial\mu})\frac{\partial\mu}{\partial t}=\nabla\lambda'_{\mu}(\nabla\mu-Fw)+\nabla\lambda'_T\nabla T \qquad (4)$$

Boundary condition of heat transfer on upper surface of the ground

$$-(\lambda+r\lambda'_{Tg})\frac{\partial T}{\partial n}-r\lambda'_{\mu g}(\frac{\partial\mu}{\partial n}-Fw)=\alpha_{(x)}(T-T_c)+r\alpha'_p(P-P_c) \qquad (5)$$

Boundary condition of moisture transfer on upper surface of the ground

$$-\lambda'_{Tg}\frac{\partial T}{\partial n}-\lambda'_{\mu}(\frac{\partial\mu}{\partial n}-nFw)=\alpha'_{p(x)}(P-P_c)+f_r \qquad (6)$$

From definition of relation between partial water vapor pressure P , tempere T and chemical potential μ

$$\mu=R_wT\ln(P/P_{s(T)}) \qquad (7)$$

where n means inward normal to earth ground and suffix c means value at crawl space, o means at outdoor air. Temperature and humidity in crawl space are treated as uniform. Domain of analysis is two dimensional space. System of equations shown above are solved by explicit finite difference method.

A part of measured values of outdoor air are shown in Fig.2 (a)• -(d). In the calculation, these value over the year are used as input data. Air change rate of underfloor space is obtained from calibration curve between outdoor wind velocity with wind direction and air change rate of the test house. During the experiment, mean air

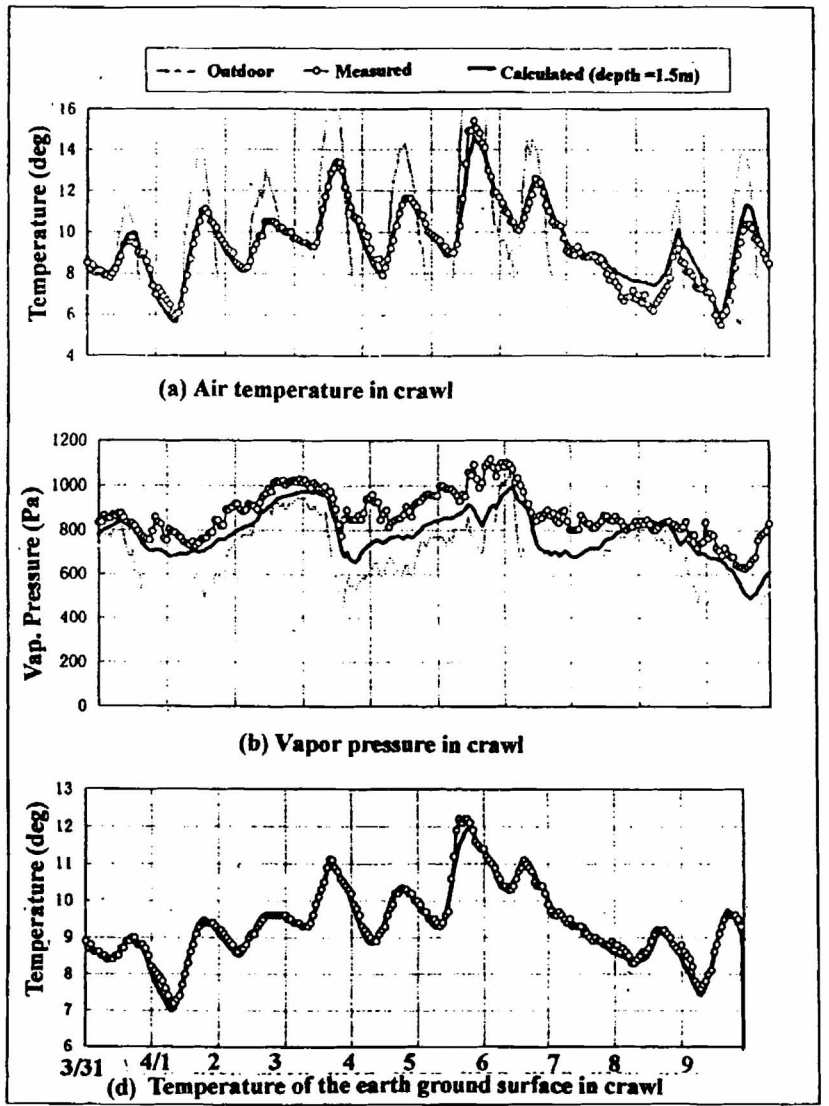

Figure 3 Comparison between measured and calculated values

Temperature and vapor pressure

(At Spring from 31st Mar. to 10th Apr.)

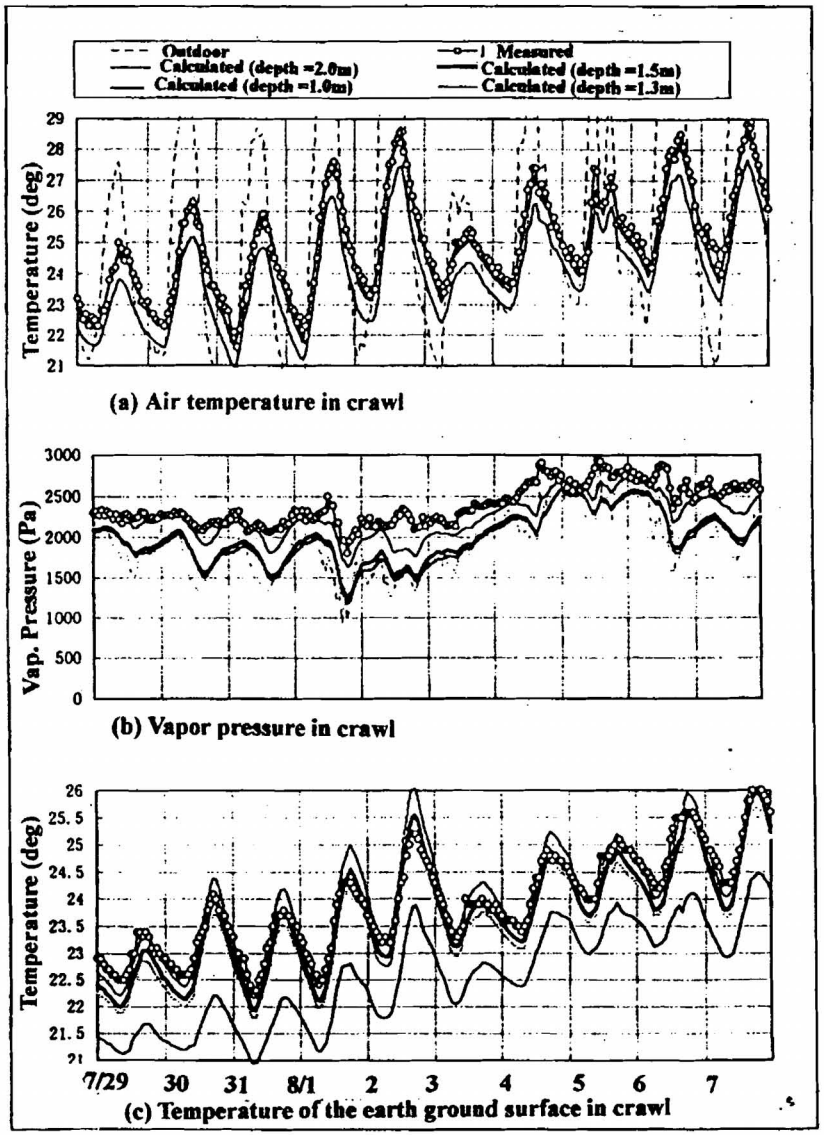

Figure 4 Comparison between measured and calculated values

Temperature and vapor pressure

(At Summer from 29th Jul. to 8th Aug.)

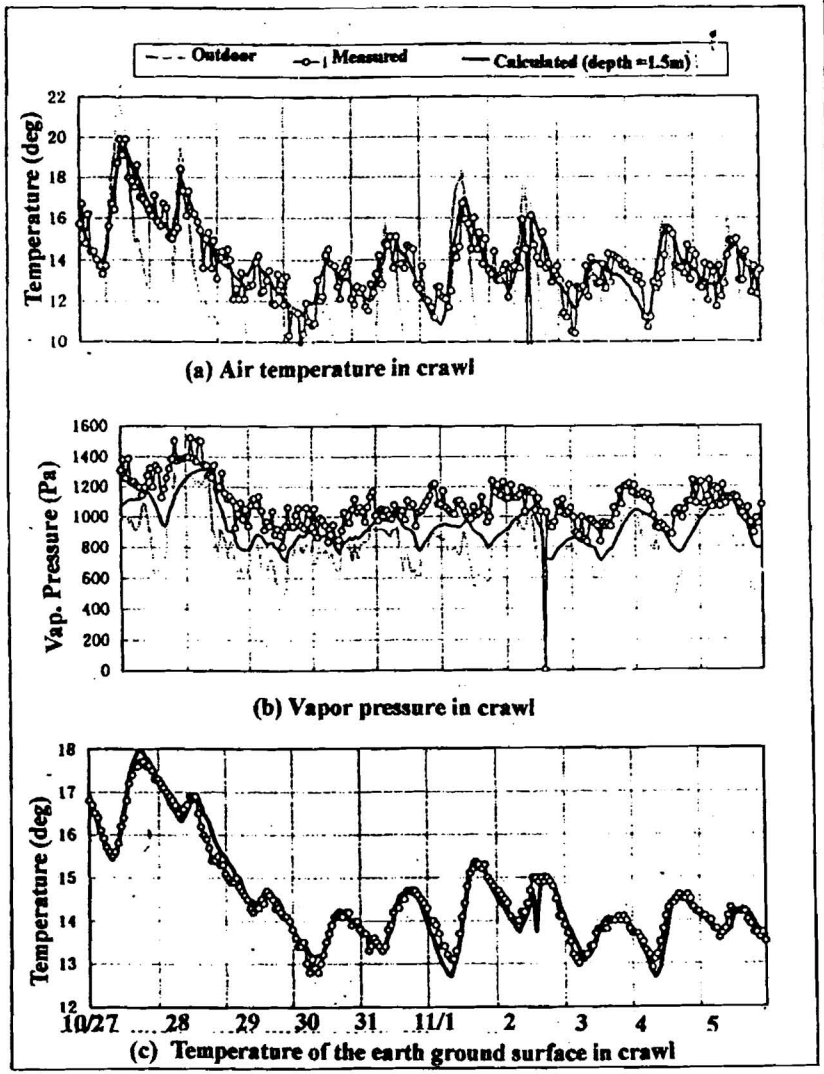

Figure 5 Comparison between measured and calculated values

Temperature and vapor pressure

(At Autumn from 27th Oct. to 5th Nov.)

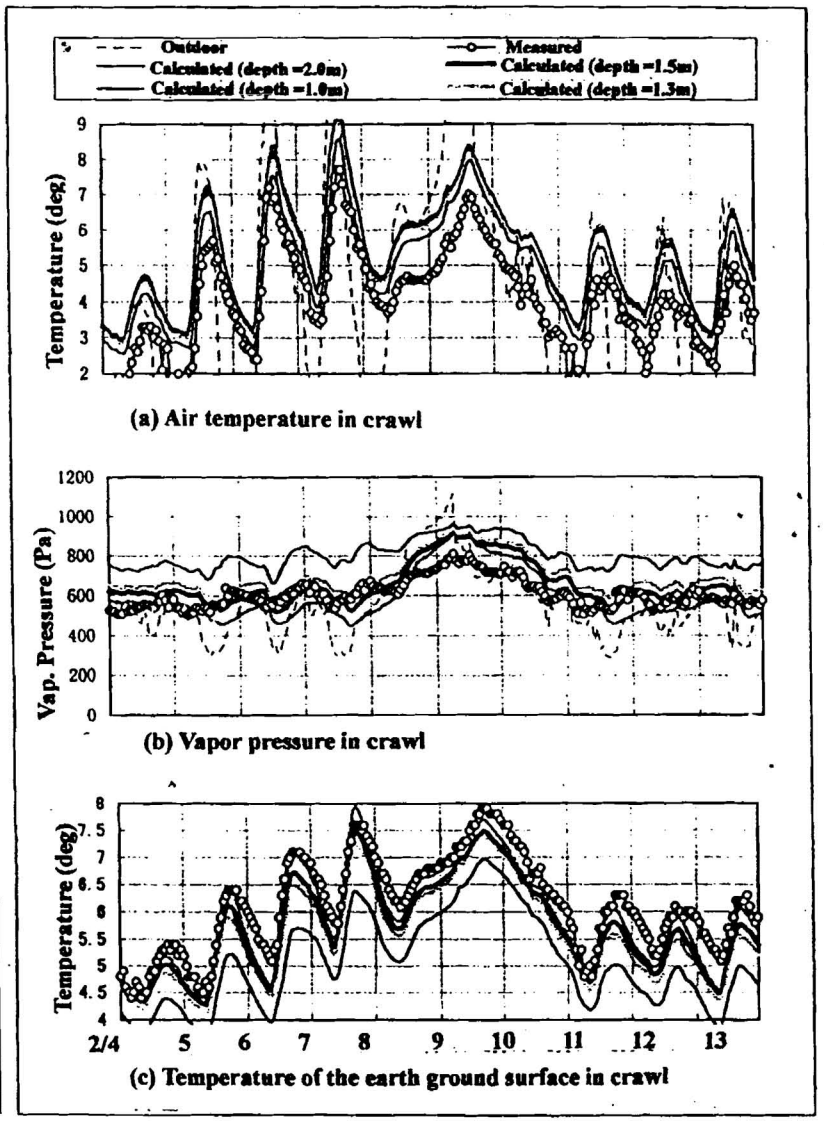

Figure 6 Comparison between measured and calculated values

Temperature and vapor pressure

(At Winter from 4th Feb. to 13th Feb.)

change rate was ca. 14 (1/h). Depth of water table was measured at the beginning of the measurement and measured depth is 1.5(m).

4 RESULTS AND DISCUSSIONS

Calculated results of temperature Tc, partial vapor pressure Pc and surface temperature of the earth ground at center of crawl space are shown in figure 3 (spring), 4 (summer) , 5 (autumn) and 6 (winter). Both of Crawl air temperature and the earth surface temperature agree well with measured value over the year, especially fair well in spring and autumn. On the other hand, of partial vapor in crawl space, calculated values are slightly small from measured values, except winter. Then, in the following, effects of depth of water table on calculated values are discussed, because it seems that their values used in the calculation are not accurate. Depth of water table was measured only at the beginning of the measurements.

Depth of water table may vary. Considering measured value, 1.5(m), sensitivity analysis are performed from 2.0 to 1.0(m). Calculeted results are shown only in figure 4 (summer) and 6 (winter). Figure 4 shows that at 1.3(m) of depth of water table, calculated vapor pressurevalues are acceptablly agree with measured values, keeping temparature showing good agreement at crawl and earth ground surface. When depth of water table ia set at 1.0(m), vapor pressure in crawl shows good agreement, on the other hand, temperature of earth ground surface is lower ca. 1.5(deg) than measured, by increased latent heat by evaporation of moisture at the earth surface. Considering much rain precipitation at beginning of summer in Japan, decrease of depth of water table might be occurred. Accounting for variations of depth of water table, calculated results show good agreenment with measured values. Then the mathematical model presented in thi paper yields reasonable prediction of thermal and hygric behavior in crawl space contacting bare soil surface.

4 CONCLUSIONS

Of the small test house, temperature and humidity variations of crawl pace contacted with bare earth ground are analyzed, applying simultaneous heat and moisture transfer equations to earth ground, considering location of water table and penetration of precipitation on bare ground surrounding the test house. Results calculated are compared with measured values over year. In addition to those, effects of depth of water table are analyzed and discussed. Conclusions are as follows

Calculated results using mathematical model presented show good agreement with measured values of temperature and vapor pressure. It is concluded that the model presented here is reasonably valid for predicting temperature and humidity in crawl space or space directly contacting to ground. Level of ground water play important roll when depth of water table decrease smaller than 2.0(m) in sand soil.

REFERENCE

[1] Matsumoto,M. and Senoo,T., Proc. AIJ Kinki, 31 17-20 (1991) (in Japanese)
[2] Matsumoto,M. and Hashimoto,T., Proc. AIJ Kinki, 93 109-112 (1993) (in Japanese)
[3] Miyata,Y., Proc. 21th Symp. Thermal Problems on Building, AIJ., 21 139-150 (1991) (in Japanese)
[4] Miyata,Y. and Matsumoto,M., Trans. AIJ .457 pp.19-28 (1993) (in Japanese)
[5] Matsumoto,M. and Hashimoto,T., An analysis of temperature and humidity variations in underfloor space , Proc. 1993 CIB W-40 meeting, CIB Publication 173 (1994)

SYNBOL

T = temperature [k]
P = pressure or partial pressure [Pa]
μ = water chemical potential referred to pure free water (= R v T ln h)[J/kg]
ϕ = moisture content [m³/m³ :vol]
t = time [s]
α = heat transfer coefficient [w/m² k]
α_T = vapour transfer coefficient related to temperature difference [kg/m² s k]
α_μ = vapour transfer coefficient related to water chemical potential difference [kg/m² sJ/kg]
c_γ = heat capacity of moist air [J/m³ K]
c_γ = water vapour capacity of moist air [Kg/m³ Pa]
$c_G \rho_G$ = heat capacity of soil [J/m³ K]
ρ = density [kg/m³]
r = heat of vapourization [J/Kg]
N = rate of air change [1/s]
λ = thermal conductivity of moist porous material [W/m k]
λ_T = moisture conductivity related to temperature gradient [kg/ms J/kg]
λ_μ = moisture conductivity related to water chemical potential gradient [kg/ms J/kg]
λ_{Tg} = moisture conductivity in gas phase related to temperature gradient [w/m k]
$\lambda_{\mu g}$ = moisture conductivity in gas phase related to water chemical potential gradient [kg/m s J/kg]
fr = precipitation [Kg/m² s]
Js = solar Radiation [J/m² s]
Sf = area of floor [m²]
Sb = total surface area of wall of under floor space [m²]
V = volume of Underfloor Space [m³]
Kf = thermal transmittance of floor [J/m² sK]
Kb = thermal transmittance of wall of under floor space [J/m² sK]

THE HYGROSCOPIC INERTIA – AN IMPORTANT FACTOR FOR THE RELATIVE HUMIDITY OF DWELLINGS WITHOUT HEATING SYSTEMS

V.P. de Freitas

THE "HYGROSCOPIC INERTIA" – AN IMPORTANT FACTOR FOR THE RELATIVE HUMIDITY OF DWELLINGS WITHOUT HEATING SYSTEMS

Vasco Peixoto de Freitas

Faculdade de Engenharia da Universidade do Porto, Rua dos Bragas, 4050-123 PORTO, PORTUGAL – E-mail: vpfreita@fe.up.pt – Web adress: http://www.fe.up.pt/sccwww/lfc/

Abstract

Hygroscopic wall and ceilings give substantial stability to the indoor relative humidity in rooms. In this paper, we analyse the importance of "hygroscopic inertia" in buildings in temperate climate regions, where there isn't buildings normally any heating systems. We present, also, the results of an experimental study that was conducted on different covering materials on which different types of paint were applied, all this with the aim of appreciating the influence of support and its paint on "hygroscopic inertia".

Key words: moisture, hygroscopicity, relative humidity, "hygroscopic inertia"

1 Introduction

The covering used on walls and ceilings play an important role in controlling the interior climate of buildings. Certain materials have a very strong hygroscopic behaviour, absorbing moisture, when the indoor relative humidity increases and releasing it into the air, when there is a reduction in the relative humidity.

Between winter and summer, in a single-family dwelling, it is possible to store over 100 kg of moisture in the covering materials.

Experiments, conducted at the Faculty of Engineering of Porto University, shown that, for a single-family house, without a heating system, whose vapour production inside was known, as we were dealing with a "laboratory house", there was a time lag and damping in the values of indoor absolute humidity with regard to outdoor absolute humidity.

These time lag and damping are due to the "hygroscopic inertia" of the dwelling which depends on furniture and equipment, but also on the nature of the covering materials for use in walls and ceilings. Hygroscopic wall and ceilings give substantial stability to the indoor relative humidity in rooms.

Nowadays, there is a growing use of non-hygroscopic materials in buildings which reduce their daily and seasonal "hygroscopic inertia".

In this paper, we analyse the importance of "hygroscopic inertia" in buildings in temperate climate regions, where there isn't buildings normally any heating systems. We

present, also, the results of an experimental study that was conducted on different covering materials on which different types of paint were applied, all this with the aim of appreciating the influence of support and its paint on "hygroscopic inertia".

2 Climate conditions inside buildings in Portugal

Taking into account the fact that we do not have heating systems in buildings, indoor temperature and relative humidity vary as follows:

Table 1 Climate conditions inside buildings in Portugal.

	Temperature (°C) *(average)*	Relative Humidity (%) *(average)*
Winter	15 – 17	80 – 90
Summer	> 24	< 50

Under these circumstances, it can be stated that the surface materials are subject to changes in relative humidity ranging from 50 % to 95 %. It should be referred that the average outdoor temperature in Portugal, in the winter, during the coldest months of the year, ranges from 3 °C to 10 °C.

3 Type of the studied materials

With the aim of analysing the behaviour of the most frequently used materials for covering of walls and ceilings, the following were tested:

Table 2 Type of the studied materials.

Designation of the samples	**Type of covering**	**Paint**	**Designation of the samples**	**Type of covering**
A	Traditional plastered A		G	Plaster + 2 mm gypsum
B	Traditional plastered A	S	H	Plaster Board
C	Traditional plastered A	T	I	Industrial plastered A
D	Traditional plastered A	U	J	Industrial plastered B
E	Traditional plastered A	V	K	Industrial plastered C
F	Traditional plastered B			

Four types of paints (S, T, U and V) were applied to the materials.

4 Results

For the experimental study, a set of over one hundred samples was prepared, using the configuration as defined in the following figure:

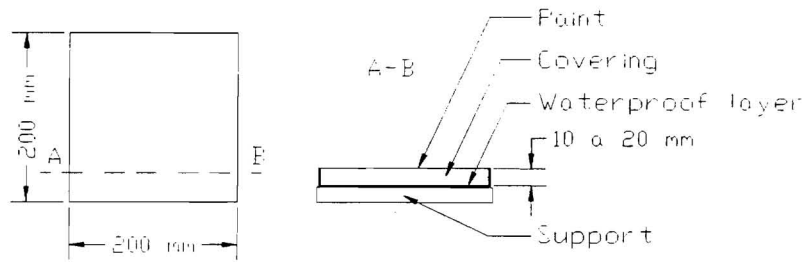

Fig. 2 Configuration of the samples.

The samples were placed in ambiences with decreasing relative humidities: 98 %, 93 %, 86 %, 75 % and 54 %, for long periods of time (3500 hours).

As we can see in figure 3, the change in the mass of the samples is very significant when the relative humidity goes from 93 % to 54 % and depends on the nature of the covering. For instance, plaster boards, 10 mm thick, can absorb or release 90 g/m² of water, while for certain types of plaster work (20 mm) that change reaches 400 g/m².

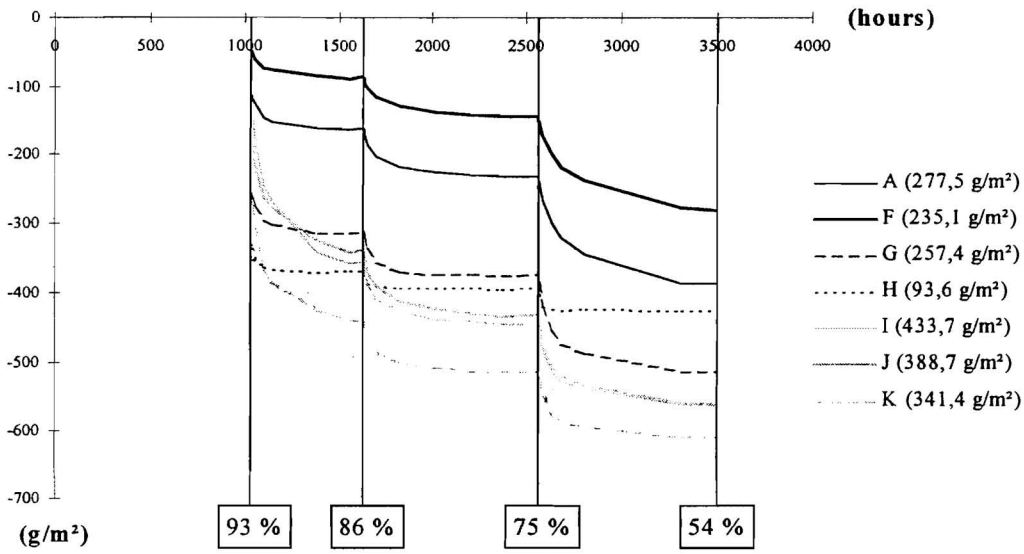

Fig. 3 Change in the mass of the coverings as a function of the change in the relative humidity.

In figure 4, it can be observed that the desorption process is very slow, thus requiring several hundreds of hours until stabilisation is attained, and the process is dependent on the relative humidity. However, the experimental study that was conducted allowed for the observation of the fact that it is especially during the first hours that the greatest

exchanges of humidity between the materials and the atmosphere took place, and that change is linear in the first 6 hours for all the materials that were studied.

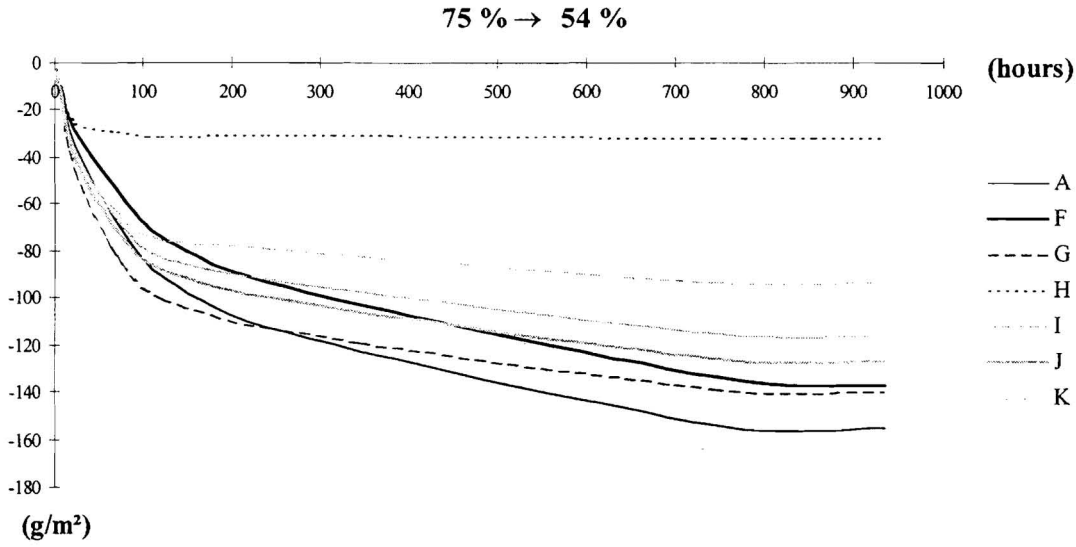

Fig. 4 Change in the mass of the samples with time.

When we paint the coverings of walls and ceilings, we are reducing their hygroscopicity. Even when using open paints, this can reduce their capacity for storing humidity by around 30 % (see figure 5). The use of washable or vitrified paints leads to even greater reductions.

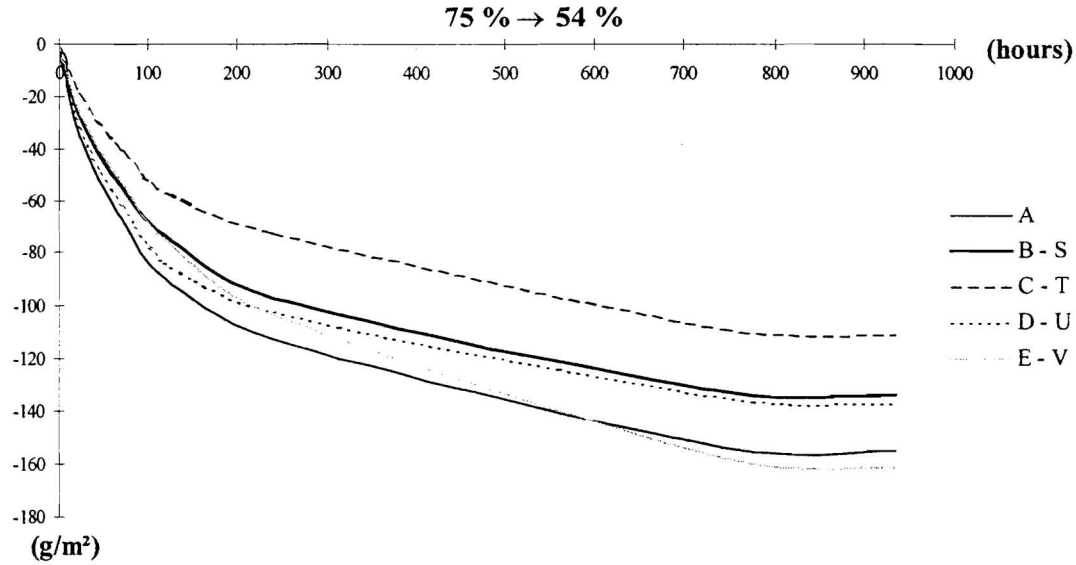

Fig. 5 Change in the mass of the samples with time, in function of the type of painting used (same support).

5 Discussion of results

The use of covering materials with a hygroscopic behaviour allows for the storage of around 25 litres of moisture between summer and winter in a room (4 m × 3 m × 2,5 m) where the walls and ceiling have a surface area of around 65 m². The use of plaster boards allows for the storage of only 5,8 litres.

We also know that, in a bedroom, around 1000 g of water vapour can be produced during the night. During that period, sometimes ventilation is highly reduced hence, the daily "hygroscopic inertia" may contribute towards controlling peaks of relative humidity in the air.

For the materials that were tested, the sorption/desorption capacity ranges from 0,1 g/(m²·h) to 0,7 g/(m²·h) for a difference in relative humidity of 1 % between the ambience and the surface of the material.

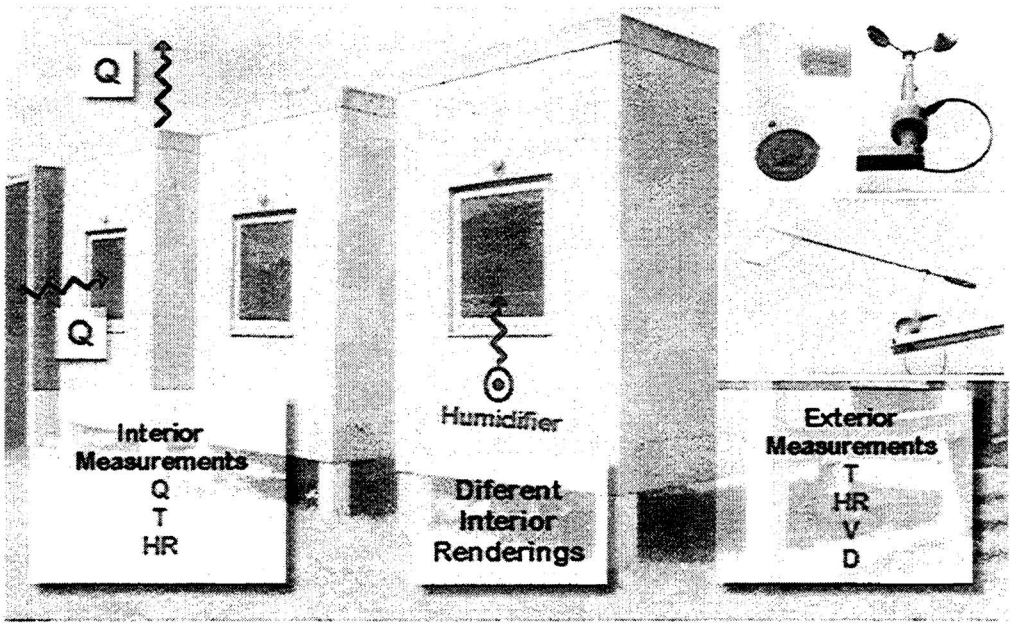

Fig. 6 Test cells.

With the aim to study the dynamic influence of the hygroscopicity of the coverings, we are developing measurements of temperature, relative humidity and ventilation in test cells (see figure 6), testing different coverings and considering different ventilation ratios. We also have at our disposal the weather station of the Faculty of Engineering of Porto University which continually measures outdoor air temperature, relative humidity, wind direction and speed, solar radiation and rainfall.

With future developments in this research, we hope to find a criterion for quantifying daily and seasonal "hygroscopic inertia", in order to minimise the phenomenon of condensation.

6 Conclusions

The main conclusions of this study, which is still in the development stage, are as follows:

- Certain materials have the ability to absorb moisture, when relative humidity ranges from 54 % to 93 %. Certain coverings may reach a storage of about 400 g/m²;
- Paint can eliminate or strongly reduce the materials' hygroscopicity ;
- In a bedroom, the walls and ceiling can store 25 litres of moisture between the summer and the winter if its configuration is adequate;
- For the tested materials, the sorption/desorption capacity ranges from 0,1 g/(m²·h) to 0,7 g/(m²·h) for a difference in relative humidity of 1 % between the ambiences and the surface of materials;
- For buildings without heating systems, the hygroscopicity of coverings and daily and seasonal "hygroscopic inertia" are an important factor for the indoor relative humidity.

7 Acknowledgement

I would like to express my greatest thanks to, Mr. Nuno Machado and Mr. Rui Gomes , Civil Engineers, for their contribution to this paper.

8 References

[1] CASTRO, RUI – "Importance of the interior coverings hygroscopicity" (in portuguese), *Master Science Thesis,* LFC/FCTUC, Coimbra, July 1998.

[2] DE FREITAS, VASCO PEIXOTO; ABRANTES, VITOR – "Étude expérimentale de l'humidité de l'air dans l'intérieur des bâtiments – Influence du comportement hygroscopique des matériaux", Healthy Buildings'88, CIB, Vol.2, pp. 201-209, Stockholm, Sweden, 5th - 8th September 1988

[3] HENS, H; ELSEN P. – "Indoor climate: influence of hygroscopic inertia on relative humidity and vapour pressure", Contribution to the CIB-W40 Sopron meeting, Hungary, September 1993

[4] HANSEN, KURT KIELSGAARD – "Sorption Isotherms - A Catalogue", The Technical University of Denmark, Denmark, 1986

[5] PADFIELD, TIM – "The role of absorbent building materials in moderating changes of relative humidity", Ph.D. Thesis, Technical University of Denmark, October 1998

[6] PLATHNER, PHILIPP; LITTLER, JOHN; CRIPPS, ANDREW – "Modelling Water Vapour Conditions in Dwellings", Third International Symposium on Humidity & Moisture, pp. 64-72, London, England, April 1998

EXPERIMENTAL STUDY OF THE DRYING OF CELLULAR CONCRETE

V.P. de Freitas, J. Castro

Experimental Study of the Drying of Cellular Concrete

Vasco Peixoto de Freitas *
José Castro **

1. INTRODUCTION

There is a growing use of cellular concrete in the Portuguese building construction, executed "*in situ*", used as form layers of flat roofs and filling layers over concrete slabs inside the buildings. The advantages of this material are its low density, easy application and low cost.

The drying of the cellular concrete, especially in case of layers of a great thickness, is very complex and long. The application of waterproofing systems or coverings (wood, linoleum, etc...) on not fully dried cellular concrete, has resulted in the occurrence of pathologies.

At the Building Physics Laboratory – LFC of the Faculty of Engineering of the University of Porto, we have carried out an experimental study with the aim of measuring the drying process of cellular concrete, under laboratory and outdoor conditions *[1]*. The measurement of the moisture content profiles of the tested material was performed by means of a gamma-ray attenuation device. In this paper, we present the experimental results of the study and give some practical recommendations on the hygrothermal implications of the use of cellular concrete.

2. THE DRYING OF BUILDING MATERIALS

The drying of materials can be expressed as a function of the differences in the vapour concentration at the surface of the material and in the atmosphere, by means of the following expression *[2]*:

$$g_v = \beta \cdot (C's - C'a) \qquad (1)$$

* Associate Professor and Head of the Building Physics Laboratory.
** Master of Science.
Faculdade de Engenharia da Universidade do Porto, Rua dos Bragas, 4099 Porto, Portugal – *vpfreita@fe.up.pt*

where

g_v - moisture flow ..... $kg/m^2.s$

β - surface transfer of moisture coefficient ..... m/s

C's - concentration of water vapour at the surface ..... kg/m^3

C'a - concentration of water vapour in the atmosphere ..... kg/m^3

When the surface is saturated, the drying flow is constant. Later, when the amount of water carried from inside the material to its surface is lower than the amount of vapour released during the drying process, the vapour concentration at the surface decreases and the drying flow tends to zero. In this phase, the water vapour is carried to the surface of the material, by means of vapour diffusion, through a layer of "dry" material. This layer of "dry" material increases during this phase *[3]*.

3. PROPERTIES OF THE CELLULAR CONCRETE BEING STUDIED

The cellular concrete being studied is made of a cement paste, with air introduced in the form of bubbles approximately 1 mm in diameter. The air is introduced by means of a chemical reaction during the preparation of the material *[4]*. The percentage of air in this type of material is around 50% of its volume. The original value of water content (saturation) can reach about 1,2 kg/kg.

Twelve cubic samples were moulded in order to determine the apparent density and to evaluate resistance to compression of the material. The density for compositions of Type I and Type II in the dry state are $440kg/m^3$ and $600kg/m^3$, respectively. The values obtained for resistance to compression ranged from 0,66 and 2,06 MPa.

The hygroscopic moisture content of the cellular concrete was evaluated, by placing a sample of material in a saturated atmosphere (RH $\cong$ 98%), where the moisture content was 0,21 kg/kg. A sample of dry material was also placed in an atmosphere with a relative humidity of about 50%, which reached a moisture content 0,08 kg/kg.

4. EXPERIMENTAL DETERMINATION OF THE MOISTURE CONTENT PROFILES

The experimental device used to measure moisture content by gamma-ray attenuation was built and calibrated at the Faculty of Engineering of Porto University – LFC and consists of a

radioactive source (Americium), a detector of sodium iodide, an electronic unit made up of a voltmeter, a temporiser, a counter, a device for measuring the counting rate and high- and low-voltage feed as well as a computer terminal with the respective software for automatically introducing and obtaining data.

The physical principle that is the basis of this measuring technique consists of the attenuation or absorption of emitted radiation when a given material is placed between the radioactive source and the detector (gammametry). The attenuation of the radiation depends on the energy of the photons, the chemical composition of the absorber and the distance between the source and the detector. It is possible to establish the relationship between the emitted (I_0) and transmitted radiation (I), depending on the value of the thickness (χ) of the specimen, the attenuation coefficient (μ) and the density of the material (ρ).

$$I = I_0 \cdot \exp. (-\mu \cdot \rho \cdot \chi) \ [\text{counts/s}] \qquad (2)$$

The value of water content can be calculated since the mass attenuation coefficient of the water (μ_w), the transmitted radiation of dry sample (I_0*) and the density of the dry material (ρ_0) are known:

$$\theta = -\text{Ln} (I/I_0^*) / (\mu_w \cdot \rho_w \cdot d) \ [m^3/m^3] \quad \text{or} \quad W = (\theta/\rho_0) \cdot \rho_w \ [\text{kg/kg}] \qquad (3)$$

The calibration of the equipment consists of the comparison between the mass variation of the samples obtained by weighing (gravimetry) and the mass variation calculated by the integration of the experimental profiles of moisture content, at the same moment of the drying process. Good agreement of the results shows that gamma-ray attenuation equipment may be considered valid for the determination of moisture distribution profiles (see figure 3).

4.1. Configuration of Samples

Cellular concrete is normally applied in constructions with one side in contact with the support, while the other side – the drying side – is exposed to climate conditions. Thus, the adopted physical model is a prismatic system that is open on one side (drying side) and "waterproofed" on the remaining five sides, so as to make sure that the drying flow in these directions is null.

The physical model was produced by a quadrangular Plexiglas mould of 3,5 mm with heights of 100, 200 and 300 mm and the interior section of 100 x 100 mm^2.

The heights chosen for the samples represent the thicknesses of cellular concrete normally used in Portugal when executing moulded layers of coverings and in filling pavements.

4.2 Drying Process

The samples of cellular concrete, with the dimensions mentioned above, were exposed to the following conditions:

- Drying in the laboratory (T = 22°C ± 2°C and RH = 50% ± 5%);
- Drying outdoors (sheltered from the rain and solar radiation).

Figure 1 shows the variation in the intensity of radiation in the dry state, by three 200-mm-high samples, which showed that density increases with depth, because the number of counts decreases. The samples are not homogeneous.

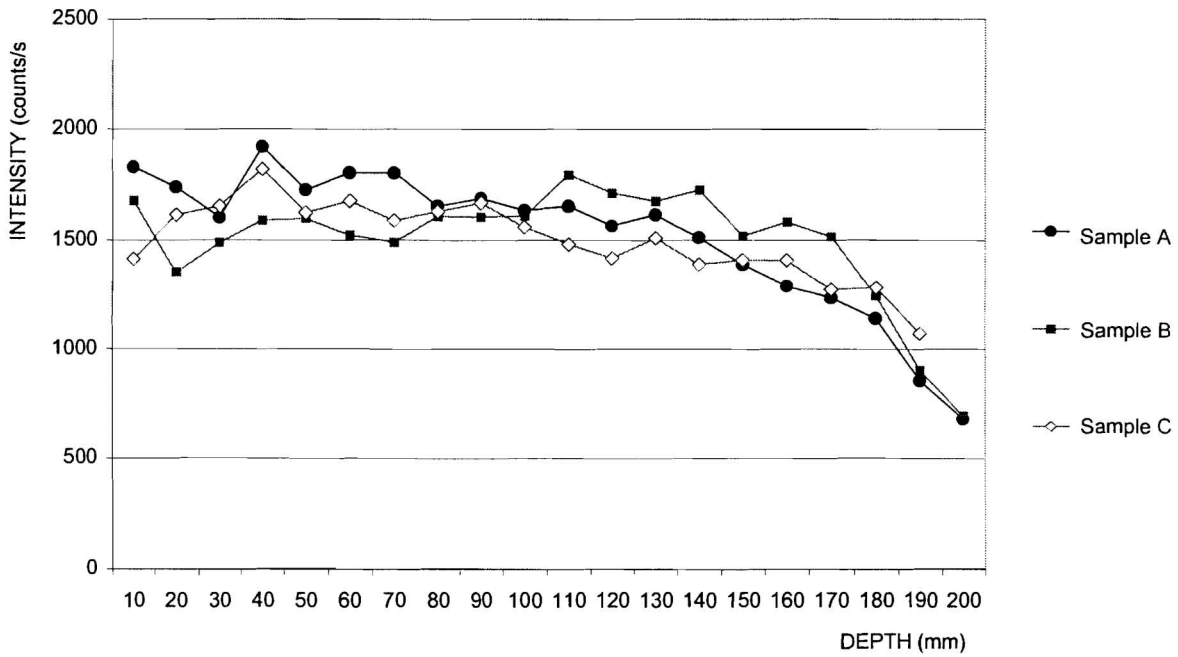

Figure 1 Variation of the intensity of radiation along the sample.

Figure 2 shows the evolution of the profiles of the moisture content in cellular concrete, obtained by means of gammametry, for 100-mm-thick samples dried in the laboratory.

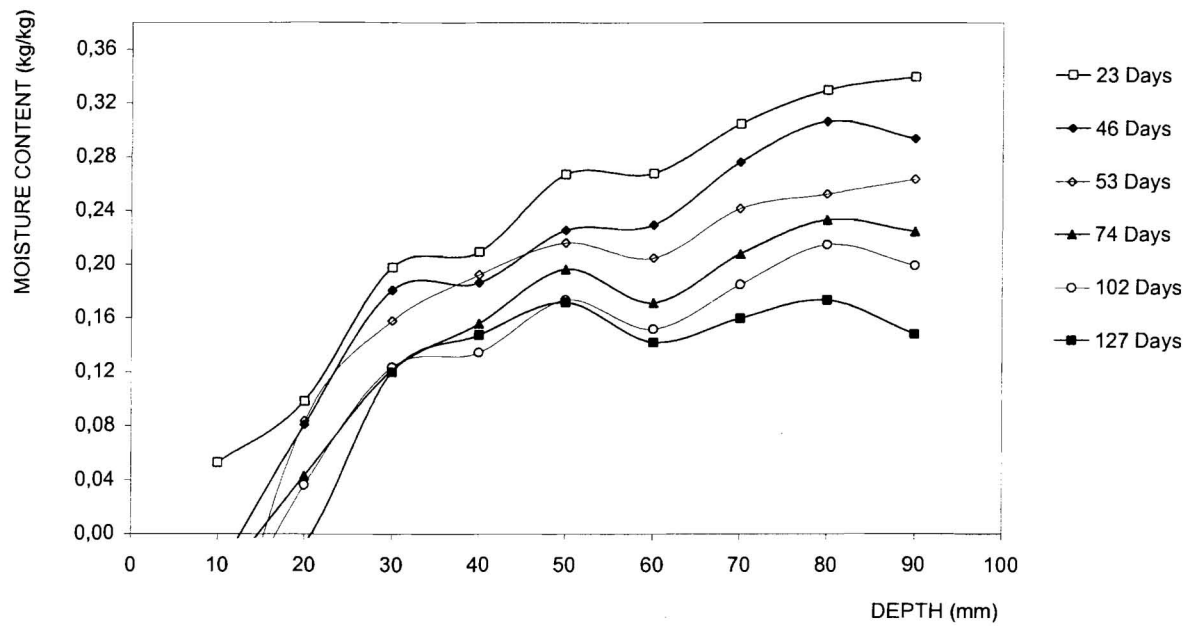

Figure 2 Profiles of the moisture content of 100-mm-thick samples when dried in the laboratory.

At the end of the drying period in the laboratory (127 days), the samples were placed in an oven at 60°C for 52 days, then for another 6 days at 105°C, until it reached the dry state. The variation of mass during the drying process, as a function of the square root of time, is shown in figure 3. In this figure, one can see the agreement between the values for the variation of mass, obtained by means of gammametry and by gravimetry.

Figure 4 shows the evolution of the profiles of the moisture content in a 100-mm-thick sample of cellular concrete dried outdoors. It should be noted that, after 68 days of drying, sheltered from rain and radiation, the samples were left exposed for 12 days, which led to a big increase in moisture content.

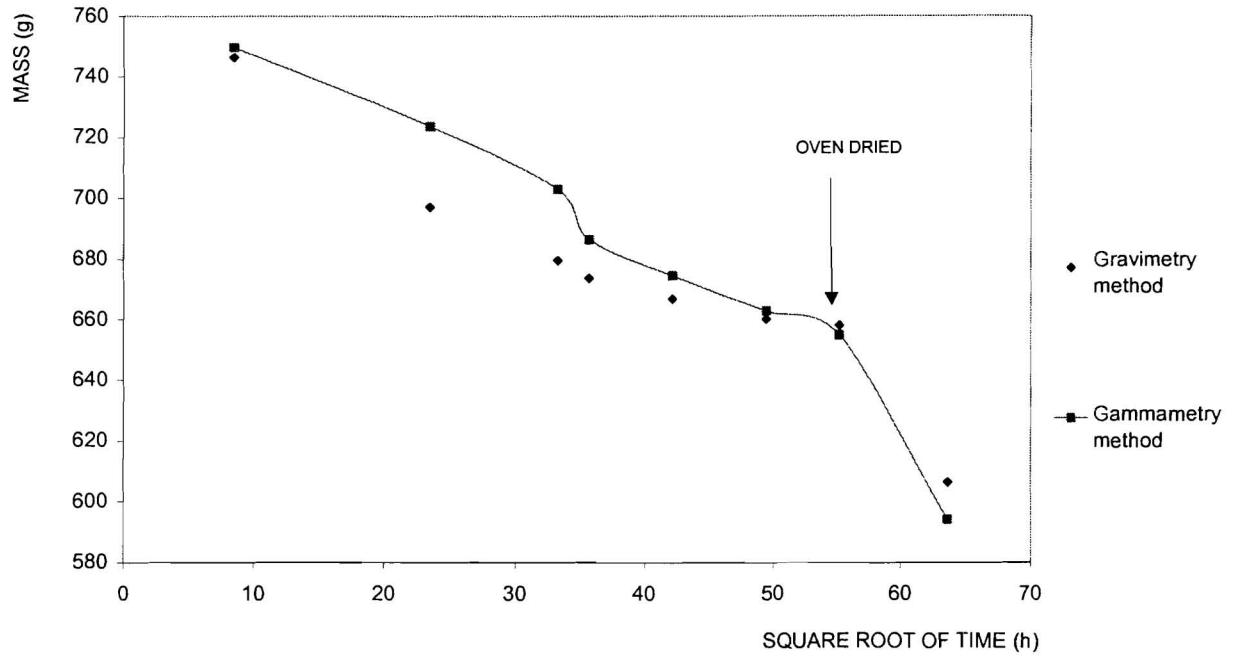

Figure 3 Comparison of the variation of the mass of a 100-mm sample calculated by gammametry and gravimetry.

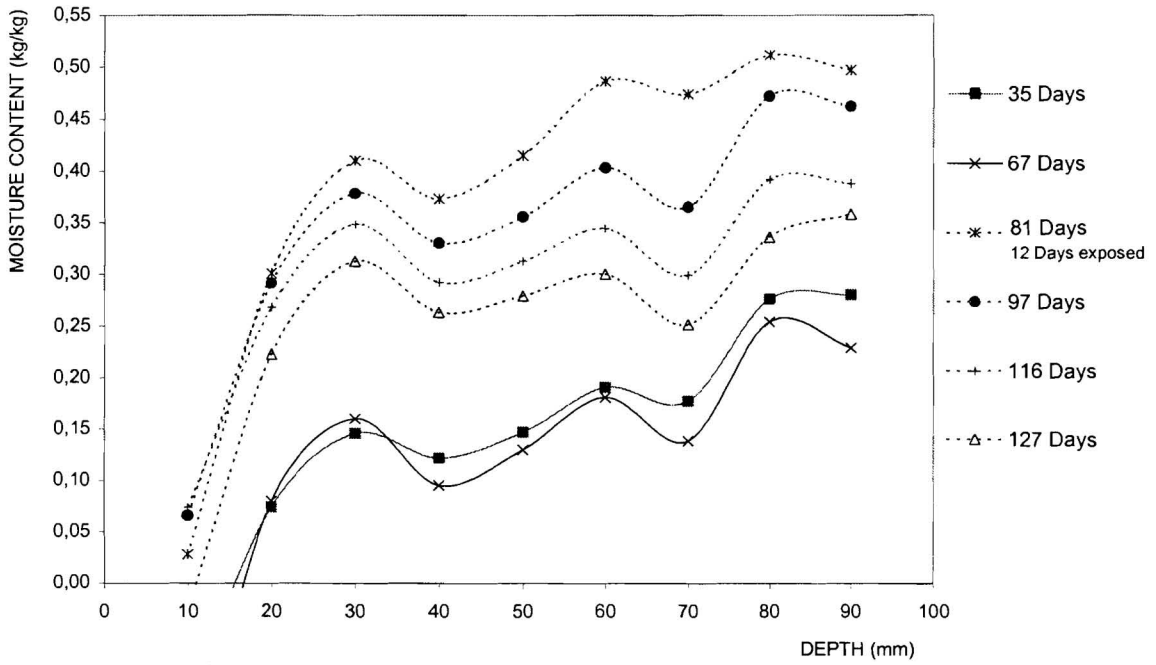

Figure 4 Profiles of the moisture content when drying in outdoor conditions of the 100-mm-thick sample (600kg/m^3).

4.3 Discussion of the Results

The average values for moisture content obtained when drying in laboratory conditions for 100- and 200-mm-thick samples are shown in Table 1. The 300-mm-thick samples are excluded from the table because the drying process is much longer.

Table 1 Values of water content of samples dried in laboratory conditions.

DENSITY (kg/m^3)	LAYER THICKNESS (mm)	MOISTURE CONTENT (kg/kg)						
		23 (days)	*30 (days)*	*46 (days)*	*53 (days)*	*74 (days)*	*102 (days)*	*127 (days)*
440	200	--	0,32	0,28	--	0,27	0,26	0,22
600	100	0,23	0,17	0,15	0,14	0,12	0,10	0,09
	200	0,23	--	0,22	0,22	0,21	0,18	0,17

For a cellular concrete of 600 kg/m^3 and thicknesses of 100 and 200 mm, after drying for 102 days, the amount of water found within it exceeds the values for the amounts of water corresponding to hygroscopic equilibrium (50% RH) by 1,2 l/m^2 and 12 l/m^2, respectively.

The moisture content observed in the samples dried in outdoor conditions were considerably higher. As an example, one should note that the average values for moisture content, measured in 100-mm-thick samples (600kg/m^3), 81 days after exposure without rain and sun between the 1st and the 69th days and under the influence of sun and rain between the 69th and 81st days, the values for moisture content exceed 0,40 kg/kg; that is, they exceed by 19 l/m^2 the values for the amount of water corresponding to the hygroscopic equilibrium.

5. PRACTICAL RECOMMENDATIONS FOR THE APPLICATION OF THIS MATERIAL

The application of cellular concrete, as a moulded layer for flat roofs or as a layer for filling pavements, executed "in situ", requires recommendations in what concerns its drying process so that it will not interfere with the hygrothermal behaviour of the construction elements in which the cellular concrete is inserted.

The thicknesses of the layer of cellular concrete to be adopted should be chosen by keeping in mind the drying time. As an example, one can refer to the fact that in the application of a 100-mm-thick layer of cellular concrete, the value of water content found in the material, after being dried for 23 days, is some 10 litres of water per m^2. To us, it seems inadvisable that one should use layers of cellular concrete over 20 cm thick when the possible drying times, without rain, are less than 120 days.

The use of cellular concrete is very complex when it is not sheltered from rainfall. Therefore, the use of protection devices is recommended, during the drying period. A cellular concrete with a density of around 440 kg/m^3 and with a thickness of 200 mm can contain over 25 litres of water per m^2 after exposure to rain for a short period.

The most common forms of protection consist of devices placed on the layer of cellular concrete. This will avoid humidification and, at the same time, allow for the development of the material's drying process.

Another type of constructive drying devices consist of making holes in the layer of cellular concrete, whose length should be greater than half its thickness, and then place perforated tubes, inside these holes to ensure the drying at different levels. These holes are later covered before the waterproofing system is placed. However, protection from the direct rain is required.

6. CONCLUSIONS

As a result of this experimental study, the following conclusions can be obtained:

- The drying of cellular concrete is a long and complex process lasting several months;
- The drying period is increased by the increase in the thickness of the applied material;
- The development of the drying process is deeply influenced by climate conditions and by the physical characteristics of the cellular concrete;
- The tested material is not homogeneous;
- The occurrence of rainfall gives rise to an increase of the drying time;
- In paragraph 5 recommendations are given to the practical application of this material.

7. REFERENCES

[1] CASTRO, José – Experimental Study of Drying Cellular Concrete, Dissertação de Mestrado, Porto, FEUP, 1998.

[2] KRISCHER, O – Die Wissenschaftlichen Grundlagen Der Trocknungstechnik – Technique du Séchage, Trad. CETIAT.

[3] FREITAS, Vasco P. de, ABRANTES, V. and CRAUSSE, P. – Moisture migration in building walls – Analysis of the Interface Phenomena – Building and Environment, the International Journal of Building Science and its Applications, vol. 31, no. 2, 1996, ISSN0360-1323, Great Britain.

[4] CORMON, Pierre – Bétons Légers d'Aujourd'hui – UTI, Paris, 1973.

SALINIZATION EFFECTS ON THE WATER SORPTION OF POROUS BUILDING MATERIALS

H.J.P. Brocken, W. Rook, O.C.G. Adan

SALINIZATION EFFECTS ON THE WATER SORPTION OF POROUS BUILDING MATERIALS

H.J.P. BROCKEN[1], W. ROOK[2], O.C.G. ADAN[1]

[1]TNO Building and Construction Research, Division of Building Technology
P.O. Box 49, NL-2600 AA Delft, The Netherlands
[2]TNO Prins Maurits Laboratory
P.O. Box 45, NL-2280 AA Rijswijk, The Netherlands
E-mail: H.Brocken@bouw.tno.nl

Abstract

The interaction of salt transport and moisture transport plays a crucial role in some deterioration mechanisms of porous building materials. For this reason it has been an important research subject for many years. Yet most research was still complicated by the lack of experimental techniques capable of measuring salt content. Therefore TNO initiated some research projects, in which the development and 'practical use' of such experimental techniques are central issues.

Part of the research focuses on the hygroscopic response of salinized porous materials. For a typical fired-clay brick and a calcium silicate brick, both salted with sodium chloride, the sorption isotherm was measured continuously by means of Microcalorimetry. The fired-clay brick contained no micropores and consequently the sorption isotherm was determined by sodium chloride only. The calcium silicate brick, however contained a reasonable amount of micropores so that the sorption isotherm was determined both by sodium chloride and by capillary condensation in the micropores. This paper shows that the measured adsorption isotherms can be predicted by a modified Kelvin equation accounting for capillary condensation at a solution-vapour interface.

Key words: sorption isotherm, Kelvin equation, salt load, brick, micropores

1 Introduction

With respect to salt crystallisation in porous building materials, durability tests were often performed by means of cyclic immersion in a salt solution and subsequent drying. Yet, such tests cannot determine the so-defined critical salt content, that is the lowest salt content that causes damage to a porous material. Repeated immersion-drying cycles cause huge salt contents to accumulate in the considered sample, leading to material in a relatively short period of time. However, actually salt crystallisation is known to be a long-term process, slowly exposing a porous material

to increasing crystallisation pressures. Therefore the critical salt content should be determined by means of a long-term test.

Nowadays, in research on salt compatibility of porous materials the long-term effect is recognized and the old durability test is replaced by a test in which the material is immersed only once. Subsequent drying introduces salts transport towards the material surface. As this situation is set, the hygroscopic response of the salted material nearby the drying surface probably dominates the damaging process. Especially the desorption isotherm, as related to the drying, is a valuable parameter in this respect.

The general method for measuring sorption isotherms is based on equilibration above saturated aqueous salt solutions. A major drawback, however, is that it offers some discrete results only, introducing inaccuracies with respect to the interpretation of the shape of the sorption isotherm. In the present work, sorption istherms were measured using microcalorimetry. This technique not only allows a continuous determination of the sorption isotherm, but moreover it distinguishes between physically different types of water vapour adsorption.

2 Capillary condensation in salted porous materials

On the basis of the definition of water activity (see e.g. Thain, 1967), for a solution-vapour interface the Kelvin equation is written as (see also Adan, 1994):

$$-\frac{2\sigma_s \upsilon_l}{RT}\frac{1}{r} = \ln\left(\frac{p_v(P_B + P_c)}{p_{vs}(P_B)}\right) = \ln\left(\frac{p_v(P_B + P_c)}{p^{\bullet}_{vs}(P_B)}\frac{p^{\bullet}_{vs}(P_B)}{p_{vs}(P_B)}\right) = \ln\left(\frac{h}{a_w(P_B)}\right)$$

or in a more convenient form:

$$h = \frac{p_v(P_B + P_c)}{p^{\bullet}_{vs}(P_B)} = \frac{p_{vs}(P_B)}{p^{\bullet}_{vs}(P_B)} e^{\left(-\frac{P_c \upsilon_l}{RT}\right)} = a_w(P_B) e^{\left(-\frac{2\sigma_s \upsilon_l}{rRT}\right)}$$

In these equations h is the relative humidity, p_v the vapour pressure above the solution-vapour interface in the capillary, $p^{\bullet}_{vs}$ the saturation vapour pressure of free pure water, p_{vs} the saturation vapour pressure of the free salt solution, σ_s the surface tension of the solution-vapour interface, P_B the barometric pressure, P_c the capillary pressure, υ_l the molar volume of liquid water, r the pore radius and a_w the water activity of the solution. The right hand side of the second equation consists of two terms. The first term accounts for the water activity, a_w, of a free ($r \rightarrow \infty$) salt solution at hydrostatic pressures equal to the barometric pressure, P_B. For pure water this term equals unity and the second equation reduces to the regular Kelvin equation as given by the second exponential term. Addition of salt to the capillary water, gives an extra reduction of the vapour pressure above the liquid-vapour interface by a factor a_w, the water activity of the free salt solution. This water activity, a_w, as well as the surface tension of the solution-vapour interface, σ_s, are a function of the concentration or molality of the solution.

3 Sorption microcalorimetry

Sorption microcalorimetry is a heat measuring sorption technique that makes it possible to measure the equilibrium moisture content during adsorption and desorption of water vapour in a porous material. Water is evaporated and the vapour is supplied to the porous material. The vapour transfer is performed in a controlled manner so that the adsorption remains close to equilibrium. By that, integration of the evaporation enthalpy represents a measure of the amount of adsorbed water vapour. Meanwhile inside the system the adsorptive vapour pressure is recorded. The measurement of such an adsorption (or desorption) cycle provides a data set of 500-1000 points in the range of 0 – 100%.

In addition to the evaporation enthalpy, also the adsorption enthalpy is integrated and subtracted from the integrated evaporation enthalpy. The resulting net adsorption energy provides information on the type of water vapour adsorption; for condensation at a water-vapour interface the net adsorption energy equals zero, while for adsorption at a pore wall surface the net adsorption energy has a negative value (release of energy).

In this paper the experimental technique will not be further elucidated. An extensive description of the method, is given by van Bokhoven (1979) and Duisterwinkel and van Bokhoven (1995). A further description of its application for measuring water vapour adsorption in porous building materials, is given by Adan (1994) and Brocken (1998). The experimental results presented in this paper are a further verification of preliminary data (Brocken, 1998).

4 Sorption isotherms

For a typical fired-clay brick and a calcium silicate brick, adsorption isotherms were measured. This was done for bricks with an artificial salt load as well as for bricks without an artificial salt load. Firstly bricks without an artificial salt load were tested. After that the same brick samples were dried and immersed in sodium chloride solutions for at least ten days, assuming that by then the concentration of the capillary water and the bulk concentration of the solution had equilibrated. For the fired-clay brick two concentrations of sodium chloride solution were used, i.e. 0.2M and 1.0M. For the calcium silicate brick only a 1.0M solution was used. After immersion the samples were air dried at (moderate) room conditions of 20°C and about 50% relative humidity for one day, followed by oven drying at 105°C for at least one day.

For non-salted bricks, adsorption isotherms are presented in Figure 1. For salted bricks, adsorption isotherms are presented in Figure 2.

For fired-clay brick, the curve for the non-salted sample hardly shows any adsorption of water vapour at high relative humidities (see Figure 1). Most of the pores in this brick are bigger than about 0.01 μm (see Brocken, 1998) so that capillary condensation hardly occurs at relative humidities less than 90%.

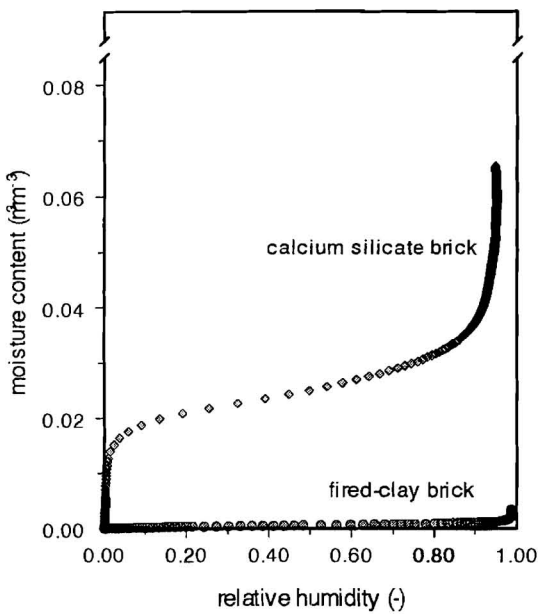

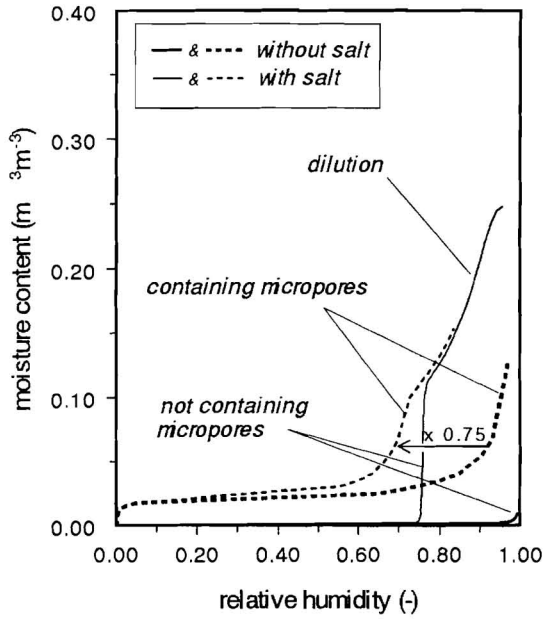

Figure 1 *[left]* Adsorption isotherms for nno-salted (•) fired-clay brick and (♦) calcium silicate brick.

Figure 3 *[right]* Schematic presentation of adsorption isotherms for bricks with and without salts, and either or not containing micropores. This presentation shows the effect of capillarity on dissolution of salts in a pore system.

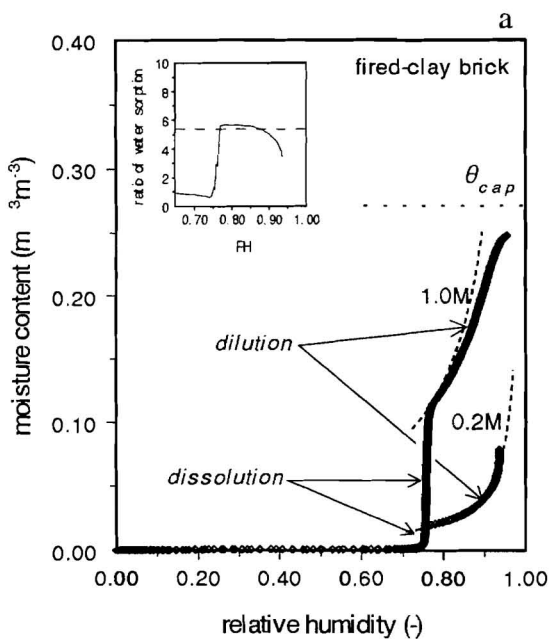

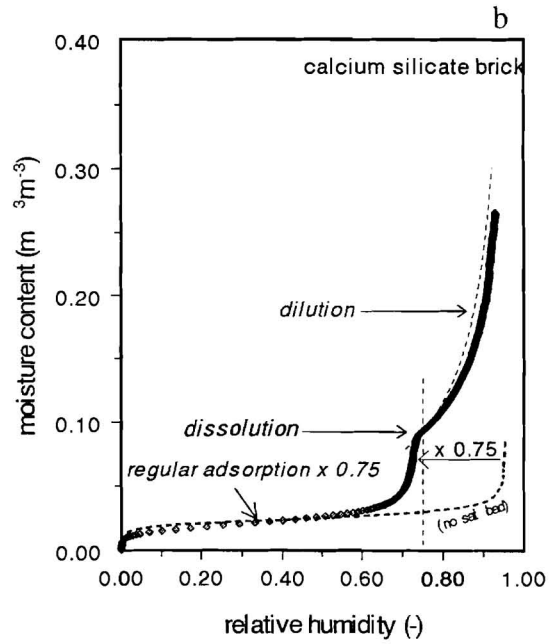

Figure 2: (a) Adsorption isotherm for fired-clay brick immersed in a 0.2M and 1.0M solution of sodium chloride. (b) Adsorption isotherm for calcium silicate brick immersed in a 1.0M solution of sodium chloride. The dashed lines indicate the simulated dilution for a free aqueous salt solution according to data adopted from Robinson and Stokes (1959).

For fired-clay brick, the adsorption isotherms of the salted samples show that in the relative humidity range up to approximately 75%, the salt load has no significant effect (see Figure 2a). At 75% relative humidity, the sorption of water (vapour) steeply increases corresponding to the introduction of a free saturated solution of sodium chloride. (With respect to the pore sizes occurring in fired-clay brick, $r \rightarrow \infty$, the saturated salt solution can be referred to as "free".)

At relative humidities above 75%, the increase of the water (ad)sorption is related to dilution of the pore solution. In Figure 2a, starting from the saturation point at 75% relative humidity, simulations based on experimental data for dilution of a "free" aqueous sodium chloride solution (see Robinson and Stokes, 1959) are added. For the brick sample immersed in a 0.2M solution of NaCl, in this region the simulated water sorption (represented by the dashed lines) and the measured water absorption agree very well; the dashed line lies through the data points. For the brick sample immersed in a 1.0M solution of NaCl, the simulation does not fully agree with the experimental data. Therefore the amount of water (ad)sorption of both brick samples was compared.

At 75% relative humidity, the (ad)sorption of water in the fired-clay brick samples immersed in a 0.2M and 1.0M solution appears to be linearly related to the salt loads, i.e. 0.4 mass% and 2.3 mass% respectively. This is reflected in the observed 1 to 5 ratio (see the inset in Figure 2a). Furthermore, with increasing relative humidity up to approximately 85%, this ratio remains the same, suggesting further dilution of the solution. For higher relative humidities, deviations occur. Presumably the capillary moisture content of the brick limits further dilution of the salt solution.

For calcium silicate brick, the curve for the non-salted samples shows a relatively large amount of adsorbed water vapour at the start of the adsorption isotherm and thereafter, for increasing relative humidities, the sorption isotherm shows a gradual increase (see Figure 1). This indicates that the calcium silicate brick contains a significant amount of micropores; at the start of the experiment first a lot of water vapour is adsorbed at the wall surfaces of these micropores.

The adsorption isotherm of the salted sample shows that up to a relative humidity of approximately 75%, the amount of water vapour adsorption is nearly the same as for the non-salted sample (see Figure 2b). Yet, in comparison to the non-salted sample, the experimental data have a "horizontal shift" which reflects the presence of a "saturated" salt solution in some pores. Up to a relative humidity of about 75%, the dry salt present in the pore system will not dilute but (partly) dissolve in the available amount of adsorbed water vapour and form a (highly) saturated salt solution. According to the modified Kelvin equation this part of the adsorption isotherm is equal to the water vapour adsorption in the untreated sample (the regular Kelvin equation), multiplied by the water activity. For a saturated sodium chloride solution, this water activity has a constant value of 0.75 (compare this part of the sorption isotherm in Figure 2b with the curve of the non-salted sample copied from Figure 1).

Complete dissolution of all salts present in the pore system is reached "before" 75% relative humidity. (75% relative humidity is indicated by the dashed vertical line.) This can also be explained from the Kelvin equation. In the case of calcium silicate brick the water (vapour) is (ad)sorbed in small pores for which the second exponential

term of the Kelvin equation is less than one. As a consequence complete dissolution of the salt present in the pores occurs at a relative humidity less than 75%.

The simulated curve for the dilution of a free aqueous salt solution is added in Figure 2b by a dashed line. This curve does not fully agree with the experimental data. Though in general it can be said that at relative humidities above 75%, the water (ad)sorption is predominantly related to dilution of the solution.

5 Conclusions

For a solution-vapour interface, the regular Kelvin equation is extended with a term accounting for the water activity of a salt solution in the pores. In this case the Kelvin equation consists of two terms; a term accounting for water vapour adsorption by capillary condensation (the exponential term from the regular Kelvin equation) and a term accounting for water vapour adsorption by the salts (the water activity). For salted porous materials that do not contain micropores (e.g. a typical fired-clay brick that mainly contains pores bigger than 10^{-6} m diameter), water vapour adsorption is fully governed by dissolution and subsequent dilution of salts in the pores (see schematic presentation in Figure 3). For salted porous materials that contain micropores, the (ad)sorption of water (vapour) is governed both by salts in the pores as well as by capillary condensation in the micropores. This effect is most predominant at relative humidities near to the water activity of the free saturated aqueous solution; that is for NaCl near to 75% relative humidity (see also Figure 3).

To understand drying of salinized porous materials, further research and evaluation of the sorption characteristics, and in particular the desorption isotherm, is needed. (Note that in the case of desorption of water vapour, so-called "hysteresis" may appear to be an important phenomenon.) For this purpose interpretation of the sorption energies will be needed.

References

[1] J.F. Thain, Principals of Osmotic Phenomena, The Royal Institute of Chemistry, Heffer, Cambridge U.K. 1967.

[2] O.C.G. Adan, On the fungal defacement of interior finishes, Ph.D. thesis, Eindhoven University of Technology, the Netherlands 1994.

[3] J.J.G.M. van Bokhoven, A method to measure the net heat of adsorption and the adsorption isotherm simultaneously, *Thermochimica Acta* 34 (1979) 109-126.

[4] A.E. Duisterwinkel and J.J.G.M. van Bokhoven, Water sorption measured by sorption calorimetry, *Thermochimica Acta* 256 (1995) 17-31.

[5] H.J.P. Brocken, Moisture transport in brick masonry: the grey area between bricks, Ph.D. thesis, Eindhoven University of Technology, the Netherlands 1998.

[6] R.A. Robinson and R.H. Stokes, Electrolyte solutions, the measurement and interpretation of conductance, chemical potential and diffusion in solutions of simple electrolytes, Butterworths Scientific Publications, London U.K. 1959.

INDICATORS OF ENERGY EFFICIENCY IN COLD-CLIMATE BUILDINGS

A. Elmroth

INDICATORS OF ENERGY EFFICIENCY IN COLD-CLIMATE BUILDINGS

-Results from a IEA-BCS Expert Working Group

Arne Elmroth, Dep. of Building Physics, Lund University, Lund, Sweden

Introduction

The purpose of this project was to develop and test new and existing indicators of a building's energy efficiency. Such indicators have many applications, such as in screening tools for energy audits, establishing measures of performance in energy-savings contracts, and tracking improvements in efficiency. These indicators should make it easier to identify houses that are truly energy efficient and to assist in comparisons with other buildings. We approached the problem by studying individual homes rather than aggregate statistics. Other IEA projects are examining indicators from an aggregate perspective. This project did not achieve all of its goals, but the analysis of individual homes provides insights and recommendations for compilation and analysis of aggregate or national data.

We explored energy indicators from the perspective of a building scientist. How does the choice of indicators affect the apparent efficiency of specific homes? And since indicators are used to compare performance, does a home's *ranking* change with the indicator? Most important, do the rankings make sense? Here again, we wanted to use our building science background to ensure that the indicators and rankings make physical sense. These questions are best answered through examination of individual houses rather than with aggregations (that is, collections of houses) because detailed characteristics are generally not collected for large groups of houses. Nevertheless, an indicator that fails to accurately rank efficiencies of individual homes is unlikely to succeed when comparing the entire housing stocks of countries.

Technical Approach

The first step in this project involved finding homes suitable for the project. These homes needed to be well-documented with both building characteristics and energy use data. Furthermore, we wanted the homes to be located in cold climates, that is, where space heating energy dominated. We hoped to acquire the following information about each building:

- One year of energy use data

- Submetered space heat
- Floor area
- Weather
- Number of occupants
- Basic construction and equipment characteristics

In addition, we expanded the compilation to include both typical and high-efficiency houses. A more diverse collection was likely to give more insights.

In spite of the "sponsor" approach, obtaining sufficient data for the homes proved to be more difficult than anticipated. Some of the problems were:

- Number of occupants was not recorded
- Lack of whole-year energy cuse data
- Failure to monitor (or report) whole-building energy use
- Lack of submetered energy use
- No information on amenities or levels of service (such as indoor temperatures)
- Inability to estimate home's overall heat loss coefficient (U-value)

The participants were sometimes asked to try to obtain more data for this project. This was achieved with some (but not complete) success.

Description of the Investigated Houses

We made compromises in order to create a diverse collection of homes and to speed up the project. As a result, some of the homes do not meet all our collection criteria. The results are still valid, but we were unable to explore as many indicators as we had initially planned. Eleven homes were finally selected for the intense examination. Those homes are shown in Table 1.

Table 1. Key to the homes

Letter	Country	City, State/Province
A	Finland	Espoo
B	Japan	Sendai, Miyagi
C	Germany	Schrecksbach, Hessen
D	USA	Moscow, Idaho
E	USA	Hanover Park, Illinois
F	USA	Missoula, Montana
G	USA	Missoula, Montana
H	USA	Eagle River, Alaska
I	Sweden	Malmo
J	Canada	Edmonton, Alberta
K	Poland	Poznan

In this report, we refer to a house by the city in which it was located or by its letter. Some features of each house are presented in Table 2. Energy data were also compiled and summarized in Table 3.

These homes represented a wide range of locations, designs, and efficiencies. Floor areas ranged from 107 to 223 m^2. Five houses were all-electric, one house was connected to a district heating system, and the remaining five burned fossil fuels for space and water heating. Two nearly identical homes–those in Missoula–were selected to show the impact when several variables were the same. A description of each house is available on the web site.[1]

Table 2. Summary of the houses' characteristics

House ID	Floor Area (m^2)	Year Built	Space Heating	Fireplace	Heat Pump	Water Heating
A	164	1991	Elec.			Elec.
B	165	1987	Oil			Oil
C	168	1987	Oil			Oil
D	325	1989	Elec.		yes	Elec.
E	112	1993	Gas	yes		Gas
F	223	1994	Elec.		yes	Elec.
G	162	1994	Elec.		yes	Elec.
H	163	1994	Elec.		yes	Elec.
I	109	1982	Elec.			Elec.
J	215	1990	Gas			Gas
K	107	1980	Dist. heat			Gas

Table 3. Summary of energy data (annual site energy)

House ID	Total Energy Use (kWh)	Space Heating (kWh)	Water Heating (kWh)	Appliances & Lighting (kWh)
A	24,108	9,020	6,232	8,856
B	11,894	3,839	4,425	3,630
C	16,414	9,610	1,512	5,292
D	18,200	8,125	1,300	8,775
E	38,101	13,774	14,829	9,498
F	21,855	4,450	3,724	13,681
G	29,595	6,580	6,570	16,445
H	16,696	8,391	3,294	5,011
I	10,300	2,200	4,200	3,900
J	45,820	27,547	7,403	10,870
K	19,653	13,244	4,472	1,937

International comparisons are complicated by inconsistent definitions of many key terms. Expressing the information in completely consistent terms proved to be impossible.

[1] Please access the web site through Alan Meier's home page: www.LBL.gov/~akmeier .

These inconsistencies undermined the accuracy of the absolute comparisons. In the end, the absence of clear and consistent definitions of basic physical characteristics–even surprisingly simple characteristics– became a major finding of this project. Four examples of inconsistent terms that could introduce significant errors are:

- Livable floor area calculation
- Calculation of heating degree-days
- Energy content of fuels
- Conversion of electrical energy into primary energy

In the complete report each of these inconsistencies are explained and the impact that they may have on the analyses is described . Several of them are characteristics that appear as the "denominator" in normalization of energy use. As such, building characteristics are just as important energy use data.

Indicators of Efficiency

Twenty different indicators of energy efficiency based on the data from the eleven homes have been calculated. These indicators are listed below.

- Total energy
- Area-normalized total energy
- Occupant-normalized total energy
- Space heat
- Area-normalized space heat
- Occupant-normalized space heat
- Climate-adjusted space heat
- Climate- and area-adjusted space heat
- Appliance and lighting energy per person
- Domestic hot water energy per person

Area adjustment means "divided by floor area", occupant normalized means "divided by the number of occupants", and climate-adjusted means "divided by degree-days". All ten of the above indicators were calculated for both site and primary energy (hence twenty different indicators). These calculations are summarized for site energy in Table 4 and Table 5.

We were unable to develop as many indicators as we hoped, because we lacked a complete data set. We particularly regretted the absence of consistent and complete information describing each building's thermal characteristics (U-values), equipment characteristics (such as heating system efficiency), and indoor temperature settings. Detailed climate adjustments were also impossible because outside temperature data were inconsistent, both in the definitions and the location of data collection.

Table 4. Total and space heating indicators expressed in terms of site energy (kWh)

House ID	Space Heat	Space Heat per m2	Space Heat per person	Space Heat per HDD	Space Heat per HDD per m2	Total Energy per m2	Total Energy per person
A	9,020	55	1,804	1.7	10.4	147	4,822
B	3,839	23.3	960	1.53	9.3	72.1	2,974
C	9,610	57.2	2,403	2.8	16.7	97.7	4,104
D	8,125	25	2,708	2.16	6.6	56	6,067
E	13,774	123.5	6,887	3.61	32.3	256.5	14,302
F	4,450	20	1,113	1.03	4.6	98	5,464
G	6,580	40.6	1,645	1.52	9.4	182.7	7,399
H	8,391	51.5	2,098	1.43	8.8	102.4	4,174
I	2,200	20	730	0.68	6.2	95	3,430
J	27,547	128	13,774	4.93	22.9	162.4	17,475
K	13,244	123.8	2,207	3.28	30.6	165.6	2,953

Table 5. Appliance, lighting, and domestic hot water indicators expressed in terms of site energy (kWh)

House ID	Appliances and Lighting	Appliances and Lighting per person	Appliances and Lighting per m2	Domestic Hot Water	Domestic Hot Water per person	Domestic Hot Water per m2
A	8,856	1,771	54	6,232	1,246	38
B	3,630	908	22	4,425	1,106	26.8
C	5,292	1,323	31.5	1,512	378	9
D	8,775	2,925	27	1,300	433	4
E	9,498	4,749	85.2	14,829	7,415	133
F	13,681	3,420	61.4	3,724	931	16.7
G	16,445	4,111	101.5	6,570	1,643	40.6
H	5,011	1,253	30.7	3,294	824	20.2
I	3,900	1,300	36	4,200	1,400	39
J	10,870	5,435	50.5	7,403	3,701	34.4
K	1,937	323	18.1	4,472	745	41.8

There are many different ways to present the results. In this study, we are most interested in how the *ranking* of the houses changes with different indicators. We considered numerous graphical displays to facilitate interpretation. Each display had its own merits and but none proved to be generally superior.

The second approach (Figure 1), a histogram, displays the approximate values and the distribution of values (but requires much more space).

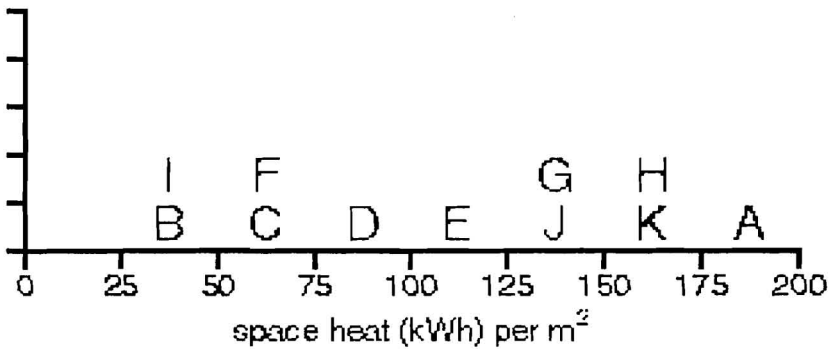

Figure 1. Histogram display of one indicator (where vertical axis represents the number of homes in that bin)

Discussion of the Indicators

These results allowed us to trace the impact of the choice of indicator on the ranking of the houses. Four detailed discussions on the following topics are presented in the complete report:

- Performance ranking of specific houses
- Implications of site vs. primary energy
- Impact of extreme situations (e.g. occupancy, plug loads, climate)
- Declining significance of space heating indicators

These discussions also draw upon additional information presented in the original documents or from the project participants.

Conclusions and Recommendations

Indicators of energy efficiency are prescriptions for condensing a large amount of information into a simple number to facilitate evaluation and/or comparison. Indicators serve many different functions. For a single house, an indicator can be used as a simple way to track its performance over time or evaluate the success of a retrofit. At a regional or national level, indicators can be used to observe the impact of energy efficiency policies on a large collection of houses.

There is no reason to expect that a single indicator will work in all cases, but it is useful to understand which indicator will be most appropriate and the data that need to be collected to support it. This project investigated the strengths and weaknesses of different indicators of energy efficiency by examining the way in which the choice of indicator affected the rankings of buildings. By understanding the implications at a single-house level, one can better interpret observed changes at the macro level.

Our major conclusions are as follows:

- Uncertainties and inconsistencies in definitions of non-energy data (the "denominator data"), such as floor area and definitions of degree-days, introduce large uncertainties in the indicators that are often larger than the uncertainties in energy data. These definitional problems undermine the value of international comparisons, especially because they introduce biases rather than random error.

- The ranking of houses by different indicators is critically dependent on the treatment of electrical energy. Houses that appear very efficient in terms of site energy may fall in apparent efficiency when this consumption is converted to primary energy at 1 kWh = 10MJ of primary energy.

- Space heating energy is declining in importance and now is less than one third of energy use, even for homes located in very cold climates. At the same time, energy use of appliances is increasing (especially when treated in terms of primary energy). Indicators need to reflect total energy use of buildings rather than focus on space heating.

- Homes with similar physical characteristics and equipment are likely to maintain their relative ranking across a broad range of indicators. Occupants and appliances certainly will affect the absolute values, but the rankings remain the same.

- The quality of the indoor environment, such as temperature, air quality, and other amenities, are not adequately reflected in any of the indicators. This rises in importance because some amenities are energy-intensive.

In this project, we sought to understand the implications of using specific indicators on large, poorly-defined groups of houses by examining the impact on a small group of well-defined homes. This approach emphasized the building science aspects of the indicators rather than the statistical aspects of large data sets. This approach was not as successful as hoped because of the complexity of attempting to develop a standard measure. Nevertheless, this project demonstrated some of the fundamental problems with indicators at both practical and physical levels.

Summary

Indicators of energy efficiency are used as screening tools for energy audits, establishing measures of performance in energy-savings contracts, and tracking improvements in efficiency. The purpose of this project was to develop and test new and existing indicators of a building's energy efficiency. We explored energy indicators from the perspective of building scientists, that is, how does the choice of indicators affect the apparent efficiency of single buildings?

We compiled detailed data on eleven houses in seven countries and calculated twenty different indicators of energy efficiency. In the course of this compilation, we found that international comparisons are complicated by inconsistent definitions of many key terms, some of which are fundamental to all indicators, such as floor area and conversions from site to primary energy.

We investigated the impact of different indicators by observing how the ranking of the houses changed. Our major conclusions were:

- The ranking of houses by different indicators is critically dependent on the treatment of electrical energy. Houses that appear very efficient in terms of site energy may fall in apparent efficiency when this use is converted to primary energy.

- Space heating energy is declining in importance, and now is less than one third of energy use, even for homes located in very cold climates. At the same time, energy use of appliances is increasing. Indicators need to reflect the total energy use of buildings rather than focus only on space heating.

- Homes with similar physical characteristics and equipment are likely to maintain their relative ranking across a broad range of indicators. Occupants and appliances certainly will affect the absolute values, but the rankings remain the same.

- The quality of the indoor environment, such as temperature, air quality, and other amenities, are not adequately reflected in any of the indicators. Environmental quality rises in importance because some amenities are energy-intensive.

These conclusions, while based on examination of only a few houses, also apply to national studies and comparisons. The difficulties in evaluating performance of individual houses have implications for measuring the success of national or regional policies to improve energy efficiency and reduce CO_2 emissions.

(The original report was written by Alan Meier, USA (Working Group Leader), Karin Adalberth, Sweden ,Sabine Busching, Germany, Arne Elmroth, Sweden, Debra Haltrecht, Canada, Tomasz Mroz, Poland, Trine Dyrstad Pettersen, Norway, Markku Virtanen, Finland, Hiroshi Yoshino, Japan)

The complete report is available on the website:
http://eetd.lbl.gov/EA/Buildings/ALAN/indicators99/

AE 990829.W40

International Council for Research and Innovation in Building and Construction

---

CIB General Secretariat:

Office address:	Kruisplein 25-G	tel:	+31.10.411 02 40
	3014 DB Rotterdam	fax:	+31.10.433 43 72
Postal address:	P.O. Box 1837	e-mail:	secretariat@cibworld.nl
	3000 BV Rotterdam	http//www.cibworld.nl	
	The Netherlands		

CIB is a world wide network of over 5000 experts from about 500 organisations, who actively cooperate and exchange information in over 50 Commissions and Task Groups. Their scopes extend to all fields in building and construction related research and development. They are listed on the next page.

They are actively engaged in initiating projects for R&D and information exchange, organising workshops, symposia and congresses and producing publications of acknowledged global repute.

It is in their ability to bring a multi-national and multi-disciplinary approach to bear on the subject matter delineated in their Terms of Reference that is their strength.

CIB Members come from institutes, companies, partnerships and other types of organisations as well as individual experts involved in research or in the transfer or application of research results. More than 130 Universities worldwide have joined.

CIB is an Association that utilises the collective expertise of its membership to foster innovations and to create workable solutions to technical, economic, social and organisational problems within its competence.

Details on Membership and Activities are obtainable from the General Secretariat at the address above.

CIB Task Groups (TG) and Working Commissions (W)

(as at 1st February 2000)

Task Groups

TG17 Protection Against Electromagnetic Radiation
TG19 Designing for the Ageing Society
TG20 Geographical Information Systems
TG21 Climatic Data for Building Services
TG22 Environmental Design Methods in Materials and Structural Engineering (also RILEM TC EDM)
TG23 Culture in Construction
TG25 Facade Systems and Technologies
TG27 Human-Machine Technologies for Construction Sites
TG28 Dissemination of Indoor Air Sciences (joint CIB-ISIAQ Task Group)
TG29 Construction in Developing Countries
TG31 Macro-Economic Data for the Construction Industry
TG32 Public Perception of Safety and Risks in Civil Engineering (joint CIB-IABSE Group)
TG33 Concurrent Engineering in Construction
TG34 Regeneration of the Built Environment
TG35 Innovation Systems in Construction
TG36 Quality Assurance
TG37 Performance Based Building Regulatory Systems
TG38 Urban Sustainability
TG39 Deconstruction
TG40 Informal Settlements
TG41 Benchmarking Construction Performance
TG42 Performance Criteria of Buildings for Health and Comfort (Joint CIB – ISIAQ Task Group)

Working Commissions

W014 Fire
W018 Timber Structures
W023 Wall Structures
W024 Open Industrialisation in Building
W040 Heat and Moisture Transfer in Buildings
W051 Acoustics
W055 Building Economics
W056 Sandwich Panels (joint CIB - ECCS Commission)
W060 Performance Concept in Building
W062 Water Supply and Drainage
W063 Affordable Housing
W065 Organisation and Management of Construction
W067 Energy Conservation in the Built Environment
W069 Housing Sociology
W070 Facilities Management and Maintenance
W077 Indoor Climate
W078 Information Technology for Construction

CIB Task Groups (TG) and Working Commissions (W) (cont)
(as at 1st February 2000)

W080 Prediction of Service Life of Building Materials and Components (also RILEM SLM)
W082 Future Studies in Construction
W083 Roofing Materials and Systems (also RILEM MRS)
W084 Building Non-Handicapping Environments
W085 Structural Serviceability
W086 Building Pathology
W087 Post-Construction Liability and Insurance
W089 Building Research and Education
W092 Procurement Systems
W094 Design for Durability
W096 Architectural Management
W098 Intelligent and Responsive Buildings
W099 Safety and Health on Construction Sites
W100 Environmental Assessment of Buildings
W101 Spatial Planning and Infrastructure Development
W102 Information and Knowledge Management in Building
W103 Construction Conflict: Avoidance and Resolution
W104 Open Building Implementation

CIB HOME PAGE

WWW.CIBWORLD.NL

The CIB home page contains the following main and publicly accessible sections:

1. General Information
2. Newsletter
3. Databases

General Information

Included is General Information about CIB in the following sub-sections:

- Introduction, including among others: CIB in the past and present
- Mission Statement
- Membership which includes information on the various types of CIB Membership and on developments in the composition of the CIB Membership
- Organisation, including the composition of the CIB Board and its Standing Committees and of the CIB General Secretariat and links with the CIB Partner Organisations
- Programme of Activities
- Services to Members, and in addition the possibilities for Members to participate in CIB's Programme of Activities
- Fee System and How To Join, including the description of the current Membership Fee Levels and the option to electronically request a Membership Application Form

Newsletters

In this section electronic copies are included of the various issues of INFORMATION, the CIB Bi-Monthly Newsletter, as published over the last couple of years. Also included is an Index to facilitate searching articles on certain topics published in all included issues of Information.

Databases

This is the largest section in the CIB home page. It includes fact sheets in separate on-line regularly updated databases, with detailed searchable information as concerns:

- ± 500 CIB Member Organisations, including among others: descriptions of their Fields of Activities, contact information and links with their Websites
- ± 5000 Individual Contacts, with an indication of their Fields of Expertise, photo and contact information

- ± 50 CIB Task Groups and Working Commissions, with a listing of their Coordinators and Members, Scope and Objectives, Work Programme and Planned Outputs, Publications produced so far, and Schedule of Meetings
- ± 100 Publications,originating to date from the CIB Task Groups and Working Commissions, with a listing of their contents, price and information on how to order
- ± 250 Meetings, including an indication of subjects, type of Meeting, dates and location, contact information and links with designated websites for all CIB Meetings (± 50 each year) and all other international workshops, symposia, conferences, etc. of potential relevance for people interested in research and innovation in the area of building and construction

Searchable Data: an Example

Searching for certain publications in the Databases in the CIB home page can be done in the following three ways:

1. In the home page itself a pre-selection is included of all recent CIB publications (published in the last 4 to 6 months). By clicking on "New Publications" the respective list will appear. By clicking on a title in this list the information fact sheet about this Publication will appear, including the option for an electronic order if it concerns a publication produced by the CIB Secretariat.
2. In the description of a Task Group or Working Commission in the database "Commissions" a pre-programmed selection is included of all publications produced under the responsibility of each Commission.
3. In the database "Publications" one can search, for example, for all publications on a certain topic, by simply typing the word that covers this topic in the box "Title" in the search page that appears when one asks for this database.

• • •

WWW.CIBWORLD.NL

DISCLAIMER

The publisher makes no representation, express or implied, with regard to the accuracy of the information contained in this book and cannot accept any legal responsibility or liability in whole or in part for any errors or omissions that may be made.

The reader should verify the applicability of the information to particular situations and check the references prior to any reliance thereupon. Since the information contained in the book is multidisciplinary, international and professional in nature, the reader is urged to consult with an appropriate licensed professional prior to taking any action or making any interpretation that is within the realm of a licensed professional practice.

CIB General Secretariat
Post Box 1837
3000 BV Rotterdam
The Netherlands
E- mail: secretariat@cibworld.nl
http://www.cibworld.nl
International Council for Research and
Innovation in Building and Construction